Zinc oxide polyvinylidene difluoride nanocomposite ultrafiltration membranes

Dissertation

zur Erlangung des akademischen Grades eines
Doktors der Naturwissenschaften
– Dr. rer. nat. –

vorgelegt von

Thorsten Hendrik van den Berg

geboren in Recklinghausen

Fakultät für Chemie
der
Universität Duisburg-Essen

2017

Acknowledgments

I would like to thank Prof. Dr. Mathias Ulbricht for giving me the opportunity to work on this topic. I would also like to thank Prof. Dr. Matthias Epple for his efforts as a co-referent for this work.

I really enjoyed the valuable discussion with all the members of the Technical Chemistry II workgroup in Essen. Especially Anne Vaterrodt, Marc Birkner, Thorsten Pieper, Matthias Quilitzsch, Jens Meyer, and Ibrahim El-Sherbini gave additional impulse to the process of this work.

Thanks to the students who worked with me on this work as well, namely Soraya Laghmari, Janina Brückerhoff, Mike Scott, Yiğit Yelkenci, and Ronald Osmond.

A special recognition for their help with the experiments goes to the apprentices I had the pleasure to work with, namely Dennis Baljak, Tom Petrick, and Torben Preisl.

Also, the technical and administrative assistance by Inge Danielzik, Tobias Kallweit, Roswitha Nordmann-Silberg, and Claudia Schenk is gratefully acknowledged.

I like to thank the European Commission for funding this project in the context of the *7 th Framework Programme for Research and Technological Development* and Sabine Paulussen for her efforts in coordinating this project. Also, I appreciate the contribution and valuable input of the project partners. Among these, a special thank-you is extended to Nino Gaeta for the opportunity to conduct the up-scaling of the membrane at GVS and to the partners at Solvay for kindly providing the membrane polymers.

Furthermore, I like to thank Smail Boukercha for his support with the SEM images and Jasmina Kovacevic for her help with the TGA measurements.

Last but not least, I want to thank my wonderful wife for her loving support and endless patience and my parents for always supporting me on my life’s journey. Without your support, I would not have seen this through.

The work presented here was performed from January 2013 till April 2016 at the Lehrstuhl für Technische Chemie II of the University of Duisburg-Essen and supervised by Prof. Dr. M. Ulbricht.

Disputation: Essen 7.12.2017

Referents:	Prof. Dr. Mathias Ulbricht
	Prof. Dr. Matthias Epple
Chairman:	Prof. Dr. Georg Jansen

Statement

I declare that this dissertation represents my own work, except where it is stated by acknowledgements and references. I only used the materials and references named and this work was not submitted to any other university before.

Signature is not included in the online version for privacy reasons.

Essen, July 2017

Table of contents

Abstract

Ultrafiltration is a widely-used membrane process for water purification. While the application of the process is an established practice, there is still a profound interest in the improvement of the membranes. The present work is about the preparation of polyvinylidene fluoride (PVDF) membranes and nanocomposite membranes with zinc oxide nanoparticles. As a first step, a basis membrane was developed which exhibited an attractive filtration performance. This membrane formulation was optimized and produced in pilot scale. Meanwhile, nanocomposite membranes were prepared using the formulation of the basis membrane as starting point. For the preparation of the dope solution, the nanoparticles were dispersed in the solvent and the polymer was added afterwards. The membranes were prepared by the non-solvent induced phase separation (NIPS) under controlled climate conditions. It was evaluated how several factors effect the agglomeration and integration of the particles during the phase separation. These were the implementation of the hydrophilic additive polyvinylpyrrolidone (PVP) in the dope, the rate of the phase separation, the surface modification of the particles with PVP, trifluoroacetic acid, acetic acid, and oxalic acid, and the presence of acrylic acid (AA) repetition units in the membrane polymer. It was found that the implementation of PVP and the reduction of the phase separation rate reduce the agglomeration tendency of the particles while the integration was not improved. The particle surface modification with carboxylic acids exhibited no influence on the membrane over the pristine particles. This can be attributed to the low surface coverage and the instability of the modification under the conditions of dope solution preparation. In contrast, the surface modification with PVP facilitated a change in the Hansen parameter of the particles. This led to a decrease of agglomeration even in hard non-solvents and improved the integration of the particles into the polymer matrix. The implementation of the copolymer P(VDF-*co*-AA) as membrane polymer induced a comparable effect under the condition that soft non-solvents were used. Since hard solvents disrupt the bonding between the polymer and the particle. Some results indicated that the increase in particle size, which is caused by agglomeration in the dope solution, can lead to a better integration of the particle because the decrease in diffusivity hinders the migration of the particles into the non-solvent phase.

Ultrafiltration ist ein weitverbreitetes Membranverfahren zur Wasseraufbereitung. Während die Anwendung dieses Prozesses etabliert ist, besteht immer noch ein großes Interesse an der Verbesserung der Membranen. Diese Arbeit beschäftigt sich mit der Herstellung von Polyvinylidenfluorid (PVDF) Membranen und der Integration von Zinkoxid Nanopartikel in diese. Zuerst wurde eine Basismembran mit attraktiver Leistung entwickelt und anschließend bis zu einem Pilotversuch optimiert. Gleichzeitig wurden Nanocomposite Membranen auf Grundlage der Basismembran hergestellt. Dazu wurden die Nanopartikel in dem Lösungsmittel dispergiert und anschließend wurde das Polymer hinzugegeben, um die Gießlösung zu erhalten. Diese wurden anhand der Scherviskosität charakterisiert. Dadurch wurde überprüft, ob Agglomerate in der Gießlösung vorhanden sind. Die Membranen wurden mittels Nicht-Lösungsmittel induzierter Phasenseparation (NIPS) unter kontrollierten Klimabedingungen erzeugt. Es wurde untersucht inwieweit verschiedene Faktoren die Integration und Agglomeration der Partikel während der Phasenseparation beeinflussen. Dazu zählen die Verwendung des hydrophilen Additivs Polyvinylpyrrolidone (PVP), die Geschwindigkeit der Phasenseparation, die Oberflächenmodifikation der Partikel mit PVP, Trifluoressigsäure, Essigsäure und Oxalsäure sowie die Anwesenheit von Acrylsäure (AA) Einheiten im Membranpolymer. Es konnte dabei festgestellt werden, dass die Verwendung von PVP in der Gießlösung sowie die Reduktion der Geschwindigkeit der Phasenseparation die Agglomeration der Partikel verringert, wobei die Integration allerdings nicht verbessert wurde. Die Oberflächenmodifikation mit Carbonsäuren war unter den Bedingungen bei der Herstellung von Gießlösungen nicht stabil und auch bezüglich der Erzeugung einer hohen Oberflächenbedeckung nicht erfolgreich. Auf Grund dieser Defizite war kein Einfluss auf die Membraneigenschaften feststellbar. Die Oberflächenmodifikation mit PVP hingegen konnte eine Änderung der Hansen Parameter der Partikel realisieren, wodurch die Agglomeration auch in harten Nicht-Lösungsmitteln unterdrückt und die Integration der Partikel in die Polymermatrix erreicht wurde. Es konnten außerdem Hinweise gefunden werden, dass eine Vergrößerung des Partikeldurchmessers durch Agglomeration vor der Phasenseparation zu einer besseren Integration der Partikel führt, da diese nicht vollständig in die Nicht-Lösungsmittel Phase migrieren. Die Verwendung des Copolymer P(VDF-*co*-AA) als Membranpolymer konnte einen ähnlichen Effekt erzeugen unter der Voraussetzung, dass kein hartes Nicht-Lösungsmittel verwendet wurde, da dieses die Bindung zwischen Polymer und Partikel stört und damit den Effekt negiert.

List of abbreviations

Ac	**Acetic acid**
ACN	Acetonitrile
BSA	bovine serum albumin
CCl_4	Carbon tetrachloride
CB	Coagulation bath
d	Day or days
DCM	Dichloromethane
DI-water	Deionized water
DLS	Dynamic light scattering
DMAc	Dimethylacetamide
DMF	Dimethylformamide
DMSO	Dimethyl sulfoxide
EG	Ethylene glycol
EtAc	Ethyl acetate
HSP	Hansen solubility parameter
IR	Infrared spectroscopy
MEK	Methyl ethyl ketone
MeOH	Methanol
min	Minutes
MWCO	Molecular weight cut off
n.a.	Not available
n.d.	Not determined
NaN_3	Sodium azide
NMP	*N*-Methyl-2-pyrrolidone
NP	Nanoparticles
NS	Non-solvent
Ox	Oxalic acid
PEG	Polyethylene glycol
PEO	Polyethylene oxide
PVDF	Polyvinylidene difluoride
PVP	Polyvinylpyrrolidone
SD	Standard deviation
SEM	Scanning electron microscopy
TEG	Triethylene glycol
TEP	Triethyl phosphate
TFA	Trifluoroacetic acid
TGA	Thermogravimetric analysis

THF	Tetrahydrofuran
TOC	Total organic carbon

List of symbols

A	Area [m²]
a	Solute radius [m]
A_m	Area corresponding to one adsorbed molecule [m^2]
c	Concentration [mol/l]
d_h	Mean hydrodynamic diameter as determined by DLS [nm]
δ_D	Hansen solubility parameter for dispersion forces [MPa$^{1/2}$]
δ_P	Hansen solubility parameter for polar forces [MPa$^{1/2}$]
δ_H	Hansen solubility parameter for hydrogen bonding forces [MPa$^{1/2}$]
δ_{Tot}	Total or Hildebrand solubility parameter [MPa$^{1/2}$]
ε	Porosity [-]
μ	Viscosity [Pa s]
J	Volume flux [m³/m² s]
P_0	Initial water permeability [l/h m² bar]
P_1	Water permeability after compaction [l/h m² bar]
p	Pressure [Pa]
M_w	Mass average molecular mass [Da]
n	Refractive index [-]
n_p	Number of pores [-]
r	Pore radius [m]
$\overline{R}$	Ideal gas constant
R	Rejection [%]
R_o	Interaction radius [-]
r_H	Hydrodynamic radius [nm]
T	Temperature [K] or [°C]
V_m	Molar volume [mol/m³]
w	Mass fraction [-]

1. Introduction

In the last century, the world water demand increased by over 600 %. This is caused mainly by the great water demand for agriculture as a consequence of the population growth in that time frame. The development is expected to continue in the upcoming years, which will further decrease the available water resources. Therefore, solving this problem is of paramount importance for a sustainable human development in the near future.[1]

The implementation of water management and sustainable technologies has the potential to decrease the water demand. In order to achieve a sufficient solution for the growing world population, it is also necessary to increase the available water resources by water treatment. Membrane technology can be a valuable contribution to the solution of water scarcity. Membrane processes are classified according to the intended application and membrane structure. The following processes are commonly used in water treatment:

- Microfiltration (MF) removes particles and bacteria.
- Ultrafiltration (UF) is used to remove viruses and colloids.
- Nanofiltration (NF) is used to remove low molecular organic molecules.
- Reverse osmosis (RO) is used for desalination.

In the last thirty years, these processes have become established in water treatment. This is caused by the advantage in energy consumption. In contrast to some conventional processes, membrane processes do not require a phase change. Also, these processes exhibit less stages and are easily scalable, which is advantageous from an engineering standpoint.[2,3]

The state-of-the-art commercial membranes are overwhelmingly polymeric membranes prepared by a phase separation process.[4] Their performance has been tremendously improved over the last decades. Still there is a great demand for improvement in terms of combining high selectivity with high permeability. The NANOPUR project[1] was designed to explore the application of novel technologies to attain that goal. The aim was the development of a membrane for water treatment, which would be structured and functionalized in the nanoscale. The combination of several techniques was used to achieve high permeability with selective properties for the removal of micropollutants which can be used at relative low pressures. Special consideration was taken that the results would be easily

[1] Project homepage: https://nanopur.vito.be/

up-scalable despite the primary concern for advancement of knowledge and not direct application.[5]

Nanotechnology is a candidate with the potential to meet the previously stated demands. The research field of nanoparticles is a relatively young as it emerged with the beginning of the new millennium.[6] With a short delay the field of nanocomposites followed as new topic and in tow with it the subject of nanocomposite membranes in water treatment. The annual publication number of this subject can be seen in Figure 1.

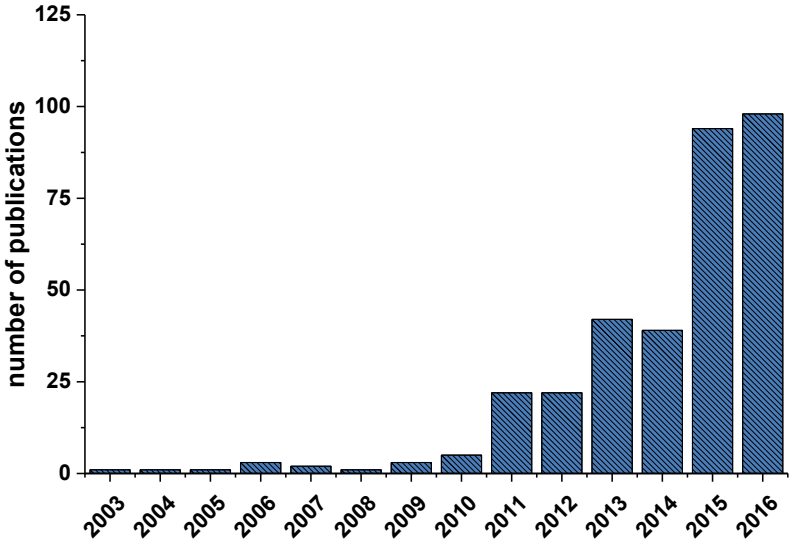

Figure 1 Number of annual publications regarding nanocomposite membranes for water treatment.[7]

The interest in the application of nanocomposites for water treatment is rooted in the possibility of combining the properties of common membrane polymers and a large variety of functional nanoparticles. These can be for example hydrophilicity to increase flux and decrease fouling tendency or mechanical strength to increase the sustainable flux. The fact, that most nanocomposite membranes are prepared by blend modification, makes this approach viable for scale-up into commercial production.[8]

The main problem with the approach is that many interesting nanoparticles are not well dispersible in the common solvents for membrane preparation. For that reason, agglomeration is likely to occur, which is not desirable as agglomerates can reduce the permeability of the membrane by pore blocking. The effective concentration of the particles is also reduced, if the nanoparticles are agglomerated. This will lead to a reduced effect on the membrane properties.[8,9]

In this work, zinc oxide nanoparticles have been selected as test subject. These are strongly hydrophilic and have been shown to increase permeability and decrease fouling in membranes. Additionally they exhibit anti-bacterial and photocatalytic properties.[10–12]

The designated membrane polymer is polyvinylidene fluoride (PVDF). Polyvinylpyrrolidone (PVP) will be used as porogenic additive. And *N*-methyl-2-pyrrolidone (NMP) is the solvent, that will be utilized to prepare the dope solutions. The effect of the zinc oxide nanoparticles on the membrane properties will be studied. It is anticipated that agglomeration and low integration of the particles into the polymer matrix will emerge because of the low mutual affinity.The affinity between the nanoparticles, the solvent and the membrane polymer will be adjusted using the following two approaches. First, the nanoparticles will be modified using carboxylic acids and polyvinylpyrrolidone, which have been shown to increase the stability of nanoparticles dispersed in NMP.[13,14] Secondly, the membrane polymer will be modified to contain acrylic acid groups. The effect should be the formation of a bond between the oxidic nanoparticle and the polymer, which could increase the mutual affinity.

Using this strategy, the influence of the affinity between the dope solution components on the membrane properties can be studied and a PVDF membrane with well-integrated zinc oxide nanoparticles should be achieved.

2. Theoretical background

2.1. Ultrafiltration

Ultrafiltration is a liquid-liquid membrane filtration processes. The application is the removal of viruses, proteins, sugars, and other macromolecules and in some instances nanoparticles from the solution. Membranes employed in this process have a pore diameter in the range of 2 to 100 nm, which corresponds to the hydrodynamic diameters of the solutes. This pore size criterion separates the ultrafiltration process from the microfiltration and nanofiltration processes, which cover pore diameter of 100 nm to 10 µm and below 2 nm, respectively.[2,15] Most commercial ultrafiltration membranes are made of polymers and are prepared by a phase separation process. The structure of these membranes is typically asymmetric, which connotes that the pore size and porosity changes over the cross-section. The top surface, also called skin layer, constitutes the selective layer of the membranes, where the smallest pore size is found. The surface porosity of this layer, which is composed by the average pore size and pore density, determines the membrane performance, which is the combined permeability and rejection. The rejection is caused by the skin layer acting as screen filter like a sieve. The underlying support structure of the membrane has no influence on the membranes permeability and rejection properties in the ideal case.[2] The ultrafiltration process and the structure of the membrane are schematically displayed in Figure 2.

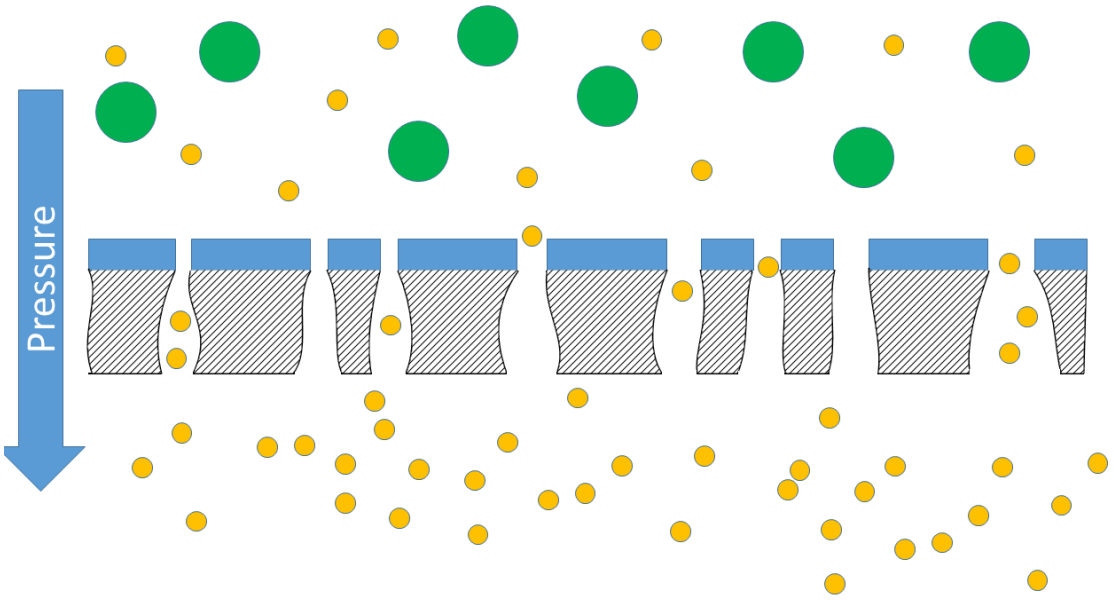

Figure 2 Ultrafiltration process with typical membrane.

Solute molecules of different size are displayed as circles. Figure is not true to scale.

The pore flow model describes the passage of the solution as viscous flow through the porous membrane. This convection is caused by the applied pressure gradient. The flow through the membrane is described by the Hagen-Poiseuille equation E-1.[15]

$$J = \frac{\varepsilon\, r^2}{8\,\tau\mu}\,\frac{\Delta p}{\Delta x} \qquad \text{(E-1)}$$

In the equation, *F* is the volume flux through the membrane given in [m³/m²s]. The surface porosity ε has no unit. It is derived from the pore radius *r* and number of pores n_P in the membrane area A_M by the following relation E-2.

$$\varepsilon = \frac{n_P r^2 \pi}{A_M} \qquad \text{(E-2)}$$

The tortuosity τ is the ratio of the pore length and the membrane thickness and has no unit. Typical ultrafiltration membranes have a very low surface porosity in the range of 0.1 to 0.05 and a tortuosity in the range of 1.5 to 2.5.[2] The three remaining parameter are the pressure gradient Δp in [Pa], the membrane thickness Δx in [m] and the viscosity of the feed solution μ given in [Pa s]. The rejection *R* can be calculated by the Ferry-Renkin equation, which is shown in E-3.[2]

$$R = \left[1 - 2\left(1 - \frac{a}{r}\right)^2 + \left(1 - \frac{a}{r}\right)^4\right] * 100\% \qquad \text{(E-3)}$$

r is the pore radius in [m] and *a* is the radius of the solute also in [m]. The equation is derived from the assumption that the solute is a spherical and travels through a cylindrical pore. The underlying approach is rooted in the definition of the rejection with the assumption that the ratio of the pore area and the area of the solute molecule is equivalent to the ratio of the solute concentration in the filtrate. With this equation, the rejection of a solute with known hydrodynamic radius can be related to the pore diameter. The calculated rejection for the different solute radii is plotted against the pore radius of the membrane, which is shown in Figure 3.

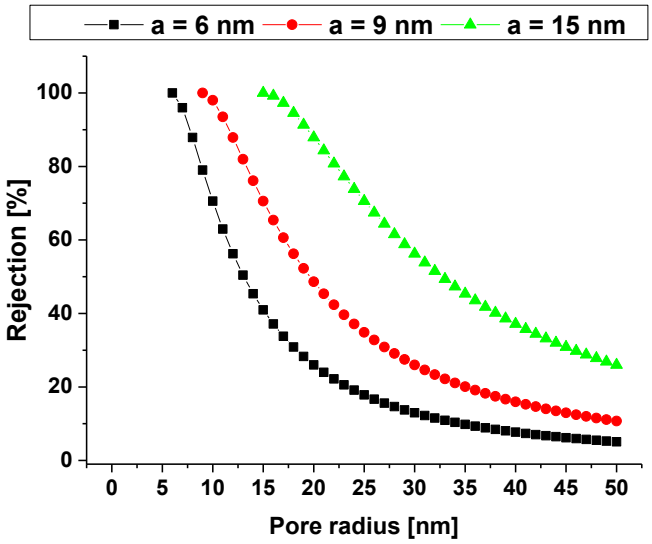

Figure 3 Calculated rejection against pore diameter.

Radius of the solute is given in the legend.

In the previous figure, the rejection increases sharply, when the pore diameter approaches the solute radius. Once the pore radius matches the solute radius, complete rejection is reached. The slope is steeper for smaller solutes. It is accepted that a rejection of 90 % can be correlated with the effective pore size of the membrane.[16] This also coincides with the definition of the molecular weight cut off (MWCO), which is defined as the molecular weight that corresponds to 90 % rejection.[2] In this thesis three solutes are used for rejection characterization: polyethylene glycol (PEG) M_w = 35 kDa, polyethylene oxide (PEO) M_w = 100 kDa and bovine serum albumin (BSA). The solute radius of these compounds is presented in Table 1.

Table 1 Radii of solutes for rejection experiments.

solute	M_w [kDa]	d_h [nm][16]
polyethylene glycol (PEG)	35	6.3
polyethylene oxide (PEO)	100	9.6
bovine serum albumin (BSA).	69	7.4

2.2. Phase separation membranes

2.2.1. Phase separation processes

Most commercial polymer membranes are prepared by phase separation processes. In these a casted polymer solution film is transformed from liquid into solid state. This is achieved by destabilizing the solution. Four varieties of the processes can be distinguished by the method, which is used to facility this:

- Thermally induced phase separation (TIPS). The phase separation is induced by a change in the temperature of the polymer solution. The system becomes unstable at the lower temperature and separates.[15]
- Solvent evaporation induced phase separation (EIPS). The polymer is solved in a volatile solvent or a solvent mixture with at least one volatile component. The volatile solvent evaporates and the decline in solvent concentration causes the polymer solution to separate.[2]
- Vapor induced phase separation (VIPS). The polymer solution is treated with a non-solvent vapor. The adsorption of the non-solvent onto the polymer film increases the non-solvent concentration to the point that phase separation occurs.[2]
- Non-solvent induced phase separation (NIPS): The polymer film is immersed in a non-solvent bath. The solvent of the polymer must be miscible with the non-solvent for this process. In the bath the solvent and the non-solvent are exchanged. This causes the system to become unstable and phase separation occurs. This process is also called immersion precipitation.[15]

2.2.2. Non-solvent induced phase separation

The previously mentioned processes can be described with the aid of a phase diagram. The following explanation will focus on the non-solvent induced phase separation, since this process is used in this work. Polymer, solvent, and non-solvent are the three components plotted in the phase diagram that describes the system. The corners of the phase diagram always refer to a pure component. The polymer and the solvent are miscible over a broad concentration range. The solvent and non-solvent are miscible in all ratios. The non-solvent and polymer are only miscible at very low concentrations or not at all. Therefore, a tertiary mixture of these components will not be stable at all compositions. When the free mixing enthalpy for these compositions is plotted over the three-component diagram, the

compositions with a mutual tangent plane form a line in the diagram called binodal. This is displayed in Figure 4.[15]

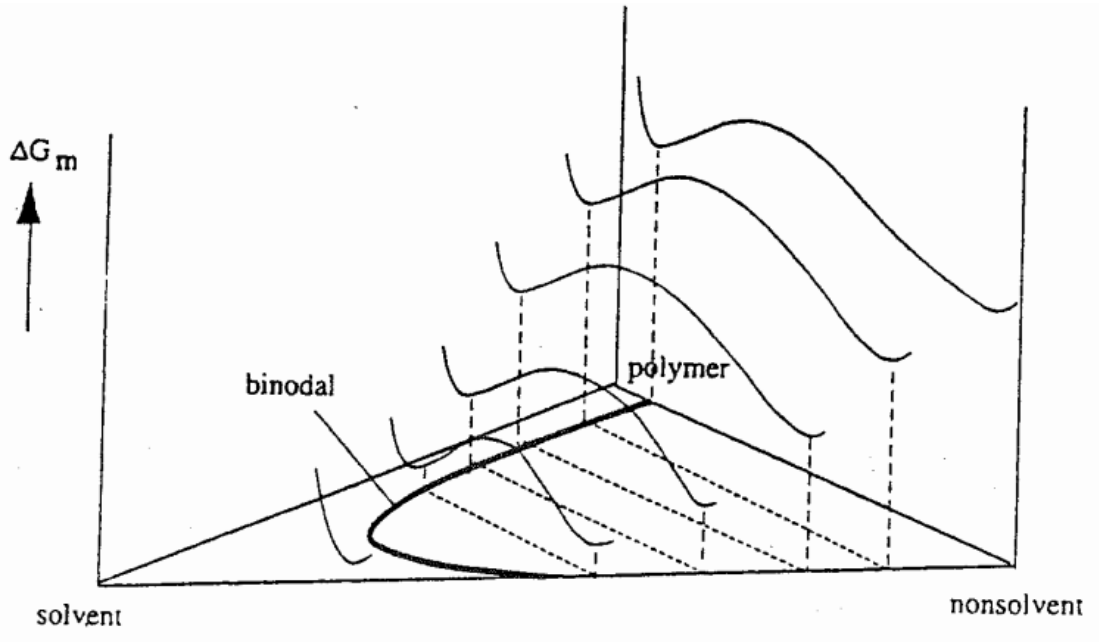

Figure 4 Derivation of the binodal line in the three-component diagram.[15]

The spinodal region is found inside the binodal region. Between the two lines a meta-stable region is located. Any tertiary composition in this region is thermodynamically unstable but will not precipitate unless a high degree of nucleation is present. The size of this region increases with the molecular weight of the polymer. The unstable two phase region is located inside of the spinodal region. Any tertiary composition in this region separates spontaneously into two phases. This separation occurs along the tie lines, which connect compositions that are in thermodynamic equilibrium. The composition of the formed phases is located on the binodal line at the end of the tie line. The position of the binodal line is specific for the system and is also temperature dependent, because of the temperature dependency of the free mixing enthalpy. In practice the binodal line is often not calculated instead it is derived from miscibility experiments A phase diagram with the previously named elements is displayed in Figure 5.[2,15]

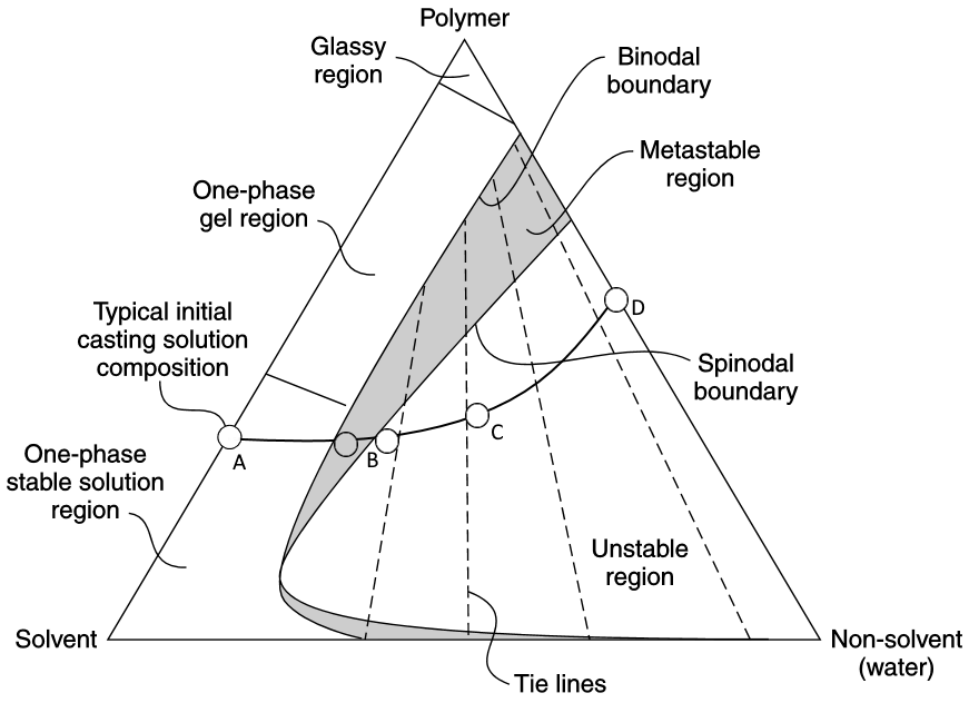

Figure 5 Schematic tertiary phase diagram for non-solvent induced phase separation. Adapted from [2]

In Figure 5, a typical dope solution composition is indicated at point A. It is located on the axis, because in this example there is no non-solvent present in the dope solution. The one phase region can be divided into three sections in order of ascending polymer concentration: stable, gel and glassy. The stable region has the lowest viscosity; a composition in this region normally produces a porous membrane. The gel region has such a high viscosity that the dope solution can be regarded as a solid gel. This is commonly encountered at a polymer concentration in excess of 30 %. The glassy region is encountered at very high polymer concentrations in excess of 90 %. In this situation, the polymer chains are no longer able to rotate. This region is not relevant for most membrane preparation applications.[2,15]

For the preparation of a porous membrane, the polymer concentration is usually located in the stable one phase region. This is applicable to point A in Figure 4, the initial dope solution composition. When the polymer film is immersed in the non-solvent bath, solvent diffuses into the coagulation bath and the non-solvent diffuses into the polymer film. This changes the composition along the indicated line to point B, as shown in Figure 4. At this point the polymer precipitates. The polymer film separates into a polymer-rich and polymer-poor phase by instantaneous liquid-liquid demixing. The polymer-poor phase grows in the interface of the polymer film, where the local non-solvent concentration is sufficient to cross the binodal line. These spots will form the pores in the finished membrane and therefore are also called nascent pores. The polymer-poor phase grows laterally and into the bulk of the polymer film

by liquid-liquid demixing. This process is synonymous with pore growth since the porous structure is formed in this fashion. The rate of pore growth is dependent on several properties of the system. The following conditions favor a rapid pore growth:

- High affinity between solvent and non-solvent
- High mutual diffusivity between solvent and non-solvent
- Low polymer concentration

The exchange of solvent and non-solvent causes the composition to change to point C in Figure 4. This is the point of solidification, at which the polymer-rich phase solidifies and no further liquid-liquid demixing is occurring. The amount of non-solvent tolerated before the polymer solidifies is mainly determined by the affinity between the polymer and the non-solvent. Hard non-solvents have a low affinity to the polymer and facilitate early solidification e.g. water. Soft non-solvents have a greater affinity to the polymer and are tolerated much longer. Solidification occurs first at the surface of the proto-membrane leading to the formation of the membrane surface. The growth of the surface pores is quenched as the consequence of the solidification. Therefore, the pore size of the selective layer is fixed at this point. The pore growth continues further into the bulk of the proto-membrane. Two cases can be distinguished for the formation of the cross-section structure. First, when the conditions for rapid pore growth are met, the non-solvent will diffuse swiftly into the bulk and the demixing will be fast. This is mostly the case at a high mutual affinity between solvent and non-solvent. The result is the formation of a structure with large macro-voids. The second case would be the formation of a sponge-like structure, which is encountered at slow demixing speed. This is facilitated when the diffusion of the non-solvent into the bulk is hindered by a dense top layer or if solvent and non-solvent have a low mutual affinity. The formation of both structures is visualized in Figure 6. The first case is shown on the right side of the figure and the second case is displayed on the left side.

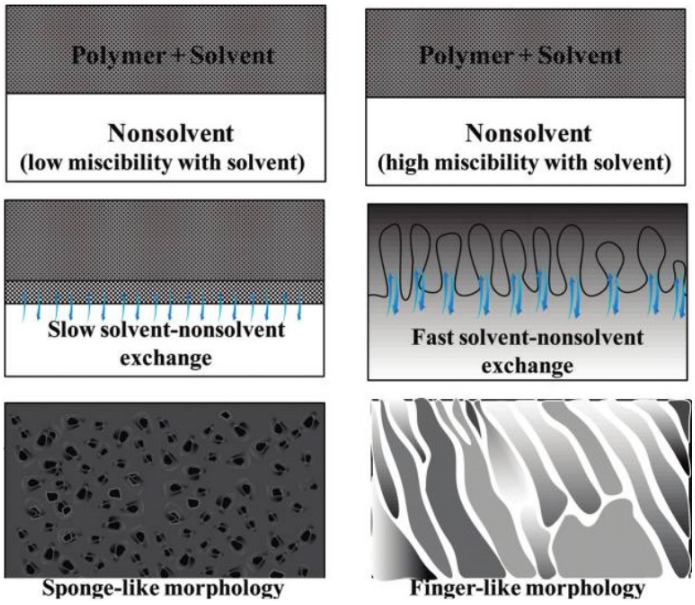

Figure 6 Membrane morphology as a consequence of demixing speed.[17]

Further, slow demixing can be achieved by adding solvent into the coagulation bath before immersing the polymer film, increasing the polymer concentration or by selecting a soft non-solvent. These conditions also favor delayed demixing. Which indicates that the composition of the proto-membrane does not met the binodal as in the previous example. The composition would change as indicated in the Figure 7.[2,15]

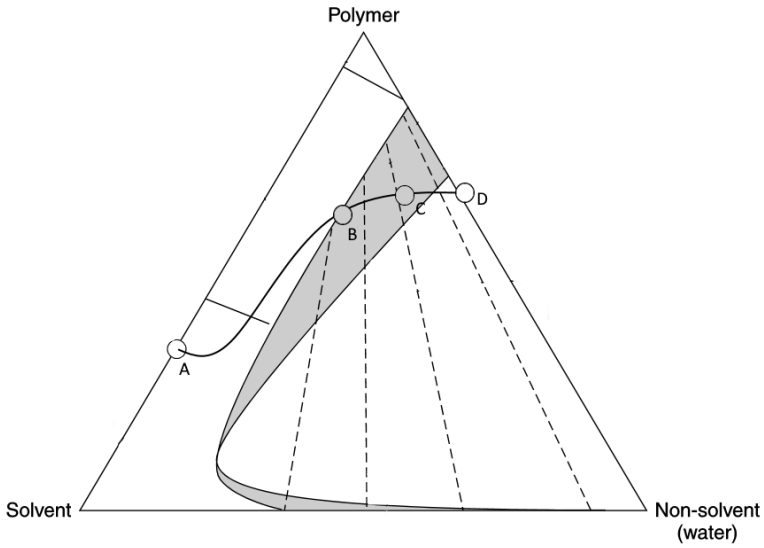

Figure 7 Schematic composition path for delayer liquid-liquid demixing. Adapted from [2].

In the figure, solvent diffuses from the proto-membrane into the coagulation bath. The polymer concentration increase consequently. When the composition crosses the binodal line, the high polymer concentration leads to a decrease of surface porosity. This can yield a dense surface if the polymer concentration is sufficiently high. Such a membrane would not be suitable for ultrafiltration. [2,15]

2.2.3. PVDF ultrafiltration membranes

In this work, polyvinylidene difluoride (PVDF) is used as base polymer for the membrane preparation. This polymer is used extensively as membrane polymer in the commercial and academic context. The reason for that can be traced back to its high mechanical strength as well as the excellent thermal and chemical stability of PVDF, which make it suitable for a large variety of applications. Furthermore, PVDF exhibits compatibility with other polymers like poly(methyl methacrylate) and polyvinylpyrrolidone, which allows for fine tuning of the membrane properties by blend modification. Solubility can be found in several strong polar, aprotic solvents e.g.: *N*-methyl-2-pyrrolidone (NMP), dimethylacetamide (DMAc), dimethylformamide (DMF) and triethyl phosphate (TEP). This allows for membrane preparation by non-solvent induced phase separation.[18–20]

In this work, NMP and DMAc are used to prepare dope solutions because it is necessitated by one of the goals to the substitution of NMP for DMAc (cf. 3.2 and 5.2.3). Both solvents have similar solubility parameters and are excellent solvents for PVDF as can be seen in Table 2. The solubility parameters are explained in 2.4.

Table 2 Hansen parameter comparison of PVDF solvents.

	δ_D	δ_P	δ_H	RED
	[$MPa^{1/2}$]	[$MPa^{1/2}$]	[$MPa^{1/2}$]	[-]
PVDF [21]	17.2	12.5	9.2	0.0
DMAc	16.8	11.5	9.4	0.1
NMP	18.0	12.3	7.2	0.2

There have been several studies done on the influence of the solvent in the preparation of PVDF membranes. Out of these, the most profound comparison of the solvents in question was done by A. Bottino et al.[19]

This study states the following differences for the solvents:

- PVDF in NMP tolerates less water before precipitating than in DMAc.
- The enthalpy of mixing is higher for DMAc-water than for NMP-water.
- The viscosity of PVDF solutions is greater in NMP than in DMAc.
- The mutual diffusivity is higher for DMAc-water than for NMP-water.

It can be concluded that the rate of pore growth will be grater for DMAc, since the difference in mixing enthalpy indicated that the driving force for the exchange of solvent and non-solvent is greater. The lower viscosity of PVDF solutions in DMAc and the high mutual diffusivity of DMAc-water enforce this even more. The lower tolerance for water in NMP means that the

delay of demixing will be shorter and that the pore growth will be terminated by solidification earlier than in DMAc. Overall it can be expected, that the membranes prepared from DMAc will have larger pore diameters.

Dope solutions with PVDF only tolerate low amounts of water, while alcohols as non-solvents are tolerated at higher concentrations. This can be seen in the phase diagram displayed in Figure 8.

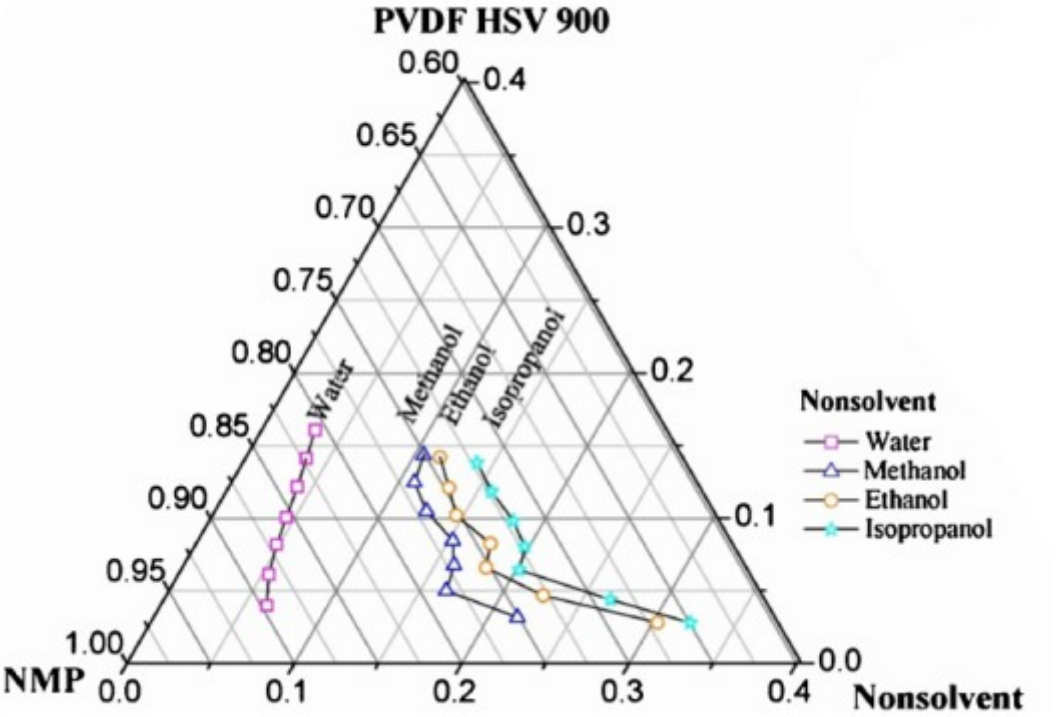

Figure 8 Phase diagram of ternary PVDF/NMP/non-solvent system at 25 °C. Adapted from [22].

The combination of the low tolerance for water as non-solvent with the high affinity of polar solvents with water leads to the emerging of macro-voids in PVDF ultrafiltration membranes.[8-10] The notable exceptions are membranes prepared from TEP. These exhibit a sponge like structure without macro-voids, which can be traced back to the low mixing enthalpy of TEP and water.[19] The other exception constitutes PVDF membranes that were prepared by the thermally induced phase separation. These usually have a sponge like structure but are normally not suitable for ultrafiltration, because of the comparable higher pore size.[18,20]

The low affinity between PVDF and water, which can be seen in the phase diagram, correlates with the hydrophobicity of the material. The increase of the hydrophilicity of PVDF membranes has been a topic in many studies. The reason behind this is the prospect to remove two problems that PVDF membranes exhibit. First, the hydrophobicity hinders the

wetting of the membrane which correlates with the reduction of the pure water permeability. Secondly, the hydrophobicity enhances the adsorption of organic foulants.[2,15,18]

Two approaches to achieve this can be distinguished; blend and surface modification. The blend modification constitutes in adding a hydrophilic additive to the membranes dope solution. The hydrophilic component can be a polymer e.g. polyvinylpyrrolidone or nanoparticles. The additive is integrated into the membrane polymer during the phase separation and the hydrophilicity is improved by the additive in the surface. Blend modification is easy employed in the commercial production of membranes, since it does not necessitate additional production steps.[2,15,18]

The approach of surface modification is applied after the membrane has been produced. The membrane surface is then treated either physically or chemically to increase the hydrophilicity. This can be achieved by the immobilization of hydrophilic polymers or nanoparticles on the surface via various chemical methods like coating, grafting to or grafting from. The physical treatment encompasses various oxidations method that increase the density of hydrophilic groups on the surface.[2,15,18,20]

2.3. Nanoparticles and nanoparticle dispersions

The International Organization for Standardization (ISO) sets the definition for nanoparticle to be a particle with a diameter between 1 and 100 nm.[23] In the recent years these particles have been of particular research interest. This is partially caused by the novelty of the research topic, but to a greater degree by the interesting properties of nanoparticles. The smaller size induces a greater surface to bulk ratio in nanoparticles compared to macroscale particles. For small nanoparticles, this can lead to every atom of the particle being a surface atom. Nanoparticles are produced by two general approaches. The *top-down* approach consists of reducing the size of a macroscale compound into nanoscale. Notable processes to achieve this are the *laser ablation*, which uses a laser beam to remove nanoscale fragments from a solid surface, or mechanical milling, which is performed by grinding a material into nanoscale. The second approach is called *bottom-up*. It consists of synthesizing the nanoparticles from low molecular precursors. This approach consists of many different processes which use different physical and chemical mechanisms to facilitate the formation of nanoscale structures.[24]

Nanoparticles are often dispersed in solvents, which are referred to as dispersion medium in this context. The resulting system consists of a continuous liquid phase, the dispersion medium, and a dispersed solid phase, the nanoparticles. This is referred to as a colloidal

dispersion. The conventional method to prepare a dispersion is ultrasound treatment also called sonication. This can be applied by a sonotrode consisting of a probe attached to a transducer, which generates ultrasonic vibrations. The probe is immersed into the dispersion medium containing the not yet dispersed nanoparticles. The ultrasound sonication breaks up agglomerates down to the primary size of the nanoparticles and distributes the particles over the dispersion medium. This process yields a stable dispersion if the treatment time is sufficient. Dispersions can become unstable by undergoing Ostwald ripening, which causes the formation of agglomerates. The agglomerates separate from the dispersion medium and sediment. The driving force, which causes this phenomenon, is that the system seeks to minimize the surface energy by increasing the size of the particles.[24]

The attractive force between the particles, which form the agglomerates, is mainly the Van der Waals force. Hydrogen bonding is only contributing to the attractive interaction if the necessary functional groups are present on the nanoparticle surface. The Coulomb force in most cases acts as repulsive force because of the identical surface charge of the nanoparticles. The interaction between the particles and the dispersion medium consists of all three aforementioned forces. Therefore, Hansen solubility parameter can be used to evaluate the interaction between these components. As mentioned in chapter 2.4, compounds with similar Hansen parameters exhibit compatibility because of the similar interactions. This holds true for nanoparticle dispersions, which are found to be stable if the components have similar Hansen parameters. In this case the interaction between the particle and the dispersion medium is favored over the particle-particle interaction. This correlates with contributions of the interactions to the cohesive energy of the system.[25,26]

It is also possible to achieve a stable dispersion if the interaction between particle and the dispersion medium is not favorable. In this case the attractive forces must be compensated by either electrostatic or steric stabilization. The mechanism of electrostatic stabilization is explained by the so-called DLVO theory, which is named after the scientists who developed it, namely Derjagin, Landau, Verwey and Overbeek. When a nanoparticle is suspended in a solvent, an electrochemical double layer is formed. The surface charge of the particle attracts counterions, which are bound to the particle and will not be removed by tangential forces. This is referred to as Stern layer. The charge of the Stern layer attracts in turn counterions, which are weakly bound. This is referred to as Gouy-Chapman diffuse layer. The border between the two layers is referred to as Stern plane.

If a tangential force is applied, a fraction of the diffuse layer will be removed. The slipping plane is the designation for the boundary between this part of the diffuse layer and the remaining layer. The electrostatic potential at this plane is referred to as zeta potential. The adsorption of ions results in an excess of charge, which depends on the surface charge of the nanoparticle and the ion strength of the electrolyte if applicable. The mechanism of electrostatic stabilization is the particle-particle repulsion caused by the Coulomb force between same charged particles. The effect is proportional to the excess charge per Coulomb's law. If the repulsion is large enough, the nanoparticles will be hindered from approaching each other and in turn prevent agglomeration by Ostwald ripening.[24]

The stabilization of dispersions by steric stabilization is facilitated by the adsorption of a polymer onto the nanoparticles. This is usually either polyvinylpyrrolidone or a form of cellulose. If sufficient polymer has been adsorbed, the solvated polymer chains will reach into the dispersion medium. When nanoparticles approach each other, the polymer chains of these particles encounter each other. The nanoparticles are kept from approaching further by the steric hindrance of the polymer-polymer interaction. This is caused by the change in free enthalpy that the interpenetration of the polymer layers would require. The magnitude of the steric stabilization is caused by the polymer type and concentration.[14,24]

2.3.1. Zinc oxide nanoparticles

Zinc oxide is a compound known to mankind for centuries. It has been widely uses as pigment, but also in rubber manufacturing and medical applications.[27] Since zinc oxide is a semi-conductor with a band gap of 3.4 eV, it has also been of research interest for electronic and optoelectronic applications.[28]

Zinc oxide is amphoteric in nature and can therefore be solvolyzed under acidic and alkaline conditions. This can occur even with water as reaction partner. The reaction equations are displayed in R-1 and R-2.[29,30]

$$ZnO(s) + 2\ H^+(aq) \rightarrow Zn^{2+}(aq) + H_2O \qquad (R\text{-}1)$$

$$ZnO + 2\ OH^-(aq) + H_2O \rightarrow [Zn(OH)_4]^{2-}(aq) \qquad (R\text{-}2)$$

The nanoparticles of zinc oxide have the same properties as the bulk material. Because of the smaller size of the nanoparticles the antibacterial[11,30,31] and photocatalytic properties [29,32] are of particular interest.

Zinc oxide nanoparticle can be produced by several processes. While most commercial processes utilize solely the bottom-up approach, a notable exception is the mechanochemical processing. This processes combines the top-down approach of ball milling with the bottom-up approach of chemical synthesis. The reaction is conducted inside the active ball mill to achieve a small particle size.[31] The nanoparticles for this study were manufactures by Evonik Industries. The production is based on the continuous flame hydrolysis of metal chlorides. This is process is dubbed the Aerosil® process.[33] The corresponding reaction for zinc oxide is presented in R-3.

$$2\ ZnCl_2 + 2\ H_2 + O_2 \rightarrow 2\ ZnO + 4\ HCl \qquad \text{(R-3)}$$

In preparation for the Aerosil® process, the zinc chloride is vaporized and the gas stream is unified with an oxygen stream. The respective gas stream is fed together with a hydrogen gas stream into the flame of the burner unit. The reaction is commenced by the thermic activation of the burner. When the gas stream reaches regions of lower temperature the zinc oxide solidifies and forms aggregates and agglomerates while passing further through the exit of the burner unit. The final particle size depends on the droplet size of the zinc oxide. Theses collide stochastically before solidification occurs and form bigger droplets. This leads to a large size distribution of the zinc oxide nanoparticles. The product gas stream is led into a cooler after which the hydrochloric acid is removed from the product.[33]

When zinc oxide is immersed in aqueous solution a zinc hydroxy layer is formed. The hydroxy groups are responsible for the dispersibility of zinc oxide in water, but also responsible for the easy solvolysis of this compound. It is also dispersible in other polar solvents like other metal oxides.[29,31,34] This hydrophilic behavior can be changed by surface modification of the particles. In the literature, examples can be found of zinc oxide nanoparticle surface modification with compounds containing carboxylic acid groups. The dispersibility of the modification changed according to the modifications affinity.[35–37]

2.4. Hansen solubility parameters

2.4.1. Fundamentals of the Hansen solubility parameters

The Hansen solubility parameters (HSP) were developed by Charles M. Hansen in 1967 during his Ph.D. thesis. At the time the Hildebrand solubility parameter δ_{Tot} was an established instrument to compare solvents. It is defined as the square root of the cohesive energy density E as shown in E-4.[25,26]

$$\delta_{Tot} = \sqrt{\frac{E}{V_m}} = \sqrt{\frac{\Delta H_V - \bar{R}T}{V_m}} \tag{E-4}$$

The cohesive energy is expressed as the Gibbs free energy necessary for the vaporization of the solvent $\Delta G_V = \Delta H_V - \bar{R}T$. This is divided by the molar volume V_m of the condensed phase. While many phenomena could be explained by correlating the Hildebrand parameter of the involved components, sometimes polymers exhibited different behavior despite having similar Hildebrand parameter. Hansen proposed to divide the cohesive energy density into the three individual contributions of the major interactions in organic matter. These are the dispersive and polar interaction together with hydrogen bonding. The dispersive interaction constitutes of the attractive London forces caused by the interaction of induced dipole moments between neighboring molecules. The corresponding cohesive energy is labeled E_D and can be derived from the vaporization energy if the molecule is an alkane, since these molecules lack the other interactions. The polar interaction is caused by the Coulomb attraction between the permanent dipoles of molecules also referred to as Debye interaction. The cohesive energy of the interaction is labeled E_P. The value can be derived from the dipole moment of the molecule. Hydrogen bonding refers to the intermolecular bonding between two polar groups over a strongly polarized hydrogen atom. This is the strongest of the three interactions. The cohesive energy originating from hydrogen bonding is referred to as E_H. The total cohesive energy E is constituted of the contributions of these interactions as shown in E-5.[25,26]

$$E = E_D + E_P + E_H \tag{E-5}$$

The relation between the Hansen solubility parameters and the Hildebrand solubility parameter can be acquired by dividing the equation E-5 by the molar volume. The result is displayed in E-6.[25,26]

$$\delta_{Tot}^2 = \delta_D^2 + \delta_P^2 + \delta_H^2 \tag{E-6}$$

The Hildebrand solubility parameter is kept in the Hansen's model. It is renamed to total solubility parameter δ_{Tot} because it describes the total cohesive energy found for the molecule. The Hansen solubility parameters generate a three-dimensional space in which all compounds can be displayed. This space is referred to as Hansen space.[25,26]

The main application of the Hansen model is of course the interpretation and prediction of solubility of polymers. The approach to this is analogous to the medieval theorem "similia similibus solvuntur". This translates to "like dissolves like" and refers to empirical rule that compounds are compatible to solvents, which exhibit the same properties in regards to polarity. To approach the problem numerically the distance between a compound, e.g. a polymer, and a solvent in the Hansen space is calculated in accordance with E-7.[25,26]

$$R_a^2 = 4(\delta_{D2} - \delta_{D1})^2 - (\delta_{P2} - \delta_{P1})^2 - (\delta_{H2} - \delta_{H1})^2 \qquad \text{(E-7)}$$

The difference of the diffusive solubility parameters is weighted with a factor "4" in contrast to the other interactions. This is an empirical coefficient that was found from the evaluation of experimental data. The interaction between the two compounds is rated by calculating the relative energy distance (RED) for the pair. This is done by the equation E-8.[25,26]

$$RED = \frac{R_a}{R_0} \qquad \text{(E-8)}$$

The radius R_0 is called interaction radius. It is the fourth parameter in Hansen's model in addition to the three solubility parameters. The radius represents the maximal difference in solubility parameter the compound will tolerate. By the calculation of the RED two cases can be differentiated. If the RED is smaller than 1, the compound will be solved. The smaller the RED is the better is the interaction. If the RED is bigger than 1, than the compound will not be solved.[25,26]

While the concept of the HSP was originally developed for polymers in solution, it has been transferred to other applications with great success. For polymers, it has been extended to the miscibility of polymers in solid state as well as the behavior of polymers at interfaces. The model was also transferred to inorganic compounds in the context of pigments and nanoparticle dispersion. Biological systems like DNA and the diffusion of solvents through organic tissue can also be described by the Hansen model.

2.4.2. Determination of Hansen solubility parameters

In the original approach the polymers are solved in a variety of solvents, which are spread over the Hansen space. The solvents are consequently rated as good or bad solvent depending on

the observed solubility of the polymer in these solvents. From this data, the solubility sphere is constructed, which contains all the good solvents and no bad solvents.[25,26] In this work, the program HSPiP Version 4.1 is used for this purpose. An example of the sphere is displayed in the Figure 9.

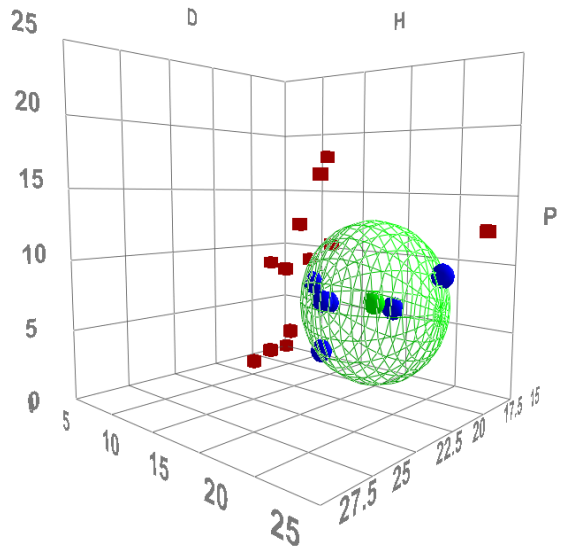

Figure 9 Example of a solubility sphere generated by the HSPiP program.
Blue spheres: good solvents; red cubes: bad solvents, green sphere: polymer, green wire sphere: solubility sphere.

The generated sphere has the determined solubility parameters as center and the radius is identical to the interaction radius R_0. The program can use different algorithms to determine the sphere. In this work, the standard fitting algorithm is applied that was suggested by Hansen in his original work.[25,26]

The algorithm tries to fit all good solvents into the sphere, while trying to minimize the amount of good solvents outside of the sphere and bad solvents inside of the sphere. In most cases this approach yields several possible spheres. The algorithm selects the best result by the obedience to the following criteria:

1. The distance to the center of the sphere should be minimal for the good solvents outside of the sphere.[25,26]
2. The distance to the center of the sphere should be maximal for the bad solvents inside the sphere.[25,26]

The software rates the best achieved result of the algorithm by assigning the value *fit*. A rating of *fit* = 1 signifies that all good solvents are inside the calculated sphere and all bad solvents are outside of the sphere. This rating is reduced depending on the number of solvents on the wrong side of the sphere and their distance to the sphere.[25]

Up to this point only a binary rating system of good and bad solvents was discussed. Under application conditions it is often found that this rating system is to narrow. In the context of polymers for example it is often found that different solvents swell the polymer in various degrees. The software allows to accommodate this by introducing a rating system of 1 to 6. A rating of 1 indicates the best compatibility and rating of 6 total incompatibility. In the software, the rating that represents the threshold for a good solvent is designated *inside*. For the determination of the Hansen sphere the inside should be set to the value that allows the best *fit* rating. This rating system can also be implemented for other applications than polymer solutions. In this work the Hansen parameters of nanoparticles are determined, therefore is the dispersion quality used to rate the compatibility of the particle with the dispersion medium.[25]

2.4.3. The oddity of water

Water is a common dispersion medium for oxidic materials and therefore relevant for this work. It is also commonly encountered and therefore interesting to evaluate. Despite the general importance of water, it is not recommended to use it as solvent for the determination of Hansen solubility parameters. The reason for this is the strong hydrogen-bonding encountered in water. When the solubility parameters for water are evaluated from the cohesive energy density as measured by the vaporization energy, the hydrogen bonding parameter is found to be δ_H = 42.3 MPas$^{1/2}$. This value exceeds the solubility parameter of most compounds by such a margin that the one would expect water to be a bad solvent for these compounds. But the experimental result often disagrees with this prediction. When water is used as good solvent in the calculation of the solubility sphere, the large distance of this solvent to the other solvents lower the fit rating of the result significantly.[25,26]

To overcome this problem the Hansen parameters of water were determined from miscibility experiments. While these results are more sensible in regard to their value for δ_H, it is generally not recommended to use water as solvent for the determination of Hansen parameter.[25,26]

2.5. Nanocomposite membranes

Nanocomposites are defined as the combination of a matrix material with a nanofiller, which must be integrated into the bulk of the matrix material. This filler material must be in at least one dimension smaller than 100 nm to be considered a nanofiller. The nanomaterial can be any nanomaterial e.g. nanoparticle, nanowire or nanogel. The matrix material can also come from a wide variety of materials. Since this work discusses polymeric membrane, the scope will be on polymers as matrix material. The common method of producing nanocomposite polymer-matrix membranes is blend modification in conjunction with a phase separation process.[8] This procedure is displayed schematically in Figure 10.

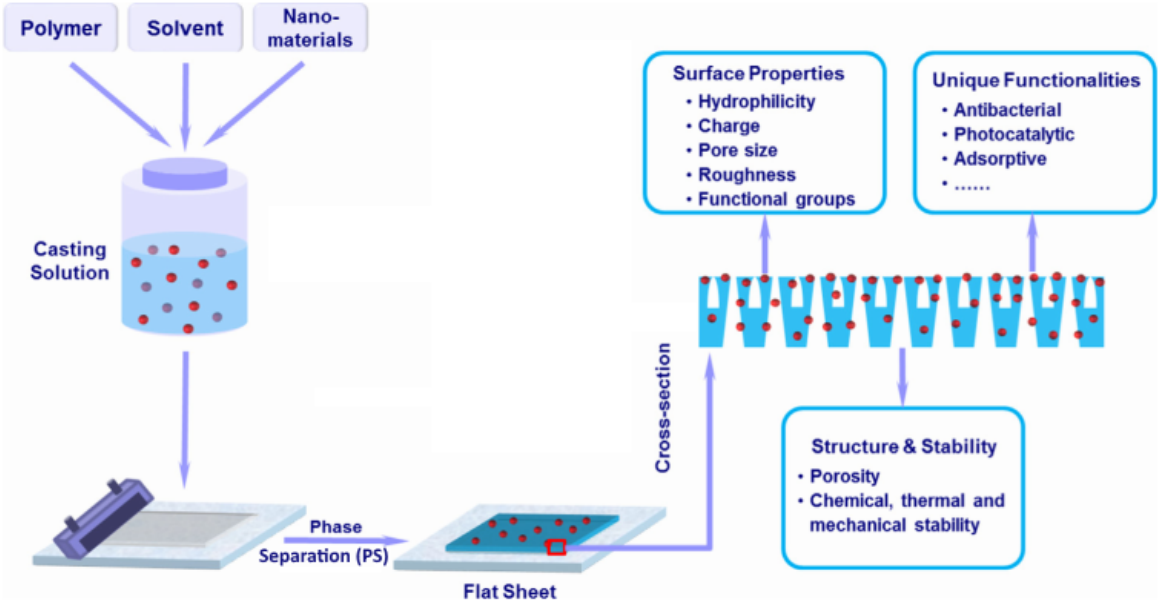

Figure 10 Conventional fabrication of flat-sheet nanocomposite membranes through the PS process and the main effects of nanofillers on final products. Adapted from [8].

The nanofiller material is added to the casting solution from which a membrane is fabricated by a phase separation process. The filler can influence the system during the phase separation. The specific influence depends on the intrinsic properties of the nanomaterial and the surface modification of the particle if applicable. The effect can often be seen in the porosity of the cross-section structure and in the skin layer morphology. After the precipitation of the membrane the filler material can be found in the bulk but also in the surface of the membrane. The mere presence of the nanofiller in the bulk can influence several membrane properties:

- Mechanical properties
- Thermal and chemical stability
- Decrease the pure water permeability by pore blocking

The nanofiller, which is immobilized at the interface of the polymer, can affect the surface properties of the membrane. This is mostly caused by the contribution of the nanomaterial's surface properties to the surface chemistry of the membrane. The hydrophilicity, charge and functional groups of the membrane surface can be altered through this mechanism. If the particle has photocatalytic, adsorptive, or anti-bacterial properties, these are added in the same way. An increase of the surface roughness is also often seen.[8]

The main problem that causes a reduction in modification effectiveness is the occurrence of agglomeration during the phase separation. The agglomeration process increases the size of the particles. The change in size reduces the overall surface area of the particles and the effective particle concentration, which impairs the expected effect of the nanoparticle modification. Furthermore, the large agglomerates can decrease the permeability of the membrane. The agglomerates block the pores and therefore inhibit the flux through the membrane. This will lead to a reduction of the pure water permeability. [9,38] The nanoparticle agglomeration is caused by the difference in affinity between the polymeric matrix material and the nanomaterial.[20] In this work the nanofiller material consist of zinc oxide nanoparticles and the matrix material is polyvinylidene difluoride (PVDF). An overview of the results of various studies is given in the following paragraphs. Additionally, a tabular summary is presented in Table 3, which contains the relevant conditions and results of the referred studies. All discussed studies cover the effect of the integration of metal oxide nanoparticles into PVDF ultrafiltration membranes. The membranes were prepared in all cases by non-solvent induced phase separation. The nanoparticles employed in these studies are titanium oxide, aluminum oxide, magnesium hydroxide and zinc oxide. Since these are metal oxides, it is expected that the effect of them on the membrane will be similar to expected effect of zinc oxide.[10]

In regards to the permeability an enhancement is seen with the addition of nanoparticles to the dope. This can be seen in eight studies, some of the authors attributed this to the increase in surface hydrophilicity caused by the hydrophilic particles.[12,39–45] This change in hydrophilicity was observed very often.[12,38–41,43–45] In five of these studies the permeability decreased at higher nanoparticle concentrations. This was attributed to the pore blocking by agglomerated.[12,40,42,44,45] In one other study, the permeability was not affected by the addition of nanoparticles.[46] No effect was observed in a different study.[38] The difference in

effect that is seen on the permeability could not be correlated with any factor in the membrane preparation.

The assessment regarding the effect of the nanoparticles on the membrane structure is as fuzzy as for the effect on the permeability. No effect whatsoever is seen in four studies.[12,38,39,41] In three studies an increase in skin layer thickness is seen.[43,45,47] The authors attribute this to the increased viscosity of the dope solution, that was caused by the addition of the nanoparticles. The macro-void formation in cross-section structure is decreased in three studies.[40,42,45] In one study an increase of macro-void formation was observed.[44]

The mechanical properties of the membrane were evaluated in some of these studies. The incorporation of the nanoparticles was found to increase in tensile strength with a decrease of elongation at break in one study.[48] The decrease of both properties was also observed in one instance.[45] But, three studies observed the increase of both properties.[12,39,40]

Table 3 Overview of nanocomposite membrane studies.

Source	NP type	Solvent	Additive	Dispersion method	Coagulant	pure water permeability	rejection	macro void formation	hydrophilicity	tensile strength	elongation at break
Oh et al. 2009[38]	TiO2	NMP	none	n.a.	*Iso*-Propanol/water 20/80	↓	n.a.	–	↑	n.a.	n.a.
Wei et al. 2011[48]	TiO2	DMAc	PVP	stirring	EtOH/water 15/85	n.a.	n.a.	n.a.	–	↑	↓
Cao et al. 2006[41]	TiO2	DMF	none	n.a.	water	↑	–	–	–	n.a.	n.a.
Song et al. 2012[43]	TiO2	DMAc	PEG	n.a.	water	↑	↓	n.a.	↑	n.a.	n.a.
Liang et al. 2012[12]	ZnO	NMP	PVP, Glycerol	5h sonication of whole dope	water	↗↘	n.a.	–	↑	↑	↑
Yu et al. 2009[40]	TiO2	NMP	PVP	stirring	water	↗↘	–	↓	↑	↑	↑
Dong et al. 2012[44]	Mg(OH)2	DMAc	PEG	NP in solvent	water	↗↘	–	↑	↑ / ↓ *	n.a.	n.a.
Yan et al. 2006[39]	AL2O3	DMAc	PVP	stirring	EtOH/water	↑	–	–	↑	↑	↑
Liu et al. 2011[45]	Al2O3	NMP	H2SO4	stirring	water	↗↘	n.a.	↓	↑	↓	↓
Yuliwati et al 2011[47]	TiO2	DMAc	LiCl	stirring	water	↗↘	↑	↓	n.a.	n.a.	n.a.

Legend

↑	Increase with NP conc.	–	no influence
↓	Decrease with NP conc.	n.a.	information not available
↗↘	increases at low NP conc., decreases at higher NP conc.	*	depends on PEG conc.

3. Aim and Concept

The aim of this work is to evaluate the influence of nanoparticle-polymer affinity on the integration of the particles into the polymer matrix and the resulting influence on the ultrafiltration performance. The pristine zinc oxide nanoparticles have a low affinity to the base polymer polyvinylidene fluoride (PVDF). In order to alter the affinity between these components two strategies are employed: nanoparticle modification and modification of the base polymer. This thesis is separated into two sections according to the topics modification of the nanoparticles and the membrane preparation.

3.1. Nanoparticle modification

In this section, the planned experiments considering the modification of zinc oxide nanoparticles are presented. The particles will be characterized by thermogravimetric analysis and infrared spectroscopy. The affinity of the particles will be evaluated by the determination of the Hansen solubility parameters.

Characterization of pristine nanoparticles

The pristine zinc oxide nanoparticle will be characterized as reference for the modification experiments. These results will also be used as reference for the experiments considering the integration of pristine particles.

Nanoparticle modification with carboxylic acids

In this work, the nanoparticles are modified with three different carboxylic acids as modification agents:

I. acetic acid (Ac)
II. trifluoroacetic acid (TFA)
III. oxalic acid (Ox)

In the literature it was shown, that the presence of acetic acid on the surface metal oxide nanoparticles improves the stability of nanoparticle dispersions in strong polar solvents.[13] The designated membrane polymer PVDF is only soluble in a few strong polar solvents. Therefore, it can be expected that the modification will alter the Hansen parameters of the nanoparticles to correspond better to the parameters of PVDF, which indicates an increase in affinity between these compounds. Therefore, the zinc oxide nanoparticles will be modified with acetic acid to replicate the cited study. Trifluoroacetic acid is the fluorinated derivate of acetic acid. Since PVDF is a fluorinated polymer, a significant additional increase in affinity can

be expected from the modification of metal oxide nanoparticles with TFA. Oxalic acid is the simplest dicarboxylic acid. The surface modification of oxidic nanoparticles with this compound should yield an increase in the number of carboxylic acid groups on the surface. This is expected to decrease the affinity between the particles and PVDF.

Nanoparticle modification with polyvinylpyrrolidone

Polyvinylpyrrolidone is a common modification agent used for the steric stabilization of nanoparticles in polar solvents. It is also compatible with PVDF. For this reason, it is expected that the adsorption of PVP on nanoparticles increases the affinity between the particles and PVDF.

3.2. Membrane preparation

In this section, the work packages presented aim to evaluate the effect of the addition of nanoparticles on the membrane properties. In the following experiments the membranes will be characterized by pure water permeability, PEG 35 kDa and PEO 100 kDa rejection properties, SEM, and mechanical characterization.

Base membrane and up-scaling

As foundation for the membrane modification a base membrane is developed in the ultrafiltration range and up-scaled into pilot scale. The target performance of this membrane is:

- Pure water permeability of ≥1000 l/h m²
- BSA rejection of ≥ 90 %
- Molecular weight cut-off ≤ 100 kDa for Dextran

These specifications originate from the objectives of the NANOPUR project. The transfer into pilot scale is also a demand of the project proposal. The project plan determined that polyvinylidene fluoride (PVDF) from the industry partner SOLVAY Specialty Polymers would be used as base polymer and polyvinylpyrrolidone as polymeric additive.

Incorporation of pristine nanoparticles

The influence of pristine zinc oxide nanoparticles on the membrane properties will be evaluated utilizing the base formulation. In this context, the effect of the PVP additive in the dope and the precipitation rate during the phase separation process will be evaluated.

Base polymer modification

For the modification of the base polymer a statistical copolymer was supplied by the project partner SOLVAY Specialty Polymers in the context of the NANOPUR project. It consists of 99 %w/w vinylidene difluoride (VDF) and 1 %w/w acrylic acid (AA) monomer. Therefore, it is referred to as P(VDF-*co*-AA). The introduction of the acrylic acid repeating units enables the formation of bonding between the polymer and metal oxide nanoparticle via the carboxylic acid group. Therefore, it is expected that affinity between the membrane polymer and the zinc oxide nanoparticles will be enhanced. A molecular weight determination was not possible for the copolymer on the in-house size exclusion chromatography set-up because of the chromatography columns incompatibility with carboxylic acid groups. The project partner assured that the molecular mass is comparable to the PVDF that is used as base polymer. Therefore, it is expected that all differences between the polymers during the membrane preparation can be attributable to the chemical difference caused by the acrylic acid groups. The conditions identified in the experiments with PVDF and pristine particles will be applied to the modified base polymer P(VDF-*co*-AA).

Incorporation of modified nanoparticles

The conditions identified in the experiments with PVDF and pristine particles will be applied to the modified nanoparticles. Membranes will be prepared from dope solutions with various amounts of modified nanoparticles. The effect of the modified particles on the membrane properties will be evaluated. For all particle modifications, it is expected that the modification agent will be partially removed by the water during the membrane preparation.[49,50] This will yield the original zinc oxide surface for the nanoparticles, which are immobilized in the membrane.

4. Experimental

4.1. Nanoparticle dispersion preparation

The dispersions are prepared using a sonotrode (*Sonoplus HD 3200* from Bandelin electronics GmbH & Co. KG). Rosette cells are used to facilitate axial mixing. These cells are available in four sizes: 20, 50, 100 and 250 ml. The filling volume must not be lower than half of the cell volume for the axial mixing to work. Two sonotrode tips are used in this work: the tip *VT 70* for volumes in excess of 50 ml and the *KE 73* for smaller volumes.

As a first step, the nanoparticles are placed in the rosette cell and overlaid with the dispersion medium. The filled cell is placed in the cooling bath of ice and DI-water. The tip of the sonotrode is submerged into the solvent. Special care is taken that the tip is not touching the walls of the cell. The set-up is presented in Figure 11.

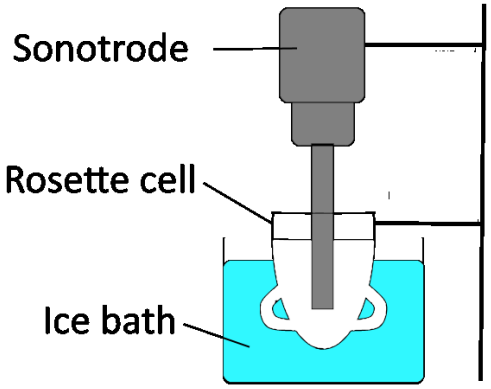

Figure 11 Diagram of the sonication set-up.

If not stated otherwise, the sample is sonicated for 10 minutes at an amplitude of 50 %. The dispersion can be used directly.

4.2. Nanoparticle Modification

This procedure describes the modification of the zinc oxide nanoparticles with various modification agent. The agents used in this work are trifluoroacetic acid, oxalic acid, acetic acid and polyvinylpyrrolidone.

As the first step, in preparation of the procedure the modification agent is solved in ultrapure water. This is done in a beaker under constant stirring. Sodium hydroxide solution is added for the adjustment of pH to the required value if the pH value is controlled. To equalize the volume of the solution to the nanoparticle dispersion ultrapure water is added. Meanwhile, a dispersion of pristine zinc oxide particles in ultrapure water is prepared as described in 4.1.

The nanoparticle concentration is kept at 25 mg/ml. After the preparation, the dispersion is filled into a beaker with stir bar. The solution and the dispersion are heated separately to 60 °C under constant stirring. When the temperature is reached, both liquids are unified and kept at 60 °C under stirring. After one hour, the heating is terminated. The solution is kept under stirring until the dispersion reaches room temperature. The particles are separated from the aqueous by centrifugation (*Universal 320* from Hettich Lab Technology) at 4500 rpm. The sediment is rinsed with ethanol twice and then dried in a vacuum oven. The mass of the dried particles m_1 is evaluated. From this value the mass retrieval is calculated as shown in E-9.

$$mass\ retrieval = \frac{m_1}{m_0 * (1 + c_{monolayer})} * 100\% \qquad \text{(E-9)}$$

$c_{monolayer}$ is the concentration of modification agent on the particle at monolayer (see 5.1.3); m_0 is the mass of the unmodified zinc oxide nanoparticles. If the available mass of the modification agent is smaller than the necessary mass for the formation of the monolayer, equation E-9 is modified to E-10.

$$mass\ retrieval = \frac{m_1}{m_0 + m_{modificaton\ agent}} * 100\% \qquad \text{(E-10)}$$

4.3. Membrane Preparation

4.3.1. Dope solution preparation

The glassware and stir bar are cleaned with acetone and dried at 40 °C in the oven. The polymers are dried at 40 °C in the vacuum oven over 72 hours and stored in a desiccator over silica gel until use. The polymer is weighed into an Erlenmeyer flask with glass joint (100 or 250 ml) and a stir bar is added. The flask is closed with the plug, sealed with parafilm and placed on a magnetic stirrer hot plate and stirred at 300 rpm. If nanoparticles are to be added, the particles are dispersed in the NMP as described in 4.1. The NMP with or without dispersed particles is now added to the polymer under stirring. The flask is then again closed and sealed. The hot plate is set to 60 °C and then stirred over 48 h to assure that the polymers are well solved. Afterward, the dope solution is rested for a few hours in the dark to remove bubbles.

4.3.2. Rheology

The shear viscosity of the dope solution is measured using a rheometer *Physica MCR301* from Anton Paar. The measurement is performed using a probe with conical geometry and diameter of 25 mm with the designation CP25-2. The sample is kept under a dry air stream

during the measurement to prevent precipitation over the course of the measurement. The measurement cell is kept at 20 °C. The shear viscosity is measured over the shear rate from 1 to 800 s^{-1}. The viscosity at 15.9 s^{-1} is selected to compare dope solutions. This value is comparable to the shear rate of the casting knife during membrane casting and the shear thinning behavior is neglectable in this range.

4.3.3. Membrane casting

The dry air circulation in the climate box is started and a period of 30 minutes is allowed for the humidity to drop below 30 %RH. The glass plates (length 35 cm) and the casting knife are cleaned with acetone inside the climate box and again a period of 30 minutes is allowed for the residual solvent to evaporate. If a nonwoven is used as substrate, the nonwoven is attached to the glass plate with duct tape. The membranes are casted using a *COATMASTER* made by Erichsen. The casting speed is fixed at 5 mm/s. This determines that the casting knife will need approximately 70 s to cover the length of the plate. A casting knife is used with a clearance of 200 µm if not stated otherwise. The casted dope solution film is directly immersed into the coagulation bath outside of the climate box. The coagulation bath consists of DI-water, if not stated otherwise. The membrane remains in the coagulation bath for one hour and is then rinsed in a fresh DI-water bath for 24 hours. For the filtration experiments the samples are taken from the wet membrane and then stored in 10 mM sodium azide solution. The rest of the membrane is submerged in ethanol overnight and then changed to *n*-hexane. The membrane is dried from *n*-hexane.

4.4. Ultrafiltration experiments

4.4.1. Dead end

The dead-end filtration set up uses the stirred ultrafiltration cell *Amicon 8050* made by Merck Millipore. Circular samples with a diameter of 44 mm are used in this cell. The device is set up as seen in Figure 12. A laboratory scale is used to quantify the amount of permeate.

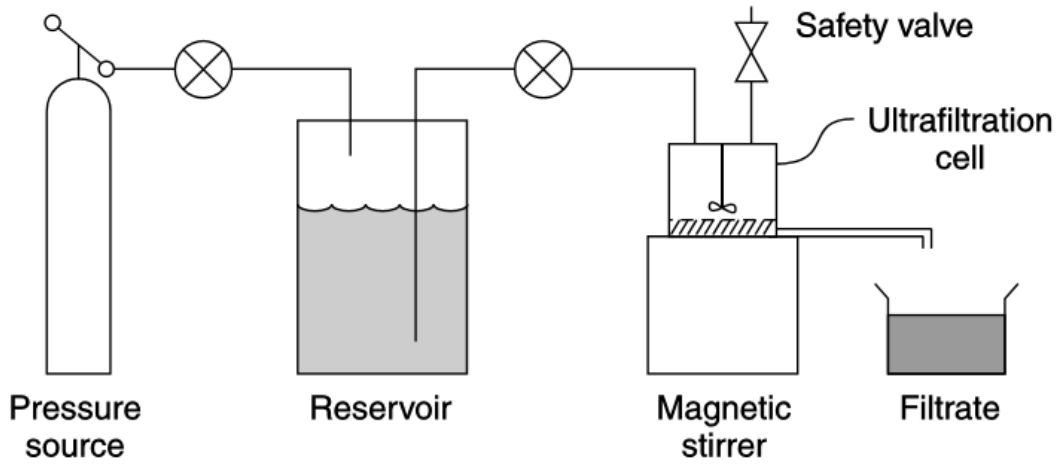

Figure 12 Dead end filtration setup.[2]

The membrane is installed in the cell and the reservoir is filled with DI-water. The magnetic stirrer is set to 400 rpm and kept there during the experiment. The pressure is set to 0.5 bar and the flux is measured over five minutes three times. The permeability P_0 is calculated as shown in E-11.

$$P = \frac{m}{A\,\Delta t\,\rho_{H_2O}\Delta p} \qquad \text{(E-11)}$$

P is given in [l/h m² bar]. m is the water mass [g] collected over the time interval Δt [h] at the transmembrane pressure Δp [bar]. A is the effective membrane area of $1.34\ 10^{-3}$ m² as specified in the user's guide of the cell.[51]

The pressure is increased to 1.5 bar for 30 minutes to compact the membrane. Afterward the permeability is measured and calculated again, which is referred to as P_1. The cell is then filled with 50 ml BSA solution (1 g/l and 10 mM NaN_3) and the pressure is set to 0.15 bar. The first two grams of permeate are discarded and the following five grams are collected. The concentration in permeate and feed are determined by TOC analysis as described in 4.5.1. The rejection R is calculated per E-12.

$$R = \left(1 - \frac{c_P}{c_F}\right) * 100\% \qquad \text{(E-12)}$$

c_P and c_F are the TOC of the permeate and feed respectively, given in [mg/l].

4.4.2. Crossflow system

The crossflow filtration setup is laboratory device *LSta05* produced by SIMA-tec GmbH. The overall area of the flat membrane sample is 100 cm², while effectively 84 cm² are used in the filtration. After installing the membrane in the cell, the feed container is filled with two liters

of aqueous sodium chloride solution (c = 50 mg/l). The salt is added to increase the conductivity of the feed over 20 µS/cm, the minimum threshold of the flow meter. The volume stream is kept at 20 l/h for the whole experiment. The steps of the filtration protocol are presented in Table 4.

Table 4 Filtration protocol for the crossflow setup.

	pressure [bar]	time [h]	feed composition
initial pure water flux	0.5	0.5	ultrapure water with 50 mg/l NaCl
Compacting	1.5	0.5	
pure water flux after compacting	0.5	0.5	
PEG filtration	0.15	1	1 g/l PEG M_w = 35 kDa; 50 mg/l NaCl
PEO filtration	0.15	1	1 g/l PEO M_w = 100 kDa; 50 mg/l NaCl

The device gives a continues reading of the flux and pressure. The mean permeability over time is calculated from this data for each stage of the experiment. The first samples of the feed and permeate are taken after 30 minutes at constant conditions and a second one after another 30 minutes. The solute concentrations are determined by TOC analysis. The rejection is calculated as stated in 4.4.1 by E-11.

4.5. Membrane characterization methods

4.5.1. Total organic carbon measurement

The amount of total organic carbon (TOC) is determined using the device *TOC-V CPN* from Shimadzu, which is equipped with the external autosampler *ASI-V*. The device is a combustion analyzer and calibrated for measurement in the range of 0 – 1000 mg/l TOC. The method can tolerate up to 10 mg/l inorganic carbon. Two milliliters of the sample are diluted with 15 ml ultrapure water to stay within the calibration range. Beforehand, the vials are cleaned with 1 M hydrochloric acid to remove possible contamination and dried at 40 °C over night.

4.5.2. Molecular weight cut off

The first step of the MWCO (Molecular weight cut off) determination is the filtration of a dextran solution. The dextran feed composition is used as presented in Table 5.

Table 5 Dextran feed for MWCO determination.

M(dextran) [kDa]	c [g/l]
40	0.6
100	0.5
500	0.4
2000	0.5
sum	2.0

All dextran fractions were acquired from Serva (Fulda). The dextran is solved in aqueous sodium azide (c = 10 mM) over night. The molar mass distribution of the feed is displayed in Figure 13.

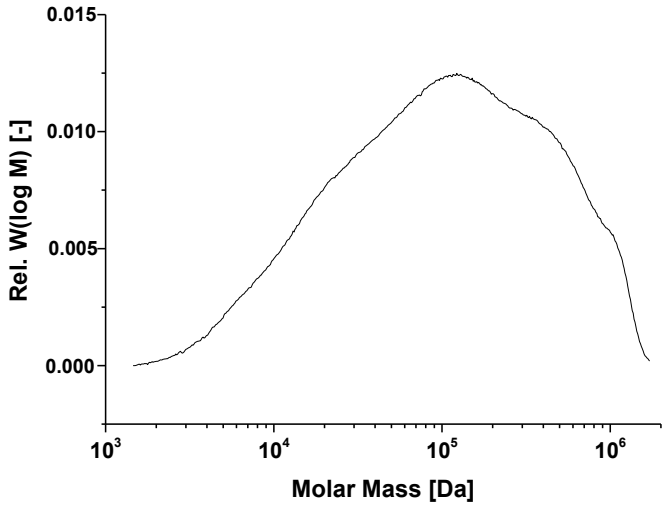

Figure 13 Molar mass distribution of feed for MWCO determination.

The distribution shows sufficient intensity in the range of 10^4 to 10^6 Da, which is adequate for the SEC measurement. The filtration is performed in dead end mode as described in 4.4.1. after the permeability P_1 was measured. The Amicon 8050 cell is filled with 50 ml feed solution. The filtration is performed under stirring (400 rpm) at a transmembrane pressure of 0.1 bar. The first 2 ml of permeate are discarded and the following 3 ml of permeate are collected for analysis. The permeate and the feed are characterized by size exclusion chromatography (SEC) to obtain the molar mass distribution of these. The sieving curve is calculated from this data. The MWCO is the molar mass which is rejected by 90 %. The SEC system employs a refractometer as detector of the model *RI-101* produced by Shodex. The column is a *2 Suprema Linear* produced by PSS. Aqueous sodium azide solution (c = 10 mM) was employed as eluent. The system was calibrated for dextran.

4.5.3. Scanning electron microscopy

The membrane morphology is analyzed by scanning electron microscopy. The device used is the *ESEM Quanta 400 FEG* from FEI. The dry samples are quenched in liquid nitrogen and then snapped in half to obtain suitable sample of the cross-section morphology. The membrane samples are sputtered with gold/palladium (80/20) to insure sufficient surface conductivity. Nanoparticle samples were spin coated onto a silica wafer from an aqueous dispersion (c = 1 mg/ml) and no sputtering was applied.

4.5.4. Mechanical characterization

The mechanical properties of the membranes are characterized regarding tensile strength, Young's modulus, and elongation at break. The tests are performed on the material testing instrument (Test Expert® II, Germany) made by Zwick Roell.

Beforehand, the samples are cut in to rectangular pieces with a 2 cm width and 10 cm length. The samples were pre-stressed at 2N with testing speed of 100 mm/min in standard climate at 25 °C and 65 %RH. Five samples of each membrane were tested and the mean value is presented in this work.

4.6. Nanoparticle characterization

4.6.1. Dynamic light scattering measurement

The *Stabisizer PMX 200C* from Particle Metrix is used for the determination of the hydrodynamic particle diameter of the dispersions. For each dispersion three measurements over 90 seconds are conducted. For the calculation, the zinc oxide particles are assumed to be spherical particle with a refractive index of n = 2.03. The viscosity and refractive index data of the solvents used for the method can be found in the appendix (cf. Table 55). The mean peak is calculated over the three measurements from the distribution by number. The standard deviation is chosen to represent the variability over the measurements.

4.6.2. Streaming Potential

The streaming potential titration is performed on the *Stabisizer PMX 200C* from Particle Metrix. The measurement cell is a polytetrafluoroethylene cylinder with a total volume of 20 ml. Within the wall of the cylinder are two metal electrodes built in. A piston, also made of polytetrafluoroethylene, is inserted into the cylinder. There are four different pistons available, which differ in grove depth. The piston 200-0001 was used for all measurements. This determines the grove depth to be 100 µm. The cylinder is filled with 10 ml of aqueous particle dispersion at a concentration of 0.1 %m/V. The measurement set-up is schematically displayed in Figure 14.

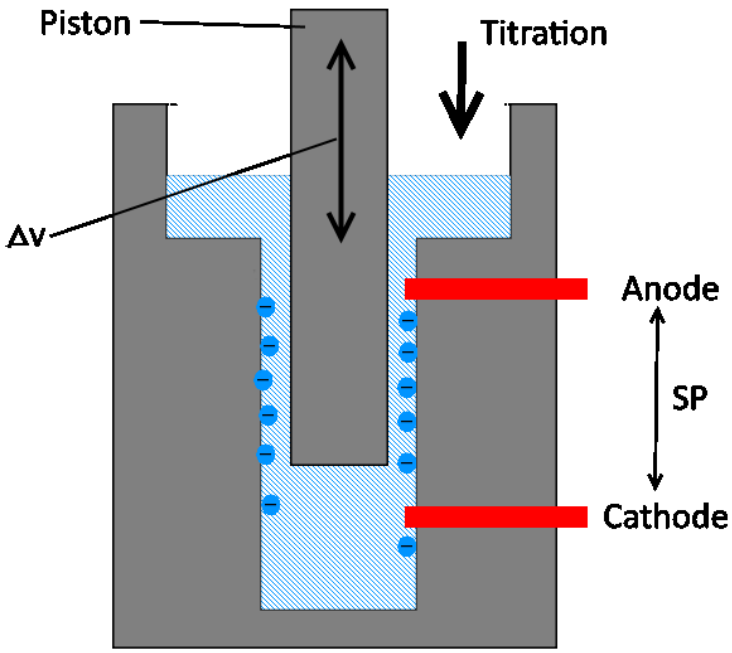

Figure 14 Measurement set-up for the determination of the particle surface potential.

A part of the dispersed particles will absorb to the surface of the measurement cell and the piston, because of the van der Waals interaction. The measurement is started by moving the piston up and down at the speed *Δv*. The movement of the piston forces the fluid to move through the grove of the piston. This current moves the mobile counter ions around the absorbed particles, which remain immobile. This induces a streaming potential between the electrodes. During the measurement, the pH value is recorded by a probe at the top of the cylinder. The device has a build in titration unit. Aqueous potassium hydroxide solution (c = 0.01 Mol/l) is added by the titration unit at a rate of 0.1 ml/min at the top of the measurement cell until the pH reaches a value of 10. The streaming potential is recorded in dependence of the pH value. The streaming potential refers to the average surface potential of all absorbed particles in the cell.

4.6.3. Zeta potential measurement

For the zeta potential characterization, the nanoparticles are dispersed in ultrapure water at a concentration of 0.1 %m/V as described in 4.1. The device used for the measurement is the *Zetasizer Nano ZS* produced by Malvern. The measurement principle is the combination of electrophoresis and laser Doppler velocimetry. An electric field is applied to the sample and the particle velocity is measured. The zeta potential is derived from the velocity change in dependence of the applied field. For each sample 12 runs are performed and the mean value is calculated. For the solvent and particle data the same values are used as in 4.6.1.

4.6.4. Hansen solubility parameter evaluation

As the first step, dispersions of the nanoparticle are prepared in all for the analysis designated dispersants. The conditions are as stated in 4.1 and the mass fraction of particles in the solvent is kept at 0.1 %w/V. The particles size of the dispersion is characterized by DLS (as described in 4.6.1) immediately after preparation and then once each day over the next four days or till the dispersion becomes unstable. Instability is reached when most particles are sedimented. The stability of the dispersion is rated according to the criteria in Table 20. The calculation will be performed with the software HSPiP 4.1 by Prof. S. Abbott and Dr. H. Yamamoto. The parameters of the used solvents are given in Table 56. The calculation will be performed using the standard sphere algorithm without consideration of the molar volume and no limitation on the interaction radius. This algorithm is described in 2.4.2 Determination of Hansen solubility parameters.

4.6.5. Infrared spectroscopy

The infrared spectroscopy of nanoparticles is measured with the *FT-IR Varian 3100 Excalibur* series from Varian Inc. The device uses the attenuated total reflection technique. The spectra are recalculated to standard (KBr) Fourier transformed spectra to correct for the wavelength dependent penetration depth of this method.

4.6.6. Thermogravimetric analysis

The thermogravimetric analysis of the nanoparticles is performed on the *STA449 F3 Jupiter* from NETZSCH. Between 15 and 40 mg of the sample are placed in an alumina crucible. The analysis is performed in the range of 30 to 800 °C. The heating rate was set to 10 K/min and an argon stream of 20 ml/min was present at all stages of the measurement.

4.6.7. Stability of the modification

The following experiment is conducted to evaluate, if the modification of the particle can persist the preparation of the dope solution as described in 4.3.1. For this 0.5 g of the modified particles are dispersed in 30 g NMP under standard conditions. The dispersion is stirred at 60 °C for two days to simulate the step conducted to solve the polymer. The particles are removed from the dispersion by centrifugation and rinsed with ethanol twice. In the next step the particles are dried in a vacuum oven. The dry particles are characterized by TGA. This procedure is also done with pristine particles as reference.

5. Results

5.1. Nanoparticles

5.1.1. Evaluation of sonication conditions

The results of the experiments are presented in this part. These were done to find adequate conditions for the preparation of dispersions in water. The unmodified zinc oxide particles were sonicated in ultrapure water for different lengths of time to find the necessary treatment time to obtain stable dispersions. The times which were evaluated at 1 to 10, 15, 20, 25, 30, 45 and 60 minutes. Also, one sample was just shaken by hand as reference which will be labeled as 0 min dispersion time. The detailed results can be found in the appendix (cf. Table 60). The observations are given in Table 6.

Table 6 Stability of dispersions at different sonication times.

sonication time [min]	observation
0	unstable
1	unstable
2	unstable
3	stable
4	stable
5	stable
6	stable
7	stable
8	stable
9	stable
10	stable
15	stable
20	stable
25	unstable
30	unstable
45	stable
60	unstable

Stability was observed between 3 and 20 minutes of treatment time. Furthermore, the possible influence of the concentration at a treatment time of 20 minutes has been evaluated. For these five dispersions were examined with concentrations ranging from 0.1 to 2 %w/V. The data is presented in Table 7.

Table 7 DLS data for the influence of the concentration.

c [%w/V]	0.1		0.5		1		1.5		2	
time	d_H	SD	d_H	SD	d_H	SD	d_H	SD	d_H	SD
[d]	[nm]	[nm]	[nm]	[nm]	[nm]	[nm]	[nm]	[nm]	[nm]	[nm]
1	97	4	93	15	90	14	105	15	100	12
6	87	10	75	6	101	10	84	8	97	1
7	95	12	92	7	81	11	90	16	83	11

All prepared dispersions were stable over the course of one week. Under these conditions, the concentration has no apparent effect neither on the particle size nor on the stability. It can be concluded that the examined conditions are suitable for the preparation of stable dispersions in water.

5.1.2. Scanning electron microscopy

As a reference for further experiments it was necessary to characterize the size and shape of the pristine particles. The scanning electron microscopy was chosen to obtain pictures of these particles. The sample was prepared by spin coating a stable aqueous particles dispersion on a silicon wafer. The obtained picture is presented in Figure 15.

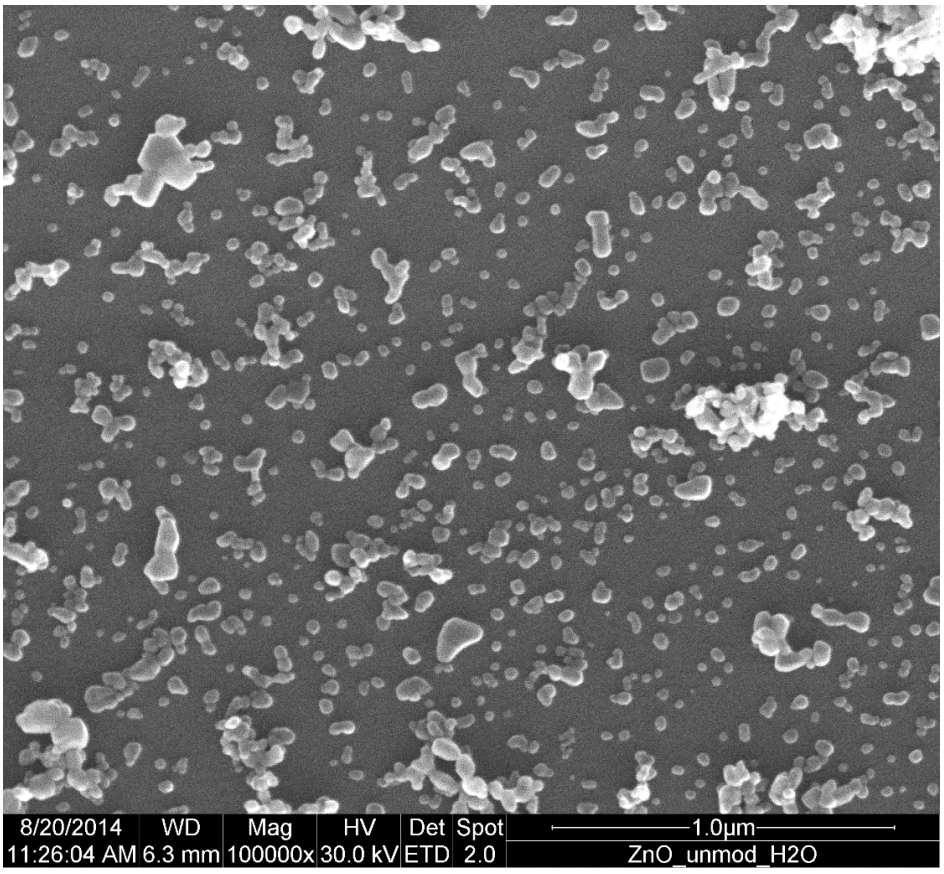

Figure 15 SEM picture of pristine ZnO NP at 100k magnification.

The scanning electron microscope pictures shows a wide size distribution of the particle. This is not uncommon for a commercial product. While most observed particles are smaller than

the 100 nm, some of the bigger particles go up to 300 nm. The shape of the particles is irregular. The size distribution and shape is caused by the production method (cf. 2.3.1).

5.1.3. Estimation of monolayer

It is necessary to know the approximate size of the monolayer, which is formed by the modification agent on the particles surface. Since reliable data was not retrievable in literature, it was necessary to estimate the size of the monolayer and the corresponding mass fraction. For the calculation, the problem was simplified using the following assumptions:

- The modification agent molecules are assumed to be spheres.
- The modification agent will form the hexagonal close packing on the nanoparticle surface.
- The zinc oxide nanoparticles are assumed to be spherical particles with a diameter of 100 nm.

Using the first assumption the radius of the sphere r_m can be calculated from the specific volume V_m of the modification agent molecule. The equation is displayed in E-13.

$$r_m = \sqrt[3]{\frac{3V_m}{4\pi}} \qquad \text{(E-13)}$$

The specific volume V_m is obtained by dividing the molar mass through the density ρ and the Avogadro constant N_A. This is shown in E-14.

$$V_m = \frac{M}{\rho N_A} \qquad \text{(E-14)}$$

The assumption of the hexagonal close packing makes it possible to calculate the surface coverage for a sphere of known radius. A section of the packing is shown in Figure 16.

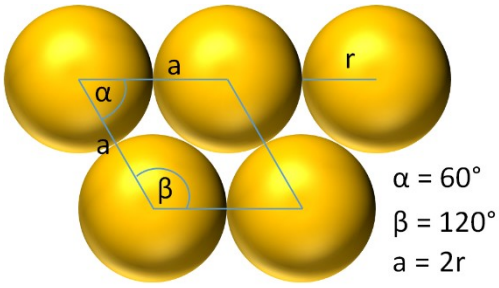

Figure 16 Hexagonal close packing of spheres on a plane surface.

In the figure above, the indicated rhombus contains one sphere with the radius *r*. The edges of the rhombus have a length of two times the radius *r* and the angles inside are 60 ° and 120 °. Therefore, the area of the rhombus is the equal to the area A_m needed for the adsorption of

one molecule. Since this specific rhombus consists of two equilateral triangles with the side length *a*, the area can be calculated by the equation E-15.

$$A_m = 2 * \frac{\sqrt{3}}{4} a^2 = 2\sqrt{3} r^2 \quad \text{(E-15)}$$

Using the last assumption, the surface area of the nanoparticle A_{NP} can be calculated as the surface of a sphere with a radius of 50 nm. The mass of the particle m_{NP} is obtained by calculating the volume of the sphere and multiplying it with the density of ZnO. The data can be found in the appendix (cf. Table 57).

$N_{monolayer}$ is calculated as shown in E-16. This variable referees to the number of molecules which are needed to form a monolayer on the particle with a 100-nm diameter.

$$N_{monolayer} = \frac{A_{NP}}{A_m} \quad \text{(E-16)}$$

The mass of the monolayer $m_{monolayer}$ is obtained by multiplying this number with the molar mass and dividing it by the Avogadro constant. This is presented in E-17.

$$m_{monolayer} = N_{monolayer}\, M_m \quad \text{(E-17)}$$

With this number the mass fraction $w_{monolayer}$ of the monolayer is calculated as shown in equation E-18.

$$w_{monolayer} = \frac{m_{monolayer}}{m_{NP} + m_{monolayer}} * 100\% \quad \text{(E-18)}$$

This calculation is done for all low molecular modification agents examined in this work. The end results are shown in the Table 8. The data and interim results can be found in the appendix (cf. Table 58).

Table 8 Calculated weight fraction for monolayer of low molecular agents.

	TFA	Ox	Ac
$w_{monolayer}$ [%]	15.9	17.1	10.8

For polyvinylpyrrolidone (PVP) the calculation must be adjusted because of the polymeric nature. There are two cases which can be discussed. The first case is that the PVP in solution adsorbs to the nanoparticle in its globular form. In this case the surface coverage can be calculated as above E-14 to E-18 but the solute radius in aqueous solution r_H is used instead of r_M. The radius can be derived from the numeric value equation $r_H = 0.5279\ M^{0.3915}$.[16] The molar mass must be given in [g/mol] to obtain the radius in [Å]. In this work PVP K-30 is used. Therefore, the molar mass of the polymer will be assumed to be 40 kDa for calculation purposes.[52] The calculation can be performed as previously stated with the known solute radius. The second case is the absorption of the polymer chain in a way that every repeating

unit has contact with the surface. This case can be calculated the same way as for the low molecular modification agents by using the values of the monomer. The data and interim results can be found in the appendix (cf. Table 59). The result for both cases is shown in Table 9.

Table 9 Calculated weight fraction of monolayer for PVP.

	repetition unit	polymer
$w_{monolayer}$	13.0 %	36.6 %
mean	24.8 %	

It is not possible to assert which adsorption modus is present in this work. Therefore, it will be assumed that the actual adsorption behavior is in between the two modes and the mean value of $w_{monolayer}$ = 24.8 % is used for all following calculations.

5.1.4. Modification of Nanoparticles

5.1.4.1. Modification with trifluoroacetic acid

In this part of the result, the result of the modification of zinc oxide with trifluoroacetic acid are presented. The first results shown refer to the modification without the control of the pH of the procedure. The mass retrieval for modifications at different ratios of TFA are shown in the Table 10.

Table 10 Mass retrieval at different TFA concentrations.

ratio(TFA/ZnO) [%]	$pH_{calculated}$ [-]	mass retrieval [%]
5	2.3	85.7
15	1.8	75.4
20	1.7	69.5
30	1.6	67.3
75	1.2	54.6
100	1.0	45.1
200	0.7	20.8

In the data presented a constant decline in the retrieved mass is emerging with an increase in TFA. The most likely reason for this is the occurrence of a solvolysis reaction (cf. 2.3.1). Instrument based loses should only have a negligible minor effect. The pH has been calculated for these reactions and the pH decrease correlates with the decrease in mass retrieval. Because of this phenomenon, it was decided to control the pH by adding sodium hydroxide to the modification agent solution before the modification to diminish the solvolysis. The results of these experiments are shown in Table 11.

Table 11 Mass retrieval at different TFA concentrations at controlled pH value.

c(TFA)	pH	mass retrieval
[%w/w(ZnO)]	[-]	[%]
200	6.3	84.2
200	7.0	86.3
200	10.0	86.3
500	7.0	86.1
1000	7.0	86.3

The data shows a stable mass retrieval for all modifications with neutral or alkaline pH value. The mass retrieval is virtually identical for all modifications in the table. This indicates that the solvolysis reaction has been impaired and did not even occur at a higher pH value.

5.1.4.2. Modification with other carboxylic acids

The results of the modification with other carboxylic acids, namely acetic acid, and oxalic acid, are reported in this part. The standard modification procedure as described in 4.2 was used. The data of these modifications are shown in Table 12.

Table 12 Mass retrieval for the modification with other carboxylic acids.

mod. agent	ratio(mod/ZnO)	pH	mass retrieval
	[%]	[-]	[%]
Ac	200	2.5	0.0
Ac	200	5.0	67.1
Ox	200	2.65	189.0

The first dataset in the table indicates that no particles were retrieved in the modification employing acetic acid without pH control. This means that the zinc oxide nanoparticles have been hydrolyzed during the procedure. The pH value was increased to 5 to reduce the loss by solvolysis for the second attempt. This value was chosen for convenience, since the emerging acetate buffer system allows an easy adjustment to this value. The modification with the adjusted pH shows a low mass retrieval, indicating that the solvolysis still occurs. The modification with oxalic acid shows a mass retrieval that is higher than 100 %. This indicates that a higher adsorption occurred than the calculation of the monolayer predicted. The Ox-modified particles segregated before the dispersion was centrifuged. The indication of this phenomenon was uncertain at the time of the experiment.

5.1.4.3. Modification with PVP

In this part the results of the modification of zinc oxide with polyvinylpyrrolidone are presented. There were two different modification procedures performed. The first one is the standard modification as described in 4.2, which will be referred to as *standard*. In the second

one PVP was added to the solvent before the sonication as described in 4.1. The separation, rinsing and washing was done exactly as for the standard modification, but no heated stirring was done. This modification will be referred to as *codispersion*. Because of the volume limitation of the largest available rosette cell, these two modification were not done at the same effective concentration. For the *standard* modification, the total volume was 400 ml, while for the *codispersion* modification only a volume of 200 ml was used. This results in a two times bigger effective concentration during the modification step. In Table 13 the mass retrieval for both modification procedures are shown.

Table 13 Mass retrieval for different PVP modification procedures.

	ratio(PVP/ZnO) [%]	mass retrieval [%]
standard	500	82.3
codispersion	500	79.1

Both procedures have a similar mass retrieval. It can be assumed that the difference is mostly caused by instrument based loses, because in the *codispersion* procedure some particles remained in suspension even after being centrifuged several times. This was not the case for the *standard* procedure.

5.1.5. IR spectroscopy

For all modified nanoparticles, IR spectroscopy was performed to assess the presence of the modification on the surface. In some spectra, a hydroxyl vibration can be seen. It can be assumed that this vibration originates from the hydroxyl groups present on the surface of the zinc oxide as well from the residual water, which can be correlated with the 0.3 % mass loss during the thermogravimetric analysis of the pristine particles (cf. 5.1.6).[53,54] The spectrum of the particles modified with oxalic acid is shown in Figure 17.

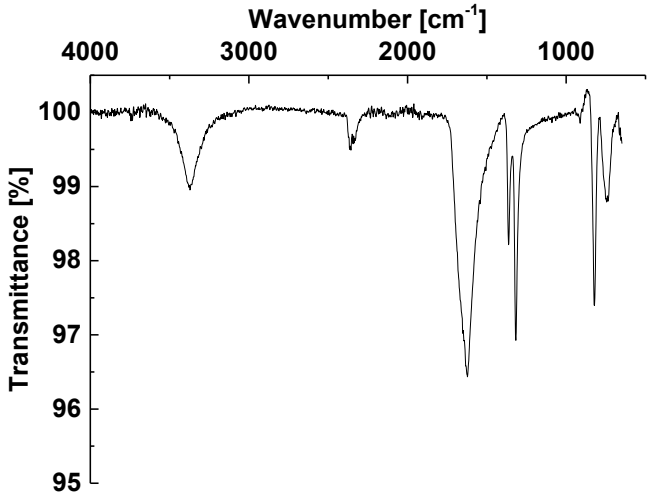

Figure 17 IR spectrum of ZnO NP modified with 200% oxalic acid.

In the spectrum above the following signals can be identified which refer to oxalic acid. The vibration of the carboxyl group can be seen at 3370 cm^{-1} and at 1623 cm^{-1}.[53,55] The vibrations at 1370 and 1314 cm^{-1} are of particular importance. These two vibrations indicate that carboxyl acid have formed dimers.[56] Therefore, it can be concluded that the adsorption of oxalic acid on the particle surface has exceeded the monolayer formation.

In Figure 18 the spectra of the acetic acid modified particles are presented. The spectra of the modified particles and of the particles after the washing as described in 4.6.7 are shown.

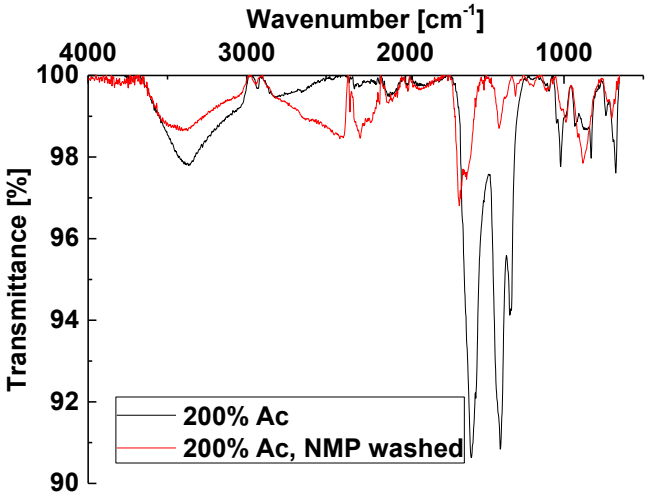

Figure 18 IR spectra of ZnO NP modified with 200% Ac before and after washing with NMP.

In the figure above the following signals can be identified which refer to acetic acid. The vibration of a hydroxyl group can be seen at 3385 cm^{-1}. This signal most likely belongs to residual water, because the peak is too broad for a carboxyl group. The *ν*(O-H) vibration of carboxyl group is not seen. This could indicate that the acetate form is present on the particle

surface. There are two vibrations referring to the carboxylate group *v*(C=O) at 1580 cm^{-1} and *v*(C-O) at 1402 cm^{-1}.[53,57] Both vibrations decrease after the washing with NMP. This might indicate the partial removal of acetate from the surface of the particles. The spectra of three trifluoroacetic acid modified particles are shown in the Figure 19. The first is modified with a ratio of 100 % TFA/ZnO at pH 1. The other two were modified with a ratio of 200 % TFA/ZnO, one at pH 7 and the other one at pH 10.

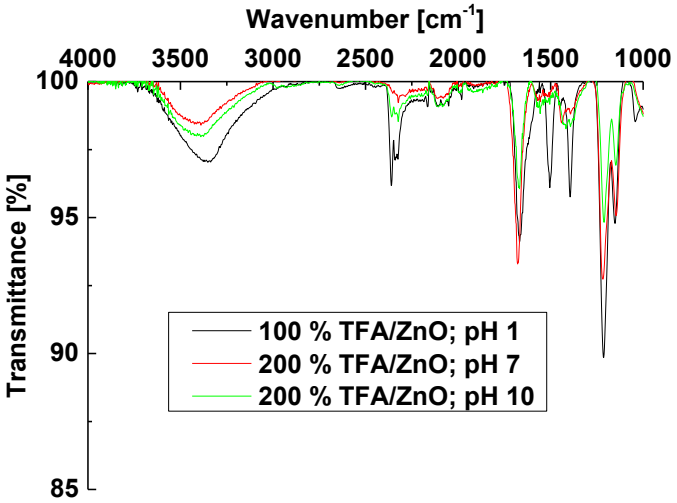

Figure 19 IR spectra of TFA modified ZnO NP with variation of TFA concentration and pH.

In the figure above the following signals can be identified which refer to trifluoroacetic acid. The vibration of a hydroxyl group can be seen at 3400 cm^{-1}. The signal is as broad as in the previous spectrum, which indicates that this vibration is most likely caused by residual water. The vibration of the carbonyl group can be seen at 1670 cm^{-1}. The pure acid exhibits *v*(C=O) at 1780 cm^{-1}. Therefore, we can assume that the carboxylate form is present on the particle surface. In the range of 1211 to 1151 cm^{-1} the vibrations of the carbon-fluorine-bond can be seen.[53,58] Over all three samples the intensity of the absorption is different. The sample with 100 % ratio of TFA/ZnO has the highest intensity, while the other two have a slightly lower absorption. This might indicate that the surface coverage is lowered with an increase of pH during modification. The IR spectra of the polyvinylpyrrolidone modified particles is shown in Figure 20.

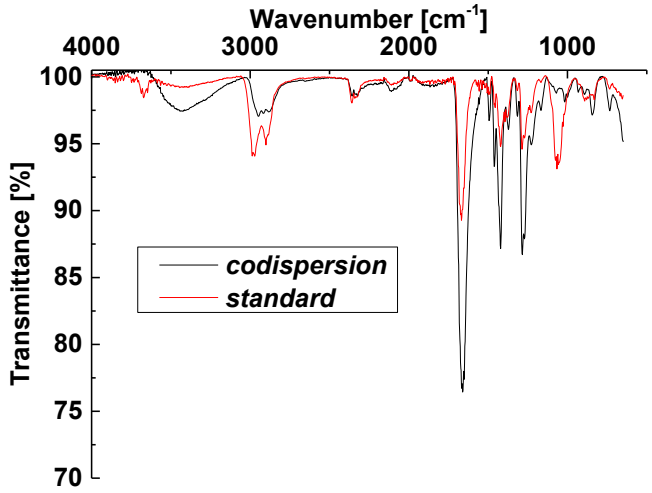

Figure 20 IR Spectra of the PVP modified ZnO NP.

In the figure above, both modification processes exhibit the same signals referring to PVP. The vibration of the carbonyl group can be seen at 1665 cm^{-1} and the signal of the methylene group can be seen at 1419 and 1285 cm^{-1}.[53,59] For the *codispersion* sample the transmittance is smaller which indicates a higher concentration of PVP on the particle. This might be caused by the difference in effective concentration between the two procedures (cf. 5.1.4.3). The *codispersion* sample was washed with NMP according to the procedure specified in 4.6.7. The spectra of the particles before and after the washing are compared in Figure 21.

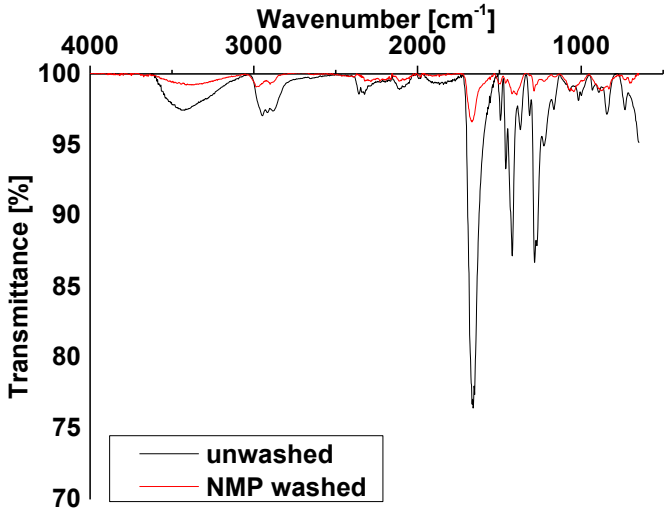

Figure 21 IR spectra of PVP modified ZnO NP before and after NMP washing.

As with the acetic acid modified particle there is a decrease of the signal after washing with NMP. This might indicate the partial removal of PVP from the surface of the particles.

5.1.6. Thermogravimetric analysis

Selected samples were characterized by thermogravimetric analysis. The amount of adsorbed modification agent can be determined from the mass loss in the gravimetric analysis. The pristine particles were measured as reference. In that measurement, a mass loss of 0.30 % was found, which most likely originates from residual water. This mass loss is subtracted from all further measurements to correct for the water content and the remaining mass loss is attributed to the absorbed modification agent. The surface coverage is calculated from the estimated monolayer (cf. 5.1.3). The results for the particles modified with trifluoroacetic acid are shown in Table 14.

Table 14 TGA results for TFA modified samples.

ratio(TFA/ZnO)	pH	residual mass	$w(TFA)_{ads}$	surface coverage
[%]	[-]	[%]	[%]	[%monolayer]
10	2.0	97.88	1.82	11.4
100	1.0	93.72	5.98	37.6
200	0.7	88.83	10.86	68.3
200	6.3	97.17	2.53	15.9
200	7.0	98.69	1.01	6.4
200	10.0	99.31	0.39	2.4
500	7.0	96.55	3.15	19.8
1000	7.0	94.90	4.80	30.2

There are two distinct trends observable in the modification with trifluoroacetic acid. First the influence of concentration and secondly the influence of pH value. By comparing the samples modified at pH 7, it becomes apparent that the surface coverage increases with an increase in TFA concentration. Therefore, the concentration of the modification agent during the procedure increase the adsorption as one would expect. The influence of the pH value can be seen in the samples modified with a ratio of 200 % TFA/ZnO. The surface coverage is drastically decreased by the pH increase pH from 0.7 to 10. The reason for this phenomenon is not clear from this data alone, but a reasonable assumption is that the adsorption mechanism is favored at low pH values. The particles modified with PVP using both procedures were characterized. The results are shown in the Table 15.

Table 15 TGA results for PVP modified samples.

	residual mass	$w(mod)_{ads}$	surface coverage
	[%]	[%]	[%monolayer]
standard	89.3	10.4	42.1
codispersion	81.5	18.2	79.5

The particles modified with the *codispersion* procedure have approximately twice the surface coverage of the particles modified with the *standard* procedure. This correlates with the difference in effective PVP concentration during the modification between the two procedures (cf. 5.1.4.3). Since the amount adsorbed PVP is higher in the *codispersion* sample, this sample is selected for the evaluation of the stability of the modification (cf. Table 17). The results of the particles modified with oxalic and acetic acid are presented in Table 16.

Table 16 TGA results for samples with Ac and Ox modification.

ratio(mod/ZnO)	pH	residual mass	$w(mod)_{ads}$	surface coverage
	[-]	[%]	[%]	[%monolayer]
200% Ac	5.0	97.4	2.3	21.7
200% Ox	2.3	43.6	56.1	327.9

In the samples modified with acetic acid a comparable surface coverage is found as in the TFA samples modified at the same ratio and pH 6.3. This might indicate that the same binding mode is present. In the oxalic acid modified sample, the calculated surface coverage exceeds the calculated monolayer. This correlates with the mass retrieval of the modification, which exceeded 100 % (cf. 5.1.4.2). Both results indicate that a higher adsorption modus than monolayer adsorption is achieved. The results of the particles which have been washed with NMP as described in 4.6.7 are shown in Table 17.

Table 17 TGA results of NMP washed samples.

	residual mass	$w(mod)_{ads}$	surface coverage
	[%]	[%]	[%monolayer]
pristine ZnO	98.6	0.0	0.0
200% Ac modified at pH 5	98.7	-0.1	0.0
500% PVP *codispersion*	92.8	5.8	26.5

The pristine particles have a lower residual mass after being washed in NMP than in the previous measurement. This mass loss most likely originates from residual NMP in the particles. This is a reasonable explanation because NMP has a boiling point of 202 °C and is therefore not easily removed by drying.[60] This mass loss is subtracted from the other samples for the calculation of the absorbed modification agent. The acetic acid modified particles have a similar residual mass as the unmodified particles. This indicates that most or all acetic acid is removed by the NMP under these conditions. Since the binding mechanism should be similar for trifluoroacetic acid, this result should be transferable to the particles modified with trifluoroacetic acid. For the PVP modified sample only a fraction of the modification remained on the particle while 68.1 % of the modification is removed from the particle. The reason for

the better stability might be the larger number of binding sites in the PVP molecule. This results in a greater binding enthalpy per molecule.

5.1.7. Surface potential measurement

The streaming potential of a pristine particle dispersion in water was measured using the titration device in the *Stabisizer PMX 200C*. The titration was always started from the pH value of the dispersion in ultrapure water. First, the titration was done using potassium hydroxide solution. The change of the streaming potential with an increase in pH value is displayed in Figure 22.

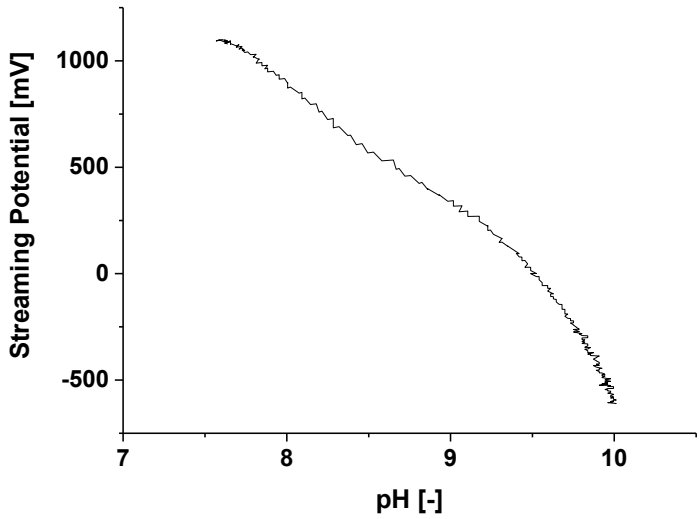

Figure 22 Streaming potential of 0.1%m/V pristine ZnO in aqueous solution depending on pH.

In the figure, it is apparent that the streaming potential decreases with increasing pH value. This behavior indicates that the surface potential of the particle decreases over the course of the measurement. The isoelectric point is encountered at a pH value of 9.5.

For the second measurement, the titration unit was equipped with hydrochloric acid solution to measure the streaming potential at low pH values. During the titration, a solvolysis reaction occurred (cf. R-1), which could be seen in the absence of any change in pH value with the addition of hydrochloric acid solution and the removal of turbidity from the dispersion. The reason for this occurrence is the geometry of the measurement cell, which does not allow instant mixing. The addition of the acid decrease the local pH value at the site of the titration severely without adequate mixing and the solvolysis is facilitated. For this reason, no results were obtained for pH values smaller than 7.

The zeta potential of the particle dispersion in water was measured using the Malvern *Zetasizer*. The values for the trifluoroacetic acid modified samples are shown in Table 18.

Table 18 Zeta potential of TFA modified NP at pH 6.8.

ratio(TFA/ZnO) [%]	pH at modification [-]	mean ZP [mV]	SD [mV]
pristine ZnO	n.a.	38.6	6.0
100	1.0	39.5	5.2
200	6.3	35.0	3.6
200	7.0	34.9	3.9
200	10.0	34.4	3.7
500	7.0	34.8	3.9
1000	7.0	24.3	3.7

The zeta potential for all TFA modified particles is comparable with the zeta potential of the pristine particle. Only the particles modified with a ratio 1000 % TFA/ZnO exhibit a significantly lower zeta potential.

The PVP and acetic acid modified particles were characterized in the same manner. The results of these particles are presented in Table 19.

Table 19 Zeta potential of other modified NP at pH 6.8.

	mean ZP [mV]	SD [mV]
pristine ZnO	38.6	6.0
200% Ac modified at pH 5	37.1	3.7
500% PVP *codispersion*	16.7	2.7

The acetic acid modified particles have a similar zeta potential as the pristine particles. The PVP modified particles have a zeta potential of roughly halve the potential of the pristine particle.

5.1.8. Hansen solubility parameter evaluation

The evaluation of the Hansen solubility parameter is performed to quantify the influence of the modification on the particles affinity. The pristine particles are evaluated as reference. The details of the DLS measurements can be found in the appendix (cf. Table 65 to Table 75) and will not be presented in this chapter. The criteria for the rating of solvents are derived from the results of the dispersions of pristine ZnO nanoparticles (cf. 5.1.1) and the recommendations from the HSPiP software handbook.[25] The criteria are listed in Table 20.

Table 20 Criteria for rating dispersions.

rating	criteria
1	$d_H \leq 120$ nm and stable over at least 3 days
2	$d_H > 120$ nm or size unstable
3	$d_H > 120$ nm and size unstable
4	size steadily increasing
6	unstable

In all experiments water is evaluated as reference, but it is not included into the dataset of the calculation. The reason for this is the recommendation by Hansen to not include water into the calculation of solubility parameters (cf. 2.4.3).[26]

5.1.8.1. Pristine nanoparticles

The pristine particles were dispersed in various solvents and the hydrodynamic diameter of the particles in the dispersion were measured over several days. From this data (cf. Table 65) the dispersibility in these solvents is rated according to the criteria. The results of the assessment are presented in the following table.

Table 21 Rating of solvents for pristine ZnO NP.

No.	solvent	rating
7	Acetone	6
10	ACN	6
52	Benzene	6
93	2-Butanol	2
156	Chloroform	6
181	Cyclohexane	6
285	DMAc	2
297	DMF	1
303	DMSO	6
306	1,4-Dioxane	3
325	Ethanol	1
328	EtAc	2
368	EG	1
417	Hexane	6
456	MeOH	1
481	MEK	4
521	NMP	6
524	DCM	6
617	THF	2
696	Water	1
697	*p*-Xylene	6
862	CCl_4	6

The pristine particles are unstable in nonpolar solvents, halogenated solvents, and solvents with carbonyl groups. There are two exceptions to this trend, DMAc and DMF stabilize the particle despite having carbonyl groups. The good solvents are polar solvents with alcohol and ether groups. The data was entered into the HSPiP program and solvents with a rating of 2 or better were considered to be good solvents for the purpose of the calculation. The sphere algorithm gave the result, which is presented in Figure 23.

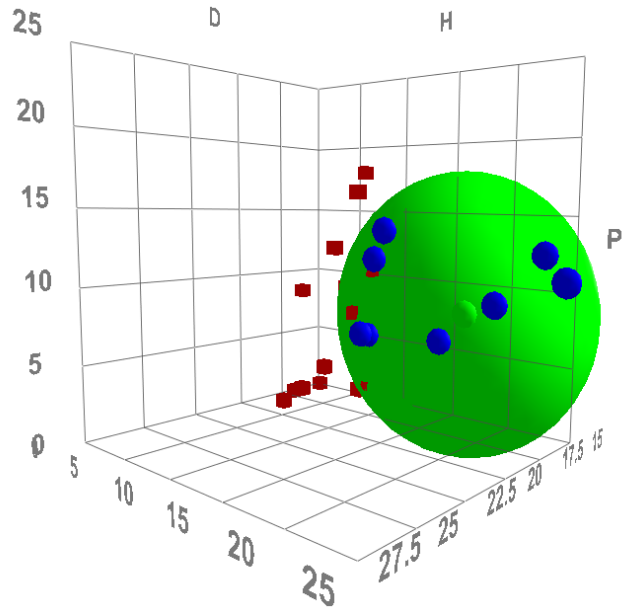

HSPiP summary

In = 8; Out = 13; Total = 21
δ_D = 15.8; δ_P =7.9; δ_H = 16.8
δ_{Tot} = 24.4
R_0 = 10.0
Fit = 1.00
Core = ±[0.65, 1.25, 0.35]
Wrong In = 0
Wrong Out = 0

Figure 23 Solubility sphere calculated for pristine ZnO NP.

The calculated sphere can be considered to be of good quality since the fit is 1 and no solvents have been wrongly assigned. The parameters indicate that the contribution of disperse interaction and hydrogen bonding are both necessary to stabilize the particle in a dispersion, while the polar interaction is of less importance. This correlates well with the observed dispersibility in the examined solvents.

5.1.8.2. Oxalic acid modified particles

The oxalic acid modified particles were dispersed in various solvents and the hydrodynamic radius of the particles was evaluated. These dispersions became unstable within a few hours. The only exception was ethylene glycol. The detailed result can be found in the appendix (cf. Table 66). The results of the rating are shown in Table 22.

Table 22 Rating of solvents for ZnO NP modified with 200% Ox.

No.	solvent	rating
7	Acetone	6
10	ACN	6
93	2-Butanol	6
156	Chloroform	6
183	Cyclohexanone	6
285	DMAc	6
297	DMF	6
303	DMSO	6
306	1,4-Dioxane	6
325	EtOH	6
328	EtAc	6
368	EG	3
417	Hexane	6
456	MeOH	6
481	MEK	6
521	NMP	6
524	DCM	6
617	THF	6
696	Water	6

No calculation is possible from this data set because the algorithm requires at least two good solvents for the calculation. Only in ethylene glycol, some dispersibility is observed. This can be explained by the higher viscosity of this solvent compared to the other solvents used in the experiment. Because of the high viscosity, the particles need longer to agglomerate and sediment. This raises the question how pronounced the effect of the viscosity is in the other calculations and if ethylene glycol should be removed from all the calculations.

5.1.8.3. Acetic acid modified particles

The acetic acid modified particles were dispersed in various solvents and the hydrodynamic diameter of the particles in the dispersion were measured over several days. From this data (cf. Table 67) the dispersibility in these solvents is rated according to the criteria. The rating of the solvents is displayed in Table 23.

Table 23 Rating of solvents for ZnO NP modified with 200% Ac at pH 5.

No.	solvent	rating
7	Acetone	1
10	ACN	1
93	2-Butanol	6
156	Chloroform	6
183	Cyclohexanone	3
285	DMAc	1
297	DMF	6
303	DMSO	6
306	1,4-Dioxane	6
325	EtOH	6
328	EtAc	2
368	EG	1
417	Hexane	6
456	MeOH	1
481	MEK	6
521	NMP	1
524	DCM	6
617	THF	2
696	Water	1
697	*p*-Xylene	6

Many solvents were assigned a similar rating as in the HSP evaluation of the pristine particles (cf. 5.1.8.1). The nonpolar solvents and the halogenated solvents are still bad solvents as one would expect. 1,4-dioxane and MEK exhibit a slightly lower score than in the evaluation of the pristine particles, which is caused by a faster agglomeration. The modification improved the rating for acetone and acetonitrile from 6 to 1. The opposite effect is seen in DMF, ethanol and 2-butanol. The solubility parameters have been calculated from this data set. Solvents with a rating of 3 or better were considered to be good solvents. The result of the calculation is presented in Figure 24.

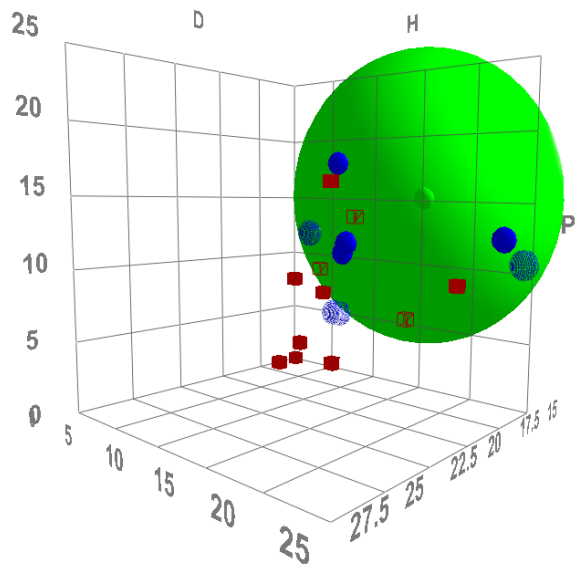

HSPiP summary

In = 8; Out = 11; Total = 19
δ_D = 11.9; δ_P =15.2; δ_H =11.4
δ_{Tot} = 22.4
R_0 = 12.7
Fit = 0.34
Core = ±[0.60, 2.05, 1.00]
Wrong In = 3
Wrong Out = 4

Figure 24 Solubility sphere calculated for ZnO NP modified with 200% Ac at pH 5.

The calculated sphere exhibits a very low fit. This indicates a low quality of the result. The reason for this is the large number of wrongly assigned solvents. These solvents are presented in Table 24.

Table 24 List of wrong in and out solvents from the calculation for ZnO NP with 200% Ac at pH 5.

Wrong in = 3	Wrong Out = 4
DMF	Tetrahydrofuran
MEK	Ethyl Acetate
2-Butanol	NMP
	Ethylene Glycol

DMF, MEK and 2-butanol were rated as bad solvents with a rating of 6. This is an impairment of the rating compared to the evaluation of the pristine particles. The wrong out solvents have a rating of 1 or 2 and except for NMP were all good dispersion media for the pristine particles.

5.1.8.4. Trifluoroacetic acid modified particles

The results of the trifluoroacetic acid modified particles will be presented in the ascending order of the surface coverage seen in the TGA measurements (cf. Table 14). The lowest coverage of 2.4 %monolayer was found in the sample modified with 200 % ratio of TFA/ZnO at a pH value of 10. The evaluation was done as in the previous experiments. The rating of the solvents is shown in Table 25 while the detailed data can be found in the appendix (cf. Table 71).

Table 25 Rating of solvents for ZnO NP modified with 200% TFA at pH value 10.

No.	solvent	rating
7	Acetone	6
10	ACN	6
156	Chloroform	2
183	Cyclohexanone	6
285	DMAc	2
297	DMF	1
306	1,4-Dioxane	2
325	Ethanol	1
328	EtAc	1
417	Hexane	6
456	MeOH	1
481	MEK	4
524	DCM	6
617	THF	1
696	Water	1
697	*p*-Xylene	6

Most solvents obtained the same rating as in the evaluation of the pristine particles. This is not surprising since only a very low degree of modification was achieved. The only exception is chloroform which improved in the rating from 6 to 2. The reason for that is not clear since it seems unlikely that the low amount of modification has an effect. The Hansen solubility parameters are calculated from the dataset. All solvents with a rating of 4 or better were considered to be good solvents for the calculation. The results are shown in the Figure 25.

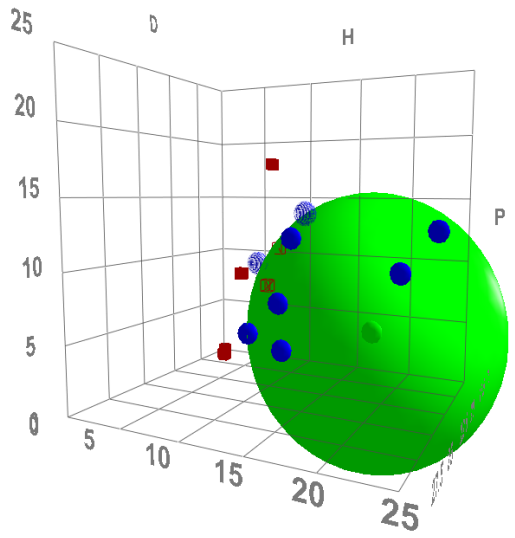

HSPiP summary

In = 9; Out = 6; Total = 15
δ_D = 15.7; δ_P =3.6; δ_H = 16.8
δ_{Tot} = 23.2
R_0 = 11.9
Fit = 0.74
Core = ±[0.90, 0.95, 0.50]
Wrong In = 2
Wrong Out = 2

Figure 25 Solubility sphere calculated for ZnO NP modified with 200% TFA at pH value 10.

The calculated sphere exhibits a fit of 0.744, which is acceptable. The wrongly assigned solvents are close to the edges of the sphere. The obtained parameters for hydrogen bonding and diffusive interaction are nearly identical to the calculated parameter of the pristine particle. The parameter for polar interaction is approximately half the value of the pristine particle. The reason for the difference is probably the lower number of evaluated solvents and not in the difference of ratings. The wrongly assigned solvents are shown in Table 26.

Table 26 List of wrong in and out solvents from calculation for ZnO NP with 200% TFA at pH 10.

Wrong in= 2	Wrong Out= 2
Acetone	DMF
Dichloromethane	MEK

The next higher surface coverage was found in the sample modified with 200 % ratio of TFA/ZnO at a pH value of 7. The surface coverage in this sample is 6.4 %monolayer. The particles were dispersed and the hydrodynamic diameter was measured over time. The detailed data is available in the appendix (cf. Table 70) and the rating is displayed in Table 27.

Table 27 Rating of solvents for ZnO NP modified with 200% TFA at pH value 7.

No.	solvent	rating
7	Acetone	6
10	ACN	6
52	Benzene	6
156	Chloroform	2
183	Cyclohexanone	6
285	DMAc	2
297	DMF	2
303	DMSO	6
306	1,4-Dioxane	2
325	Ethanol	2
328	EtAc	1
368	EG	2
417	Hexane	6
456	MeOH	1
481	MEK	4
521	NMP	6
524	DCM	3
617	THF	1
696	Water	1
697	*p*-Xylene	6

As in the previous sample it can be asserted that most solvents have a similar rating as in the evaluation of the pristine particles. Chloroform has a good rating of 2 as in the evaluation of the previous sample- The rating of dichloromethane was improved to 3. This might indicate that the modification enhances the stability in halogenated solvents. This would match with the expected effect of the modification since it would introduce halogenated groups to the particle surface. The Hansen sphere was calculated from this data. Solvents with rating of 3 or better were considered as good solvents for the calculation. The results are displayed in Figure 26.

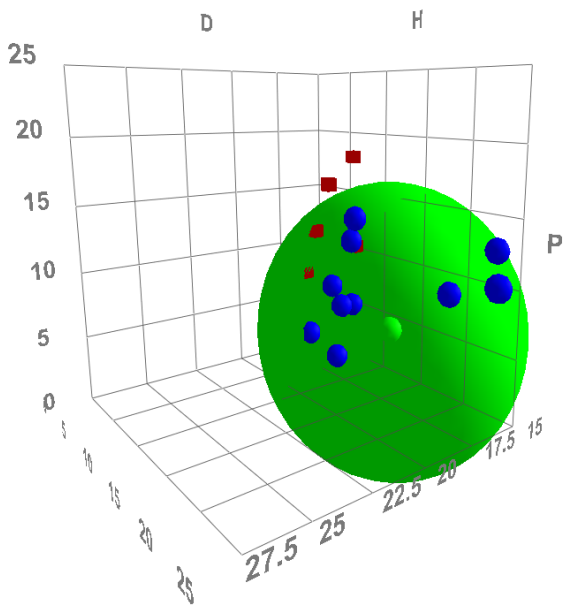

HSPiP summary

In = 10; Out = 9; Total = 19
δ_D = 17.6; δ_P = 6.0; δ_H = 16.3
δ_{Tot} = 24.8
R_0 = 11.0
Fit = 1.00
Core= ±[0.70, 0.70, 0.30]
Wrong In = 0
Wrong Out = 0

Figure 26 Solubility sphere calculated for ZnO NP modified with 200% TFA at pH value 7.

The calculated sphere exhibits an optimal fit of 1. No solvents have been wrongly assigned by the algorithm. When the sphere was calculated considering solvents with a rating of 2 as good solvents, DCM was calculated to be wrong in and several good solvents considered to be wrong out. This indicates that the change in the solvent rating is not an artifact.

The next sample in order of ascending surface coverage are the particles modified with 200 % ratio of TFA/ZnO at a pH value of 6. The surface coverage in this sample is 15.9 %monolayer. The particles were dispersed in several solvents and the DLS measurements were performed over several days as usual. The detailed data can be found in the appendix (cf. Table 69) and the rating of the solvents is presented in Table 28.

Table 28 Rating of solvents for ZnO NP modified with 200% TFA at pH value 6.

No.	solvent	rating
7	Acetone	6
10	ACN	2
93	2-Butanol	6
156	Chloroform	6
183	Cyclohexanone	2
285	DMAc	6
297	DMF	1
303	DMSO	6
306	1,4-Dioxane	2
325	Ethanol	6
328	EtAc	1
368	EG	1
417	Hexane	6
456	MeOH	1
481	MEK	6
521	NMP	6
617	THF	1
696	Water	1
697	*p*-Xylene	6

Again, most solvents have a similar rating as in the previous evaluations. Chloroform is not following the trend from the previous two samples and was not rated as a good dispersion medium for this sample. A rating of 6 was determined. The rating of cyclohexanone and acetonitrile improved to 2. While ethanol and DMAc were down rated to a 6. The Hansen solubility parameters are calculated from the data. All solvents with a rating of 2 or better were considered to be good solvents. The results are shown in Figure 27.

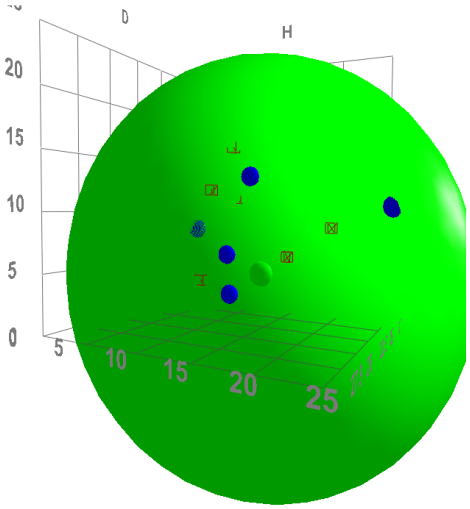

HSPiP summary

Possible δD bad fit
In = 8; Out = 10; Total = 18
δ_D = 23.33; δ_P =5.54; δ_H = 17.29
δ_{Tot} = 29.56
R_0 = 16.4
Fit = 0.212
Core= ±[0.25, 0.80, 0.60]
Wrong In = 6
Wrong Out = 4

Figure 27 Solubility sphere calculated for ZnO NP modified with 200% TFA at pH value 6.

The calculation of the sphere was problematic. It was not possible to obtain a sphere with a good fit. Several solvents are wrongly assigned by the algorithm as shown in Table 29.

Table 29 List of wrong in and out solvents from calculation for ZnO NP with 200% TFA at pH value 6.

Wrong in = 6	Wrong Out = 4
2-Butanol	Acetonitrile
Chloroform	Cyclohexanone
DMAc	Ethyl Acetate
DMSO	Methanol
Ethanol	
NMP	

Also, the calculated interaction radius *R* is with a radius of 16.4 higher than in all previous calculation. The software rated the calculation as possible bad fit for δ_D the parameter of the dispersive interaction because of the number of bad solvents inside the sphere.

The next highest surface coverage was found in the sample modified with a 500 % ratio of TFA/ZnO at a pH value of 7. The material was dispersed in several solvents and the hydrodynamic diameter is measured over several days. The detailed data can be found in the appendix (cf. Table 72) and the solvent rating is presented in Table 30.

Table 30 Rating of solvents for ZnO NP modified with 500% TFA at pH value 7.

No.	solvent	rating
7	Acetone	6
10	ACN	6
52	Benzene	6
93	2-Butanol	6
156	Chloroform	3
183	Cyclohexanone	3
285	DMAc	6
297	DMF	6
303	DMSO	6
306	1,4-Dioxane	3
325	Ethanol	6
417	Hexane	6
456	MeOH	1
481	MEK	6
521	NMP	6
524	DCM	3
617	THF	1
696	Water	1
697	*p*-Xylene	6
862	CCl4	6

Many solvents obtain a similar rating as in the evaluation of the pristine particles and the previous discussed TFA modification. But there are also some differences. In this samples evaluation chloroform is again a stable solvent as well as dichloromethane. This indicates that halogenated solvents can stabilize the sample. Acetonitrile was again evaluated to be a bad solvent. As in the previous sample, ethanol and 2-butanol are evaluated to be bad solvents, indicating an intolerance for alcohols with alkyl chains longer than methyl. In this evaluation DMF was rated to be bad solvent as well as DMAc. Therefore, all solvents with carbonyl groups are rated as bad solvents except for cyclohexanone. The Hansen sphere was calculated from this data set. Solvents with a rating of 3 were treated as good solvents. The results of the calculation are shown in Figure 28.

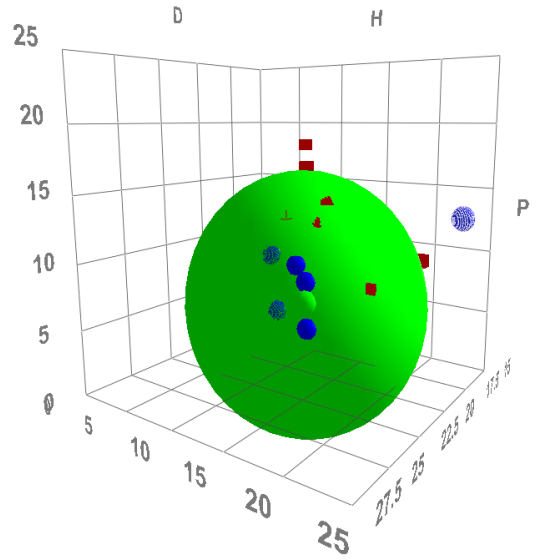

HSPiP summary

Possible δD bad fit
In = 6; Out = 13; Total = 19
δ_D = 20.9; δ_P =6.4; δ_H =13.2
δ_{Tot} = 25.5
R_0 = 10.2
Fit = 0.51
Core= ±[0.20, 0.45, 0.55]
Wrong In = 1
Wrong Out = 3

Figure 28 Solubility sphere calculated for ZnO NP modified with 500% TFA at pH value 7.

The fit of the calculated sphere exhibits a value of 0.51 which is far from optimal. But this was the best achievable result from the dataset. Only THF and MeOH had a rating of 1 and no solvent had a rating of 2. If only these solvents would have been considered good solvents for the calculation, neither of these solvents were found in the calculated sphere but several bad solvents were found inside. Since no solvent was rated as 4, the only sensible inside solvent rating was 3. The result was rated by the software to have a possible bad fit for δ_D, which is caused by the number of wrong in and out solvents. These solvents are presented in Table 31.

Table 31 List of wrong in and out solvents from calculation for ZnO NP with 500% TFA at pH value 7.

Wrong in = 1	Wrong Out = 3
NMP	Chloroform
	Cyclohexanone
	Methanol

The calculated solubility parameters for the hydrogen bonding and polar interaction are slightly lower in the calculation than for the pristine particles. The parameter of the disperse interaction is higher than in the pristine sample but that is most likely caused by the quality of the calculation.

The second highest surface coverage is found in the sample modified with a ratio of 1000 % TFA/ZnO at pH value 7. The evaluation was conducted in the same way as in the previous samples. The detailed results can be found in the appendix (cf. Table 73). The rating of the solvents is shown in Table 32.

Table 32 Rating of solvents for ZnO NP modified with 1000% TFA at pH value 7.

No.	solvent	rating
7	Acetone	6
10	ACN	6
52	Benzene	6
93	2-Butanol	6
156	Chloroform	3
183	Cyclohexanone	3
285	DMAc	6
297	DMF	2
303	DMSO	6
306	1,4-Dioxane	2
325	Ethanol	6
456	MeOH	1
481	MEK	6
521	NMP	6
524	DCM	4
617	THF	1
696	Water	1
697	*p*-Xylene	6
862	CCl_4	6

The solvents acquired the same rating as in the previous sample except for DMAc which exhibits a rating of 2 instead of 6. This indicate overall the same affinities and incompatibilities for the modified particle. The Hansen sphere was calculated from this data set. Solvents with a rating of 2 were treated as good solvents. The results of the calculation are shown in Figure 29.

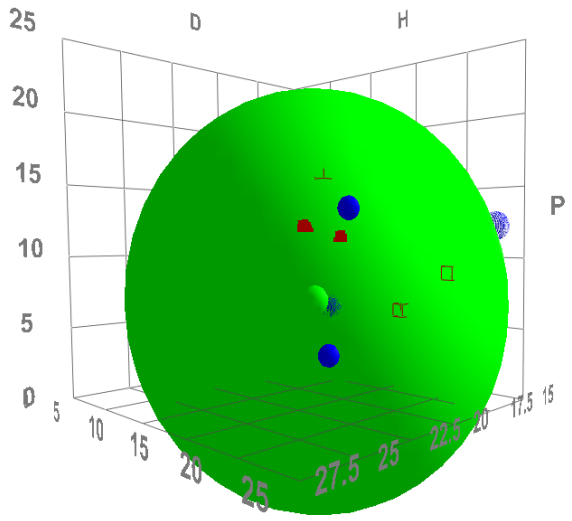

HSPiP summary

Possible δ_D bad fit
In = 4; Out = 14; Total = 18
δ_D = 22.2; δ_P =7.4; δ_H =16.3
δ_{Tot} = 28.5
R_0 = 13.3
Fit = 0.62
Core = ±[0.15, 0.85, 0.60]
Wrong In = 1
Wrong Out = 2

Figure 29 Solubility sphere as calculated for ZnO NP modified with 1000% TFA at pH value 7.

The result for this sample is similar to the result of the particles modified with a ratio of 500 % TFA/ZnO at pH value of 7. This is not surprising since the data set is nearly identical. The wrong in and out solvents vary as can be seen from Table 33.

Table 33 List of wrong in and out solvents from calculation for ZnO NP with 1000% TFA at pH value 7.

Wrong In = 1	Wrong Out = 2
2-Butanol	Methanol
	Tetrahydrofuran

The fit has a value of 0.619 which is acceptable. The same conclusion can be applied as in the previous evaluation, that the change in solvent parameter is insignificant when the quality of the fit is considered.

The highest surface coverage of 37.6 %monolayer was found in the sample modified at a TFA/ZnO ratio of 100 % at a pH value of 1. The preparation of the dispersion and measurements were performed as indicated in the method part. The rating of the solvents is shown in Table 34 while the detailed data is included in the appendix (cf. Table 68).

Table 34 Rating of solvents for ZnO NP modified with 100% TFA.

No.	solvent	rating
7	Acetone	6
10	ACN	6
52	Benzene	6
93	2-Butanol	1
156	Chloroform	6
183	Cyclohexanone	4
285	DMAc	1
297	DMF	1
303	DMSO	6
306	1,4-Dioxane	4
325	Ethanol	3
328	EtAc	1
368	EG	1
417	Hexane	6
456	MeOH	1
481	MEK	6
521	NMP	6
524	DCM	6
617	THF	1
696	Water	1
697	*p*-Xylene	6
862	CCl_4	6

The solvents exhibit similar ratings as in the evaluation of the pristine particles. Only minor differences were found. MEK was rated a 6 instead of 4 and a few other solvents went up or down one rating. The calculation of the solubility parameter was conducted with solvent rated 3 and better considered to be good solvents. The result of the calculation is presented in Figure 30

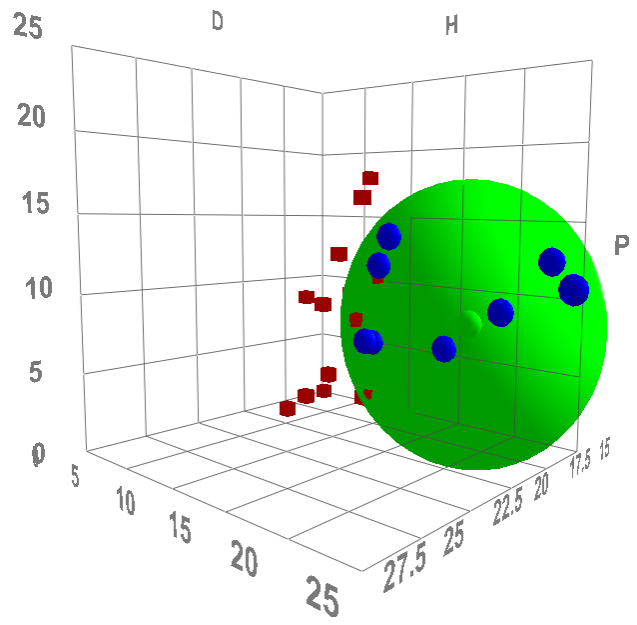

HSPiP summary

In = 8; Out = 13; Total = 21
δ_D = 15.9; δ_P =7.8; δ_H =16.9
δ_{Tot} = 24.4
R_0 = 10.0
Fit = 1.000
Core = ±[0.65, 1.25, 0.35]
Wrong In = 0
Wrong Out = 0

Figure 30 Solubility sphere calculated for 100% TFA modified ZnO NP.

The calculation yields a result which is virtually identical to the result of the pristine particle (cf. Figure 23). This is not surprising since the underlying data is nearly identical.

5.1.8.5. Polyvinylpyrrolidone modified particles

The particles modified with both procedures were dispersed in various solvents and the hydrodynamic diameter of the particles in dispersion were measured over several days.

For the particles from the *standard* procedure the solvent rating is presented Table 35. The hydrodynamic diameter of the evaluation can be found in the appendix (cf. Table 74).

Table 35 Rating of solvents for PVP modified NP from standard procedure.

No.	solvent	rating
7	Acetone	6
10	ACN	2
93	2-Butanol	1
156	Chloroform	3
183	Cyclohexanone	6
285	DMAc	1
297	DMF	1
303	DMSO	6
306	1,4-Dioxane	6
325	Ethanol	2
328	EtAc	6
368	EG	1
417	Hexane	6
456	MeOH	1
481	MEK	1
521	NMP	1
524	DCM	3
617	THF	2
696	Water	1
697	*p*-Xylene	6

The nonpolar solvents have the same low rating as for the pristine particles. The halogenated solvents chloroform and DCM were improved to a rating of 3. This is not surprising since PVP is well compatible to these solvents. The alcohols are still good solvents although ethanol is rated lower. The solvents with carbonyl group exhibit the same rating as before except for NMP, which is improved to 1. From this data set the solubility parameters have been calculated. Solvents with a rating of 3 or better were considered to be good solvents for the calculation. The results are shown in Figure 31.

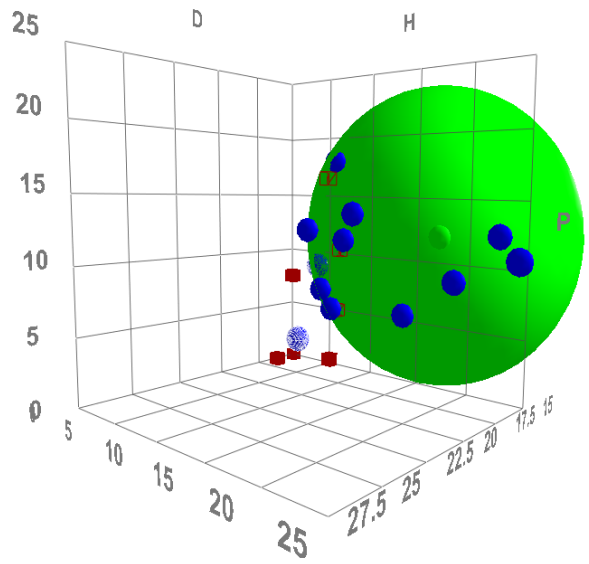

HSPiP summary

In = 12; Out = 7; Total = 19
δ_D = 14.0; δ_P=11.9; δ_H=16.0
δ_{Tot} = 24.4
R_0 = 11.9
Fit = 0.49
Core = ±[0.20, 0.80, 0.30]
Wrong In = 3
Wrong Out = 2

Figure 31 Solubility sphere calculated for ZnO NP modified with 500% PVP by standard procedure.

The calculated sphere has a fit of approx. 0.5, which indicates a not particularly good result. The reason for this are the solvents which end up in the wrong side of the spheres. These solvents are listed in Table 36.

Table 36 Wrong in and wrong our solvents for PVP modified NP by standard procedure.

Wrong in = 3	Wrong Out = 2
Acetone	Chloroform
DMSO	MEK
Ethyl Acetate	

No stability was found for acetone, DMSO and ethyl acetate. They don't conform to the calculated spheres since their solubility parameter are close to good solvents. MEK and chloroform are in the same situation but on the other side of the calculated sphere.

The particles modified with the *codispersion* procedure were dispersed and characterized by dynamic light scattering over several days. The solvents were rated based on these measurements. The solvent rating for the particles is presented in Table 37. The details of the hydrodynamic radii can be found in the appendix (cf. Table 75).

Table 37 Rating of solvents for PVP modified NP by codispersion.

No.	solvent	rating
7	Acetone	6
10	ACN	6
93	2-Butanol	2
156	Chloroform	3
183	Cyclohexanone	6
285	DMAc	2
297	DMF	2
303	DMSO	2
306	1.4-Dioxane	6
325	Ethanol	4
328	EtAc	6
368	EG	1
417	Hexane	6
456	MeOH	2
481	MEK	6
521	NMP	1
524	DCM	3
617	THF	6
696	Water	1
697	*p*-Xylene	6

The rating of the solvents indicated a large compatibility with various solvents. NMP, chloroform and DCM exhibit a good rating as with the other PVP modified sample. THF, MEK and ethanol gained a better rating than in the previous evaluation. Acetonitrile is rated as 2 in contrast to previous rating of 6. The solubility parameters were calculated from the data. For the calculation solvents with a rating of 2 or better were regarded as good solvents. The results are presented in Figure 32.

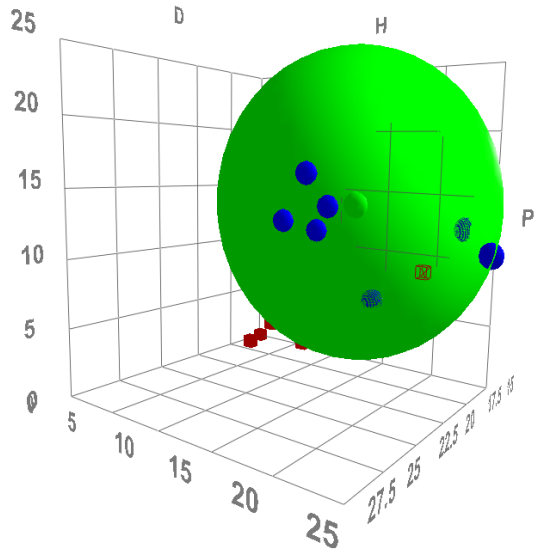

HSPiP summary

Possible δD bad fit
In = 7; Out = 12; Total = 19
δ_D = 19.4; δ_P =14.3; δ_H = 16.4
δ_{Tot} = 29.2
R_0 = 11.3
Fit = 0.83
Core = ±[0.65, 1.30, 0.95]
Wrong In = 1
Wrong Out = 2

Figure 32 Solubility sphere calculated for ZnO NP modified with 500% PVP by codispersion.

The calculated sphere exhibits a good fit with a value of 0.83. Despite the satisfactory fit the result was rated to be a possible bad fit for the parameter δ_D by the software. The reason for that is that the parameter δ_D is above 19 and only few solvents were tested with a parameter that exceeds this value. Therefore, the edge of the sphere on that axis is not properly confined by a bad solvent and some uncertainty remains. This does not necessitate a bad fit, but indicated the possibility of a bad fit.[25] This will be further debated in the discussion part (cf. 6.1.5). The wrong in and out solvents are presented in Table 38.

Table 38 Wrong in and wrong our solvents for PVP modified NP by codispersion

Wrong in = 1	Wrong Out = 2
Ethanol	2-Butanol
	Methanol

5.2. Membranes

5.2.1. Evaluation of casting conditions

The relative humidity in the ambient air during the casting process is the major environmental influence on the production of many polymeric membranes. Therefore, it is desirable to keep the humidity at a constant low value during the membrane preparation. A climate box was constructed by a former PhD student in the workgroup to control the humidity during the casting. The casting set-up within in the climate box is displayed in Figure 33.

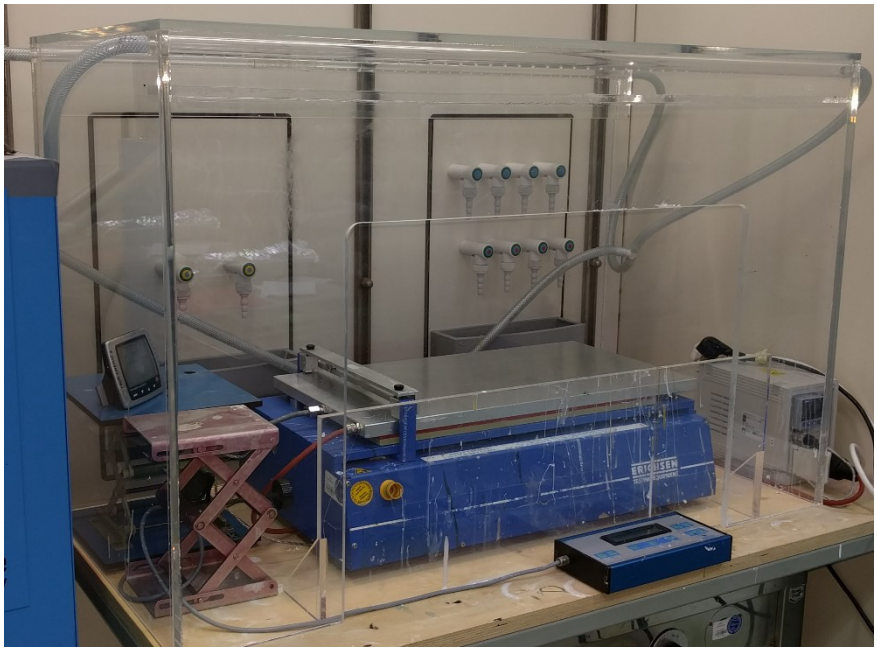

Figure 33 Climate box with casting devices inside.

This box is purged with compressed air from the in-house compressor system. This air has a lower humidity than the ambient air and therefore the relative humidity decreases in the box. A beneficial side effect is that the purging removes dust from the air in the box. This decreases the chance of the formation of defects in the membrane caused by dust particles.[2]

The reliability of the climate box to effectively reduce the humidity is expected to have vital influence on the membrane preparation as stated earlier. For that reason, the efficiency of the dry air purge is evaluated to find suitable conditions for the membrane preparation. The evaluation is performed by measuring the relative humidity in the climate box without the purge. Then the dry air purge is activated and the relative humidity is measured every minute for 15 minutes. The purge is then deactivated and a wait of 30 minutes was allowed till the relative humidity returned to the initial value. The measurement is repeated twice and the mean values are calculated. The ambient conditions during the measurements were

measured. The temperature exhibited a value of 19.2 °C and the relative humidity measured at 46.8 %RH. The result is presented in Figure 34.

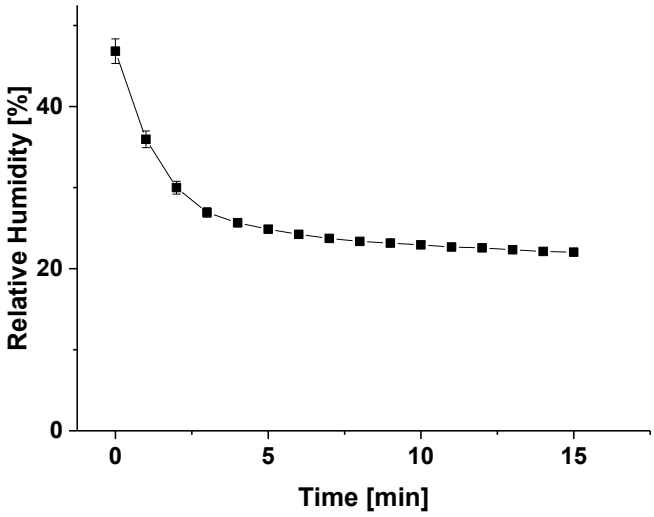

Figure 34 Mean relative humidity (n= 3) in casting box with dry air purge.

The standard deviation of the measurements is so small that the error bars are hardly seen around the data points. It is also important to note that the temperature in the climate box remained constant during the measurements. Hence the change in relative humidity is caused by the change in partial pressure of water and not of the equilibrium vapor pressure. The figure clearly shows that the dry air purge decreases the relative humidity efficiently and keeps it at a stable, low value after approximately 10 minutes. It was decided to implement a 30-minute-long purge before starting the membrane preparation to eliminate any variation of the conditions.

As a next step, the effect of the ambient humidity on the dope film before the coagulation was evaluated. Dope solution films are prepared at a thickness of 200 µm with and without dry air purge. The dope consists of 16 % PVDF and 1 % PVP K-30 in NMP. The weight of the films is measured every five minutes over 85 minutes. The experiment is repeated once for each condition and the mean weight change is calculated. The ambient temperature was 19.0 °C during the experiment. The relative humidity exhibited a value of 36.5 %RH without dry air purge and 20.7 %RH with activated purge. The mean weight change is presented in Figure 35; the error bars indicate the standard deviation.

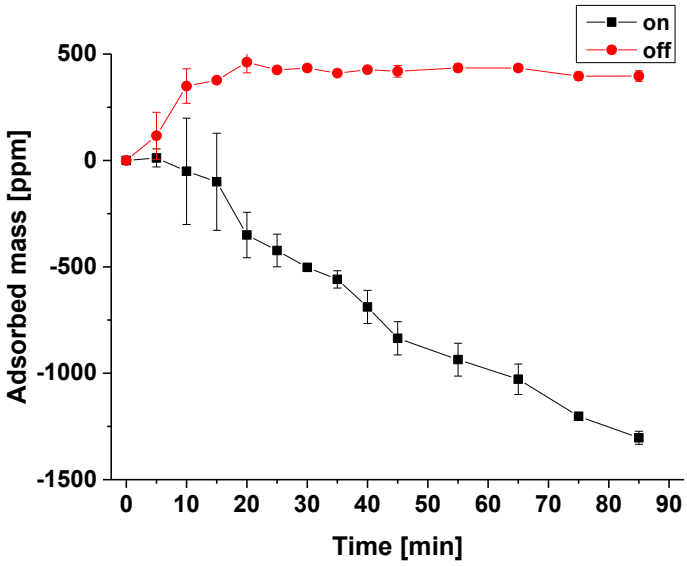

Figure 35 Mass changes of dope films (16 % PVDF and 1 % PVP in NMP) in the activated and deactivated dry air purge(n=2).

The observation of the experiment is that without humidity control the dope film exhibits an increase in mass over the first twenty minutes which ceases after approximately 20 minutes. At this time the film had not shown any signs of precipitation. While the sample with active dry air purge has a stable mass over the first five-minute interval and a steady mass decrease afterwards.

5.2.2. Development of base membrane

The first aim of the membrane development is to find a suitable dope solution formulation for the membrane preparation. As stated in chapter 3.2, the prepared membrane should meet the following performance criteria:

- Pure water permeability of ≥1000 l/h m²
- BSA rejection of ≥ 90 %
- Molecular weight cut-off ≤ 100 kDa for Dextran

As base polymer polyvinylidene difluoride (PVDF) from Solvay *Solef 6010* was selected. This polymer is only compatible with a limited number of solvents. Accordingly, NMP was chosen since it is a well-established solvent for PVDF. As hydrophilic additive polyvinylpyrrolidone (PVP) was selected. The brand *Luvitec K-30* from BASF was selected because it is a commonly employed for this purpose. The composition of the dope was varied and membranes were prepared as described in the method part (cf. 4.3). The membranes were characterized by dead end filtration of BSA and dextran solution (cf. 4.4.1). The composition of 16 % PVDF and 1 % PVP produced membranes which suited the performance requirement the most of all

examined compositions. The mean values and standard deviation of the characterization results are shown in Table 39.

Table 39 Performance of base membrane.

	16% PVDF. 1% PVP	SD
water permeability P_1 [l/ h m² bar]	476 (n = 30)	87
BSA rejection [%]	87 (n = 17)	8
MWCO(Dextran) [kDa]	107.4 (n = 3)	3.4
initial water permeability P_0 [l/ h m² bar]	1134 (n = 30)	430

The rejection data in the table fits the goal performance very well. The BSA rejection of 87 ± 8 % corresponds well with the aim of 90 %. The standard deviation of 8 % is acceptable, since the filtrations were conducted with the *Amicon 8050* cell which only has an effective membrane area of 13.4 cm². Therefore, the variation of the pore size over the membrane area emerges in the standard deviation of the result. The MWCO of 107 kDa with a standard deviation of 3 kDa is acceptable for the aim of 100 kDa. The initial water permeability has a value of 1134 ± 430 l/h m² bar. This exceeds the goal value of 1000 l/h m² bar. The permeability after compaction is just over 40 % of the initial value. This indicates an asymmetric structure with finger-like voids, which cause the membrane to be compressed during the compaction procedure. The high standard deviation of the permeability data is caused by the variation of the pore density over the membrane area. SEM pictures of the membrane were taken. A picture of the selective surface and the cross-section morphology are presented in Figure 36.

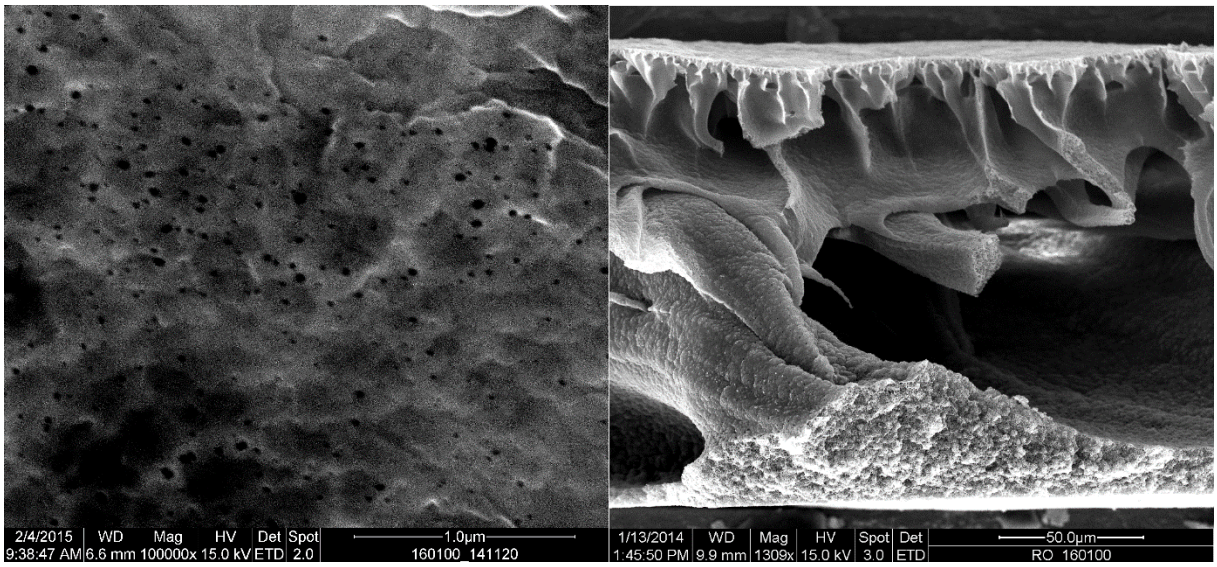

Figure 36 SEM picture of base membrane (16% PVDF, 1 % PVP K-30).

Left: top surface at 100kx magnification; right: cross-section at 1309x magnification.

The top surface shows a high porosity with some pore size distribution. This correlates with the previous seen deviation in permeability and rejection. The structure of the surface is uneven. The cross-section morphology exhibits an asymmetric structure with large macro-voids. This correlates with the previously seen decrease of permeability during compaction. The high porosity and uneven surface are typical for PVDF precipitated from NMP.[18] Since the reproducibility was good and the performance satisfactory, this dope solution composition was selected for the integration of nanoparticles by blend modification.

From the variation of the dope solution composition another composition was found to be interesting. Based on the previously discussed composition the PVDF concentration is increased by one and a half percent to 17.5 % PVDF while keeping the PVP concentration at 1 %. The evaluation of the performance is done likewise as for the precious composition. The results of the evaluation are shown in Table 40.

Table 40 Performance of base membrane for up-scaling.

	17.5% PVDF. 1% PVP	**SD**
water permeability P_1 [l/ h m² bar]	489 (n = 9)	150
BSA rejection [%]	n.d.	n.a.
MWCO(Dextran) [kDa]	80.4 (n = 1)	n.a.
initial water permeability P_0 [l/ h m² bar]	912 (n = 9)	200

The performance of the membrane is very similar to the previous evaluated performance. The pure water permeability before and after compaction is comparable considering the standard deviation. The rejection was improved as indicated by the decrease of the MWCO was 80 kDa. Overall this constitutes a performance improvement over the previous membrane formulation. The morphology of the membrane was examined by SEM. The pictures of the selective surface and cross-section are shown in Figure 37.

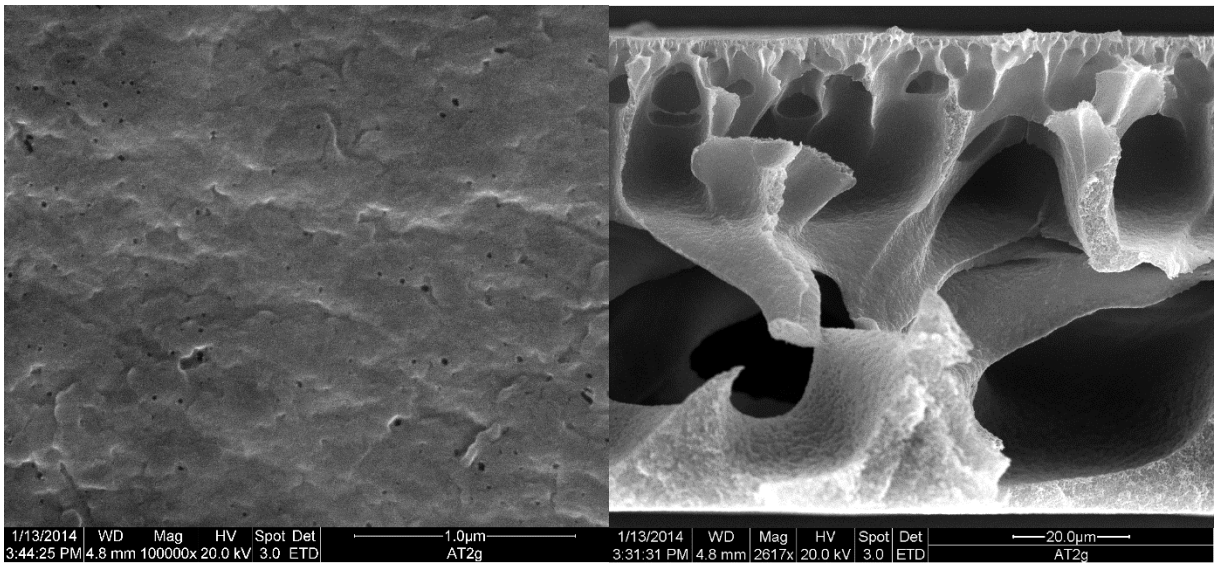

Figure 37 SEM picture of base membrane for up-scaling (17.5% PVDF, 1% PVP K-30).

Left: top surface at 100kx magnification; right: cross-section at 2617x magnification.

The cross-section morphology of the membrane is very similar to the previous membrane. The large macro-voids again explain the large loss of permeability during the compaction. The top surface is smoother than before and shows a lower pore density. This is caused by the higher polymer concentration during the phase separation. Since the performance was slightly better than the previous composition, the dope composition of 17.5 % PVDF and 1 % PVP K-30 in NMP was chosen as base composition for the up-scaling experiments.

5.2.3. Transfer to up-scale-able system

In the previous part, the dope solution formulation of 17.5 % PVDF and 1 % PVP K-30 in NMP was selected as basis for the up-scaling of the membrane into pilot scale. The first necessity for the transfer to pilot scale is the successful preparation of the membrane on a nonwoven support. The industry partner supplied the nonwoven *NOVATEXX 2483* produced by Freudenberg Filtration Technologies SE & Co. KG. In the first preparations, the casting knife gap was kept at 200 µm as in the previous experiments. These membranes showed a very uneven surface with some spots where the nonwoven extended through the membrane surface. The casting thickness was increased to 400 µm to overcome that problem. The membranes prepared in this manner had a sufficient surface quality. Thickness measurement were conducted of the nonwoven, the membrane and a reference membrane prepared on a glass substrate. The results are shown in Table 41.

Table 41 Thickness of membranes (17.5% PVDF, 1% PVP K-30 in NMP) on different substrates.

	membrane thickness [mm]		
	mean	SD	n
nonwoven	0.0773	0.0029	5
membrane prep. on glass	0.3036	0.0156	5
membrane prep. on nonwoven	0.2962	0.0050	5

The reference membrane prepared on the glass support and the membrane prepared on the nonwoven have virtually the same thickness of approx. 300 µm. The nonwoven itself has a thickness of 77 ± 3 µm. Under the assumption that overall porosity is not changed by the support type it can be asserted from the constant membrane thickness that the dope solutions penetrates the nonwoven. The industry partner informed us at this point that this is unwanted and suggested to increase the dope viscosity to 8 Pas or more to eradicate the issue. The polymeric additive was exchanged to *Luvitec PVP K-90* to achieve the desired viscosity. This polymer has an approx. ten times higher molar mass than PVP K-30. Both types of PVP have a comparable effect on the demixing process when the same mass fraction is employed.[52] The substitution increased the viscosity but the desired value was not reached. Therefore, the mass fraction of the additive was increased to 2 % which generated an acceptable shear viscosity in the dope solution. The measured viscosities are shown in the Figure 38.

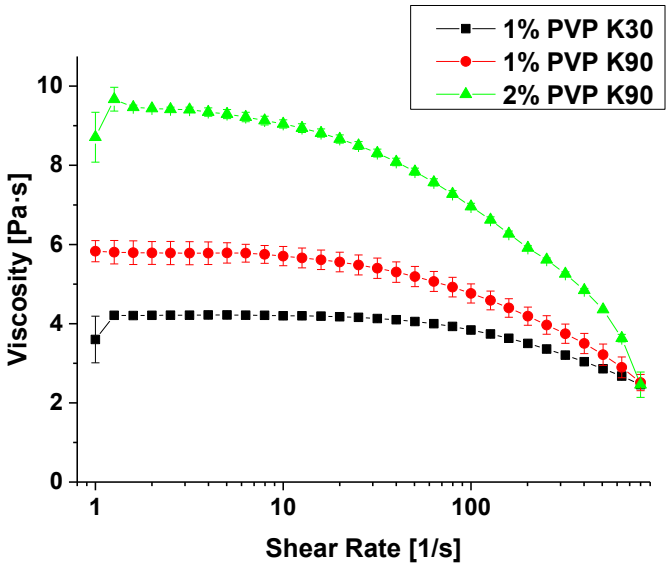

Figure 38 Influence of the PVP type on concentration on the shear viscosity of a dope with 17.5 % PVDF in NMP.

In the figure, it can be seen that the viscosity increases with the substitution of PVP K-30 for PVP K-90. When the viscosity is compared at a shear rate of 15.9 s^{-1} the initial value is 4.19 ± 0.02 Pa s which increased to 5.61 ± 0.25 Pa s after the substitution. The increase of the PVP mass fraction then increased the dope viscosity to 8.82 ± 0.11 Pa s. It can also be noted that an amplification of the shear thinning behavior occurs as consequence of the change in

dope solution composition. Membranes are prepared from the original dope solution and the dope solution with 2 % PVP K-90 on both types of substrate. The membranes are characterized by dead-end filtration of PEG 35 kDa. The results are presented in Table 42.

Table 42 Transfer from glass substrate to nonwoven, influence on membrane performance.

		permeability [L/h m² bar]				rejection [%]		n
PVP type and concentration	**substrate**	**P_0**	**SD**	**P_1**	**SD**	**PEG 35kDa**	**SD**	
1 % PVP K-30	**glass**	1371	147	930	80	53	6	8
	nonwoven	4863	866	2087	659	54	1	7
2 % PVP K-90	**glass**	1028	57	929	126	76	12	4
	nonwoven	2426	694	1244	402	85	3	5

From the data in the table three effects can be asserted. First, the membrane prepared from the original dope solution has a higher permeability after compaction J_1 when casted at a thickness of 400 µm compared to the results in the previous part. The second effect is that the transfer onto the nonwoven support increases the permeability without influencing the rejection. Third, the change of the dope compositions increased the rejection and decreased the permeability. The background of these effects is discussed in 6.2.3.

The next task was the change of the solvent from NMP to DMAc. The industry partner only had the permission to discharge aqueous DMAc solution into the sewage, rendering all formulations containing NMP unusable.

The composition of the dope solutions was altered by increasing the mass fraction of PVDF and PVP K-90 because of the effect of the solvent substitution (cf. 2.2.3). This should increase the viscosity and therefore slow down the diffusion during the phase separation. And additionally, decrease the tolerance of water. This should cause an earlier termination of the pore growth. The measured shear viscosities of the dope solutions are shown in Figure 39.

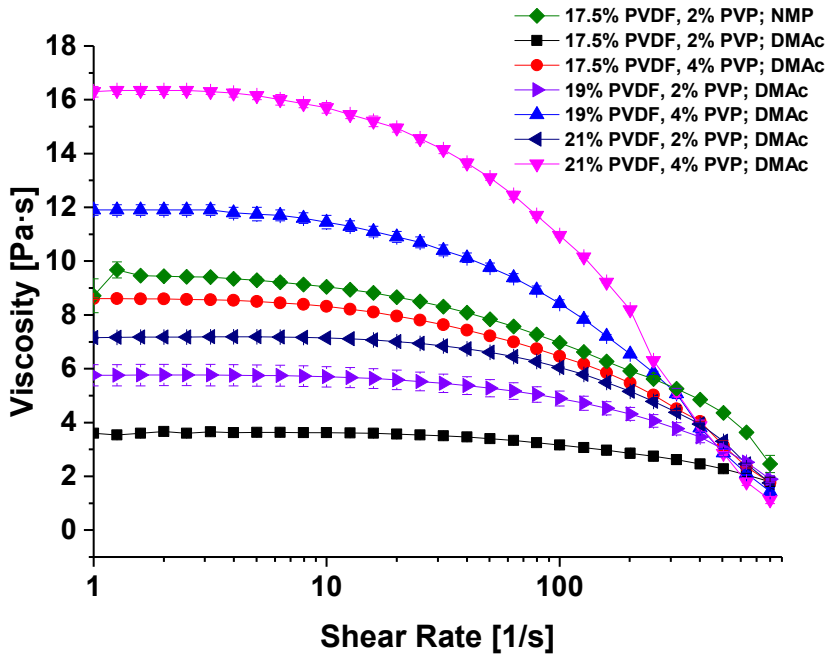

Figure 39 Influence of polymer concentration and solvent of dope solution shear viscosity.

From the data presented in the figure it can be seen that for the previously used composition (green diamond) the viscosity drops to than less half by changing the solvent to DMAc (black square). The viscosity then increases with the adjustment of the polymer concentration, but only the dope solutions with a mass fraction of 4 % PVP reach or exceed the viscosity of the NMP formulation. Membranes were prepared from these dope solutions on nonwoven and characterized by crossflow filtration of PEG 35 kDa and PEO 100 kDa. The results of these filtrations are shown in Table 43.

Table 43 Performance of membranes prepared from DMAc.

	permeability [L/h m² bar]				rejection [%]				n
	P_0	SD	P_1	SD	PEG 35 kDa	SD	PEO 100 kDa	SD	
17.5% PVDF; 2% PVP; NMP	2426	694	1244	402	85	3	n.d.	n.a.	5
17.5% PVDF; 2% PVP; DMAc	2277	145	1836	249	0	0	50	4	2
17.5% PVDF; 4% PVP; DMAc	1742	n.a.	1268	n.a.	17	n.a.	52	n.a.	1
19% PVDF; 2% PVP; DMAc	1713	n.a.	1135	n.a.	16	n.a.	75	n.a.	1
19% PVDF; 4% PVP; DMAc	1794	n.a.	711	n.a.	44	n.a.	72	n.a.	1
21% PVDF; 2% PVP; DMAc	2167	n.a.	1494	n.a.	2	n.a.	68	n.a.	1
21% PVDF; 4% PVP; DMAc	899	n.a.	558	n.a.	64	n.a.	78	n.a.	1

The filtration data indicates that the change of the solvent decreases the rejection while increasing the pure water permeability P_1. This agrees with the previously stated solvent differences (cf. 2.2.3). The data reveals that the increase of the polymer concentration leads

to the decrease of pure water permeability P_1 and increase in rejection for both solutes. This can be explained by the increase in viscosity increase seen in Figure 39.

From the experiment the composition of 21 % PVDF and 4 % PVP K-90 in DMAc was selected for the up-scaling with the industry partner. The performance of the membrane was characterized by crossflow filtration of PEG 35 kDa and PEO 100 kDa. The performance of this membrane is presented in Table 44 with the performance of the lab scale membrane as reference.

Table 44 Performance of the membrane (21 % PVP, 4 % PVP K-90 in DMAc) from lab and pilot scale.

	permeability [L/h m² bar]				rejection [%]				n
	P_0	SD	P_1	SD	PEG 35 kDa	SD	PEO100 kDa	SD	
lab scale	899	n.a.	558	n.a.	64	n.a.	78	n.a.	1
pilot scale	215	8	204	9	91	2	86	1	3

The performance of the pilot scale membrane differs significantly from the membrane prepared in lab scale. The permeability P_0 is reduced by a factor of four and P_1 by a factor of two while the rejection is increased. SEM pictures of the up scaled membrane were prepared to determine the reason for this deviation. These are presented in Figure 40.

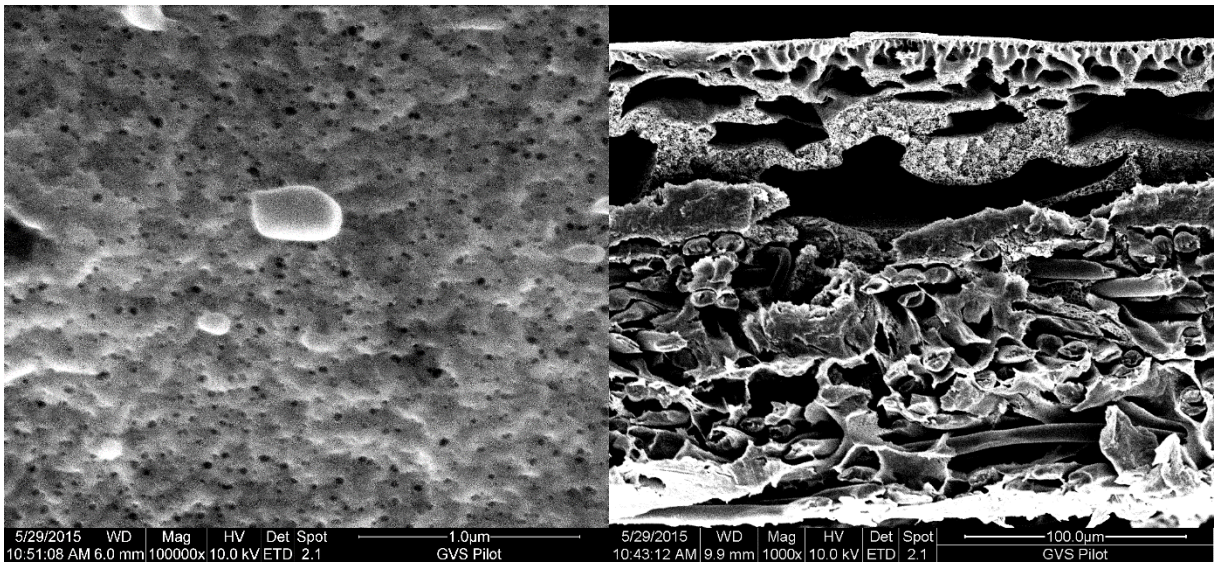

Figure 40 SEM picture of the up scaled membrane (21% PVDF, 4 % PVP K-90 in DMAc).

Left: top surface at 100kx magnification; right: morphology at 1000x magnification.

The surface of the membrane shown in Figure 40 is well porous and exhibits a slight pore size deviation. Such a structure conventionally indicates a high permeability. Therefore, the reason for the decline in permeability should not be correlated to the surface morphology. In the picture of the cross-section morphology a dense layer can be seen at the bottom of the PVDF structure above the nonwoven. This might be the reason for the change in membrane performance.

The thickness of the membranes is measured to further evaluate the performance change. The data is presented in Table 45.

Table 45 Thickness comparison of lab scale and up scaled membranes

	membrane thickness [mm]		
	mean	**SD**	**n**
lab scale	0.3023	0.0224	8
pilot scale	0.2386	0.0059	9

The difference in mean thickness between both membranes is 64 µm, which refers to 21 % of the original thickness. This indicates that the dense layer reduces the thickness of the membrane. The standard deviation of the thickness measurement is approximately four times smaller for the pilot scale membrane than for the lab scale membrane. The smaller standard deviation indicates that the up scaled membrane is more homogeneous than the pilot scale membrane.

5.2.4. Adjustment of morphology

It is necessary to slow down the precipitation speed to obtain a more sponge-like morphology with minimal macro-void formation for some planed experiments (cf. 3.2). Two strategies are applied simultaneously to achieve this goal.

First, the polymer concentration is increased to increase the viscosity of the dope solution. This will slow down the exchange speed of solvent and non-solvent and consequentially slow down the speed of the pore growth. Second, the coagulation bath is enriched with solvent. This is done to decrease the driving force for the solvent non-solvent exchange and delay the solidification. Both measures are known to be effective for changing the kinetics of the phase separation and lead to a more sponge-like morphology (cf. 2.2.2). [15]

For the adjustment of viscosity, dope solutions were prepared in NMP with 16 % PVDF and the addition of 1, 3 and 5 % PVP K-30 and dope solutions of 1 % PVP K-30 with 18 or 20 % PVDF. These were characterized by rheology. The results are presented in Figure 41.

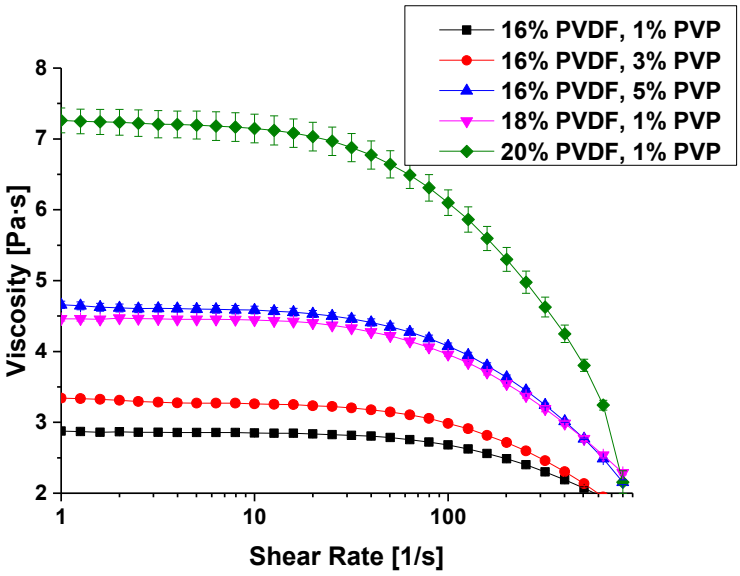

Figure 41 Increase of shear viscosity of different dope solutions in NMP

The viscosity increases with an increase in polymer concentration as seen in previous results and the shear thinning behavior is more pronounced at higher polymer concentration as one would expect.[61]

Membranes were prepared from the dope solutions with 16 % PVDF and 1 % PVP K-30. A mixture of DI-water with 10 and 15 %Vol NMP were used as coagulation bath (CB). At higher concentrations, the membrane did not precipitate completely. The SEM pictures of the cross-section morphology of these membranes are presented in Figure 42.

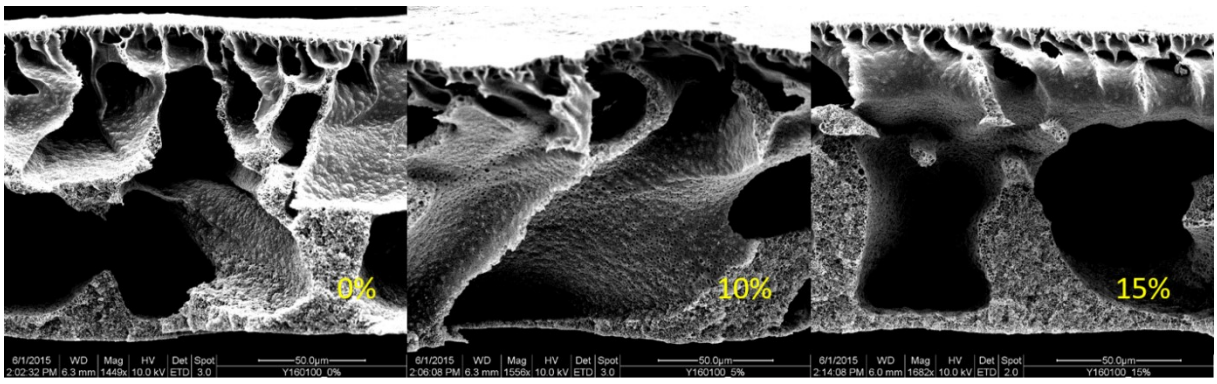

Figure 42 SEM pictures of the cross-section morphology of membranes from a dope solution of 16% PVDF and 1% PVP in dependence of the amount of solvent in CB.

Solvent content is indicated in the picture. Magnification left to right: 1449x. 1558x and 1682x.

In the figure above, it can be seen that the morphology is not changed by the addition of NMP to the coagulation bath. The reason for that is most likely the low amount of NMP that was added.

Membranes were prepared from the dope solutions with 16 % PVDF and 3 % PVP K-30 next. The coagulation bath consisted of DI-water with 10 and 15 %Vol NMP. As in the previous

sample it was not possible to use higher NMP concentrations. The SEM pictures of the cross-section morphology of these membranes are presented in Figure 43.

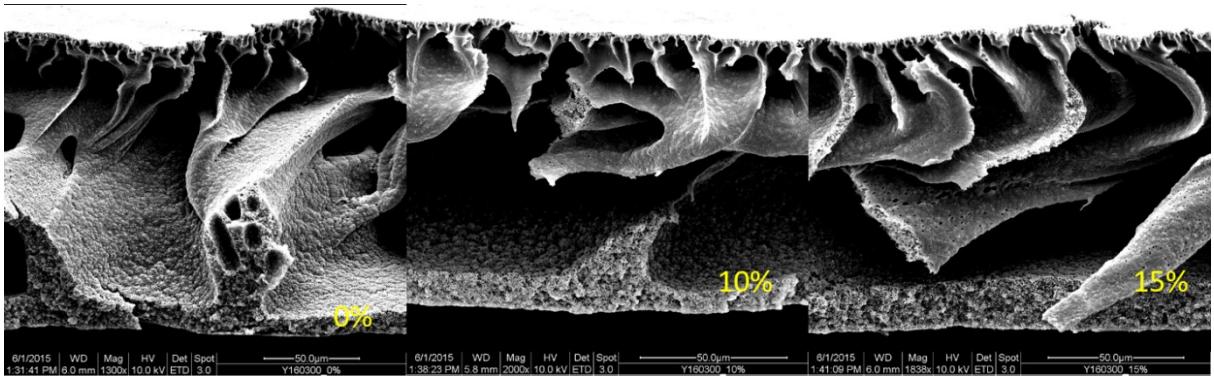

Figure 43 SEM pictures of the cross-section morphology of membranes from a dope solution of 16% PVDF and 3% PVP in dependence of the amount of solvent in CB.

Solvent content is indicated in the picture. Magnification left to right: 1300x, 2000x and 1838x.

As before the morphology has not been changed.

Membranes were prepared from the dope solutions with 16 % PVDF and 5 % PVP K-30. DI-water with 10 and 15 %Vol NMP were used as coagulation bath. Like in the previous preparation, it was not possible to use higher concentrations. The SEM pictures of the cross-section morphology of these membranes are presented in Figure 44.

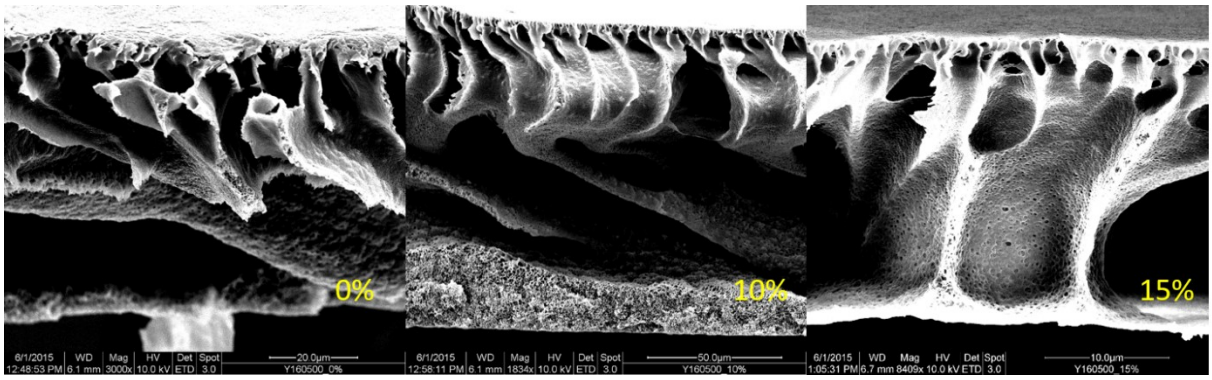

Figure 44 SEM pictures of the cross-section morphology of membranes from a dope solution of 16% PVDF and 5% PVP in dependence of the amount of solvent in CB.

Solvent content is indicated in the picture. Magnification left to right: 3000x, 1834x and 8409x.

The morphology has not been changed as previously seen. To conclude, it can be stated that a concentration of 16 % PVDF in the dope solution is not precipitating in coagulants soft enough to facilitate a sufficient change in the morphology.

Next membranes were prepared from the dope solution with 18 % PVDF and 1 % PVP K-30. The same coagulation bath compositions were used as in the previous experiments because as before the precipitation was not facilitated at higher concentration. The SEM pictures of the cross-section morphology of these membranes are presented in Figure 45.

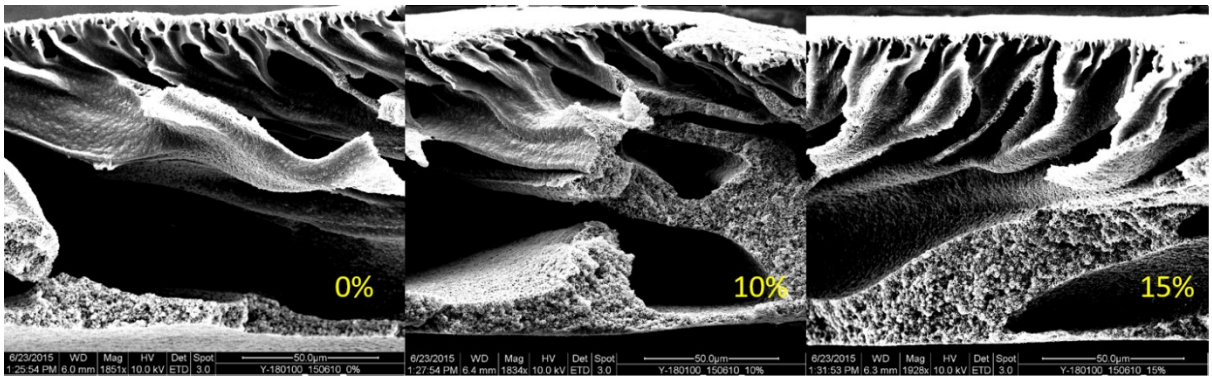

Figure 45 SEM pictures of the cross-section morphology of membranes from a dope solution of 18% PVDF and 1% PVP in dependence of the amount of solvent in CB.

Solvent content is indicated in the picture. Magnification left to right: 1851x, 1834x and 1928x.

The increase in PVDF concentration made the cross-sections morphology slightly denser than in the previous membranes. But the addition of the NMP to the coagulation bath had no apparent effect as before.

During the membrane preparation from the dope with 20 % PVDF and 1 % PVP K-30 a coagulation bath was used containing 10, 15, 25, 40 and 50 %Vol NMP and DI-water. The previous encountered problem did not occur, the dope solution precipitated in all coagulants. This indicates that the PVDF concentration was chosen sufficiently for the preparation. The cross-section morphology was characterized by SEM. The pictures are presented in Figure 46.

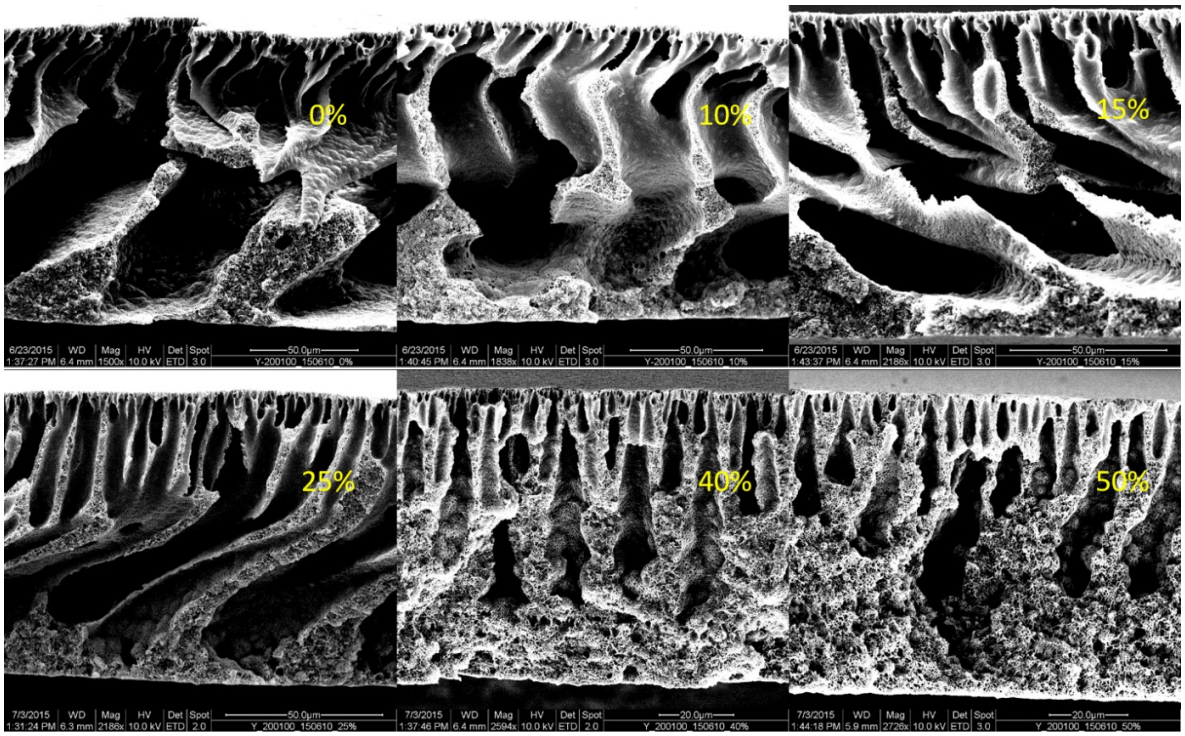

Figure 46 SEM pictures of the cross-section morphology of membranes from a dope solution of 20% PVDF and 1% PVP in dependence of the amount of solvent in CB.

Solvent content is indicated in the picture. Magnification left to right: 1st row 1500x, 1838x and 2186x; 2nd row 2188x, 2594x and 2726x.

The increase in PVDF concentration lead to a slightly denser cross-section structure than observed in the previous membranes. The influence of the NMP in the coagulation bath on the morphology is virtually non-existing up to a concentration of 15 %Vol. At a concentration of 25 %Vol the morphology becomes a more regular finger-like structure with smaller voids. At 40 and 50 %Vol NMP in the coagulation bath the membranes exhibits virtually identical structure. The formation of macro-voids has been reduced and the morphology contains finger-like and sponge-like domains. The performance of these membranes was characterized by the crossflow filtration of PEG 35 kDa. The results are presented in Figure 47.

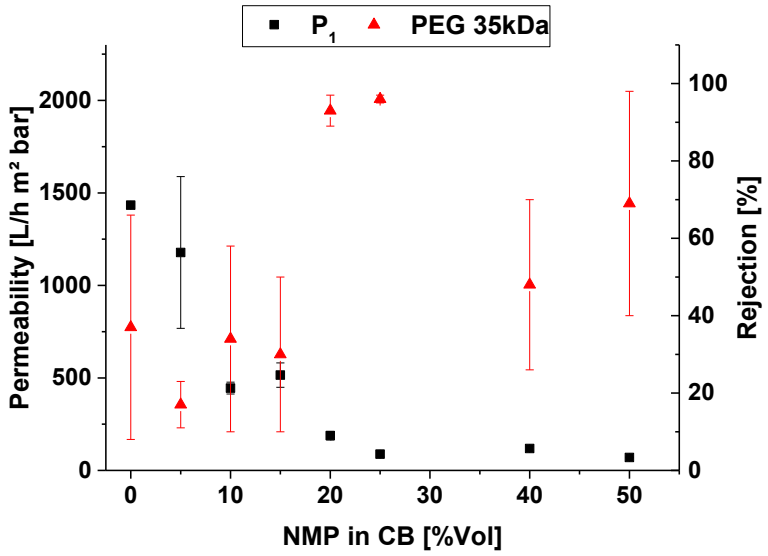

Figure 47 Influence of NMP in the coagulation bath; 20 % PVDF and 1 % PVP in the dope.

The permeability of the membranes decreases of with the increase of NMP in the coagulation bath.

5.2.5. Incorporation of pristine nanoparticles

5.2.5.1. Standard dope solution composition

The results of the experiments with pristine nanoparticles are presented in this part. The first step was the preparation of dope solutions. These contained 16 % PVDF and 1 % PVP K-30 in NMP and pristine zinc oxide nanoparticles were added at a concentration of 5, 10, 15, 20, 25 and 50 %w/w(PVDF). The viscosity of these dope solutions was characterized using rheology. The results are presented in Figure 48.

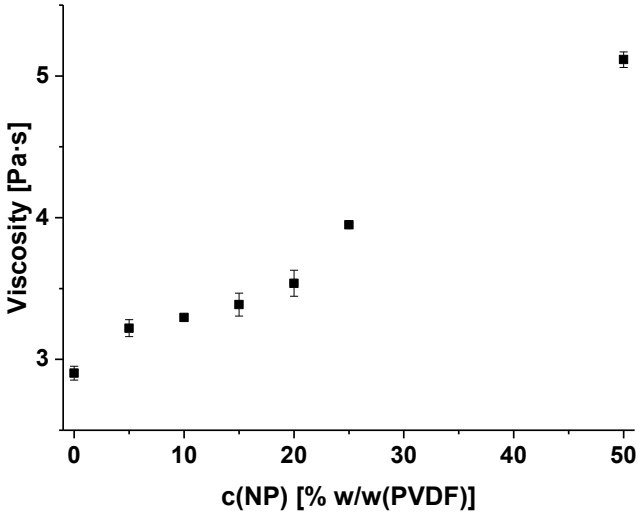

Figure 48 Shear viscosity at 15.9 s^{-1} for dope solutions (16% PVDF and 1% PVP in NMP) with various amounts of pristine ZnO nanoparticles.

In the figure above it can be seen that the viscosity of the dope solution increased nearly steadily with the addition of the nanoparticles. The reason for the increase can be traced back to the interaction between the particles and the solvent.

Membranes were prepared form these dope solutions. The standard conditions were used as defined in 4.3.3. The membranes were characterized by the crossflow filtration of PEG 35 kDa and PEO 100 kDa. The results of these filtrations are presented in Figure 49 while the numeric values can be found in the appendix (Table 76).

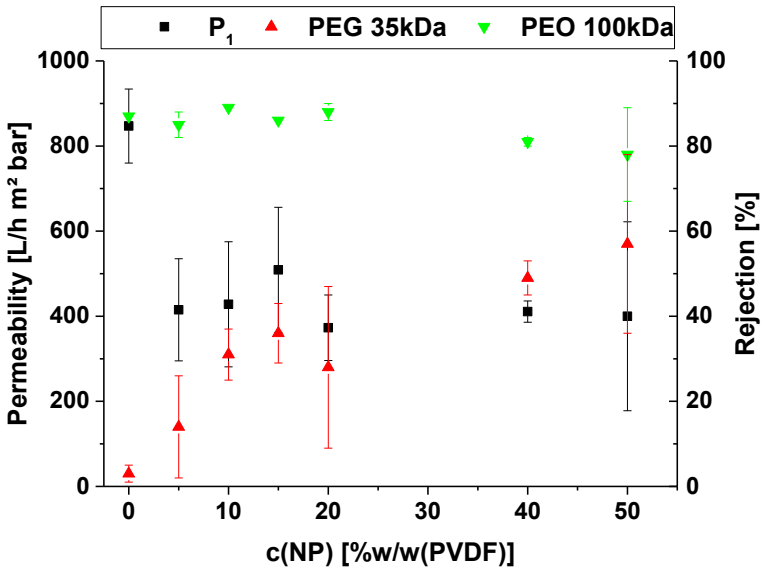

Figure 49 Performance of membranes with pristine ZnO nanoparticles.

The following trends can be asserted from the data in the figure above. The permeability drops initially with the addition of zinc oxide particles. But with the further increase in particle concentration in the dope solution no influence on the permeability is seen.

The rejection for PEO 100 kDa remains constantly just under 90 % for all examined membranes. The rejection for PEG 35 kDa increases from just above zero to approx. 50 %. The membrane with 0 and 50 %w/w(PVDF) ZnO particles were characterized by SEM. The pictures of the top surface morphology are shown in Figure 50.

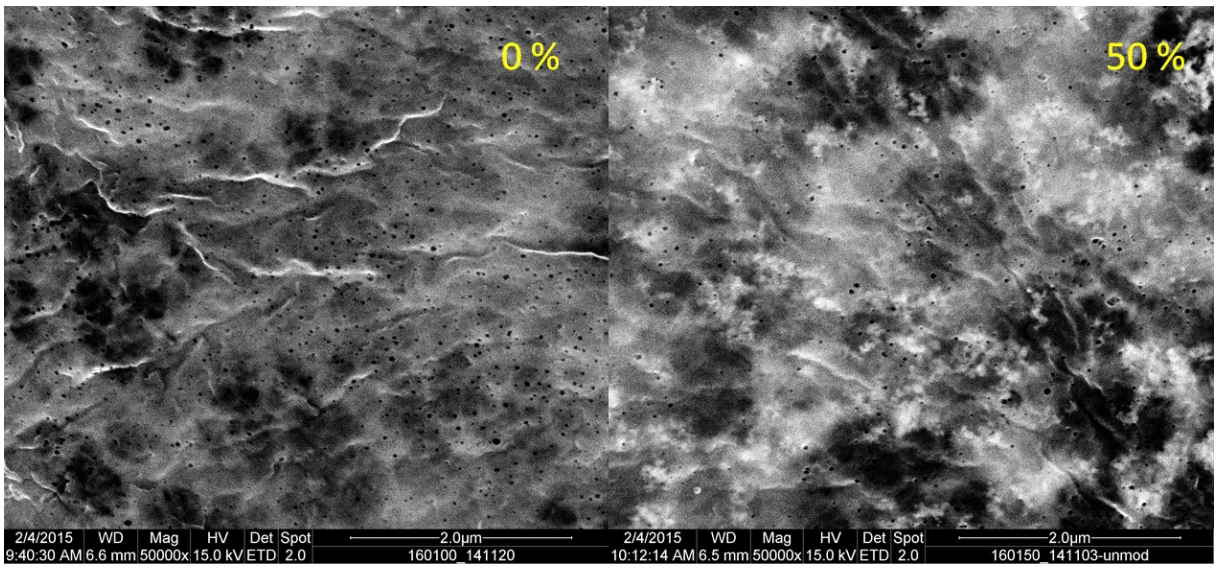

Figure 50 Top surface of membranes with and without pristine ZnO NP.

Concentration [%w/w(PVDF)] of NP in dope solution indicated in picture. Magnification: 50kx.

In the picture, the pore size is not changed by the introduction of the nanoparticles. But a lot of agglomerates are noticeable below the skin layer as indicated by the bright spots in the picture. No particles are seen on the top surface or integrated into the surface.

The pictures of the cross-section morphology are shown in Figure 51.

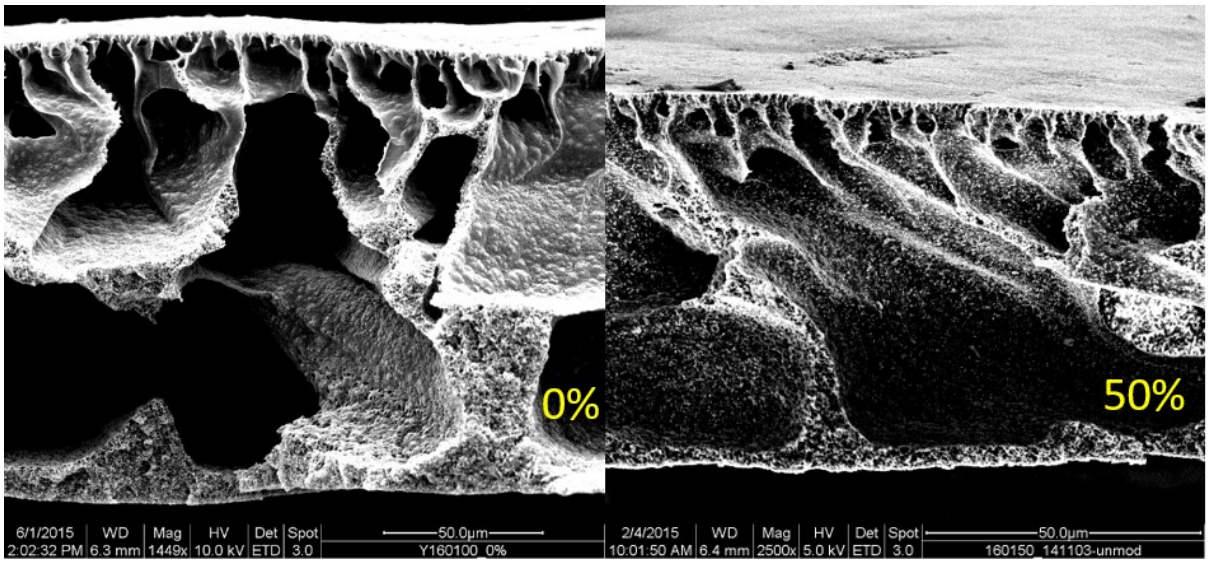

Figure 51 Cross-section of membranes with and without pristine ZnO NP.

Concentration [%w/w(PVDF)] of NP in dope solution indicated in picture. Magnification left: 1449x and right 2500x.

It can be seen in the figure above, that both membranes exhibit the same cross-section morphology. In the membrane with 50 %w/w(PVDF) ZnO bright spots can be seen through the whole cross-section. This area is displayed in a higher magnification in Figure 52.

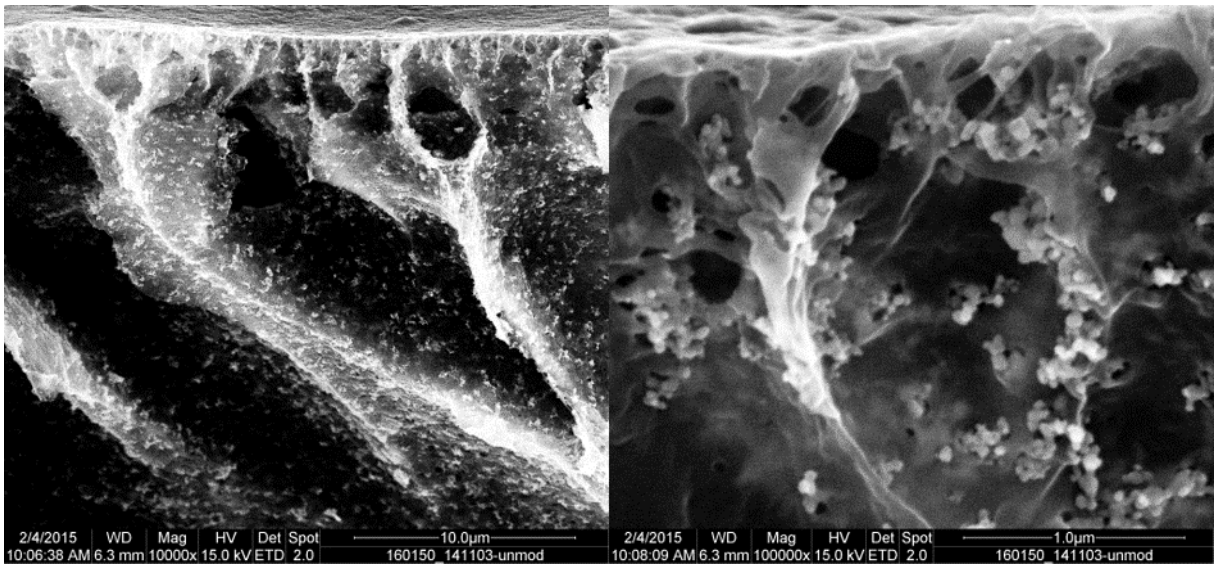

Figure 52 Agglomerates of NP in membrane with 50%w/w(PVDF) NP.

Magnification left: 10kx and right 100kx.

At the higher magnification, it can be clearly seen that the particles are agglomerated. The agglomerates sit on the wall of the voids or inside pores of the sponge-like domains. Therefore, it can be stated that the integration of the particles into the polymer matrix is poor. This aggress with the prediction based on the material characteristics. The high amount of agglomeration was not expected from the viscosity data (cf. Figure 48).

5.2.5.2. Dope solutions without PVP

To evaluate the influence of the hydrophilic additive PVP, dope solutions without this compound were prepared. The PVDF concentration was kept at 16 % as in the previous experiments. The viscosity of these dope solutions was characterized; the results are presented in Figure 53.

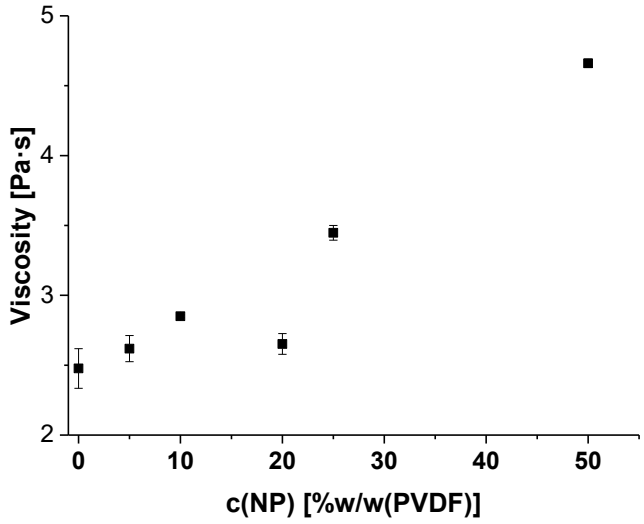

Figure 53 Shear viscosity at 15.9 s^{-1} for dope solutions (16% PVDF in NMP) with various amounts of unmodified ZnO nanoparticles.

As in the previous experiment the viscosity increases steadily with the particle concentration. The data point at 20 %w/w(PVDF) is an outlier of this behavior which is most likely caused by a weighing mistake during the dope solution preparation. The steady increase indicates that mostly the interaction between NMP and zinc oxide is responsible for the viscosity increase. As before no indication of agglomeration can be found in the data.

Membranes were prepared according to the standard procedure. The membranes were characterized by the crossflow filtration of PEG 35 kDa and PEO 100 kDa. The results of these filtrations in Figure 54, the detailed results can be found in the appendix (cf. Table 77).

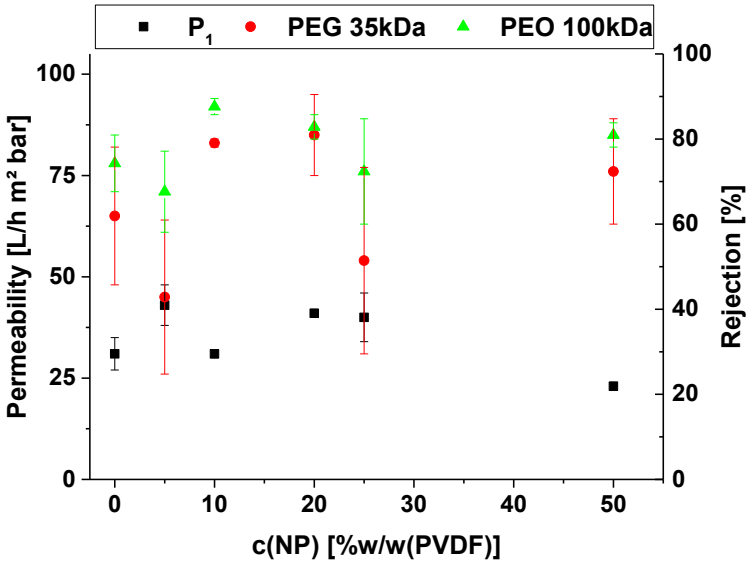

Figure 54 Performance of membranes (16% PVDF) with pristine ZnO nanoparticles.

The permeability is greatly reduced by the omission of PVP from the dope solution. The hydrophilic additive PVP enhances the pore initiation during the phase separation, therefore is the reduction in permeability to be expected. The addition of nanoparticles to the dope solution seems not to influence the membrane performance even at high concentrations. Which negates any porogenic effect of the particles. The membrane with 0 and 50 %w/w(PVDF) ZnO particles were characterized by SEM. The pictures of the top surface morphology are shown in Figure 55.

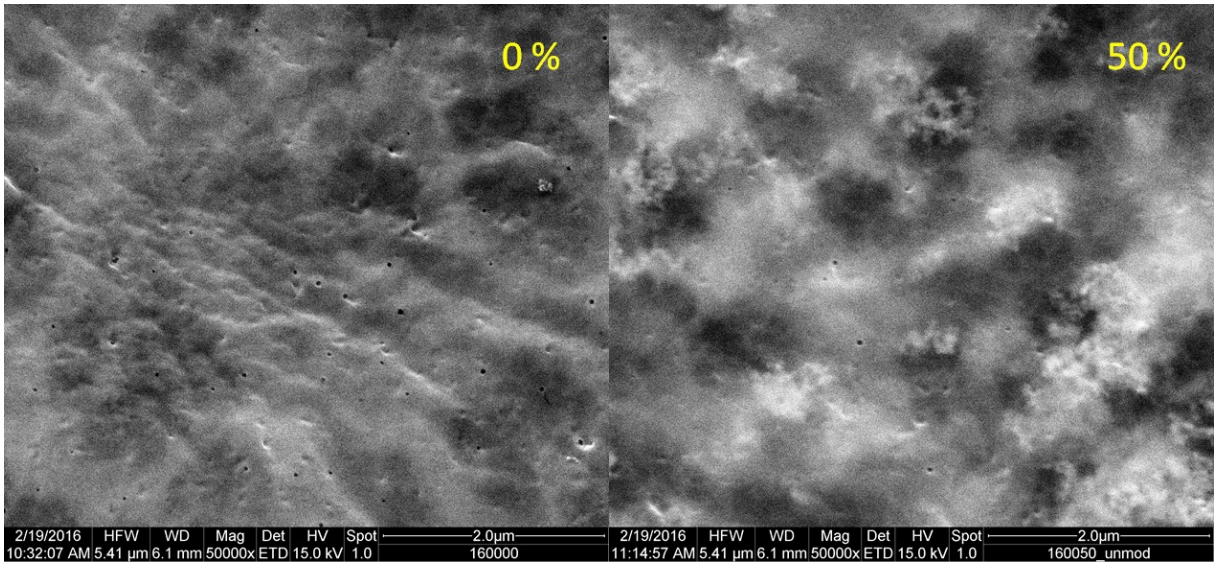

Figure 55 Top layer of membranes with and without pristine ZnO NP and no PVP in dope solution. Concentration [%w/w(PVDF)] of NP in dope solution indicated in picture. Magnification 50kx.

The surface has a very low pore density, which explains the comparable low permeability of these membranes. The introduction of the particles does not seem to influence the pore structure. As in the previous experiments many agglomerates can be noticed below the skin

layer as indicated by the bright spots in the picture. No particles are seen on the top surface or integrated into the surface. The membrane cross-section was characterized by SEM. The results are presented in Figure 56.

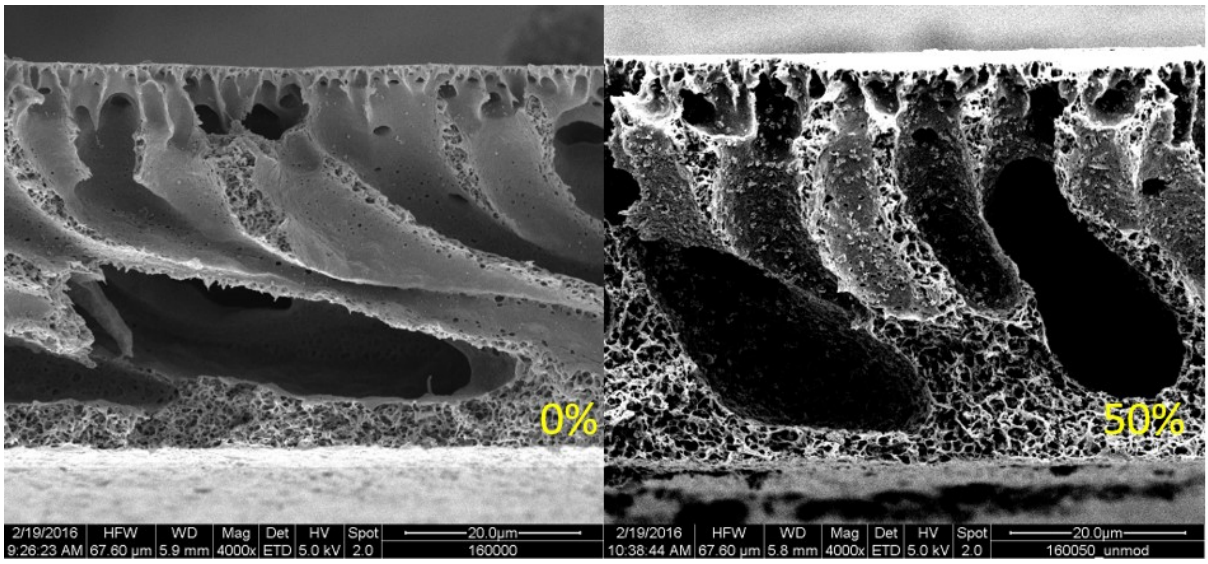

Figure 56 Cross-section of membranes with and without pristine ZnO NP and no PVP in dope solution. Concentration [%w/w(PVDF)] of NP in dope solution indicated in picture. Magnification 4kx.

The omission of the PVP does not change the cross-section morphology. As before large macro-voids are found in the structure. The addition of nanoparticles has no influence of the morphology. Agglomerate can be spotted on the walls of the macro-voids. A picture of the agglomerates at higher magnification is shown in Figure 57.

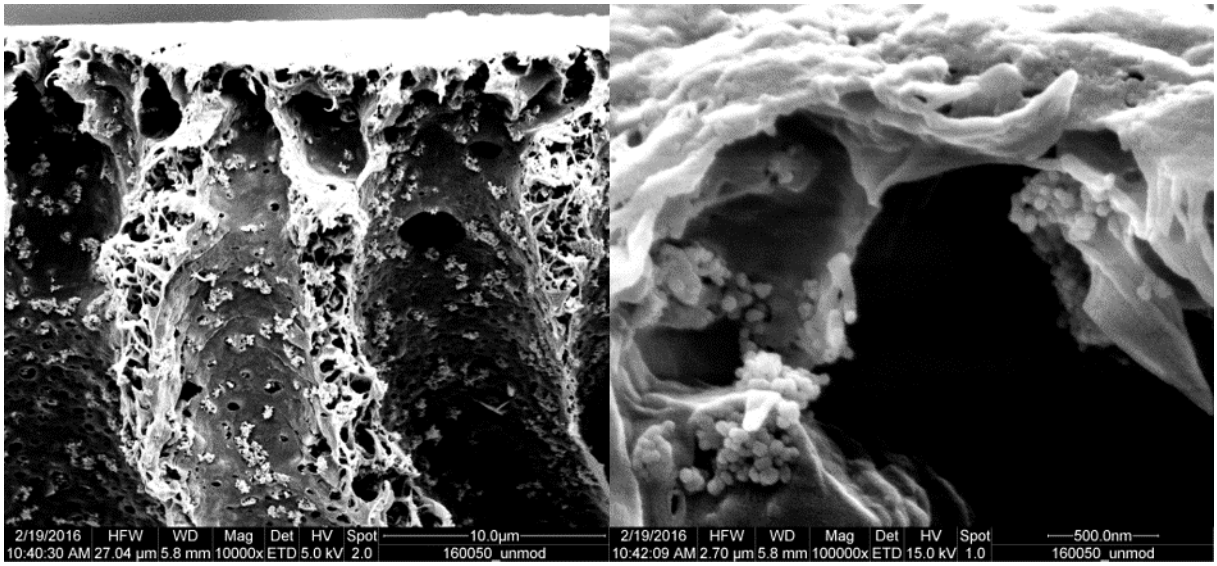

Figure 57 Agglomerates of NP in membrane with 50%w/w(PVDF) NP and no PVP in dope solution. Magnification left: 10kx and right 100kx.

The higher magnification reveals that all particles are aggregated. The integration into the polymer matrix seems to be poor. The explanation for the poor integration is analogous to the previous experiments (cf. 5.2.5.1). The agglomerates seem to be slightly bigger than in the

membranes with PVP. This could indicate that the PVP in the dope solution has a stabilizing effect on the particles during the phase separation.

5.2.5.3. New morphology

The next step was the evaluation of the influence of the precipitation rate on the nanoparticle during phase separation. The conditions were changed according to the findings in chapter 5.2.4. The PVDF concentration was increased to 20 % and 1 % PVP was added. The following nanoparticle concentrations were selected for the experiment: 5, 10, 20 and 50 %w/w(PVDF). The viscosity of these dope solutions was characterized; the results are presented in Figure 58.

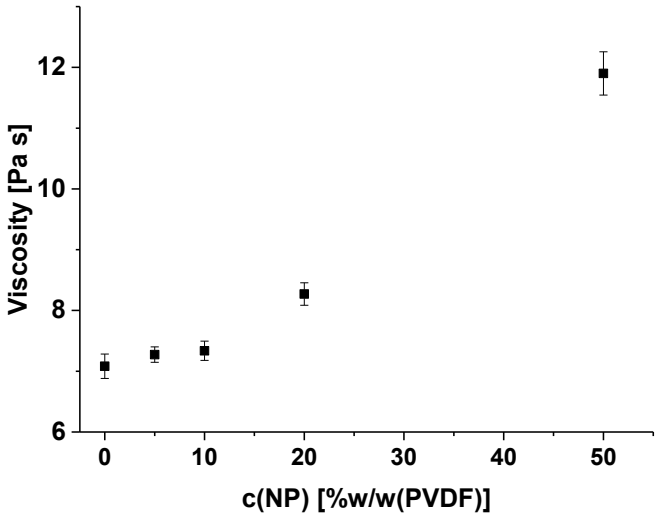

Figure 58 Shear viscosity at 15.9 s^{-1} for dope solutions (20% PVDF and 1% PVP in NMP) with various amounts of unmodified ZnO nanoparticles.

The viscosity increases steadily as in the previous experiments. This shows again that apparently no agglomeration occurred in these samples. Membranes were prepared from these dope solutions by precipitation in the soft coagulation bath which consisted of DI-water and NMP at a ratio of 50 %Vol each. The membranes were characterized by the crossflow filtration of PEG 35 kDa and PEO 100 kDa. The results of these filtrations in Figure 59, the detailed results can be found in the appendix (cf. Table 78).

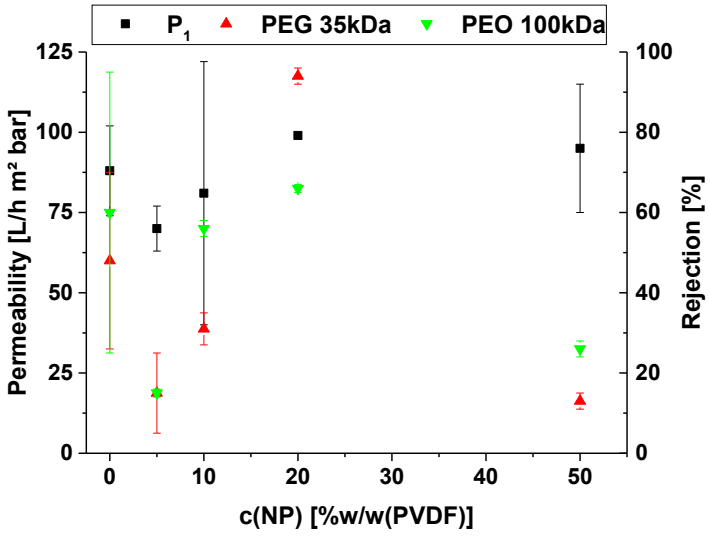

Figure 59 Performance of membranes with unmodified ZnO nanoparticles coagulated in solvent blend.

All membranes show a low permeability, which is caused by the precipitation conditions as discussed in 6.2.4. There is no distinct influence of the nanoparticle addition on the membrane performance. The performance of all membranes is nearly identical except for the PEG 35 kDa rejection in the membrane with 20 %w/w(PVDF) ZnO particles.

The top layer morphology of these membranes was characterized by SEM. The pictures of the membrane with 50 %w/w(PVDF) nanoparticles and without particles are shown in Figure 60.

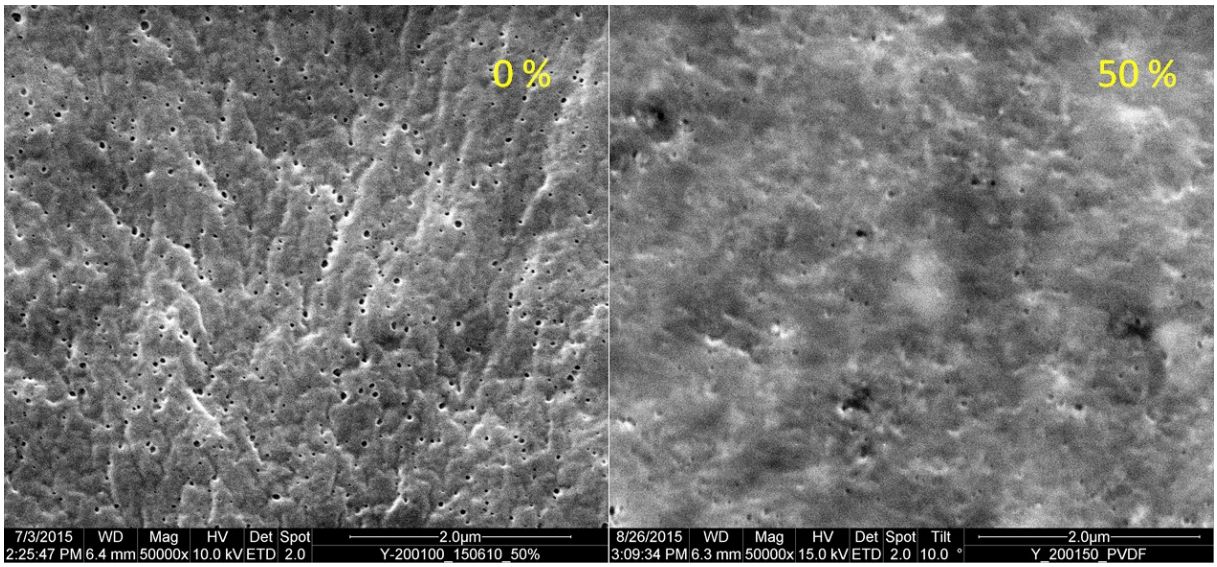

Figure 60 Top layer of membranes with and without pristine ZnO NP prepared by slow precipitation. Concentration [%w/w(PVDF)] of NP in dope solution indicated in picture. Magnification: 50kx.

The introduction of the nanoparticles made the membrane surface smoother and decreased the number of pores. The reason for this is not clear. There is no indication of particles on the surface or integrated into the skin layer. Also, the previously seen agglomerates under the top

surface are not present. The cross-section morphology of these membranes was characterized by SEM. These are displayed in Figure 61.

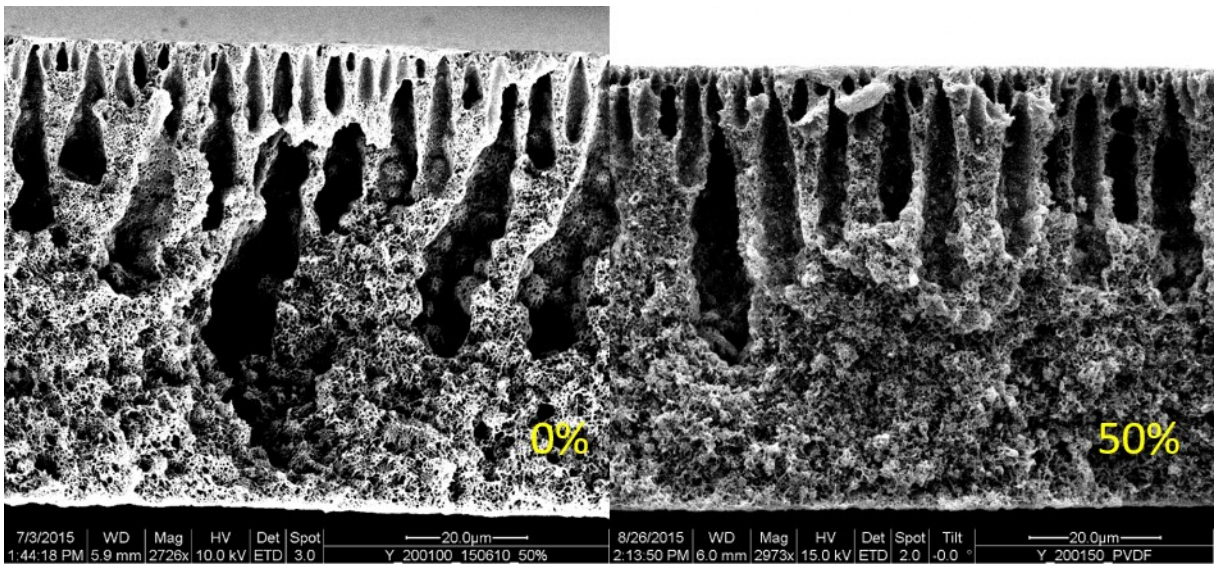

Figure 61 Cross-section of membranes with and without pristine ZnO NP prepared by slow precipitation. Concentration [%w/w(PVDF)] of NP in dope solution indicated in picture. Magnification left: 2726x and right 2973x.

By comparing both pictures it becomes clear that no influence on the morphology is seen as consequence of the addition of nanoparticles. In contrast to the previous samples no agglomerates are discernible at this magnification. These might be hidden by the porous structure. Therefore, it is necessary to view the structure at a higher magnification. This is shown in Figure 62.

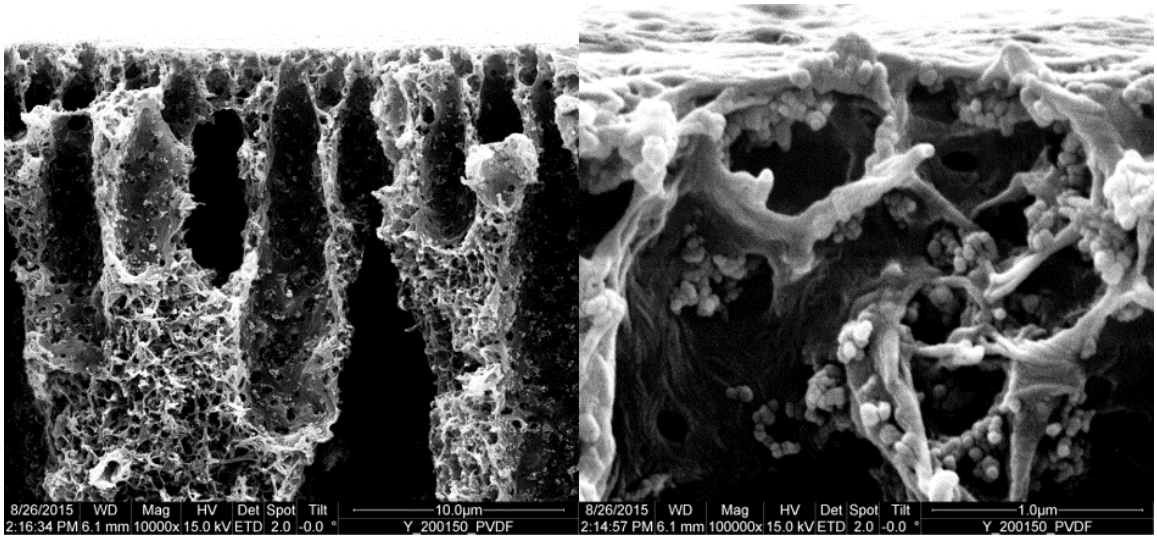

Figure 62 Agglomerates of NP in membrane with 50%w/w(PVDF) NP prepared by slow precipitation. Magnification left: 10kx and right 100kx.

The higher magnification reveals that agglomerates are still present, although these are better distributed than before and smaller in size. The decrease of the precipitation rate did not improve particle integration since the particles and agglomerates are sitting on the surface of

the PVDF structure. This indicates that the rapid precipitation rate is not the cause for the previously seen agglomeration and poor integration. Hence, it is the consequence of the intrinsic incompatibility between the materials.

5.2.6. Incorporation of TFA-modified nanoparticles

While the modification with TFA did not produce high surface coverage nor change the particle characteristics as previously seen (cf. 5.1.4.1 and 5.1.8.4), it was decided to investigate, if the obtained modification might be sufficient to realize an effect on the membrane. The particle modification performed at a ratio of 100 % TFA/ZnO and no pH control were chosen for the evaluation. These modification parameters produced an acceptable mass retrieval, which made it feasible to obtain a sufficient amount of modified particles to conduct these experiments. And the surface coverage achieved at these parameters was rated among the best attained values. Dope solutions were prepared at the usual composition of 16 % PVDF and 1 % PVP in NMP. These solutions were characterized by rheology. The results are presented in Figure 63.

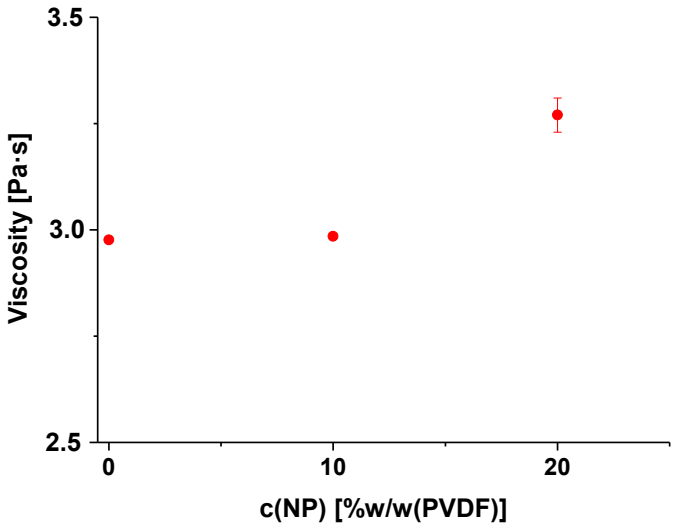

Figure 63 Shear viscosity at 15.9 s^{-1} for dope solutions (16% PVDF and 1% PVP in NMP) with various amounts of TFA-modified ZnO nanoparticles.

The viscosity is increased by the addition of the modified particles. The increase is comparable to the increase, which was seen in the experiments with the pristine particles at the same composition. This indicates that the particles are not agglomerated in the dope solution. Membranes were prepared from these dope solutions. The preparation was performed by the standard procedure as described in 4.3.1. The membranes were characterized by crossflow

filtration of PEG 35 kDa and PEO 100 kDa. The results of these filtrations are shown in Figure 64. The detailed results can be found in the appendix (cf. Table 79).

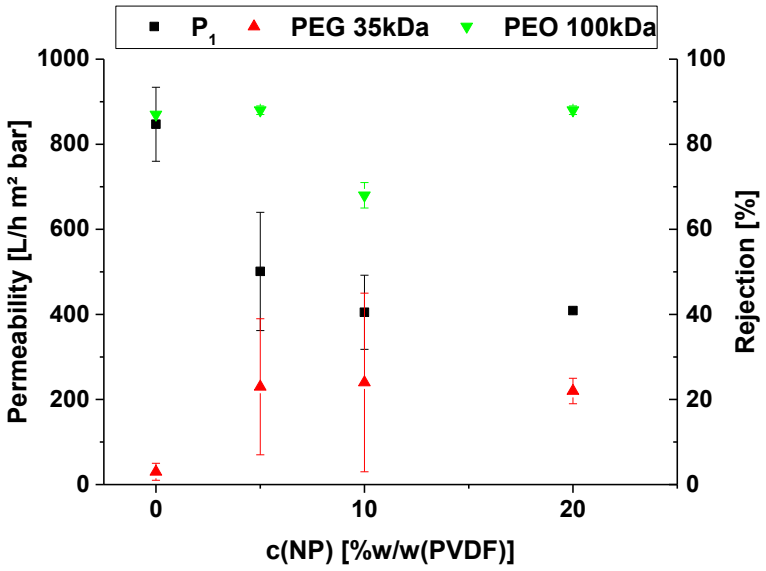

Figure 64 Performance of membranes (16% PVDF and 1% PVP) with TFA-modified ZnO nanoparticles.

In the graph, the rejection of PEO 100 kDa is not influenced by the addition of the particles. The rejection for PEG 35 kDa is marginally increased while the permeability is decreased by approximately 50 % of the initial value. This decrease is reached by the addition of 10 %w/w(PVDF) particles and is not further enhanced by the increase of the concentration to 20 %w/w(PVDF). The structure of these membranes was characterized by SEM. The cross-section morphology of the membrane with the addition of 20 %w/w(PVDF) particles is presented in Figure 65.

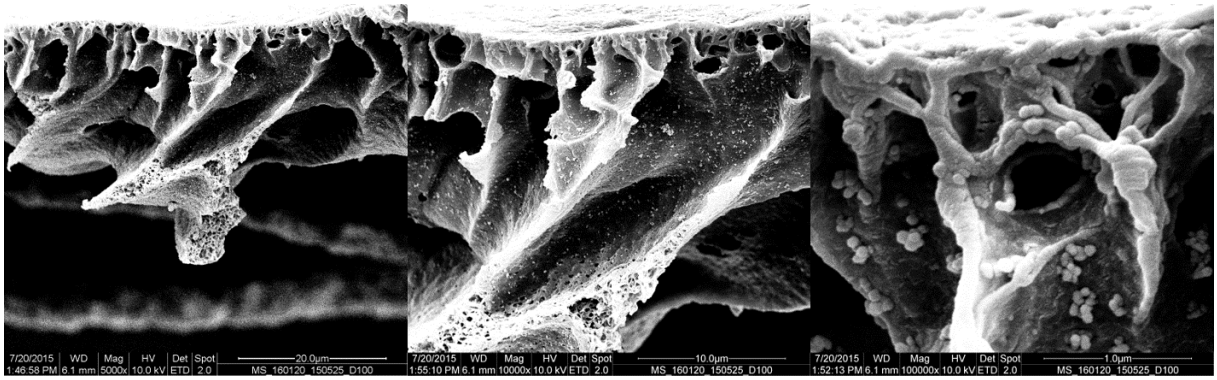

Figure 65 Cross-section of the membrane with 20%w/w(PVDF) TFA modified particles.

Magnification left to right: 5kx, 10kx and 100kx.

The first picture of the membrane morphology reveals a similar structure to membrane with pristine particles (cf. Figure 51). The porous bottom layer is not focused well because the membrane did not break evenly in the sample preparation. The other two pictures show that the particles are agglomerated and not well integrated in the polymer matrix. The size of the

agglomerates appears to be smaller in size than in the membrane with the pristine particles, which were prepared under the same conditions.

5.2.7. Incorporation of acetic acid modified nanoparticles

While the modification with acetic acid did not produce a significant surface coverage (cf. Table 16) and didn't realize a conclusive influence on the Hansen parameter (cf. 5.1.8.3), these experiments were conducted to see if any effect will be found in the membrane preparation. The dope solution composition of 16 % PVDF in NMP without the addition of PVP was chosen for this evaluation. These solutions were characterized by rheology. The results are shown in Figure 66.

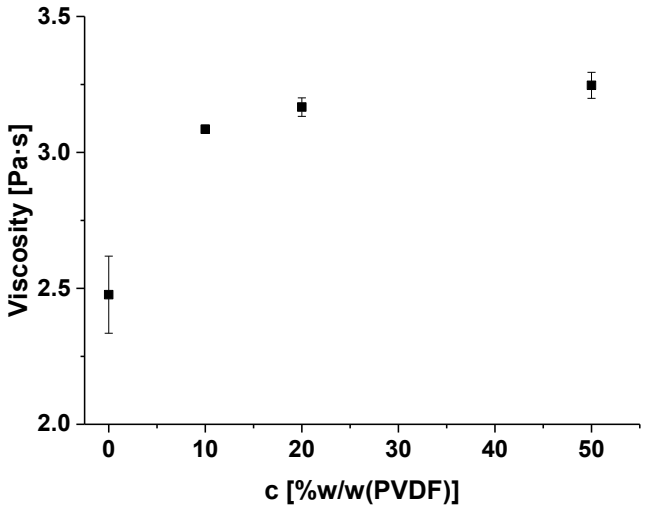

Figure 66 Shear viscosity at 15.9 s^{-1} for dope solutions (16% PVDF in NMP) with various amounts of Ac-modified ZnO.

In the figure, an increase in shear viscosity is caused by the addition of the particles. In contrast to the previous experiment is the increase not a linear behavior. The viscosity increases initially with the addition of 10 %w/w(PVDF). While the further increase in particle concentration only produces a small increase in viscosity. This behavior might indicate the formation of agglomerate in the dope solution.

Despite these findings, membranes were prepared from theses dope solutions by precipitation in DI-water. The membranes were characterized by crossflow filtration of PEG 35 kDa and PEO 100 kDa. The results of these filtrations are shown in Figure 67. The detailed results can be found in the appendix (cf. Table 80).

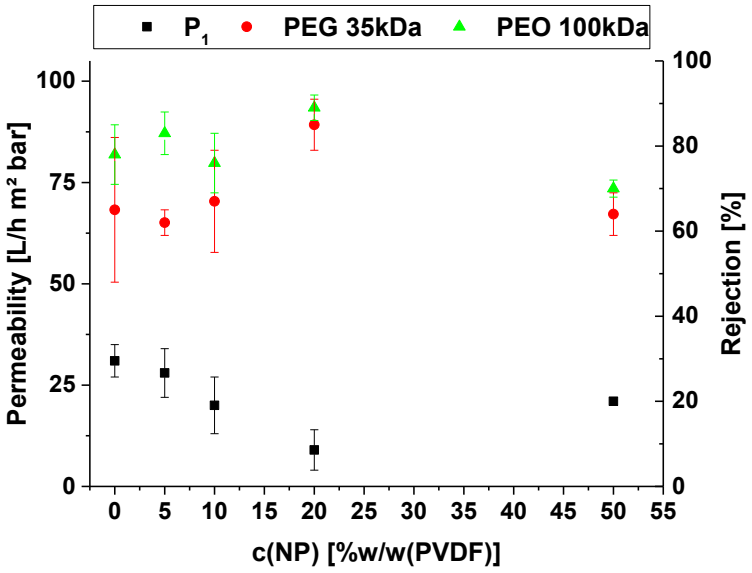

Figure 67 Performance of membranes with Ac-modified ZnO nanoparticles

The rejection performance of the membrane is not significantly influenced by the addition of the modified particles. The same can be asserted for the pure water permeability.

In the range of the particles concentration between 0 and 20 %w/w(PVDF) a classical trade off relation between permeability and rejection for PEG 35 kDa seems to emerge but this might be incidental since the performance change is very small. The skin layer of the membrane with 50 %w/w(PVDF) is displayed in Figure 68.

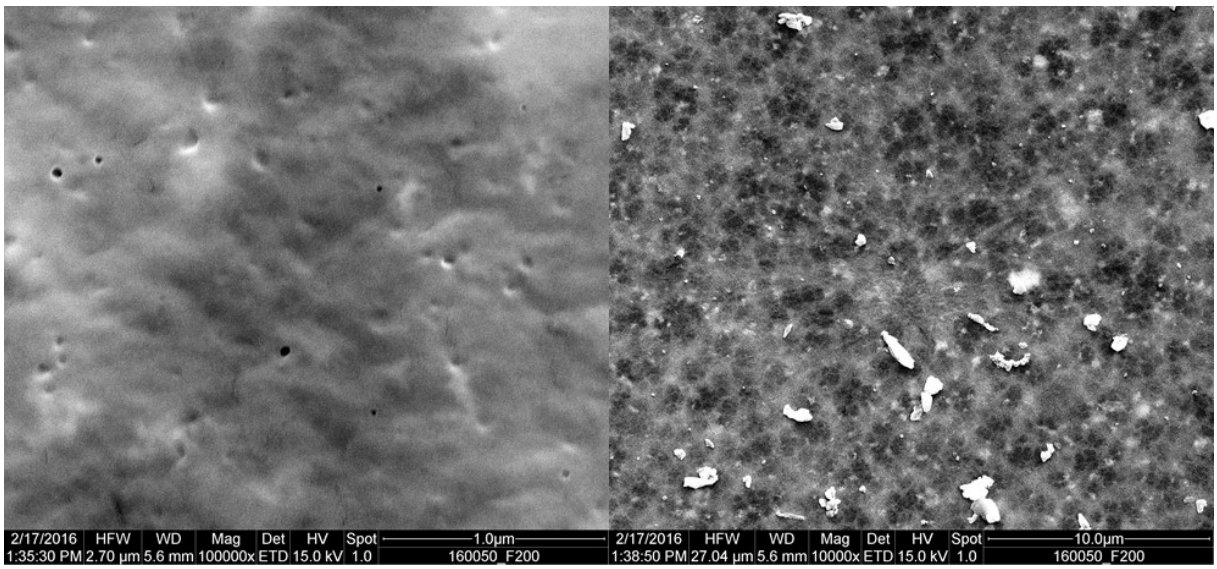

Figure 68 Top surface of membrane (16% PVDF) and 50%w/w(PVDF) Ac-modified particles. Magnification: left 100kx; right 10kx.

The picture of the surfaces reveals a very low porosity with small pores. This agrees with the observed pure water fluxes and is most likely caused by the omission of PVP in the dope solution (cf. 5.2.5.2). The lower magnification reveals agglomerates on the surface. The cross-

section morphology of these membranes was characterized by SEM. The membrane with the highest particle concentration is displayed in Figure 69.

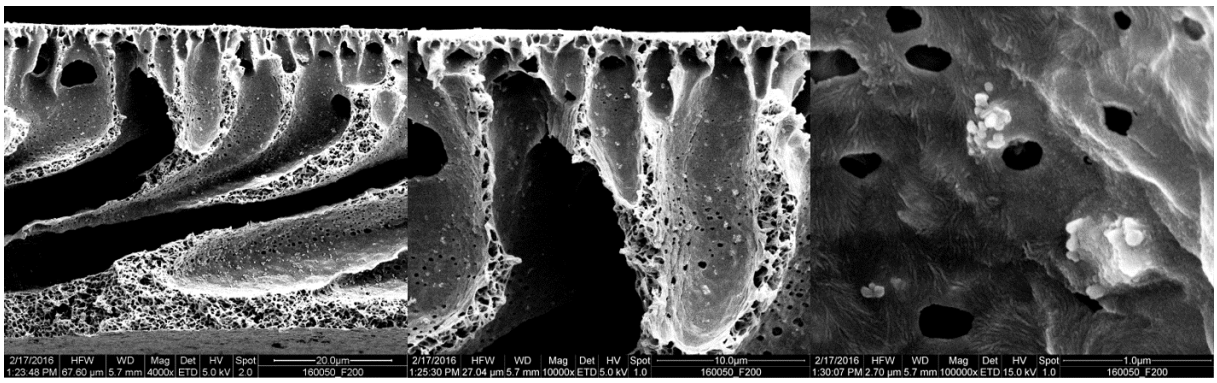

Figure 69 Cross-section of membrane (16% PVDF, 1% PVP) and 50%w/w(PVDF) Ac-modified particles. Magnification left to right:5kx, 10kx and 100kx.

The picture shows a similar structure as seen in the membranes with pristine particles prepared under similar conditions (cf. Figure 56). The particles are agglomerated and can be seen over the whole structure. In the last picture, it can be seen that the agglomerates are bigger than in previous experiments. The agglomerates are partially embedded in the polymer matrix, which indicates a better integration than seen in the previous experiments.

5.2.8. Incorporation of PVP-modified nanoparticles

Both evaluated polyvinylpyrrolidone (PVP) modifications showed promising influences on the particle stability in NMP (cf. 5.1.8.5). Since the surface coverage was higher in the particles, which were modified with the *codispersion* procedure (cf. Table 15), it was decided to employ these particles for the integration into the membrane. The dope solution composition of 16 % PVDF in NMP with no addition of PVP was selected for these experiments. The dope solutions were characterized by rheology. The data is presented in Figure 70.

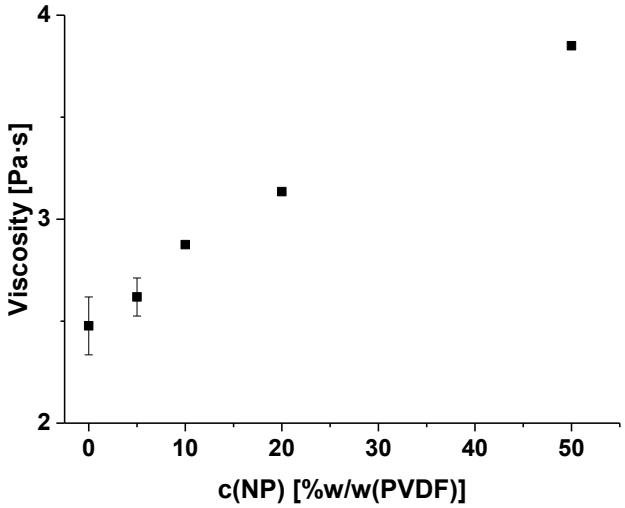

Figure 70 Shear viscosity at 15.9 s^{-1} for dope solutions (16% PVDF in NMP) with various amounts of PVP-modified ZnO nanoparticles

It can be clearly seen that the addition of the nanoparticles induces a steady increase in viscosity. The increase has a smaller slope than the increase with the pristine particles in the same system (cf. Figure 53).

Membranes were prepared according to the standard procedure as stated in 4.3. These were characterized by the crossflow filtration of PEG 35 kDa and PEO 100 kDa. The detailed data can be found in the appendix (cf. Table 81), while a graphic representation is presented in Figure 71.

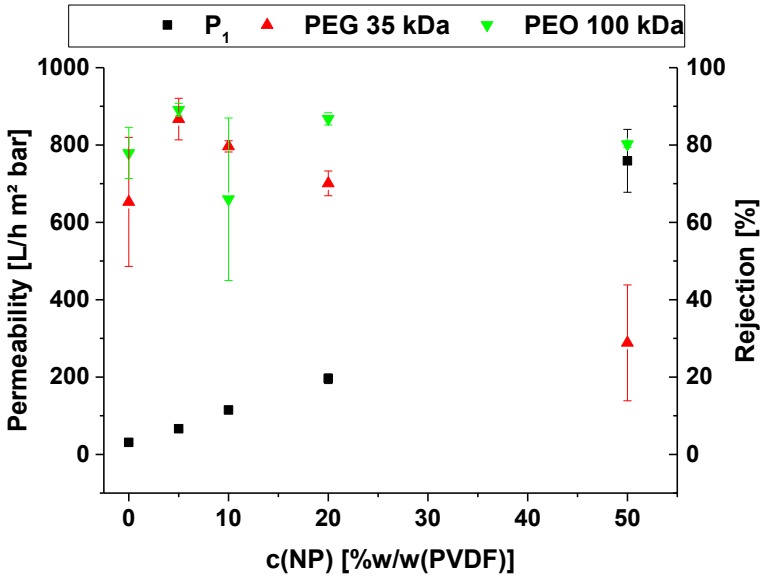

Figure 71 Performance of the membranes with PVP-modified ZnO nanoparticles.

The data in the figure indicates a tradeoff relation between PEG rejection and pure water permeability. The rejection for PEO 100 kDa was not influenced by the nanoparticle

implementation. This indicates that the pore size was increased by the addition of the particles. This applies most likely also to the number of pores. Since the PEO rejection remains constant, one can assert that the pore size is below 10 nm (cf. 2.1).

The morphology of the membranes was characterized by SEM. The pictures of the cross-section are shown in Figure 72.

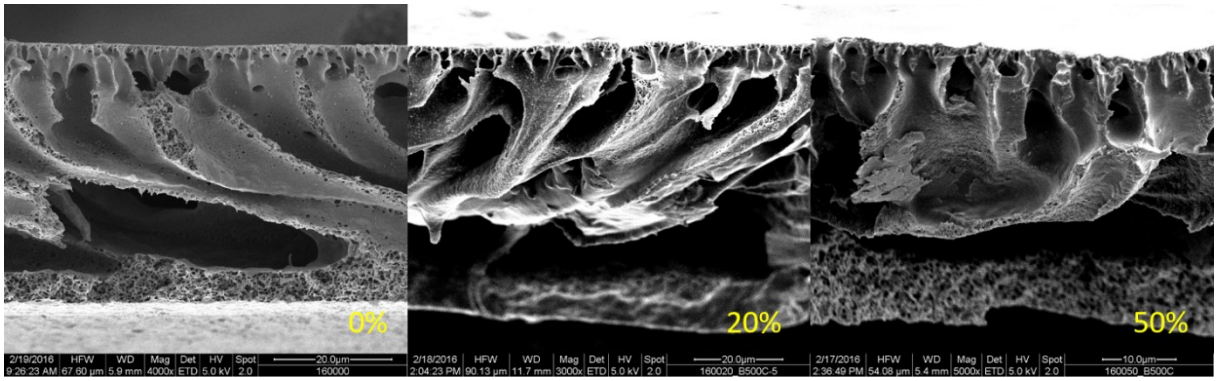

Figure 72 Cross-section of membranes with and without PVP modified particles and no PVP in dope solution Concentration [%w/w(PVDF)] of NP in dope solution indicated in picture. Magnification left to right: 4kx, 3kx and 5kx.

In all pictures, virtually the same morphology is seen, asymmetric with prevalent macro-voids. In two samples the sponge-like bottom layer is not well focused, which was caused by subpar breaking during the sample preparation. In contrast to all other characterized membranes no agglomerates are noticeable in the cross-section in theses samples. To verify the presence or absence of agglomerates the membrane with 50 %w/w(PVDF) modified particles is observed at a higher magnification. The pictures are presented in the following figure.

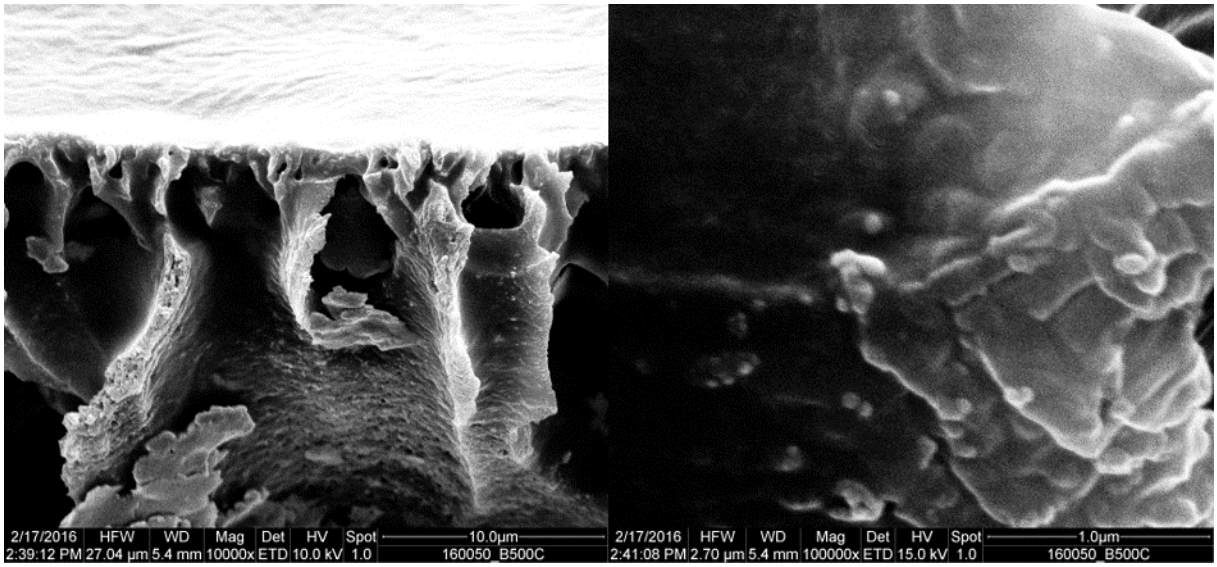

Figure 73 Cross-section of membrane (16% PVDF in dope) and 50%w/w(PVDF) PVP modified particles. Magnification left to right: 10kx and 100kx.

At the higher magnification, it can be seen that the particles are not aggregated and are well integrated into the polymer matrix. This could have been expected, since the calculated Hansen parameter were significantly changed by the modification (cf. 5.1.8.5).

The pictures of the top surface of the membrane are presented in Figure 74.

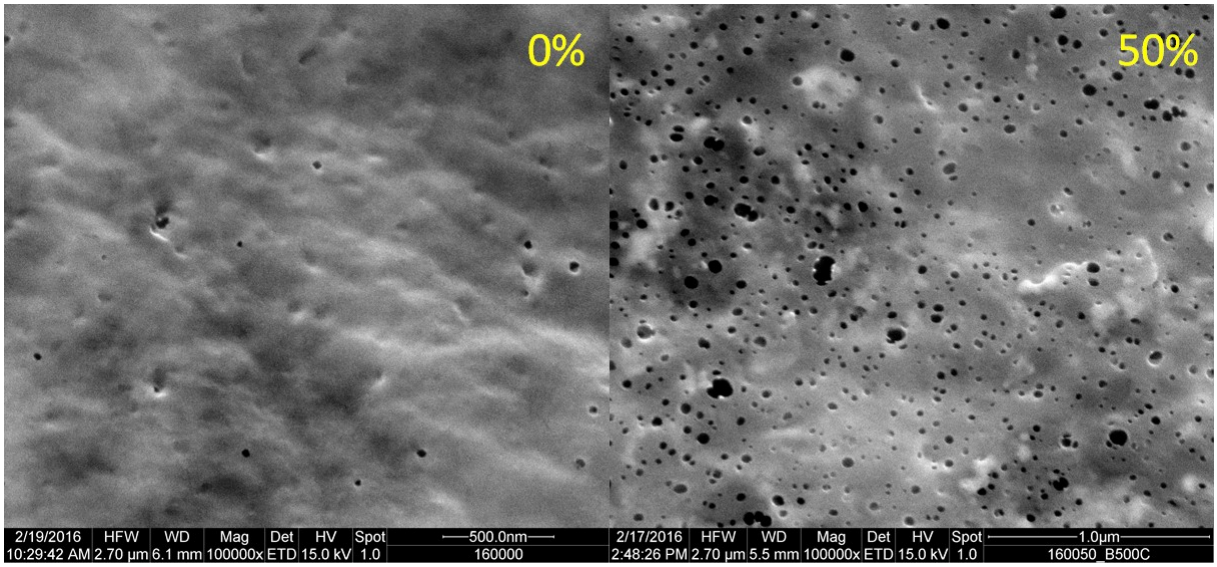

Figure 74 Top surface of membranes (16% PVDF in dope) with and without 50%w/w(PVDF) PVP modified particles. Magnification: 100kx.

By comparing the two pictures in the figure above it can be asserted that the addition of the PVP-modified nanoparticles increased the surface porosity. This phenomenon would be expected as effect of PVP as membrane additive. Therefore, it is reasonable to assume that PVP, which has desorbed from the particles, is causing the formation of pores in the surface. This alone should explain the change in membrane performance, which has been seen in the filtration experiment.

5.2.9. Implementation of modified base polymer

The experiments presented in this part were done to evaluate the influence of the novel base polymer on the nanoparticle integration (cf. 3.2). As in the previous experiment, the dope solution consisted of 16 % base polymer, in this case P(VDF-*co*-AA), and 1 % PVP K-30 in NMP. The addition of pristine zinc oxide nanoparticles was done at the following ratios 3, 5, 10, 15, 20, 25 and 50 %w/w(copolymer). These dope solutions were characterized by rheology. The shear viscosity data is shown in Figure 75.

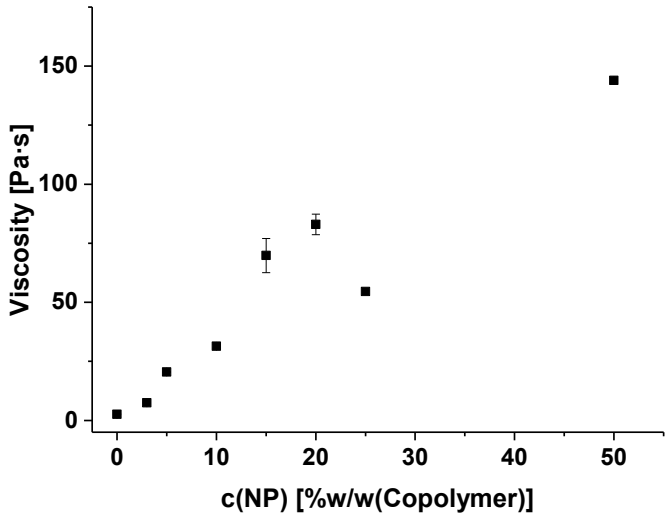

Figure 75 Shear viscosity at 15.9 s^{-1} for dope solutions (16% P(VDF-co-AA) and 1% PVP in NMP) with various amounts of pristine ZnO nanoparticles.

The viscosity of the dope solution without nanoparticles is comparable to the viscosity of the dope solution prepared with PVDF at the same composition (cf. Figure 48). It can be easily seen from the data that the viscosity increases linearly with the addition of the nanoparticles. This trend indicates the absence of agglomerates. However, the dimension of the increase is up to two orders of magnitude larger than measured in the same compositions with PVDF as base polymer. This is a strong indication that the acrylic acid group of the copolymer forms a bond to the zinc oxide particles. Membranes were prepared from these dope solutions to see if this interaction influences the structure and consequentially the performance of the membranes. The preparation was performed according to the standard procedure (cf. 4.3.3). The membranes were characterized by cross-flow filtration of PEG 35 kDa and PEO 100 kDa. The results are presented in Figure 76. The detailed data can be found in the appendix (cf. Table 82).

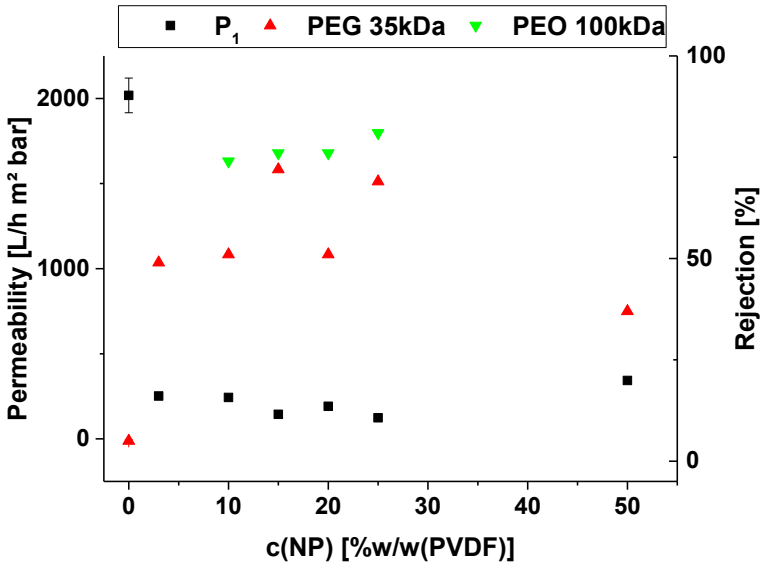

Figure 76 Performance of membranes from novel copolymer with ZnO nanoparticles, coagulated in water.

The membrane without the addition of particles has a performance which exhibits profound differences to the PVDF membrane prepared under the same conditions. The change of base polymer increased the permeability from approx. 800 to 2000 l/h m² bar (cf. Figure 49). The introduction of the zinc oxide nanoparticles reduced the permeability and increased the rejection. This effect is comparable to the behaviour exhibited by PVDF membranes in the blending with zinc oxide nanoparticles (cf. 5.2.5). This is suprising when the vast difference in viscosity is considered. The membrane structure was characterized by SEM to evaluate this finding further. The pictures are presented in Figure 77. The membrane with the highest nanoparticle content and the membrane without particles were chosen for the comparision.

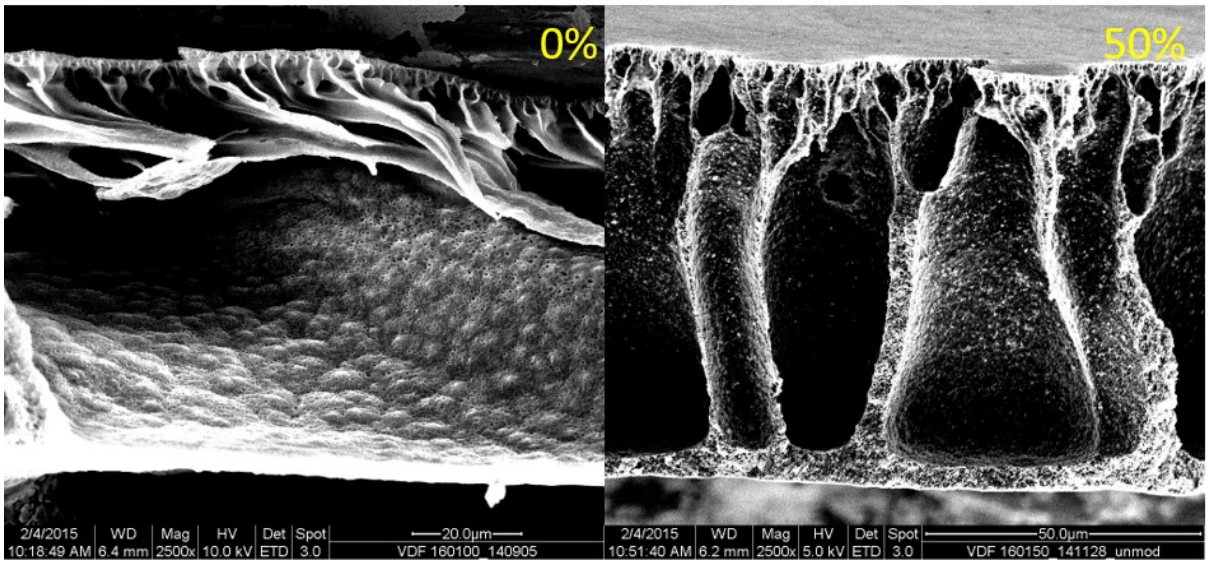

Figure 77 Cross-section of membrane (16% P(VDF-co-AA) and 1% PVP in dope) with and without 50 %w/w(PVDF) pristine particles.

Concentration [%w/w(PVDF)] of NP in dope solution indicated in picture. Magnification: 2500x.

The membrane without nanoparticles shows a higher content of macro-voids in the cross-section morphology compared to the PVDF membrane (cf. Figure 51).

The membrane with the addition of nanoparticles shows a similar morphology as the PVDF membrane (cf. Figure 51). This indicates that the high viscosity is not influencing the cross-section structure in the magnitude that could have been expected. Over the whole structure agglomerates can be seen. This is in direct contradiction to the expectation that the bond between the copolymer and the particles, which has been observed in the viscosity increase, will decrease the agglomeration tendency during the phase separation. The top layers of the respective membranes are presented in Figure 78.

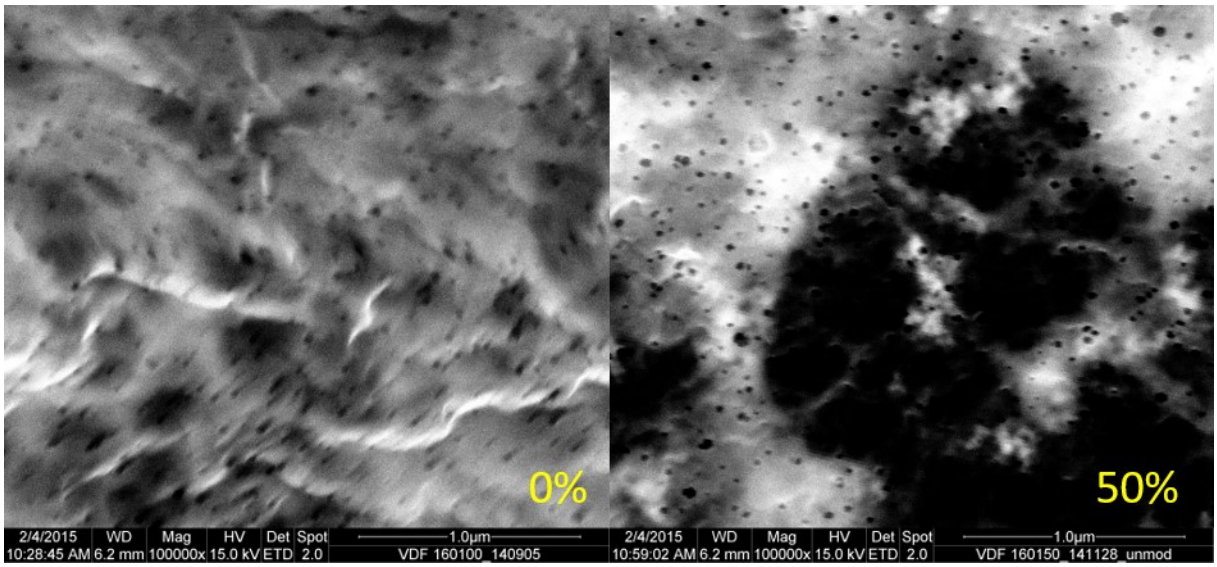

Figure 78 Surface of membrane (16% P(VDF-co-AA) and 1% PVP in dope) with and without 50 %w/w(PVDF) pristine particles.

Concentration [%w/w(PVDF)] of NP in dope solution indicated in picture. Magnification: 100kx.

The picture of the membrane without particles is blurry because of focus problems during the SEM measurement. Despite that, it can be asserted that both membranes have a comparable top layer morphology. The pore number and size seems to be close to identical. The surface of the membrane with nanoparticles displays many bright spots. These are caused by nanoparticles under the polymer layer, which increase the conductivity in these areas. This might indicate that the cause for the change in membrane performance is predominantly the pore blocking by agglomerated under the skin layer. The cross-section below the top surface of the membrane is shown at a higher magnification in Figure 79.

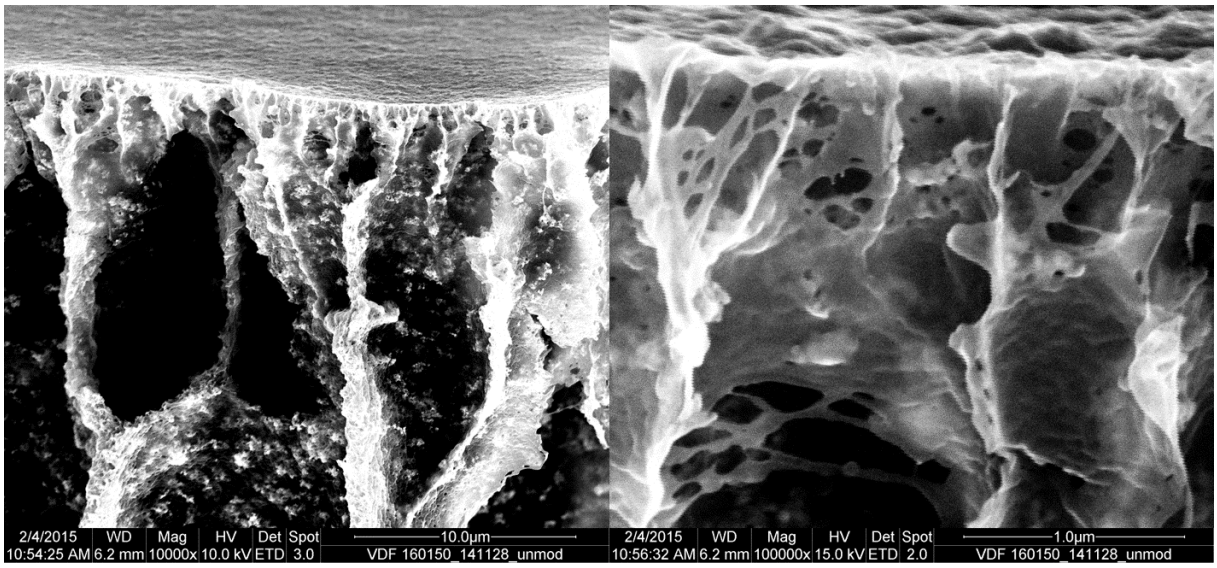

Figure 79 Cross-section of membrane (16% P(VDF-co-AA) and 1% PVP in dope) and 50%w/w(PVDF) pristine particles. Magnification left to right: 10kx and 100kx.

The agglomerated nanoparticles are clearly seen in the morphology of the membrane. The agglomerates are of comparable size to the ones found in PVDF membranes coagulated under comparable conditions (cf. Figure 52). It is interesting that the agglomerates appear to be better integrated into the polymer matrix than seen before in any other sample. This can be interpreted as the effect of the bonding between the copolymer and the zinc oxide nanoparticles.

It was decided to evaluate the performance of the novel base polymer at lower precipitation rate. Therefore, the conditions identified in 5.2.4 were applied to this system. The base polymer concentration was increased to 20 % and the PVP content was kept at 1 %. The evaluated nanoparticle content was decided to be 0, 5, 10, 20 and 50 %w/w(copolymer). The viscosity of these dope solution has been measured and the results are presented in Figure 80.

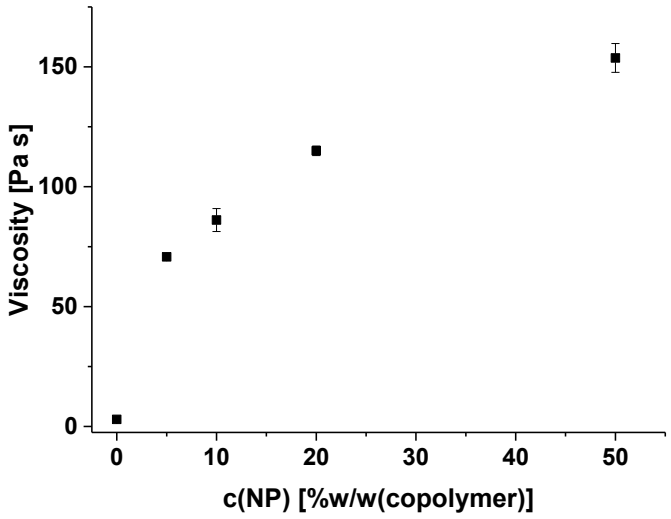

Figure 80 Shear viscosity at 15.9 s^{-1} for dope solutions (20% P(VDF-co-AA) and 1% PVP in NMP) with various amounts of ZnO nanoparticles.

The measured viscosity increase at the higher copolymer concentration is greater than in the previous experiments. The slope of the viscosity increase is virtually linear, which indicated that agglomeration is not present in the dope solution. Membrane were prepared from these dope solutions by precipitation in the soft coagulant. The performance of these membranes was evaluated by the crossflow filtration of PEG 35 kDa and PEO 100 kDa. The results of the filtrations are presented in Figure 81. The detailed results can be found in the appendix (cf. Table 83).

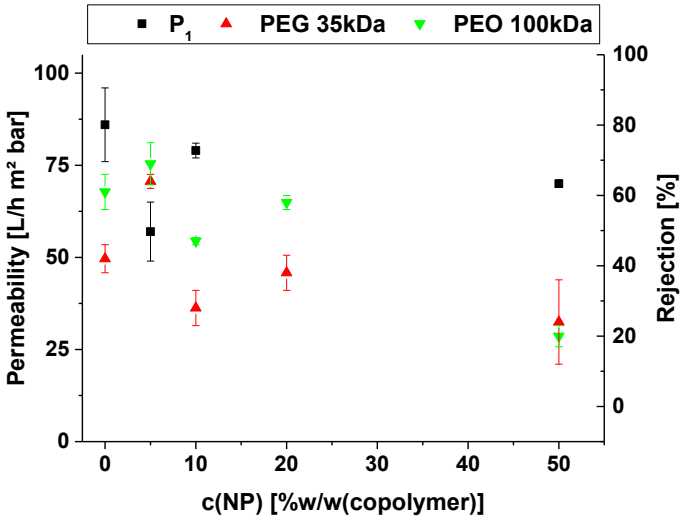

Figure 81 Performance of membranes from novel copolymer with ZnO nanoparticles. coagulated in solvent blend.

The permeability of the membrane without nanoparticles is changed similar to the change seen in the PVDF membrane (cf. Figure 59). The rejection characteristics of the membrane without nanoparticles are improved by the change of coagulant because the previously

discussed influence of acrylic acid is suppressed under these conditions. This yields an overall comparable membrane performance to the PVDF membrane (cf. Figure 59).

The introduction of the nanoparticles causes a decrease in the rejection for both solutes. This could either indicate an increase in pore size or the occurrence of defects in the top layer. The permeability shows a slight decrease with the increase in nanoparticle concentration. This change is small enough to be considered insignificant. SEM pictures were prepared to further evaluate the phenomena leading to the change in performance. The pictures of the cross-section morphology are presented in Figure 81.

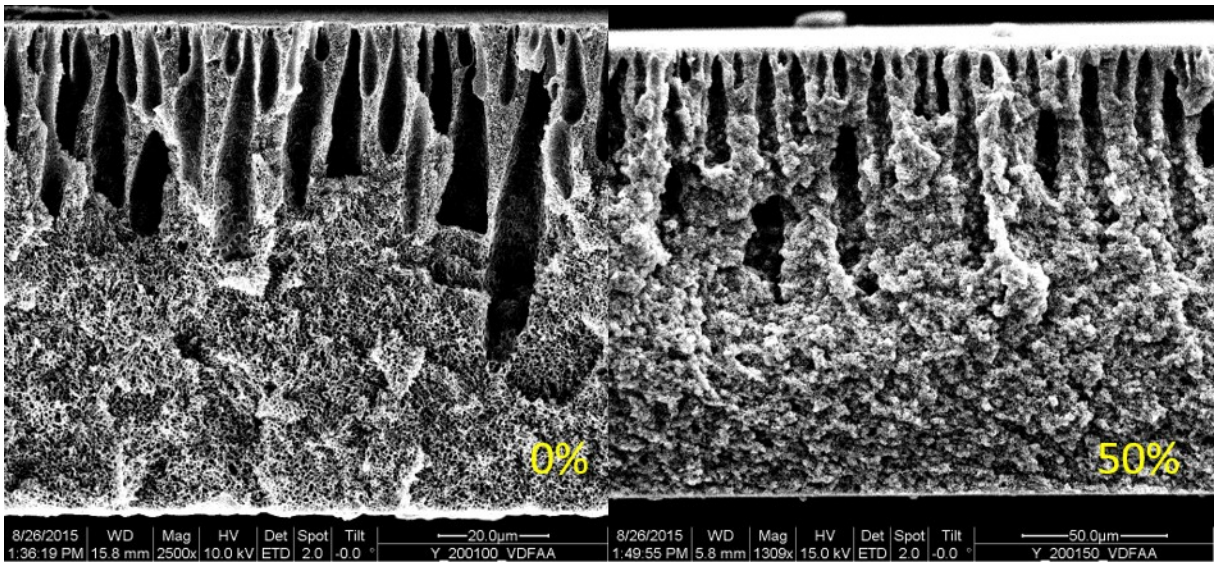

Figure 82 Cross-section of membrane (20% P(VDF-co-AA) and 1% PVP in dope) with and without 50%w/w(PVDF) pristine particles.

Concentration [%w/w(PVDF)] of NP in dope solution indicated in picture. Magnification left to right: 2500x and 1309x.

The membrane without nanoparticles exhibits a pronounced finger structure with a porous substructure. The finger structure is more distinct than in the PVDF membrane prepared under the same conditions (cf. Figure 61). Agglomerates cannot be found in the structure at this magnification. The cross-section of the membrane with 50 %w/w(copolymer) zinc oxide nanoparticles is presented at higher magnification in Figure 83.

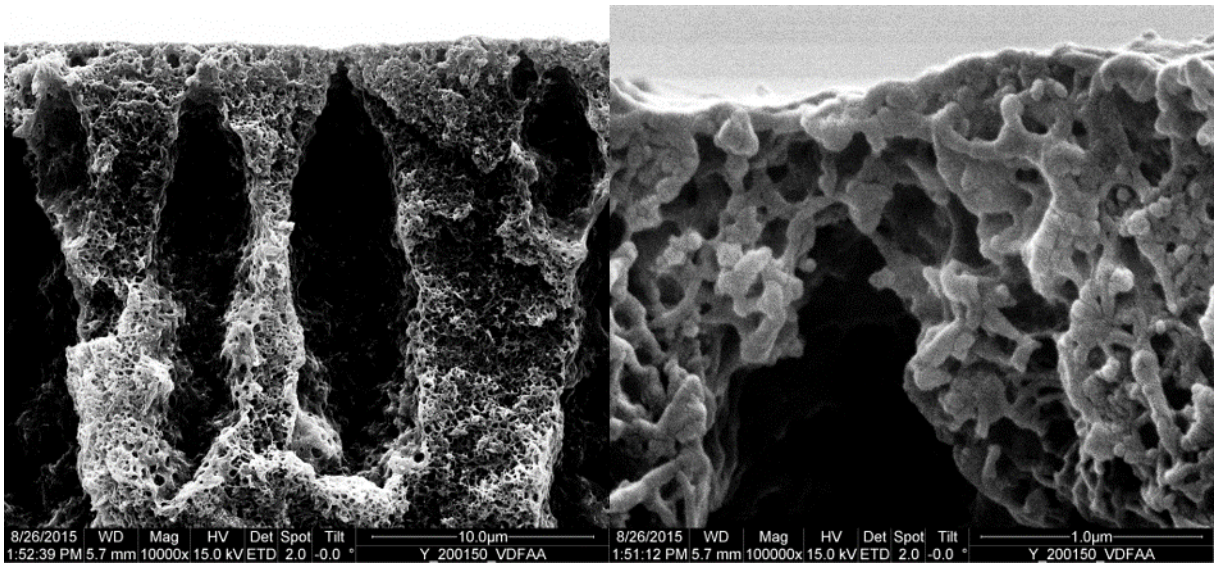

Figure 83 Cross-section of membrane (20% P(VDF-co-AA) and 1% PVP in dope) and 50%w/w(copolymer) pristine particles. Magnification left to right: 10kx and 100kx.

Both pictures show no indications of agglomeration of the particles. The shape of the particles in the membrane structure can only be recognized at the magnification of 100,000. This is a manifestation of good integration into the polymer matrix. In Figure 84, the top surface of the membranes with and without nanoparticles are presented.

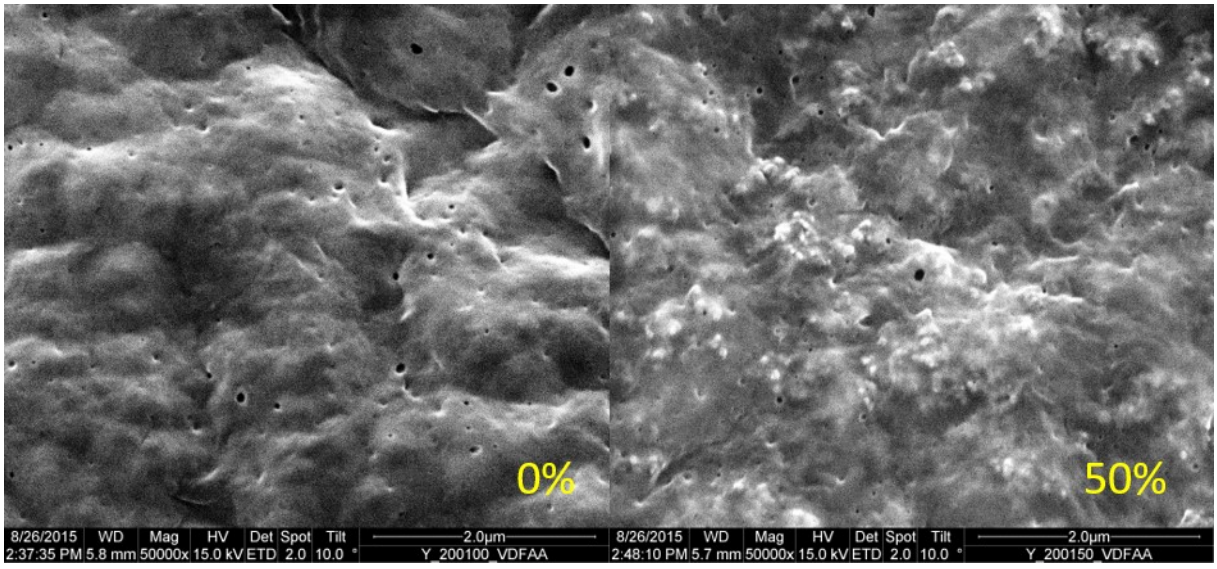

Figure 84 Surface of membrane (20% P(VDF-co-AA) and 1% PVP in dope) with and without 50 %w/w(base polymer) pristine particles. Magnification: 50kx.

Both membranes have a comparable surface structure with low pore density. The most distinct difference is that particles are integrated into the skin layer of the membrane with 50 %w/w(P(VDF-co-AA)) nanoparticles. There are no indications of defects discernible around the particles.

5.2.10. Mechanical characterization

The morphology of the membrane is one of the greatest influences on the mechanical characterization since a high content of macro-void decreases the stability under mechanical stress. It was decided to apply the conditions identified in 5.2.4 to minimize the emerging of this effect. This should yield a more homogenous structure over all samples and ensure that any change in mechanical characteristics can be ascribed to the influence of the employed nanoparticles. The membranes were prepared from 20 % base polymer and 1 % PVP K-30 in NMP and precipitated in a coagulation bath of NMP and water in a ratio of 50 %Vol/50 %Vol. The only exception was the membrane with the PVP-modified particles. The addition of PVP was omitted in this dope solution (cf. 5.2.8). The nanoparticle content was set to 50 %w/w(base polymer) to observe a pronounced effect in the measurement. Samples prepared were from these membranes and the characterization was conducted as described in 4.5.4. The mean values and standard deviation of the results for each membrane type are presented in Table 46.

Table 46 Results of the mechanical characterization for various membranes.

base polymer	c(NP) in dope [%w/w(base polymer)]	NP type	tensile strength [N]	SD	elongation at break [%]	SD	E [N/mm²]	SD
PVDF	0	none	3.66	0.7	43.0	10.5	1.03	0.27
PVDF	50	pristine	4.45	0.3	39.4	6.5	1.75	0.14
PVDF	50	PVP modified	4.12	0.4	63.5	26.8	1.01	0.13
P(VDF-*co*-AA)	0	none	4.34	0.3	33.2	28.5	1.65	0.25
P(VDF-*co*-AA)	50	pristine	7.42	0.9	14.2	12.8	2.47	0.31

In the data above, it is apparent that both base polymers without particles show a comparable tensile strength and elongation at break. The Young modulus is bigger for the membrane prepared from P(VDF-*co*-AA), which might be traced back to intermolecular binding between the acrylic acid groups. The incorporation of pristine particles increases the tensile strength and Young modulus in both membrane types. The effect is greater for the membranes prepared from P(VDF-*co*-AA). This is most likely caused by the better integration, which was previously seen in this sample type. It also indicated that at least some nanoparticles were integrated into the PVDF matrix of the membrane, while no indication could be found in the SEM picture. The elongation at break was not influenced in the case of the PVDF membranes. In the P(VDF-*co*-AA) membrane the elongation at break was decreased by the introduction of

the nanoparticles. This can be explained by the bonding between the base polymer and the nanoparticles, which increased the rigidity of the membrane. The PVP modified nanoparticles did not alter the tensile strength nor the Young modulus. Both values are virtually identical to the membrane without particles. The elongation at break was significantly increased by the introduction of the modified particles. This could imply that the well-integrated particles create a structure that is able to endure more strain without breaking.[62]

6. Discussion

6.1. Nanoparticle modification

6.1.1. Evaluation of sonication conditions and particle size

The SEM picture revealed that the pristine particles exhibit a polydisperse size distribution (cf. Figure 15). This is reflected in the DLS measurements by the PDI, which exhibited values in excess of 0.5. It is recommended to use the modus of the size distribution under these conditions to compensate for the particle size dependency of the Rayleigh scattering.[24,63] The intensity of the scatter light is proportional to the particle size by the sixth power. Therefore, larger size particles will be overrepresented in the mean diameter of the particle size distribution. This was applied in the measurement procedure (cf. 4.6.1). While this improves the accuracy of the size measurement, it can be asserted from the observed polydispersity that the result will only represent the averaged particle size. The measured hydrodynamic diameter should be viewed as quality attribute of the dispersion and not as representation of the actual particle size for the previously stated reason.

In the evaluation (cf. 5.1.1) of the sonication, it was found that stable dispersions are obtained at a sonication time between 5 and 25 minutes. This can be explained in the following way. If the sonication is below 5 minutes, the mechanical stress is insufficient to break up agglomerates and distribute the particles in the solvent cage. If the sonication time exceeds 25 minutes, the dispersion quality is deteriorated by the excessive collisions between the particles which leads to the formation of aggregates. Based on this result a sonication time of 10 minutes was chosen for the dispersion procedure as described in 4.1. It can be assert that these conditions are sufficient to obtain stable dispersions in good solvents as demonstrated for water. No impact of the concentration was found on the dispersion quality.

6.1.2. Acetic acid modification

A low mass retrieval was found in the modification of the zinc oxide nanoparticles with acetic acid (cf. Table 12). The TGA confirmed that some acetic acid molecules were absorbed to the particle surface (cf. Table 16). The absorption band of acetic acid are easily seen in the infrared spectrum of the modified particles (cf. Figure 21). The binding mode of acetic acid can be determined from the infrared spectrum. In the literature the following binding modes for acetic acid on metal oxides with the corresponding vibrations are discussed. [64]

Table 47 Acetic acid binding modes to zinc oxide.[64]

	unidentate	bidentate	bridging
	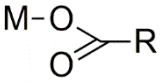	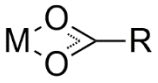	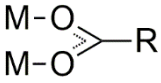
$\nu_{C=O}$ [cm^{-1}]	1577	1550	1600
ν_{C-O} [cm^{-1}	1425	1456	1441
$\Delta\nu$ [cm^{-1}]	152	94	159

When the wavenumbers in the table are compared to the current measurement, no direct match can be found. The difference between the absorption bands in the measurement is approx. 182 cm^{-1} and that value exceeds the differences of all presented binding modes. As a reference the unbound carboxylate is considered which exhibits a difference between the two vibrations more of more than 200 cm^{-1}. This value exceeds the difference found in the present samples. A reasonable explanation for the difference between the result for the acetic acid modified particles and the literature values is that the current sample has unbound acetate molecules in addition to the bound ones. This superposition of the infrared absorption of both species may be the reason for the obtained value which lies in between the value for the bound and unbound carboxylate.

The mass retrieval was lower than for the modification with trifluoroacetic acid at comparable pH value and lower than oxalic acid. The same can be asserted for the surface coverage lower than for the other modification agents. Both aspects might be caused by the ability of the weak acid to form a buffer system and the consequential stability of the pH value. The surface charge of oxidic particle is generally dependent on the pH value of the ambient solution. The zeta potential of zinc oxide particles has been examined by Berg et al. as shown in Figure 85.[65]

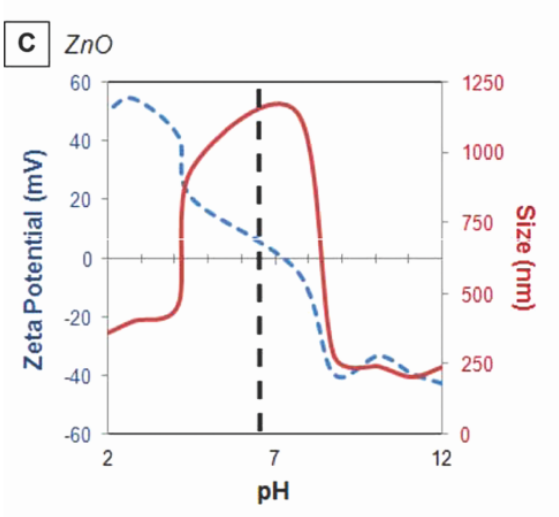

Figure 85 Zeta potential of zinc oxide NP in dependence of the pH.[65]

In the figure, the zeta potential of zinc oxide nanoparticles decreases with increasing pH. The isoelectric point is indicated by the dashed line and has a value of approx. 7.1. The zinc oxide particles exhibit a strong positive surface charge at low pH values. Therefore, the also positively charged oxonium ions are repulsed and the solvolysis is kinetically hindered. Since acetic acid is a weak acid, the pH values can be assumed to be generally higher. Therefore, the charge of the particle is lower than for the other carboxylic acids. Under these conditions, the oxonium ions can approach the particle and react with the zinc oxide as shown in R-1 (cf. 2.3.1). The solvolysis reaction consumes the oxonium ions and the zinc oxide from the nanoparticle. The reaction products water and zinc ions remain in solution. The removal of oxonium ions from the solutions causes in the case of weak acids the deprotonation of more acid molecules and therefore an increase in the concentration of the conjugated base. This can lead to the formation of a buffer system with a pH value close to the pK_a of the acid. The pH increase reduces the zeta potential of the particle. This leads to a reduction of the repulsion of oxonium ions and the kinetic hindrance of the solvolysis reaction. This is a possible explanation for the low mass retrieval in this modification with acetic acid.

The lower surface coverage of the particles can also be explained by the same phenomenon. In the literature Sakohara et al.[64] discuss the bonding from the acetate form of the acid to the metal atom of zinc oxide. This indicates that the negatively charged acetate needs to get into contact with the particle. At low pH value the particle is positively charged and the attraction to the acetate is high. If a buffer is formed by the previously mentioned mechanism, the zeta potential of the particle and the attraction is also reduced. Resulting in a decrease of the surface coverage.

The zeta potential of the acetic acid modified particles was measured (cf. Table 19). The value of the modified particles is virtually identical to the value of the pristine particles. The reason for this is most likely the low surface coverage of 21.7 $\%_{monolayer}$ (cf. Table 16). The Hansen parameters of the modified particles were determined despite low surface coverage. The result of the calculation is presented in Table 48 with the data for the pristine particles as reference.

Table 48 Comparison of Hansen Parameter analysis of pristine and Ac modified ZnO NP.

sample	pH at modification	surface coverage	δ_D	δ_P	δ_H	δ_{Tot}	R_o	fit
	[-]	[$\%_{monolayer}$]	[$MPa^{1/2}$]	[$MPa^{1/2}$]	[$MPa^{1/2}$]	[$MPa^{1/2}$]	[-]	[-]
pristine ZnO	n.a.	0	15.8	7.9	16.8	24.4	10	1
Ac mod	5	13.5	11.9	15.2	11.4	22.4	12.7	0.34

The HSP analysis of the modified particles exhibits a very low fit. This originates from solvents being designated wrong in and out by the algorithm of the program. A differentiated assessment of these solvents is conducted to further evaluate the quality of the analysis. Their respective HSP and RED are displayed in Table 49.

Table 49 Wrong in and out solvents for analysis of Ac modified NP with RED.

	Wrong In				
	δ_D	δ_P	δ_H	rating	RED
	[$MPa^{1/2}$]	[$MPa^{1/2}$]	[$MPa^{1/2}$]	[-]	[-]
DMF	17.4	13.7	11.3	6	0.87
MEK	16	9	5.1	6	0.95
2-Butanol	15.8	5.7	14.5	6	0.99
	Wrong out				
	δ_D	δ_P	δ_H	rating	RED
	[$MPa^{1/2}$]	[$MPa^{1/2}$]	[$MPa^{1/2}$]	[-]	[-]
THF	16.8	5.7	8	2	1.1
EtAc	15.8	5.3	7.2	2	1.04
NMP	18	12.3	7.2	1	1.04
EG	17	11	26	1	1.44

Ethylene glycol has a RED of 1.44 which is far from a compatible solvent. This might indicate that the stability in that ethylene glycol is a consequence of the (cf. 6.1.4). The RED values of the other solvents are very close to 1 and just slightly on the wrong side of the interaction sphere. Therefore, the calculation was repeated but without ethylene glycol in the dataset. This altered the result as displayed in Figure 86. Only solvents with a rating of 1 were considered as inside solvents for the calculation.

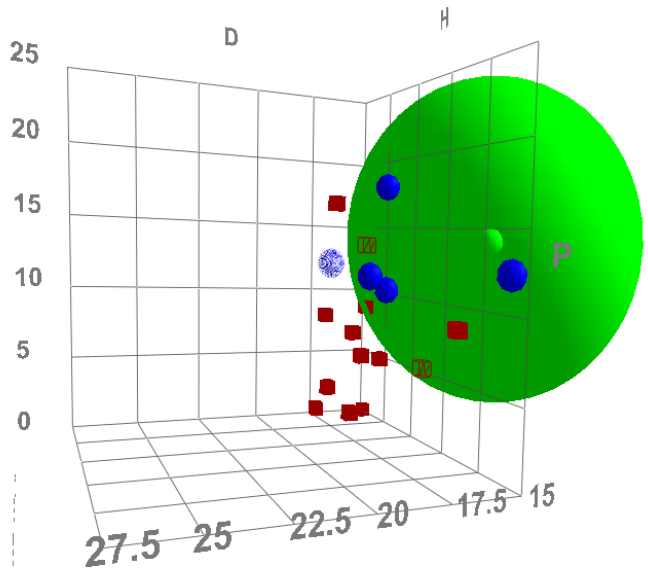

HSPiP summary

In = 5; Out = 13; Total = 18
δ_D = 12.2; δ_D =14.3; δ_H =12.2
δ_{Tot} = 22.4
R_0= 11.4
Fit= 0.771
Core= ±[0.60, 1.55, 0.80]
Wrong In= 2
Wrong Out= 1

Figure 86 Refined HSP analysis of Ac modified NP.

The exclusion of ethylene glycol greatly improved the fit to 0.771 which is an acceptable value. The solubility parameters are only slightly changed while the number of wrongly fitted solvents is reduced. The following table shows the wrong in and out solvents of the refined calculation in detail.

Table 50 Wrong in and out solvents for refined analysis of Ac modified NP with RED.

Wrong In					
	δ_D [MPa$^{1/2}$]	**δ_P [MPa$^{1/2}$]**	**δ_H [MPa$^{1/2}$]**	**rating**	**RED**
DMF	17.4	13.7	11.3	6	0.91
2-Butanol	15.8	5.7	14.5	6	1.00
Wrong out					
	δ_D [MPa$^{1/2}$]	**δ_P [MPa$^{1/2}$]**	**δ_H [MPa$^{1/2}$]**	**rating**	**RED**
NMP	18	12.3	7.2	1	1.12

MEK, tetrahydrofuran and ethyl acetate were removed from the list of misclassified solvents by the recalculation. The RED value for DMF and 2-Butanol shifted closer to 1 while the RED value for NMP increased. 2-Butanol is not neighboring any good solvents. This indicates that the solvent was just falsely assigned by the fitting algorithm. DMF and NMP are very close to each other in the Hansen space. Therefore, a similar behavior should be expected. The stability of the modified particles in NMP is in the direct agreement with the literature finding.[13] This makes the possibility of a false positive result for this solvent unlikely. A possible explanation for the different stability in DMF is that the amount of immobilized acetic acid is too low to

sufficiently stabilize the particles. This makes sense since the surface coverage is only 21.7%$_{monolayer}$ (cf. Table 16).

When the modified particles were washed with NMP at 60 °C and then characterized by TGA, it was found that all acetic acid is removed (cf. Table 17). This seems to contradict the stability of the particles in NMP. The only difference between the experiments is the temperature. This could indicate that the temperature increase leads to the dissociation of the bond. Therefore, it could be that in the dispersions the modification is still present because these were stored at room temperature. The instability of the bond agrees with some literature findings although in this publication more than three washing cycles at room temperature were necessary to remove the acetic acid modification.[49] Therefore, the assumption that the bound is more stable under ambient conditions is partially supported.

6.1.3. Trifluoroacetic acid modification

The modification of zinc oxide nanoparticles with trifluoroacetic acid was studied under various conditions. In all cases, the absorption bands of trifluoroacetic acid were seen in the infrared spectrum of the modified particles (cf. Figure 19). The absorption bands of the carbonyl function in these samples are displayed in Table 51. The respective bands of pure trifluoroacetic acid are displayed as reference.

Table 51 Comparison of the carbonyl group absorption in different samples. Ratio of TFA/ZnO and pH value during modification are given in the sample designation.

	deprotonated TFA[66]	100% TFA/ZnO; pH1	200% TFA/ZnO; pH 7	200% TFA/ZnO; pH 10
$\nu_{C=O}$ [cm^{-1}]	1783	1667	1678	1671
ν_{C-O} [cm^{-1}]	1447	1504	1505	1505
$\Delta\nu$ [cm^{-1}]	336	163	173	166

The wavenumber of the absorption of all modified particles are in the same range which indicates that all samples have a similar binding mode. The difference between the two absorptions is closest to bridging mode (cf. Table 47). The reference exhibits different vibration compared to the modified samples. Therefore, it can be asserted that no unbound TFA is present in the samples. Since the modified samples exhibit virtually identical vibrations, it can be concluded that the binding mode is independent of the pH value which was present during the modification procedure.

In the experiments, it was seen that the mass retrieval of modification procedure is reduced by the solvolysis reaction R-1 (cf. 2.3.1). The evidence for this is the decreases in mass retrieval that was observed with decreasing pH value (cf. Table 10). This was further proven by the increase in mass retrieval which was the consequence of rising the pH value to neutral (Table 11). The solvolysis might be slowed down by the zeta potential of the zinc oxide at low pH as previously discussed (cf. 6.1.2).

While the mass retrieval was improved by the pH value increase, a detrimental effect was seen for the surface coverage (cf. Table 14). In the experiments, it was seen that the surface coverage decreased with the increase in pH value. The reason for this behavior might be caused by the effect of the pH value on the zeta potential of the particle as previously discussed (cf. 6.1.2). The surface coverage also increased with the increase of the TFA/ZnO. This is most likely caused by the higher effective concentration. While the modification agent TFA was present on all modified samples, the zeta potentials of these showed no significant difference compared to the pristine particles. The zeta potentials are compared in Figure 87.

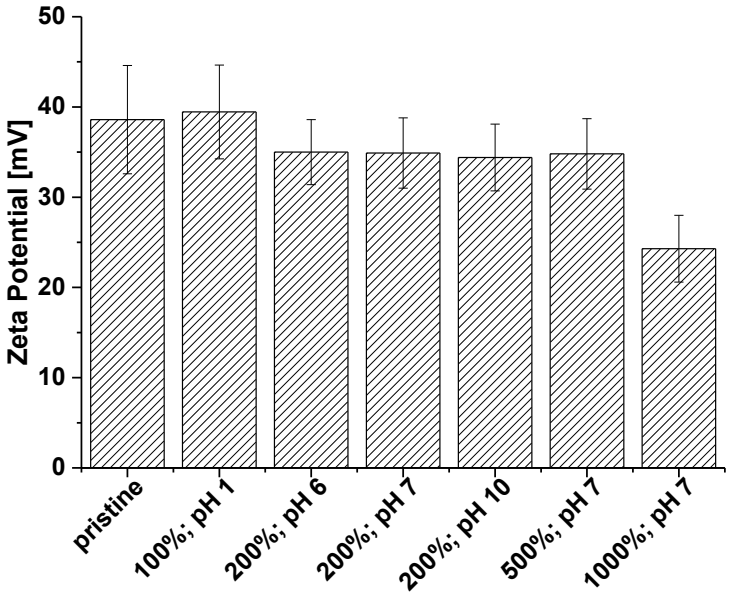

Figure 87 Zeta potential of TFA modified ZnO NP in ultrapure water at pH 6.8. Ratio (TFA/ZnO) in modification and pH value at modification given on x-axis.

Only the sample modified with 1000 % TFA/ZnO at a pH value of 7 exhibits a deviating zeta potential. The reason for that is not clear since the surface coverage is smaller than in other samples (cf. Table 14). Since other samples modified at the same pH value show no change in zeta potential, the pH value can be omitted as reason for the change.

The comparison of the available HSP analyses results is shown in Table 52. The result for the pristine particles is included as reference.

Table 52 HSP comparison of TFA modified particles.

ratio (TFA/ZnO) [%]	pH at modification [-]	surface coverage [%monolayer]	δ_D [MPa$^{1/2}$]	δ_P [MPa$^{1/2}$]	δ_H [MPa$^{1/2}$]	δ_{Tot} [MPa$^{1/2}$]	R_o [-]	fit [-]
pristine	n.a.	0	15.8	7.9	16.8	24.4	10.0	1.00
100	1.00	24.3	15.9	7.8	16.9	24.4	10.0	1.00
200	6.30	10.3	23.3	5.5	17.3	29.6	16.4	0.21
200	7.0	4.1	17.6	6.0	16.3	24.8	11.0	1.00
200	10.0	1.6	15.7	3.6	16.8	23.2	11.9	0.74
500	7.0	12.8	20.9	6.4	13.2	25.5	10.2	0.51

The comparison shows no significant change in the Hansen parameter for the modified particles. There is also no apparent relation between the surface coverage and the solubility parameter in the data. This is not unexpected since the surface coverage remains low. The particles with the highest and third highest surface coverage 200 % at pH 0.7 and 1000 % at pH 7 were not analyzed. In the case of the first not enough particles were available since the mass retrieval of the modification is around 20 %. In the case of the later it was not done for time reasons. Nevertheless, this should not dispute the previous statement since no trend was found in the data.

As a résumé for the modification of nanoparticles with trifluoroacetic acid it can be concluded that only a partial success was achieved. While the problem of the solvolysis reaction could be solved, the realized surface coverages were not satisfactory. This is also consequently the reason for the lack of influence on the particle properties as seen in the zeta potential and Hansen parameter.

6.1.4. Oxalic acid modification

Oxalic acid shows a high binding tendency to the zinc oxide particle, which was seen in the uptake that exceeded the estimated monolayer adsorption. There are indications of an intermolecular binding between the oxalic acid molecules. This can be seen in the infrared spectrum (cf. Figure 17), the thermogravimetric analysis (cf. Table 16) and the mass retrieval of the modification (cf. Table 12). This leads to the assumption that the formation of the oxalic acid dimers in combination with the bonding to the zinc oxide particles creates an intra-particular bonding. Figure 88 displays this binding between nanoparticles.

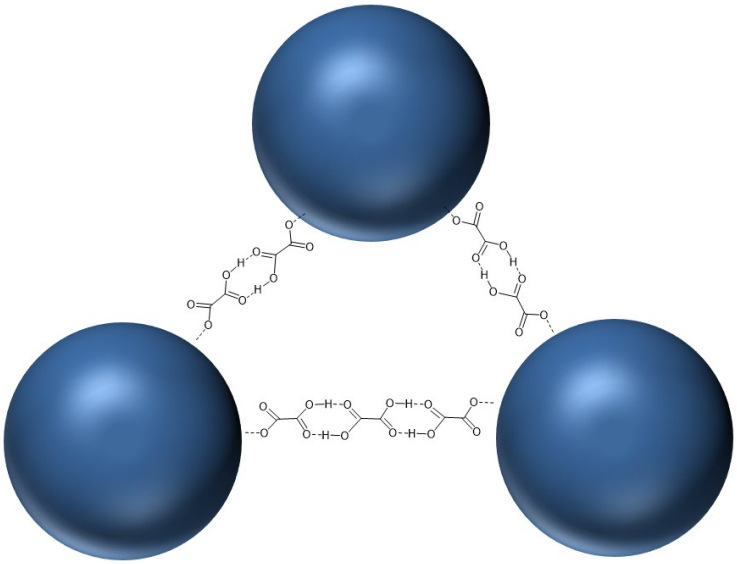

Figure 88 Exemplary inter-particular binding by oxalic acid dimers and trimers.

This explains why the oxalic acid modified particles are not dispersible in all solvents except for ethylene glycol (cf. Table 22). This also raises the question if this is solely caused by the viscosity of ethylene glycol. Since methanol and ethanol, which were also evaluated, have very similar solubility parameter they should be able to stabilize the modified particle. But the particles were not dispersible in said compounds. Therefore, it is likely that the dispersibility in ethylene glycol is just a result of the higher viscosity.

The case, that no solvolysis was found during the modification, can be explained in the following way. First, oxalic acid is a stronger acid than acetic acid. This can be concluded by comparing the pKa values. Oxalic acid exhibits two acid dissociation constants: $pKa_1 = 1.4$ for the dissociation of the first carboxylic group and $pka_2 = 4.4$ for the second group.[67] While the pKa of acetic acid is 4.76. Therefore, it is possible that the pH is lowered sufficiently to inhibit the mechanism which was explained in 6.1.2. Second, it was concluded that oxalic acid formed intermolecular bonds which caused the particles to aggregate and sediment. This removed the zinc oxide from the bulk of the solution and prevented the solvolysis reaction.

6.1.5. Polyvinylpyrrolidone modification

Two modification procedures were used for the modification of particles with PVP: first the *standard* procedure and secondly the *codispersion* procedure. Both are described in detail in 5.1.4.3. Of these two lead the modification by *codispersion* to the higher amount of PVP attached to the surface (cf. Table 15). This is most likely a result of the higher effective PVP concentration in the *codispersion* method. This resulted from the volume limitation of the largest available rosette cell. The effect of different surface coverage is also seen in the

absorption of these samples in the infrared spectra (cf. Figure 20). Both modification procedures have similar mass retrievals with the *codispersion* procedure giving a slightly lower retrieval. This is caused by some particles which were not segregated by centrifugation. This did not occur in the particles modified with the standard procedure. For both procedures, a reduction in mass retrieval is caused by instrument-based losses. Both particle types show similar dispersibility during the HSP analysis. A short overview over selected solvents is presented in Table 53. The RED to PVP is given for each solvent as reference of compatibility.

Table 53 Comparison of dispersible solvents for pristine and PVP modified ZnO particles.

		pristine	*standard* modification	*codispersion* procedure	RED to PVP
No.	**solvent**	**rating**	**rating**	**rating**	**[-]**
7	Acetone	6	6	6	1.09
10	ACN	6	2	6	1.20
93	2-Butanol	2	1	2	0.84
156	Chloroform	6	3	3	1.12
285	DMAc	2	1	2	0.88
297	DMF	1	1	2	0.76
303	DMSO	6	6	2	0.79
306	1,4-Dioxane	3	6	6	1.03
325	Ethanol	1	2	4	0.68
328	EtAc	2	6	6	1.12
417	Hexane	6	6	6	1.60
456	MeOH	1	1	2	0.78
481	MEK	4	1	6	1.15
521	NMP	6	1	1	0.92
524	DCM	6	3	3	1.01
617	THF	2	2	6	1.01
697	*p*-Xylene	6	6	6	1.40

The PVP seems to stabilize the particles in chloroform, DCM, DMSO and NMP. And the opposite seems to happen for 1,4-dioxane, ethyl acetate, MEK and THF. This correlates with the solubility of PVP in those solvents as indicated by the RED. The RED was calculated using literature data for PVP (δ_D = 21.4 $MPa^{1/2}$; δ_P = 11.6 $MPa^{1/2}$; δ_H = 21.6 $MPa^{1/2}$). [26] Between the two samples it can be asserted that the *codispersion* sample complies better with the behavior of PVP. This can be explained by the higher surface coverage of this sample (cf. Table 15). This

is reinforced by the calculated Hansen parameter for these samples which are shown in Table 54.

Table 54 Comparison of HSP for PVP modified particles.

	δ_D [MPa$^{1/2}$]	δ_P [MPa$^{1/2}$]	δ_H [MPa$^{1/2}$]	δ_{Tot} [MPa$^{1/2}$]	R_o [-]	fit [-]
pristine	15.8	7.9	16.8	24.4	10.0	1.00
***standard* modification**	14.0	11.9	16.0	24.4	11.9	0.49
***codispersion* procedure**	19.4	14.3	16.4	29.2	11.3	0.83
PVP[26]	21.4	11.6	21.6	32.5	17.3	n.a.

The calculated Hansen parameters for the particles modified by the *codispersion* procedure are close to the parameter of pure PVP. The sample modified by the *standard* procedure is further away from the parameter of PVP. This is the direct consequence of the respective surface coverage. Since the Hansen parameter change is more pronounced for the samples modified by the *codispersion* procedure, this sample was selected for all following experiment. The modification with PVP lowered the zeta potential of the particle from 38.6 ± 6.0 mV to 16.7 ± 2.7 mV (cf. Table 19). This can be explained by the shielding of the surface charge because of the PVP adsorption. When the modified particles were washed with NMP at 60 °C and then characterized by TGA, partial stability was seen in the TGA (Table 17) and infrared spectra (Figure 21). Approximately 32 % of the initial PVP modification remained on the particles. This is a much better stability than what was seen in the acetic acid modification. The reason for the better stability of the modification with the polymer PVP is most likely the greater number of binding sites per molecule compared to the previously used agents.

6.2. Membranes

6.2.1. Evaluation of casting conditions

It has been shown that the climate box can reliably maintain a low humidity for the membrane preparation (cf. Figure 34). Despite the low humidity, a constant mass decrease was found for the dope solution films during the evaluation of the effect of active climate box. While only a small increase was found in the reference experiment with the deactivated climate box (cf. Figure 35). This observation correlates with the expected adsorption of water from the ambient air. In the former experiment, the effect of the evaporation of the dope solvent NMP can be seen. The solvent has a high boiling point of 202 °C and a corresponding low vapor pressure at room temperature.[18] Therefore, one could expect a virtually nonexistent mass loss by evaporation. However, the air is exchanged constantly by the dry air purge. And this removes the solvent vapor over the dope film yielding more solvent evaporation. The resulting mass loss is higher than anticipated.

A similar explanation can be found for the stable mass in the experiment without the dry air purge. Since NMP is a hydrophilic compound one could expect a constant mass increase which is not observed. This can be explained by the lack of air convection in the climate box without the dry air purge. The solvent absorbs the water from the vapor phase until an equilibrium is reached and the water vapor pressure is decreased accordingly. Since the vapor phase is not renewed by air convection, the equilibrium remains stable and no further mass increase is observed.

The question remains how much influence can be expected by the exposure of the dope film to the ambient air during the transfer into the coagulation bath. This can be evaluated by comparing the residence time of the film inside of the climate box with the transfer time into the coagulation bath. The speed of the casting knife is set to 5 mm/s for the membrane casting (cf. 4.3.3). The distance, which is covered by the casting knife during the preparation, was measured to be 33 cm. This determines that the dope film will be exposed to the air for 66 seconds during the casting. The total time inside of the climate box is obtained by adding 30 seconds for the handling to the casting time. This adds up to a total time of 93 seconds. The transfer of the dope film into the coagulation bath requires less than five seconds. It can be concluded from these values that the dope film will spend less than 5 % of the time before coagulation outside of the climate box. Therefore, it can be stated that the predominant influence of ambient conditions must occur in the climate box.

It has been shown that utilization of the climate box leads to stable, reproducible conditions for the membrane preparation. The absorption of ambient water by the dope solution film can be successfully suppressed by this strategy. The influence of ambient conditions on the membrane preparation can therefore be omitted in all membranes in this work.

6.2.2. Development of base membrane

Two suitable dope solution formulations were found: 16 %PVDF with 1 % PVP K-30 and 17.5 % PVDF with 1 % PVP K-30. Both produce a membrane with a virtually identical cross-section structure. The performance difference between both follows the normal trade-off relation between permeability and rejection. The increase in polymer concentration decreased the permeability P_0 from 1134 to 912 l/h m² bar while improving the MWCO from 107 to 80 kDa. The lower concentration formulation will be used for the nanoparticle experiments. The higher concentration formulation will be used for the up-scaling experiments.

6.2.3. Transfer to upscale-able system

The dope solution formulation with the higher polymer concentration was selected as basis for the transfer to the upscale-able system. The formulation contained 17.5 % PVDF and 1 % PVP K-30 in NMP. There were two obstacles to overcome for the successful transfer. First, the membrane preparation needed to be transferred from the glass support on to a nonwoven support. Secondly, the solvent NMP needed to be substituted for DMAc.

When the original formulation was casted on the nonwoven support, the dope penetrated greatly into the nonwoven structure. The final membrane showed spots where the nonwoven reached into the skin layer. To overcome the penetration of the dope into the nonwoven, two strategies were employed. First the casting thickness was increased from 200 to 400 µm. Secondly, the shear viscosity of the dope solution was increased to 8.8 Pa s.

The increase of the casting thickness increased the pure water permeability with no change in dope solution composition. This might be caused by an increase in the formation of macro-voids since there is more space available for the growth of the void.[68] After the initiation of the phase separation nuclei of macro-voids are formed just beneath the top layer. This is the same for both casting thicknesses. The growth of the macro-void is facilitated through the exchange of solvent and non-solvent by means of diffusion. The growth is limited the amount of solvent available beneath the top layer which is greater for higher casting thicknesses. Therefore, the bigger casting thickness provides the possibility for more pronounced macro-

void formation.[15,69] Consequently, this can increase the channeling of permeate through the membrane. Thus, leading to a higher pure water permeability.

The viscosity was adjusted by increasing the molecular mass of the PVP. This was done by changing from K-30 (M_w = 18 kDa) to K-90 (M_w = 228 kDa).[52] As one would expect, the dope with the higher molecular weight additive showed an increase in shear viscosity. Since this increase was not sufficient to reach or exceed a viscosity of 8 Pa s, the PVP concentration in the dope solution was increased to 2 %. A sufficient viscosity increase was achieved by this measure. The performance of the membranes on glass substrate was comparable for both dope solution compositions. The modified dopes solution formulation yielded membranes with an increased rejection and a decreased permeability. This is the emerging effect of the viscosity increase. During the phase separation, the pore growth happens by the diffusive exchange of solvent and non-solvent. When the viscosity is increased, the diffusion is slowed down and the pore growth is slowed down accordingly. This brings forth smaller pores causing the change in membrane performance that was seen in these samples.

After both strategies were tried on the glass substrate, both dope solution formulations were transferred onto the nonwoven substrate. For both it was seen that the casting on the nonwoven increases the permeability with no significant effect on the rejection properties. The similar rejection implies that the pore size is not significantly changed. The constant rejection was expected since the rate of pore growth mainly depends on the dope solution composition. The cause for the increase in permeability is not clear. The most probable reason is that the integration of the nonwoven into the support structure of the membrane caused a better channeling of the permeate during the filtration experiment. The thickness measurements (cf. Table 41) indicate that even with the adjusted conditions some of the dope penetrated the nonwoven. The thickness of the membrane prepared on the nonwoven is smaller than the sum of the thickness of the nonwoven and the membrane prepared on a glass substrate. However, this constitutes no problem for the further experiment since the sever penetration of the dope was suppressed. Therefore, the first problem was solved. The next step consisted in changing the solvent form NMP to DMAc. This was necessary since the industrial partner only had a permit to discharge DMAc into the sewage. The solvent was changed in the adjusted dope solution formulation of 17.5 % PVDF and 2 % PVP K-90. The change in solvent decreased the viscosity of the dope solution (cf. Figure 39). This caused an increase in permeability and a decrease in rejection. Since the pore growth is enhanced at a

lower viscosity. By increasing the polymer concentration in the dope solution, the viscosity was increased beyond the initial value. The increase of the viscosity over the value of the dope in NMP was necessary to reach a similar performance. This is caused by a few key differences between the solvents:

- DMAc requires less water to induce phase separation[19]
- DMAc has a higher enthalpy of mixing with water than NMP[19]
- PVDF solutions in DMAc have a lower viscosity than the same concentration in NMP[19]
- The diffusivity of water in DMAc is higher than in NMP and therefore the system also has a higher mutual diffusivity[19]

The first difference determines that the occurrence of demixing will be earlier when DMAc is used as solvent which increases the time available for pore growth. The second difference determines that the driving force for the exchange of solvent and non-solvent will be higher in DMAc. The third and fourth differences determine that the exchange rate of solvent and non-solvent will be higher for DMAc. This indicates that the rate of pore growth will be bigger in DMAc than in NMP. These factors together necessitate a higher polymer concentration in DMAc to slow down the pore growth to such an extent that a comparable performance is achieved. This becomes apparent when the performance of the membrane prepared from 17.5 % PVDF, 2 % PVP K-90 in NMP and 17.5 % PVDF, 4 % PVP K-90 in DMAc are compared. Despite the comparable viscosity of 8.8 and 8.1 Pas at a shear rate of 15.9 s^{-1}, the rejection is much lower for the DMAc membrane. This indicates a larger pore diameter. This shows the effect of the difference of diffusivity, driving force and tolerance of water between the two solvents.

The dope solution composition of 21 % PVDF and 4 % PVP K-90 in DMAc showed a comparable rejection but a lower permeability than the membrane produced from the NMP formulation. Despite the differences the performance was still close enough to the goal performance that the up-scaling experiments were performed. A membrane was produced in pilot scale. This membrane underperformed in regard of the permeability compared to the membrane produced in lab scale. The thickness measurements (cf. Table 45) show that the up scaled membrane is thinner than the membrane prepared in the lab scale. The SEM picture of the membrane is shown in Figure 89.

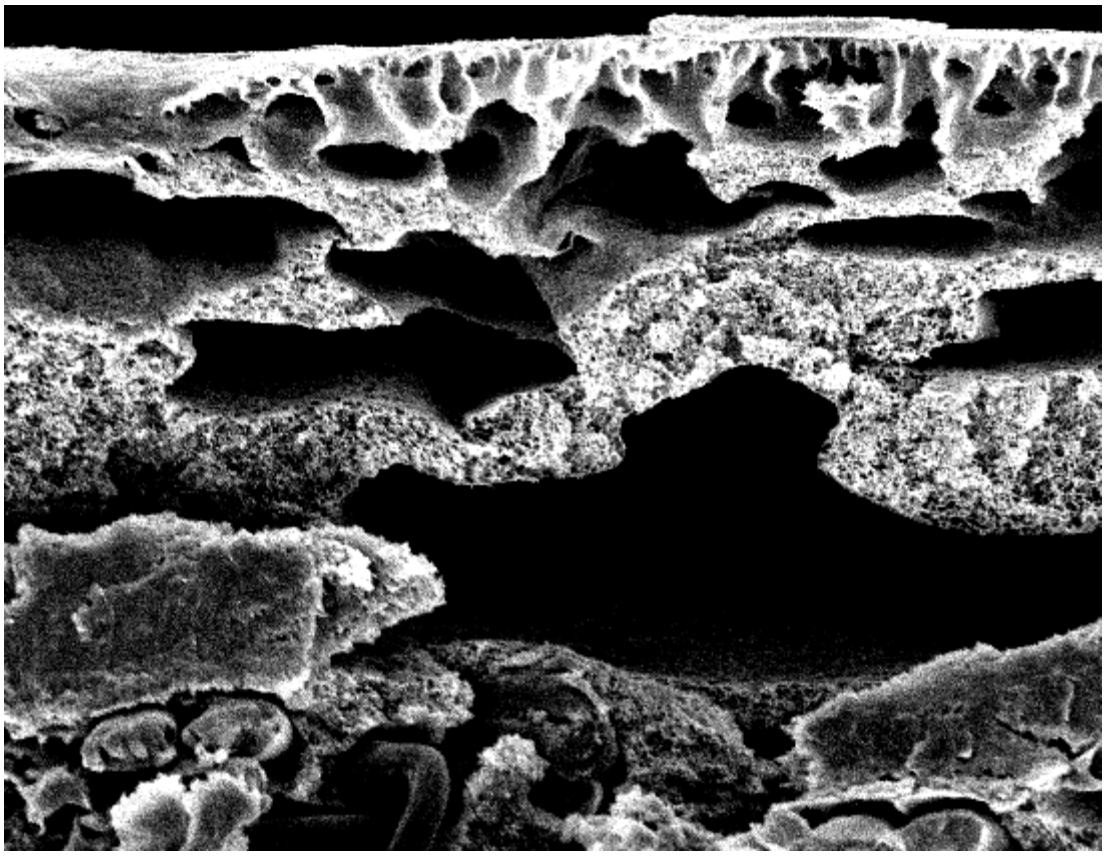

Figure 89 Segment of the up scaled membrane morphology. Magnification 1000x.

In the segment of the SEM picture a layer can be observed between the nonwoven and the porous PVDF morphology. The structure in this part seems to be less porous then the remaining polymeric parts of the membrane. It is likely that this layer is causing the decrease in permeability. This hypothesis is supported by the SEM picture of the membrane top surface (cf. Figure 40) which shows that the top surface is sufficiently porous. Therefore, it can be asserted that the permeability decrease is not caused by the top layer morphology of the membrane. The reason for the occurrence of the dense layer might be the setup of the pilot plant. A part of the pilot plant is displayed in Figure 90.

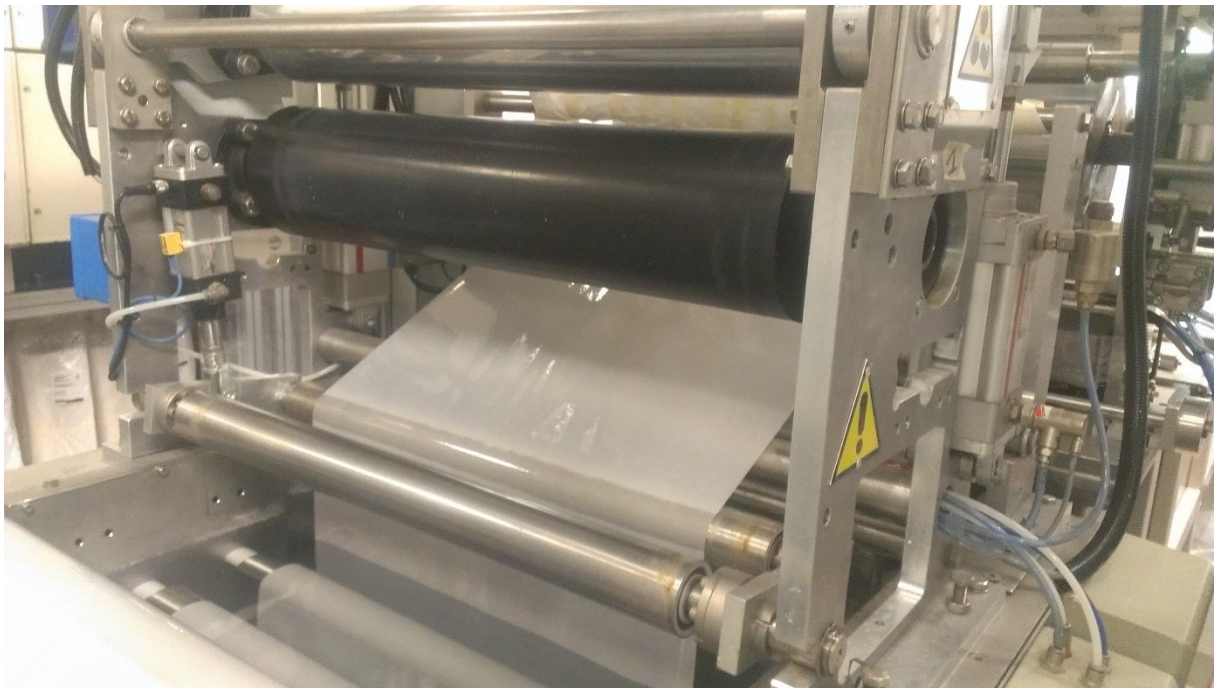

Figure 90 Pilot setup.

In the picture the proto-membrane can be seen entering the coagulation bath. A few of the rollers can be seen over which the nonwoven support is conveyed. At the bottom of the bath are more rollers present which redirect the nonwoven upward. These rollers contact the top surface of the precipitating membrane. If it is assumed that the membrane has not solidified in the lower part of the structure, it can be followed that the dense layer is caused by the compression of the precipitating polymer film onto the nonwoven by the rollers. A possible solution might be the decrease of the casting thickness. This would enable the precipitating film to reach full solidification before the rollers contact the top surface in the coagulation bath.

6.2.4. Adjustment of morphology

To change the morphology of the membrane from a finger-like to a sponge-like structure the exchange rate of solvent and non-solvent must be decreased. A twofold strategy is conventionally employed to achieve this. The first part is to increase the viscosity of the dope solution to hinder the diffusion of the solvent and non-solvent in the forming membrane. This is achieved by raising the polymer content of the dope solution. The second part is the introduction of solvent into the coagulation bath. This decreases the difference in chemical potential between the two phases and therefore the driving force for the solvent exchange. The compatibility between the polymer and the coagulation bath is also increased by this approach which delays the phase separation and solidification. The combination of both approaches was employed to change the morphology of the membrane in this work.

The result was a partial success. The morphology was changed in the way that most of the structure consisted of porous sponge-like domains. However, the formation of finger-like voids was not sufficiently suppressed (cf. Figure 46). This is caused by the intrinsic tendency of the polymer PVDF for precipitate in a structure with large macro-voids from NMP.[19] The achieved change in morphology can be seen as the best achievable result for the specific system. The addition of solvent to the coagulation bath was done to such an extent that demixing was drastically delayed, which yielded a denser membrane structure as indicated by the change in performance (cf. Figure 47). This is caused by two effects. First, the softer coagulant leads to the formation of fewer nascent pores in the top layer of the proto-membrane. Second, the delayed solidification causes the formation of a thicker top layer (cf. 2.1). The rejection is not improved in the same magnitude as the permeability is decreased. This can be attributed to the fact that the softer coagulation bath delays the solidification. Which leads to a longer time available for pore growth. Overall, the achieved change of morphology is sufficient for the scheduled experiments, since the main objective is the comparison of different coagulants. Any further increase of the delay would most likely produce a membrane with an unsuitable structure for ultrafiltration.[15] It is possible that a better morphology could have been obtained from a system with different solvent and coagulant. However, this would not have been suitable for the comparison with the other experiments presented in this work.

6.3. Nanocomposite membranes

6.3.1. Incorporation of pristine nanoparticles

Several aspects can be discussed regarding the experiments with the incorporation of unmodified zinc oxide nanoparticles. First, the formulations with and without PVP are compared to evaluate the influence of PVP on the system. The viscosities of both formulations are presented in Figure 91 as a function of the amount of added nanoparticles.

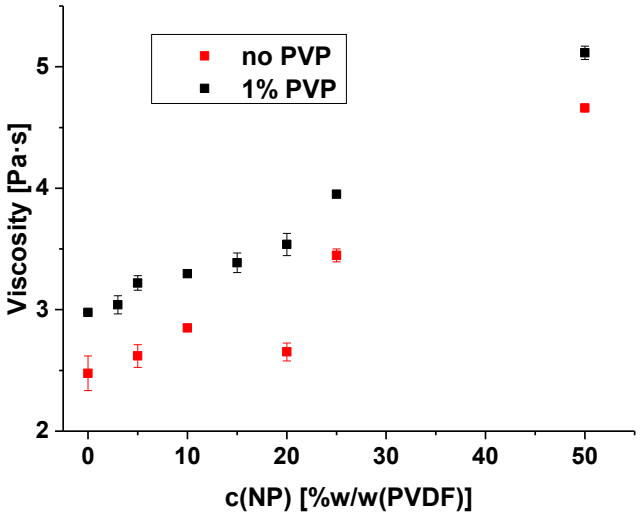

Figure 91 Comparison of shear viscosity at 15.9 s^{-1} of dope solutions (16 %PVDF in NMP) with and without 1% PVP and various amounts of pristine ZnO nanoparticles.

When the viscosity of the dope solutions with and without PVP are compared, it becomes apparent that both have the same development in dependence of the added nanoparticles. The dope solutions without PVP exhibit smaller viscosities than the other which is caused by the lower polymer content. The increase of the viscosity is caused by the interaction of the nanoparticles with a component of the dope solution. NMP contains an amide group, which can form a bond to the surface of metal oxides like zinc oxide. The same groups can be also found in PVP. Therefore, it can be proposed that the interaction with these compounds contributes to the viscosity increase.[14,70] Since the viscosity increases steadily with the nanoparticle concentration regardless of the presence of PVP, it is reasonable to assume that the dominant effect for the viscosity increase consists in the interaction between the solvent and the nanoparticles. It also indicates that the particles do not agglomerate. Otherwise a nonlinear increase of the viscosity would be expected with an increase in particle concentration. This is surprising since the particles were not stable in the pure solvent (cf. 5.1.8.1). This is true for both formulations. This is caused by the higher viscosity which hinders

the Oswald ripening as the Brownian motion of the particles is reduced. The comparison of the effect on the permeability for both systems is shown in Figure 92.

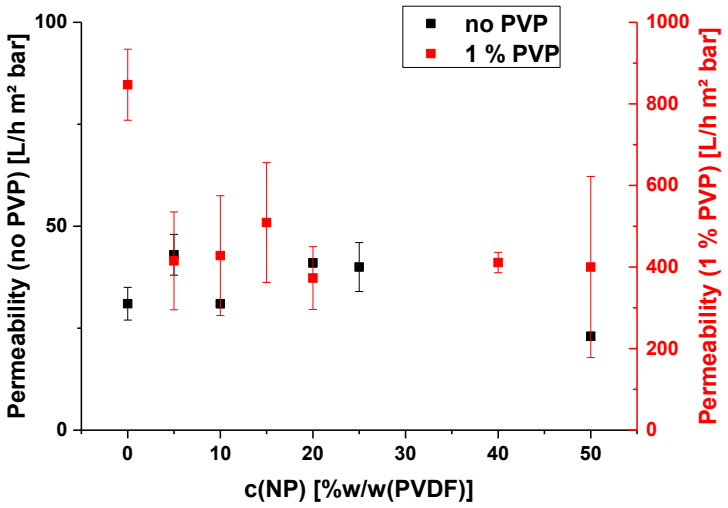

Figure 92 Permeability comparison for membranes (16 %PVDF in NMP) with and without 1% PVP and various amounts of pristine ZnO nanoparticles.

The main difference between the membranes seems to be the presence of PVP in the dope solution which increases the permeability. This is the expected porogenic effect of a hydrophilic additive. No significant difference is observed regarding the effect of the nanoparticles on the permeability. The effect that the oxidic particles increase the permeability by increasing the hydrophilicity of the membrane, as it is discussed in chapter 2.5, cannot be observed. A possible explanation would be that the particles are not present in the skin layer and have therefore not the possibility to interact with the feed. This is supported by the SEM pictures of the top surface (cf. Figure 50 and Figure 60) in which no particles are visible. In the membrane with PVP a decrease is seen with the introduction of a low concentration of nanoparticles that is not seen in the membrane without PVP. The reason is most likely pore blocking. Although this explanation is not conclusive since one would expect the effect to be more pronounced at higher concentrations and this is not the case. The decrease in permeability is not observed in the membrane without PVP most likely because of the already low permeability. The presence of pore blocking is supported by the agglomerates which were found in the structure below the top layer (cf. Figure 50 and Figure 60).

The rejection for PEG 35 kDa is compared for both systems as presented Figure 93.

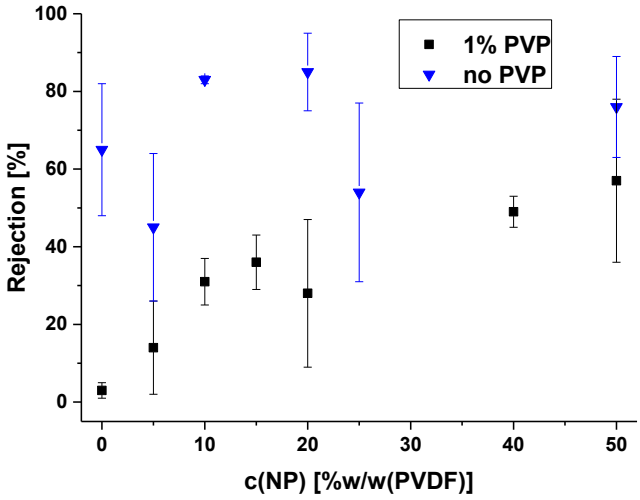

Figure 93 Rejection of PEG 35 kDa comparison for membranes (16 %PVDF in NMP) with and without 1% PVP and various amounts of pristine ZnO nanoparticles.

Regarding the rejection of PEG 35 kDa, no effect is observable for the membranes with no PVP. An increase in rejection is observed for the membranes with 1 % PVP. This increase is normally caused by a reduction in pore size. The viscosity increase caused by the nanoparticles could lead to this reduction. However, since it is only observed in the membrane with PVP, this raises the question if the PVP is necessary for this effect to realize. Another possibility is that the rejection in the membrane without PVP was too high to see this effect. This cannot be determined from the data available. Using this data, it is only possible to state that the nanoparticles do not cause the formation of defects in the top layer; otherwise a drop in rejection should have been observed. The rejection for PEO 100 kDa is compared for both systems in Figure 94.

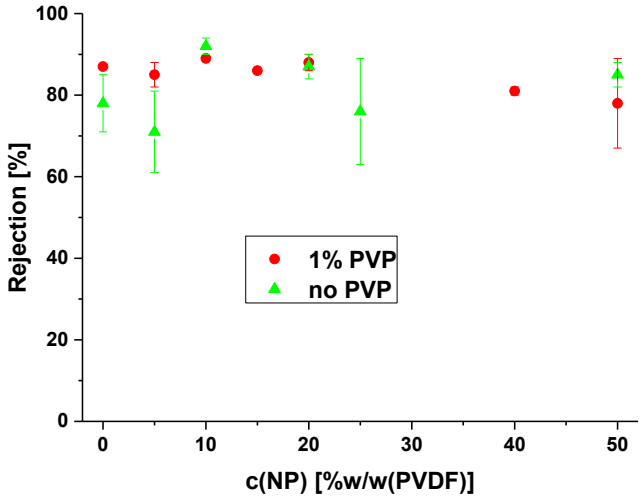

Figure 94 Rejection of PEO 100 kDa comparison for membranes (16 %PVDF in NMP) with and without 1% PVP and various amounts of pristine ZnO nanoparticles.

It can be asserted from the data in the figure that the introduction of nanoparticles has no significant effect on the rejection of PEO 100 kDa. This validates the assertion that the nanoparticles do not lead to the formation of defects in the skin layer. Also, the increase that was seen for the rejection of PEG 35 kDa in the membrane without PVP cannot be established for this solute. When one compares the overall structure of the membranes by comparing the SEM pictures in Figure 51 and Figure 56 there is no apparent difference. The agglomerates inside of the membrane structure are compared in Figure 95 for both membranes.

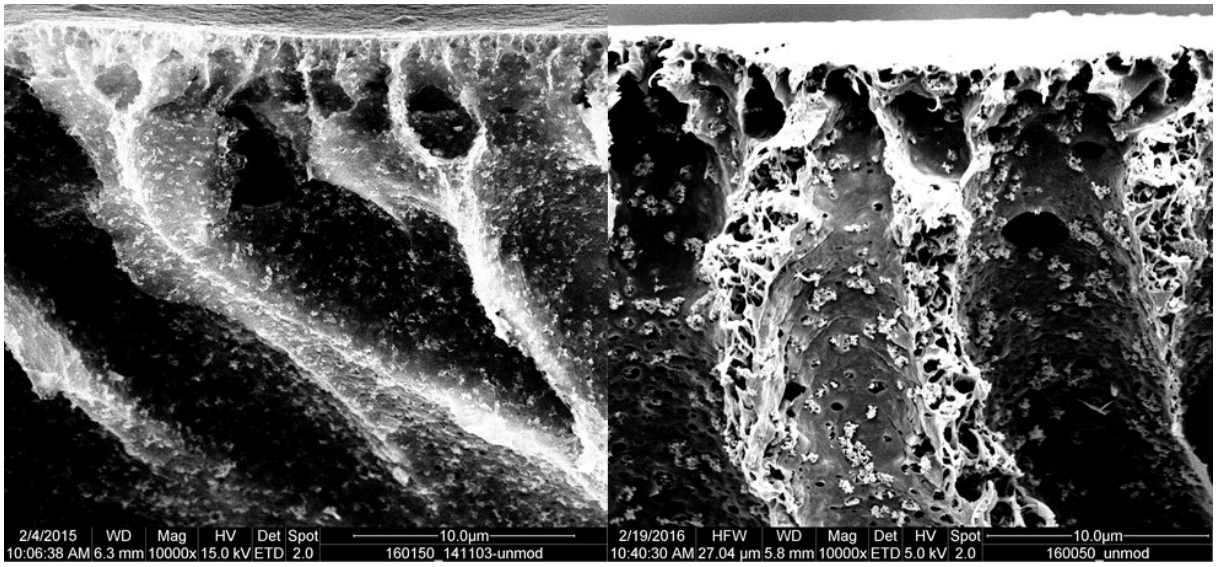

Figure 95 Agglomerates of NP in membrane at 50%w/w(PVDF) NP with and without PVP in dope solution. Left:1 % PVP; Right: no PVP; Magnification 10kx.

The comparison of the SEM pictures reveals that in the membrane with 1 % PVP the size of the agglomerates decreased is in comparison to the membrane without PVP. There are two

possible reasons for that. First, the PVP might bind to the particles and the resulting stabilization decreases the agglomeration. Second, the influence of the PVP on the phase separation process might decrease the agglomeration tendency. At this point it cannot be discerned if one of these factors or a combination of both is responsible for the lower agglomeration. If the integration of the nanoparticles is influenced cannot be determined by the previous picture. The same membranes are shown at a higher magnification in Figure 96.

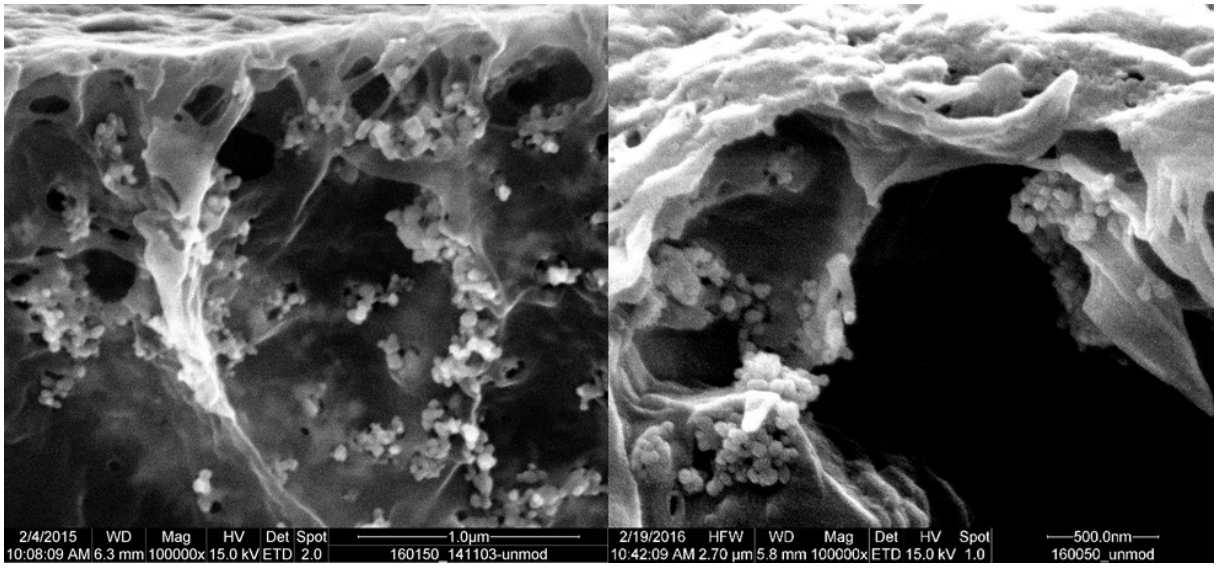

Figure 96 Agglomerates of NP in membrane at 50%w/w(PVDF) NP with and without PVP in dope solution. Left:1 % PVP; Right: no PVP; Magnification 100kx.

The agglomerates show no difference regarding their integration into the polymer matrix. The same size difference is seen as in the previous figure. As a conclusion, no clear influence of the PVP in the dope solutions can be seen on the nanoparticle integration.

The discussion is continued with the influence of the nanoparticles at slower phase separation conditions. The dope solution and the coagulation bath composition were adjusted in accordance to the results from chapter 6.2.4. The addition of ZnO nanoparticles exhibited no effect on the membrane performance (cf. Figure 59) or structure (cf. Figure 61) at the slower coagulation speed. Also, the agglomeration was also apparent (cf. Figure 62) and the integration was as poor as in the previous samples. The only difference is that the agglomerates were slightly smaller.

The tensile strength of the membrane with 50 %w/w(PVDF) NP and no NP was tested. The results are displayed in Figure 97.

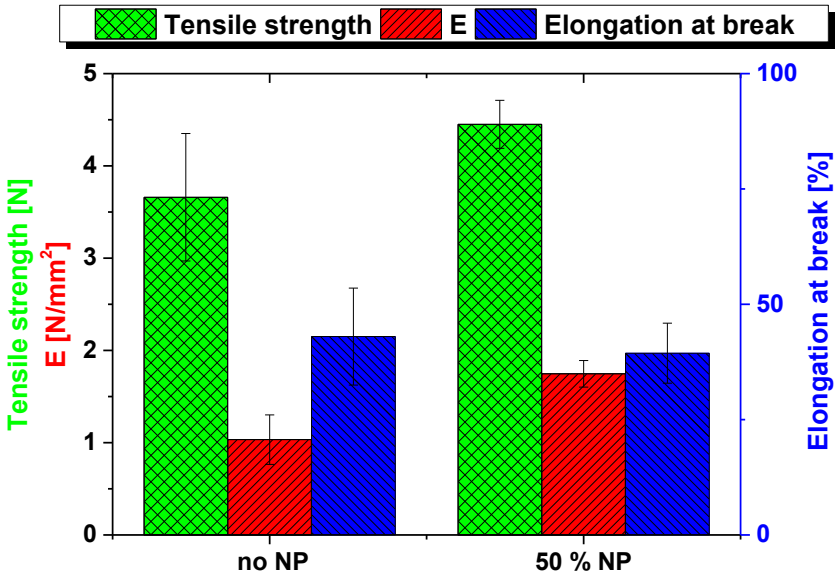

Figure 97 Comparison of mechanical properties for membranes with and without 50 %w/w(PVDF) NP.

The tensile strength and elongation for both samples are comparable considering the standard deviation. This can be explained by the lack of interaction between PVDF and zinc oxide. The Young modulus is increased by the incorporation of the nanoparticles. This can be explained by the nanoparticles acting as physical cross-link between polymer chains which distributes the load over more chains and increases the restoring force.[71] This also indicates that at least some particles are integrated into the polymer matrix. These particles were not seen in the SEM pictures because the bulk material cannot be analyzed specifically by breaking porous material. It might have been possible by cutting the sample but this was not done.

All results discussed in this chapter indicate that the pristine zinc oxide nanoparticles have little to no effect on the membrane. This is unexpected considering that there are examples to be found in the literature where zinc oxide was employed as additive even in similar system (cf. 2.5).[10,12,47]

However, this finding can be explained in the following way. When water is introduced during the phase separation the hydrophilic zinc oxide will predominantly bind to water molecules. This is supported by the results of the Hansen parameter analysis for the unmodified particle (cf. Figure 23). And as stated above, it is unlikely that a bond to PVP is hindering this. This implies that most of the nanoparticles will end up in the polymer-poor phase during the phase separation as it is rich in water. This phase has a lower viscosity and therefore are the particles no longer hindered from agglomerating. By this mechanism most particles will end up in the walls of the cavities instead in the bulk of the polymer. This explains most of the findings in

this part. And since little to no interaction occurs between the polymer-rich phase and the nanoparticles, the influence on the phase separation process is marginal. The attempt was made to quantify the nanoparticle content of membranes via thermogravimetric analysis to verify the explanation. The result was inconclusive because the nanoparticles influence the behavior of the polymer during the measurement. This led to the calculated nanoparticle content exceeding the maximal possible content (cf. Table 84).

The previously mentioned studies exhibit some differences to the present experiments which explain the divergence in the findings. Balta et al.[10] used polyether sulfone as base polymer which contains sulfone and ether groups. These can bind to metal oxides and therefore increase the affinity of the nanoparticles to the polymer-rich phase. This is visualized in Figure 98.[8,72]

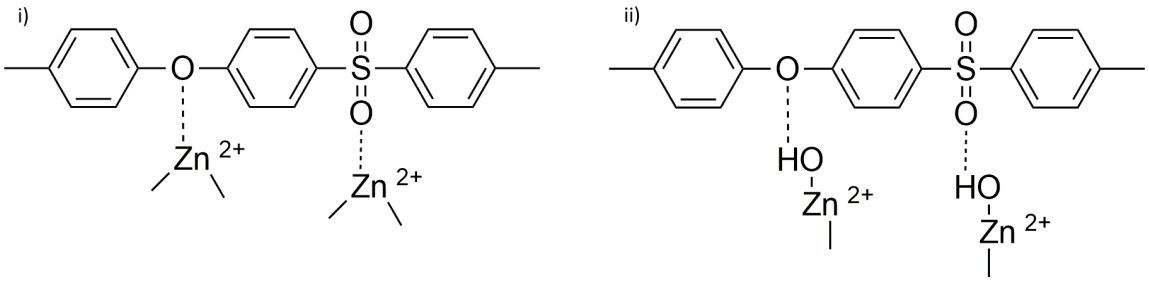

Figure 98 Possible binding modes between PES and ZnO.
i) coordinative bond; ii) hydrogen bond. According to [72]

In the case of Liang et al.[12] glycerol was added to the dope as non-solvent additive. This decreases the delay time that occurs before the phase separation and solidification of the polymer. Therefore, it could be that the zinc oxide has not enough contact time with water or that the water concentration at this point is too low to enable the previously described mechanism.

Two similar study to this work were published by Cao et al.[41] and Yuliwatis and Ismail[47]. In both studies PVDF was used as base polymer and titanium oxide nanoparticles were used. These studies find a beneficial effect on the membranes structure and performance which was like the effect of a hydrophilic additive. While not the exact same components are used in both studies, there is one mutual aspect which could help to understand the different findings to our study. In the article by Cao et al.[41] there is no evaluation on the efficiency of the dispersion conditions used and no determination of the particles size under the applied conditions. Therefore, it is possible that the particles are not optimally dispersed and consequentially bigger than the primary size of the particle of 10 and 25 nm respectively. A

bigger particle exhibits a much lower diffusivity and is therefore less likely to migrate into the polymer-poor phase during the phase separation. This can also be applied to the study of Yuliwati and Ismail.[47] While they did also not evaluate the efficiency of the dispersion conditions and consequent particle size, they evaluated the viscosity increase in the dope solution. This is displayed in Figure 99.

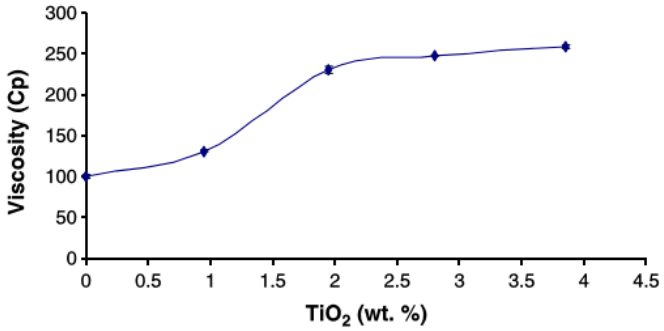

Figure 99 The viscosity of PVDF spinning dope with various TiO2 content.[47]

The graph of the viscosity as a function of the titanium oxide concentration in this study shows an unsteady slope. That means that the relative viscosity of the particles is unstable. This can indicate the presence of aggregates.[73] It is reasonable to deduct that the particle size is increased by aggregates at higher titanium oxide concentrations. In the study a significant effect on the membrane performance is only observed at concentrations which correspond to the viscosity plateau. This argumentation is also supported by a study from Bottino et al.[74] In which zirconia oxide particles with a size of around 5 µm were used as an additive for the blend modification of PVDF membrane. Here a similar effect of the metal oxide in the dope solution is observed. This could be an indication of the effect of bigger particles.

6.3.2. Incorporation of trifluoroacetic acid modified nanoparticles

In this part, the influence of the TFA modified particles on the membrane performance is compared to the one of pristine particles. The evaluated particles were modified with a ratio of 100 % TFA/ZnO. This lead to the modified particles consisting to 6 % of TFA which refers to a surface coverage of 37.6 $\%_{monolayer}$ (cf. Table 14). The viscosity of the dope solutions with both particle types are compared in Figure 100.

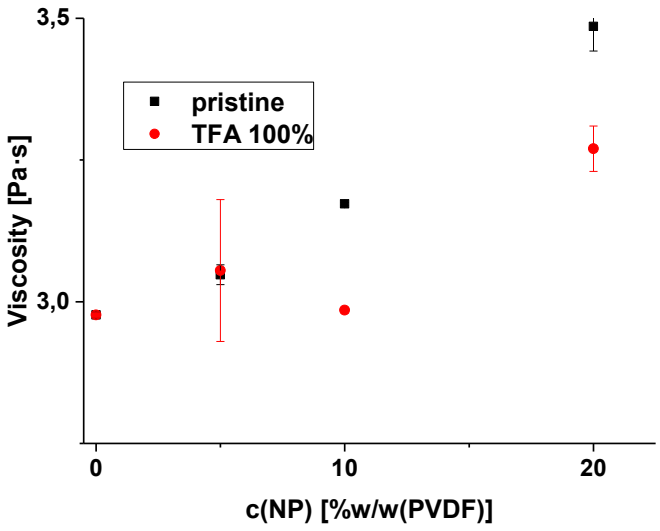

Figure 100 Shear viscosity at 15.9 s^{-1} for dope solutions (16% PVDF and 1% PVP in NMP) with various amounts of TFA-modified and unmodified ZnO nanoparticles.

When the viscosity increase for both particle types is compared, it can be asserted that the viscosity of the dope solutions with the modified particles is smaller than the ones with the pristine particles. This can be explained in the following way. The modified particles consist of zinc oxide and the trifluoroacetic acid. The zinc oxide content is therefore reduced in comparison to the pristine particle which is only consists of zinc oxide. This gives a lower effective nanoparticle concentration which is responsible for the lower shear viscosity. In chapter 6.1.2 it was discussed that the bonding between acetic acid and zinc oxide particles does not seem to be stable under the conditions that were used for the preparation of the dope solution. Since a similar bonding is present in these particles, it can be assumed that the TFA is removed from the particles. The effect of the desorbed TFA on the viscosity of the dope solution is not clear. Since it is a low molecular weight molecule, it is reasonable to assume that it will lower the viscosity by lowering the effective polymer concentration. This might also be contributing to the lower viscosity that was found for the dope solutions with the modified particles. The pure water permeability is compared in Figure 101 for both particles types.

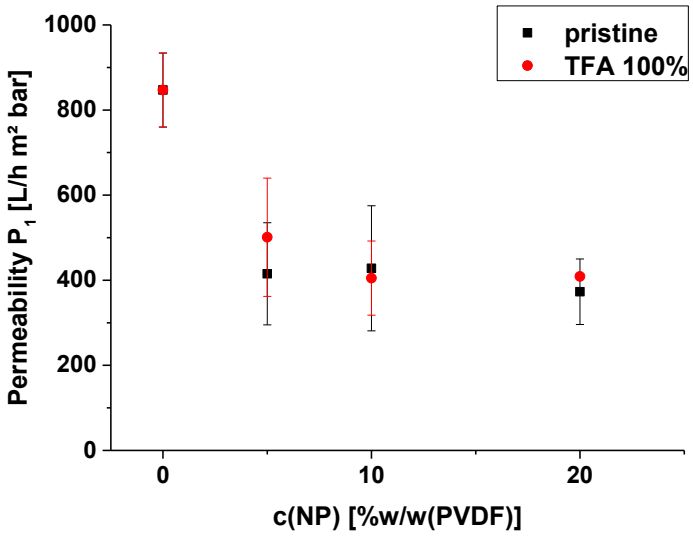

Figure 101 Permeability comparison for TFA-modified and modified nanoparticles.

The difference in regard of the permeability is only marginal. This can be explained by the virtually identical composition with the slightly lower nanoparticle content as discussed in the previous paragraph. The rejection performances of these membranes are presented in Figure 102.

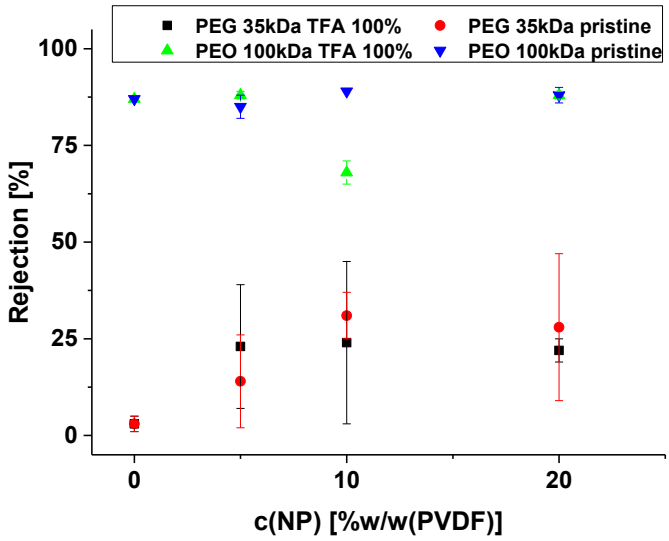

Figure 102 Rejection comparison for TFA-modified and modified nanoparticles.

As for the permeability, no difference is found in the results which cannot be explained by the different nanoparticle content. As a conclusion, one can establish that the TFA-modified particles exhibit no difference to the unmodified particles as additive. This is reasonable considering the results discussed in chapter 6.1.3 in which only a low surface coverage and no change in Hansen solubility parameter were obtained. Additionally, the instability of the bonding of carboxyl acid to the particle, which was discussed in chapter 6.1.2, severely reduces

the potential impact of nanoparticle modification on the membrane structure and performance.

6.3.3. Incorporation of acetic acid modified nanoparticles

In this part, the influence of the acetic acid modified particles on the membrane performance is compared to the one of pristine particles. The viscosity of the dope solutions with both particle types are compared in Figure 103.

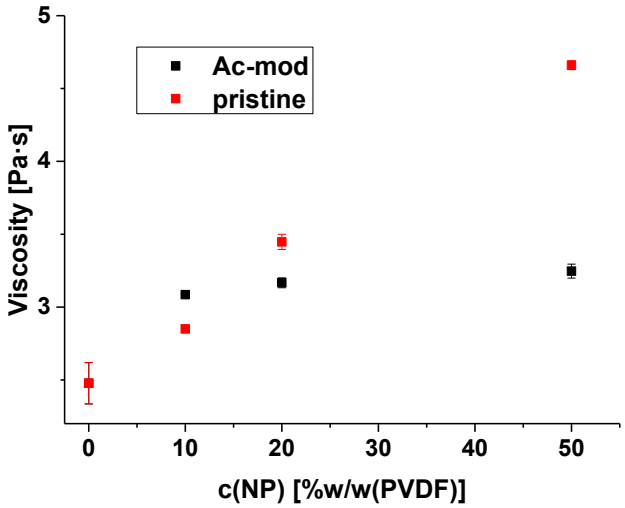

Figure 103 Shear viscosity at 15.9 s^{-1} for dope solutions (16% PVDF in NMP) with various amounts of Ac-modified and unmodified ZnO nanoparticles.

The viscosity of the dope solution with a high concentration of Ac-modified particles is lower than the reference sample with pristine particles. This might be caused by the agglomeration of these particles.[73] Why the modified particles tend to agglomerate under these conditions cannot be determined with certainty from the data. The agglomeration is surprising since the Ac-modified particles were evaluated to be stable in NMP (cf. Table 23) and the pristine particles, which were evaluated to be unstable in this solvent (cf. Table 21), did not agglomerate in the dope solution prepared under the same conditions. In the analysis of the infrared spectrum of the modified particles in chapter 6.1.2 indications of unbound acetate were found. If the carboxylate groups of the molecules were directed towards the solvent, the agglomeration could be the consequence of a decrease in compatibility with NMP. This makes sense in the respect that NMP is not a good solvent for carboxylic acid. However, this contradicts the results of the HSP evaluation. Another possible explanation would be that the zeta potential of the particles was reduced by the pH conditions during the modification which led to more agglomeration because of the reduced electrostatic repulsion.[65] While this

explanation agrees with the literature, it is not supported by the zeta potential measurements of the modified particles. The measured value for the modified particle is virtually identical with the value for the pristine particles (cf. Table 19).

The effect of the modified particles on the membrane performance will be discussed next. The pure water permeability for the membranes with the Ac-modified particles and pristine particles are compared in Figure 104.

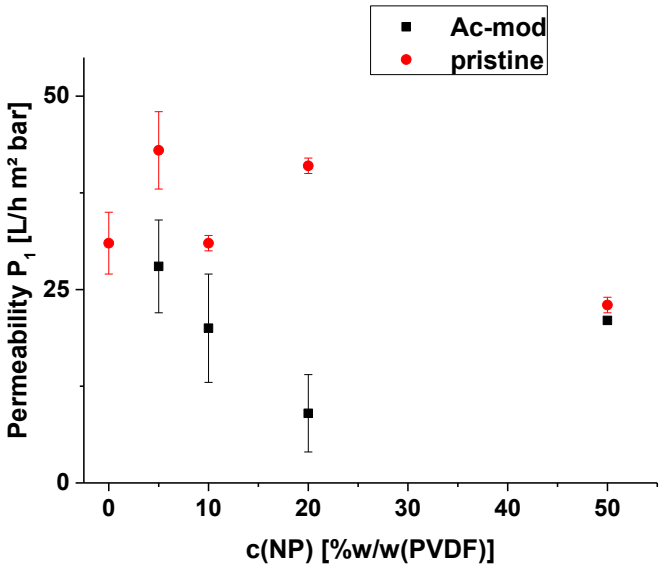

Figure 104 Permeability comparison for Ac-modified and unmodified nanoparticles.

The permeability of the membranes with acetic acid modified particles is lower than the reference samples. The lower permeability might be caused by the agglomeration of the particles. To evaluate if this phenomenon is caused by a change in pore size, the rejection performance of both membrane types is compared. The rejection data is presented in the Figure 105.

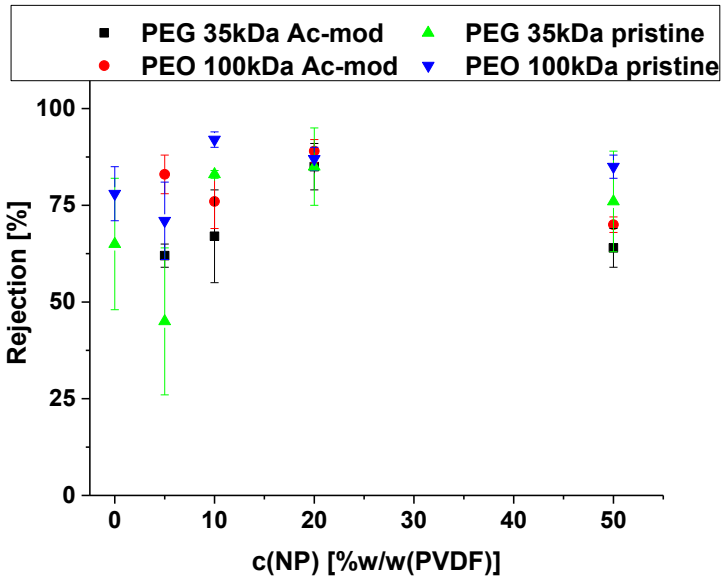

Figure 105 Rejection comparison for Ac-modified and modified nanoparticles.

In regard of the rejection the results are comparable for all samples. This indicates that the membranes have comparable pore sizes. Therefore, it can be concluded that the observed differences in permeability are most likely caused by pore blocking. The cross-section morphology of the membranes with 50 %w/w(PVDF) nanoparticles is compared in Figure 106.

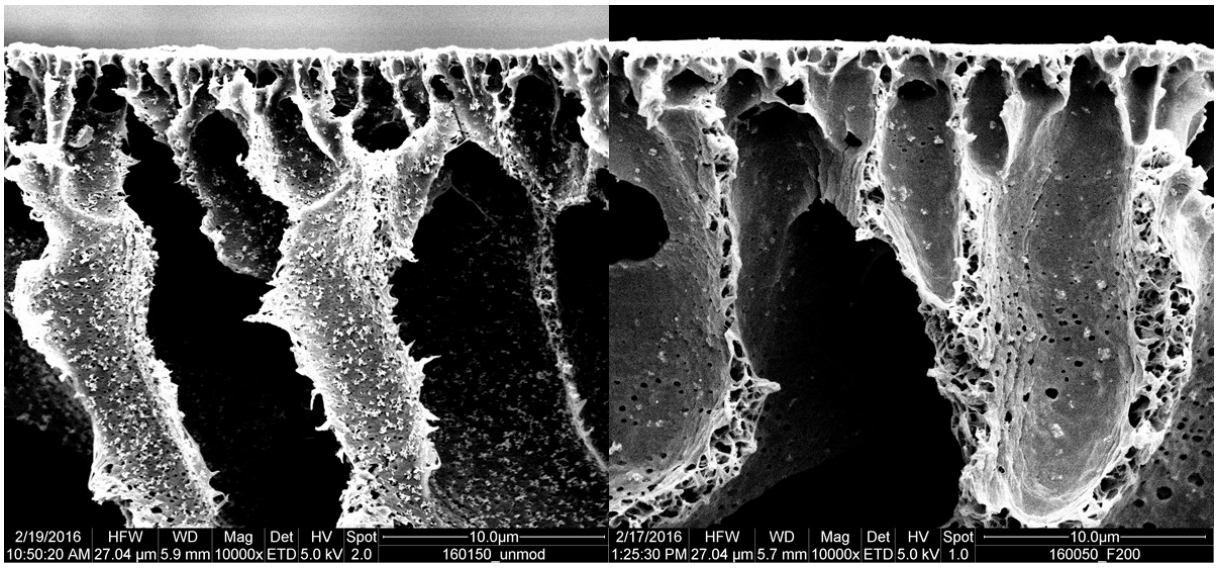

Figure 106 Comparison of the cross-section for pristine and Ac modified NP.

Left: 50% pristine NP; right: 50% Ac modified NP. Magnification 10kx.

The agglomerates of the modified particles appear to be significant bigger than the agglomerates of the pristine particles. The agglomerates of the modified particles are better integrated into the polymer matrix compared to the pristine particles (cf. Figure 69). This can be explained by the slower diffusion of the bigger agglomerates during the phase separation which hinders the agglomerates to move into the polymer poor phase. This might also explain the presence of agglomerate on the skin layer as seen in Figure 68.

Overall the Ac-modified zinc oxide particles do not perform differently to the pristine particles except for the severe agglomeration which is already present in the dope solution. The reason for the agglomeration in the dope solution is not totally clarified. The reasons for the inefficiency of the acetic acid modification is most likely the initially low surface coverage and the removal of the modification during the preparation of the dope solution that was discussed in chapter 6.1.2.

6.3.4. Incorporation of PVP-modified nanoparticles

The effect of the PVP-modified particles will be discussed in this part. The particles which were modified by the *codispersion* process were used in the experiments because of the higher degree of modification as discussed in chapter 6.1.5. The viscosity of the dope solutions in dependence of the fraction of PVP-modified particles and the reference are shown in the Figure 107.

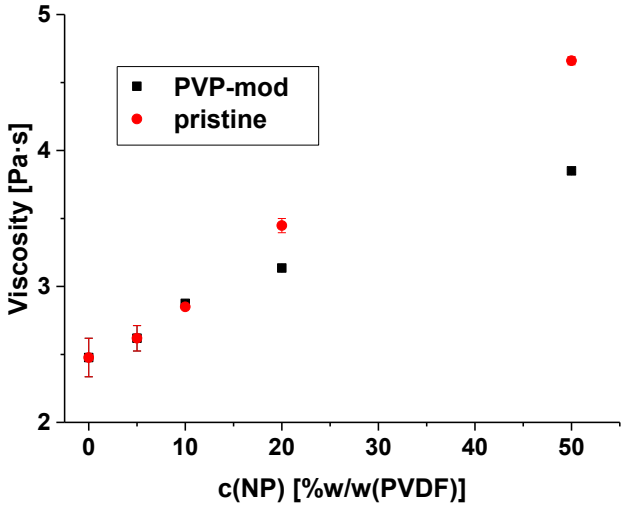

Figure 107 Comparison of shear viscosity at 15.9 s^{-1} of dope solutions (16 %PVDF in NMP) with various amounts of PVP-modified and unmodified ZnO nanoparticles.

By comparing both measurement presented in the figure above it can be determined that the PVP-modified particles exhibit a comparable increase in viscosity. Although the slope of the increase is smaller. This is might be caused by the mass of PVP which is adsorbed to the particle, therefore the effective mass of added zinc oxide is reduced by this margin (cf. Table 15). This should lead to a less pronounced viscosity increase as was seen in this experiment. The data is plotted in the dependence of the mass fraction of the particles. Since the modified particle consist to approx. 18 % of PVP (Table 15), is the amount of metal oxide in the dope reduced by this margin.

In the results, it was seen that the permeability of the membranes increases with the concentration of PVP-modified particles in the dope while the rejection for PEG 35 kDa decreases (cf. Figure 71). This indicates an increase of the pore size as effect of the nanoparticle addition.

It has already been seen that the PVP can be partially removed from the particles by NMP during the dope solution preparation as discussed in chapter 6.1.5. Therefore, it can be assumed that the amount of unbound PVP in the dope is increased with an increase of the particle concentration. The explanation for the increase in the pore size is that the unbound PVP acts as hydrophilic additive. This causes the development of a membrane performance like the membrane with PVP in the dope solution. For the membrane with 50 % PVP-modified nanoparticles the amount of unbound PVP can be calculated to be 0.995 % if the ratio of removed PVP is comparable to the previous experiments (cf. 5.1.6). The membrane performance of the membrane with the modified particles and other membranes with 1 % PVP are compared in Figure 108.

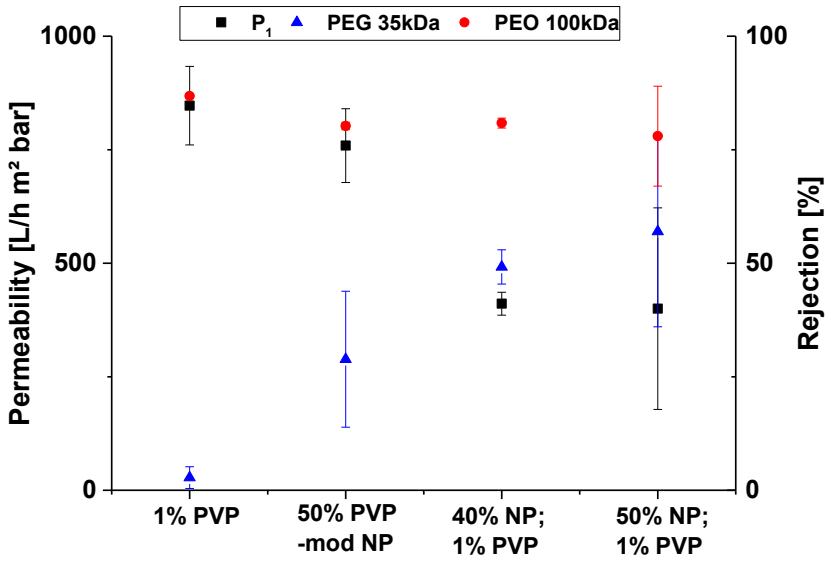

Figure 108 Comparison of performance for various types of membranes.

When the performance of the membrane with 50% PVP-modified is compared with the reference membranes two things can be asserted. First, the membrane with the modified particles has a higher pure water permeability than the membranes with pristine particles. This indicates that pore blocking is not present in the membrane with the PVP-modified particles. Second, the PEG 35 kDa rejection is higher for the membranes with nanoparticles compared to the membrane without nanoparticles while the rejection for PEO 100 kDa is

comparable for all membranes. The membrane with PVP-modified particles exhibits the smallest rejection among these samples, although the rejections are very similar when the standard deviation of the results is considered. The reason for this can be traced back to the smaller viscosity of the dope solution with the modified particles. The viscosity is decelerating the exchange of solvent and non-solvent during the phase invasion. The dope solution with a higher viscosity exhibits consequentially a slower pore growth. This leads to smaller pores and higher rejection.

The cross-section of the membranes with the highest nanoparticle content are shown in Figure 109.

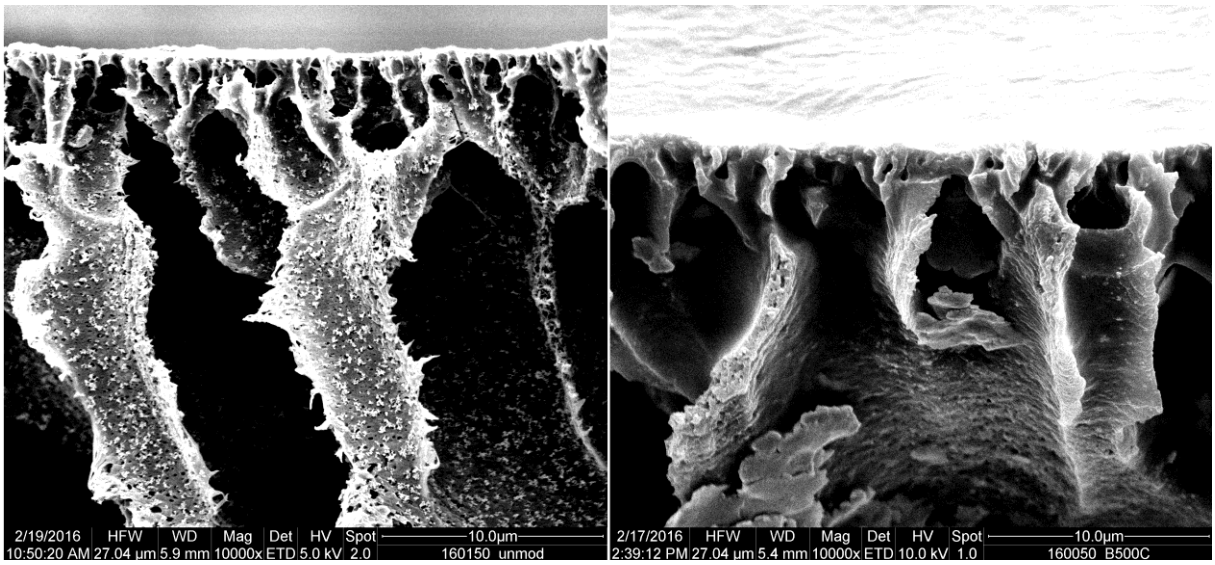

Figure 109 Comparison of the cross-section for pristine and PVP modified NP.

Left: 50% pristine NP; right: 50% PVP modified NP. Magnification 10kx.

In the picture, it can be seen that both membranes have the same morphology. The main difference is the lack of nanoparticle aggregates on the wall of the finger-like voids in the membrane with the PVP-modified particles. It can be asserted that agglomeration is not present in the membrane with PVP-modified particles. The nanoparticles in the cross-section are shown at a higher magnification in Figure 110.

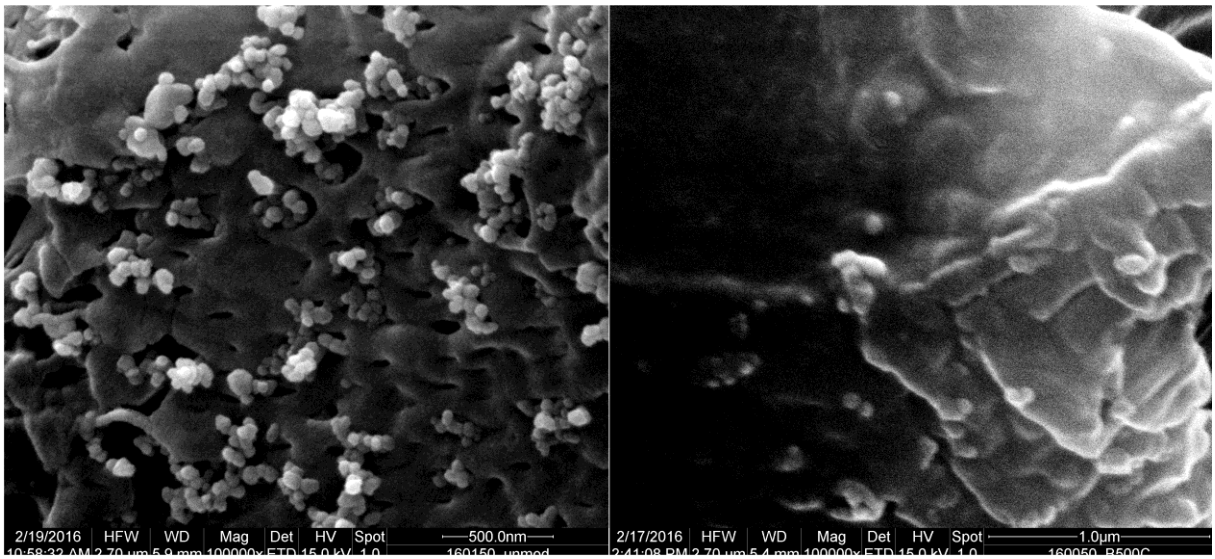

Figure 110 Comparison of nanoparticles in the cross-section for pristine and PVP modified NP.

Left: 50% pristine NP; right: 50% PVP modified NP. Magnification 100kx.

The higher magnification reveals that the PVP-modified particles are far better integrated into the PVDF-matrix than the pristine particles. This is a direct consequence of the modification which changed the affinity of the particle to be close to PVP as it was seen in the Hansen parameter analysis (cf. Figure 32). The mechanical properties of the membranes are compared in Figure 111.

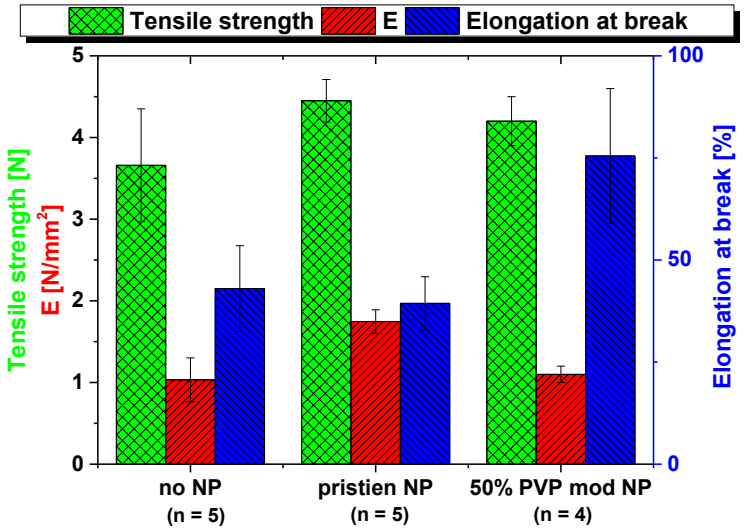

Figure 111 Comparison of the tensile strength of membrane samples with PVP-modified particles.

The membrane with the PVP-modified shows no improved tensile strength over the membrane with pristine particles and the membrane without particles. The value is comparable for all three samples. The Young modulus was also not improved with the introduction of the PVP modified particles which is unlike the effect of the pristine particles. This is surprising since one would normally expect a change in these characteristics with the

integration of nanoparticles into a polymer matrix. Only the elongation at break is changed by the integration of the modified particles. The membrane with PVP-modified particles showed a higher elongation at break over the other samples. Although the standard deviation of this measurement is larger than in the other samples. This originates most likely from an inhomogeneous distribution of the particles of the membrane structure. A possible explanation for the increase in ductility is that the particles, which are well dispersed over the polymer-rich phase, decrease the formation of crystalline domains during the phase separation.

In the results, it was seen that the PVP modified particles are no agglomerated. Therefore, one would expect that these particles have a greater influence on the mechanical properties compared to the pristine particles.[62]

A possible explanation for this is the nature of the modification. The particles were modified with PVP and the modification showed stability under the conditions used to prepare the dope solution. Therefore, one can expect that the particles are still cover with PVP in the finished membrane. The lack of influence on the mechanical properties might be caused by the fact that the modified particles interact similarly to PVP with the polymer matrix. The reference membrane has a similar PVP content to the membrane with PVP-modified particles as was discussed earlier in this chapter.

6.3.5. Implementation of modified base polymer

The effect of the copolymer P(VDF-*co*-AA) as base polymer on the integration of pristine particles will be discussed in this part. The viscosity of dope solutions, which contained 16 % base polymers and 1 % PVP, are compared in Figure 112.

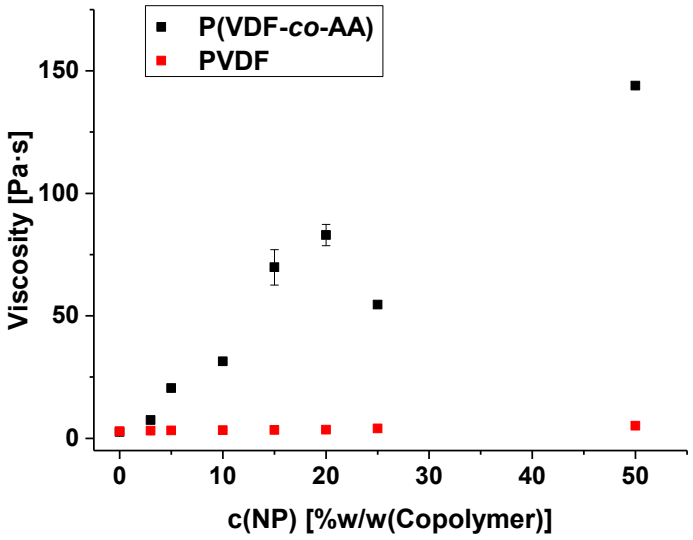

Figure 112 Comparison of shear viscosity at 15.9 s^{-1} of dope solutions (16 % PVDF or P(VDF-co-AA) in NMP) with various amounts of unmodified ZnO nanoparticles.

It can be asserted that the viscosity for the dope solutions with the copolymer increases steadily but the increase is up to two magnitudes larger than for PVDF. This behavior has two indications. First, it indicates that agglomerates are not present in the dope solution as in most experiments. Second, the bonding between the acrylic acid segments of the polymer and the zinc oxide nanoparticles increases the shear viscosity. The same comparison can be conducted for the dope solutions with the higher base polymer content. The viscosity data for the dope solutions, which contain 20 % base polymer and 1 % PVP, is presented in Figure 113.

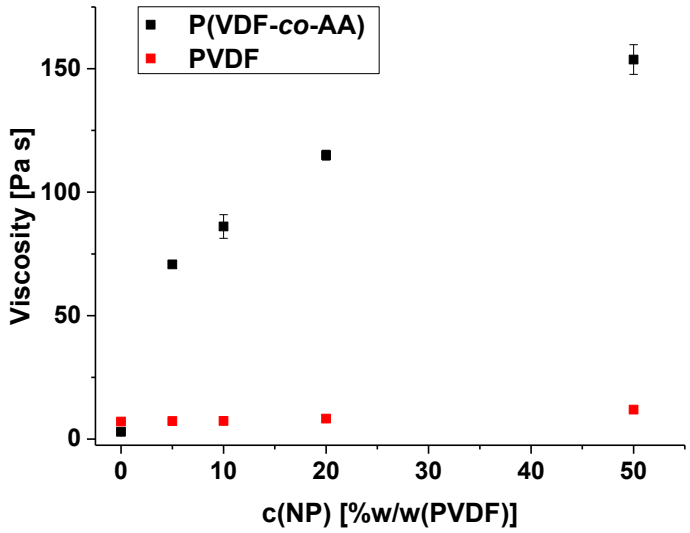

Figure 113 Comparison of shear viscosity at 15.9 s^{-1} of dope solutions (20 % PVDF or P(VDF-co-AA) and 1% PVP in NMP) with various amounts of unmodified ZnO nanoparticles.

The increase in viscosity is even more pronounced than in the evaluation of dope solutions with 16 % base polymer. This is not surprising since the viscosity was compared at a certain ratio of base polymer to nanoparticles. Therefore, the same relative amount of bonding is present in the dope. But by the changing the polymer concentration the absolute number of bonds was increased in the same magnitude. This yielded a greater increase in viscosity.

The performance of the P(VDF-*co*-AA) membranes, which were prepared form the dope solution with the lower polymer concentration by precipitation in water, is comparable to the performance of the PVDF membranes prepared under the same conditions except for the membrane without nanoparticles (cf. Figure 76).

The membrane without nanoparticles exhibits a higher pure water permeability. This can be explained by the presence of the acrylic acid segments in the base polymer. These groups are very hydrophilic and increase the driving force for the solvent non-solvent exchange. This leads to a shorter delay before demixing and a more rapid pore growth. The obtained membrane is more porous and exhibits larger pore sizes for these reasons. The structure is responsible for the encountered performance. These findings agree with reports covering a membrane preparation from a blend of PVDF and PAA.[75]

The case, that the membranes with zinc oxide nanoparticles exhibit a comparable performance regardless of what kind of base polymer is used, can be explained by the influence of water during the phase separation. The strong non-solvent breaks the bond between the acrylic acid segments and the zinc oxide since both components are hydrophilic.

An indication of this can be seen in Figure 79. In this picture the particles appear to be agglomerated which support the explanation that the exposition to water disturbs the bond between the particle and the copolymer. The question remains why the influence of the acrylic acid segments on the phase separation, that was seen in the membrane without nanoparticles, is not observed in the other membranes. A possible explanation for this phenomenon is that the hydrophilicity of acrylic acid segments is masked by the bond to the zinc oxide particles. This causes the negation of the shorter delay of demixing and leads to a similar structure as obtained from PVDF. However, this cannot be asserted with certainty from the present data. Membranes were prepared under the conditions, which were identified in chapter 5.2.4, from the dope solutions with higher polymer concentration to obtain a more sponge like morphology. The membranes exhibited a cross-section morphology with a more pronounced finger structure if no nanoparticles were implemented and a less pronounced finger structure if nanoparticles were implemented. The development of a more pronounced finger like structure can be traced back to the previously discussed effect of the acrylic acid groups. The more rapid demixing is the cause for this structure. The introduction of nanoparticles decreased the size of the finger voids which is generally caused by an increase in viscosity during phase separation.[15] This is the most pronounced structural change that was seen so far by the implementation of zinc oxide nanoparticles. Thus, it could indicate that the bonding between particle and base polymer remains stable during the phase separation. It could also indicate that the previously mentioned masking of hydrophilicity by the bond is present under these conditions. However, this cannot be distinguished from the effect of viscosity from this data. The cross-section of the membrane with 50 % nanoparticles for both polymers are compared at high magnification in Figure 114.

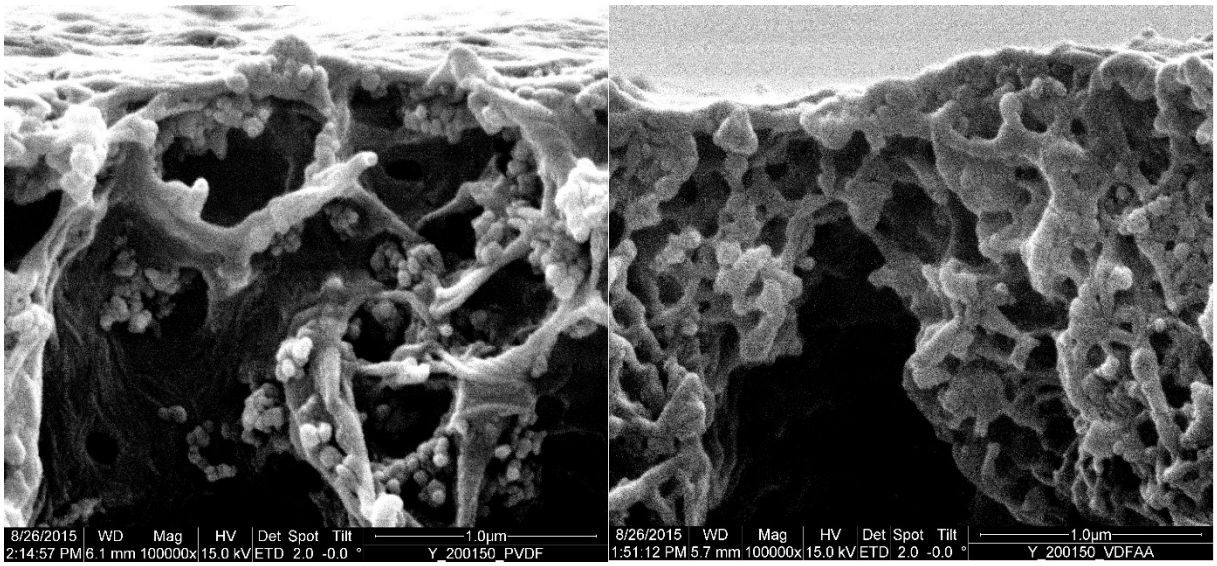

Figure 114 Comparison of nanoparticles in the cross-section of membranes from both polymers with 50% pristine NP. Left: PVDF; right: P(VDF-co-AA). Magnification 100kx.

By comparing both picture is can be asserted that the copolymer membrane exhibits fewer visible aggregates in the morphology. This indicates that the bond between the copolymer and the particles remains stable during the phase separation process when soft coagulation conditions are used. The pure water permeability of both membrane types is compared in Figure 115.

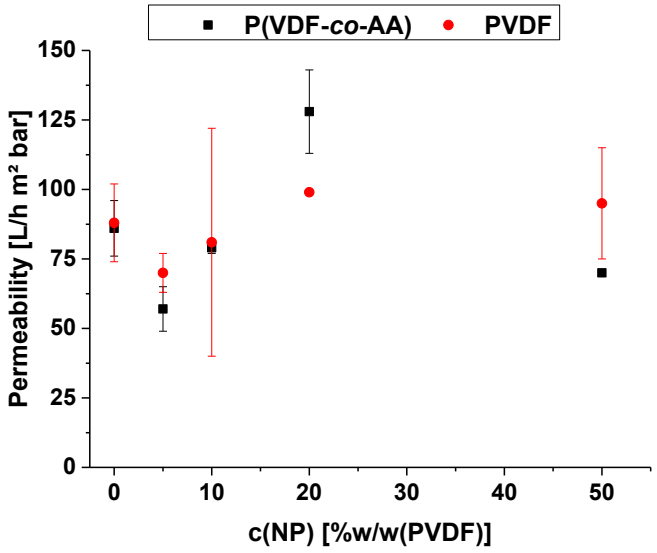

Figure 115 Comparison of permeability with both membrane polymers.

The permeability is comparable for both membrane polymers. This can be explained by the fact that both membranes were prepared under the same slow precipitation conditions. The skin layer morphology is predominantly determined by the conditions of the phase separation process, which causes both membranes to have a similar structure. This is supported by the

SEM pictures Figure 116 in which the surface morphology of the membranes with 50 %w/w(base polymer) is compared.

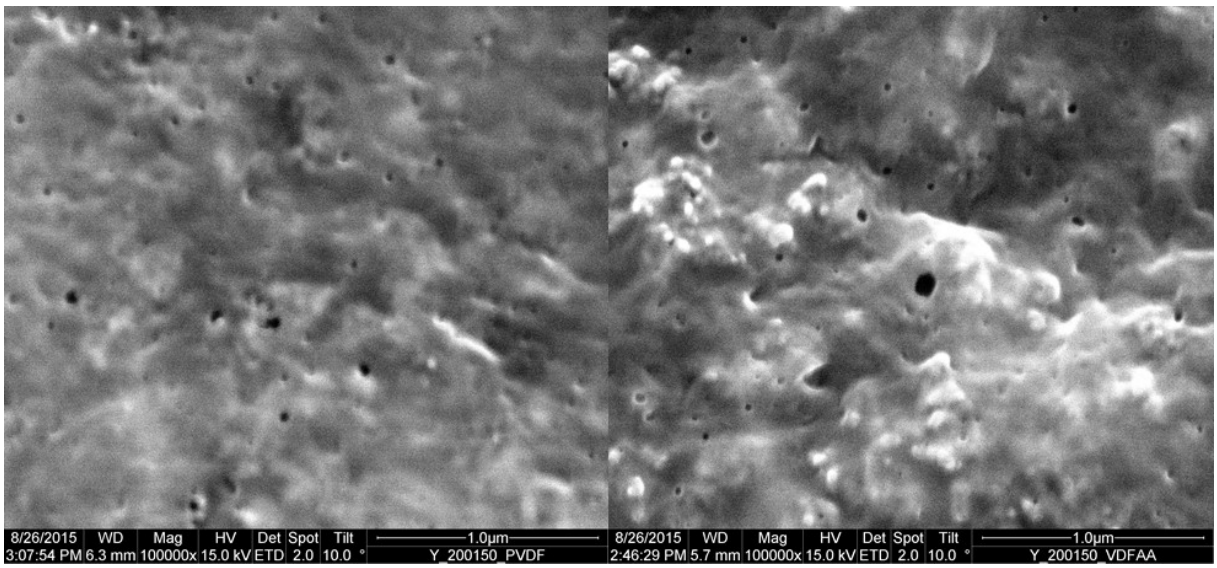

Figure 116 Comparison of skin layer morphology of membranes from both base polymers with 50% pristine NP. Left: PVDF; right: P(VDF-co-AA). Magnification 100kx.

In the figure, both membrane surfaces have comparable porosity and structure. The only difference between the two membranes is that the PVDF membrane surface is smooth and the P(VDF-*co*-AA) is rough because of immobilized nanoparticles below the skin layer. The same can be said when membranes with and without nanoparticles are compared like in Figure 60 and Figure 84.The rejection data for both membrane types is compared in Figure 117 to evaluate if any effect on the pore size can be determined.

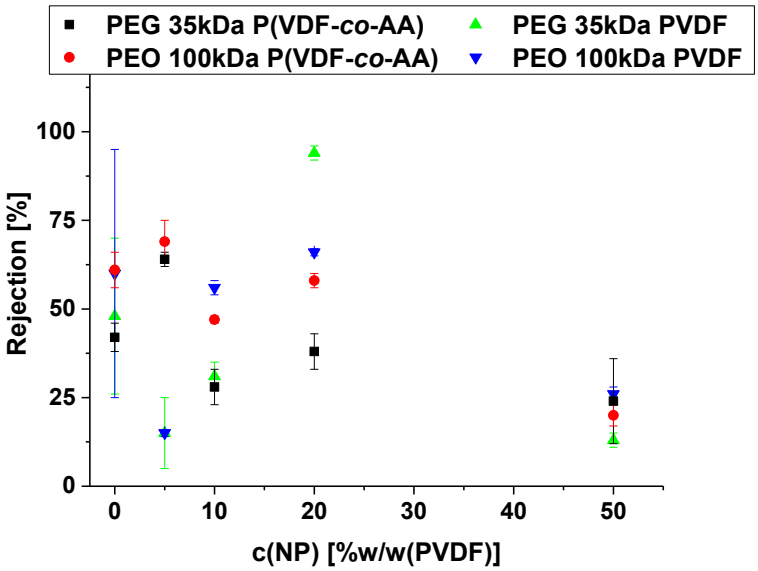

Figure 117 Comparison of rejection with both membrane polymers.

The rejection performance is comparable for base polymers. A behavior is not recognizable since the data exhibits a strong variance. A difference in terms of pore size between the two

polymers cannot be discerned. The results of the mechanical characterization are displayed in Figure 118.

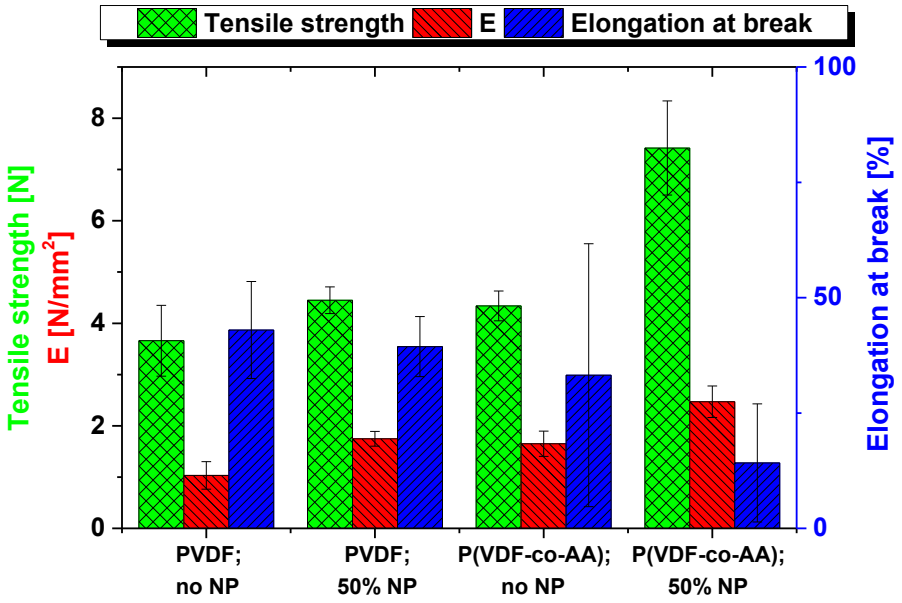

Figure 118 Comparison of the tensile strength of membrane samples with P(VDF-co-AA) and PVDF.

Both membranes without zinc oxide particles show comparable characteristics. The main difference is that the copolymer membrane has a high variation of elongation at break. The reason behind this can be traced back to the fact that P(VDF-*co*-AA) is a statistical copolymer. Therefore, the acrylic acid segments are spread irregularly over the polymer chain and the concentration of these groups per polymer chain can differentiate. This can lead to the formation of domains in the membrane where the concentration of these groups is higher than the average over the membrane. This is further enforced during the phase separation by the favored arrangement of identical groups during precipitation. The boundaries of these domains can act like grain boundaries under mechanical stress and facilitate breakage. Since the occurrence of these domains is statistically determined, a variation of the elongation at break is to be expected. When zinc oxide particles are introduced into the membrane with P(VDF-*co*-AA) shows a big increase in tensile strength and a decrease in elongation at break. This can be explained by the reinforcement of the material by the bond between the acrylic acid group of the base polymer and the zinc oxide. This in consequence also makes the material more rigid but also more brittle. Additionally, this is an indication that the bond is still present after the phase separation.

6.3.6. Overall discussion of nanoparticle integration

When all the results from the integration of the nanoparticles are discerned, two phenomena can be discussed. First and foremost, in contrast to many literature reports, that were mentioned in the background chapter, no indication was found that the pure water permeability was increased by the implementation of oxidic nanoparticles. In literature, the proposed explanation is that the hydrophilic nanoparticles increase the hydrophilicity of the membrane. An increase in hydrophilicity is often correlated with an increase in pure water permeability. In most SEM pictures of membrane surface of the current membranes no particles were found on or integrated into the skin layer. Since this severely reduces the interaction between the feed and the zinc oxide particle, it is not surprising that the effect was not observed. This also raises the question, why no particles were found in the skin layer in this work. While it is not possible to clarify this case with absolute certainty from the available data, one can exclude the materials or the phase separation conditions as reasons. The previously mentioned studies used similar or identical materials and the phase separation conditions were also identical or like the ones used in this work (cf. Table 3). This leaves only the dispersion quality respectively the sonication conditions as potential cause. In the afore-mentioned studies, the particles were just stirred into the dope solution or the dope solution was sonicated as a whole which can be expected to be of low efficiency because of the high viscosity of typical dope solutions. In chapter 6.3.1 it has been established that the dispersion quality in this work is sufficient to exclude the possibility of agglomeration in the dope solution before the phase separation. Therefore, it can be concluded that the main difference between these experiments is the particles size in the dope solution. The difference between the obtained membranes must be explained by the different behavior of the differently sized particles during the phase separation. The biggest difference between particles consisting of the same material but differing in size will be the diffusivity of the particles. The proposed mechanism, that explains the difference in the findings, is displayed in Figure 119.

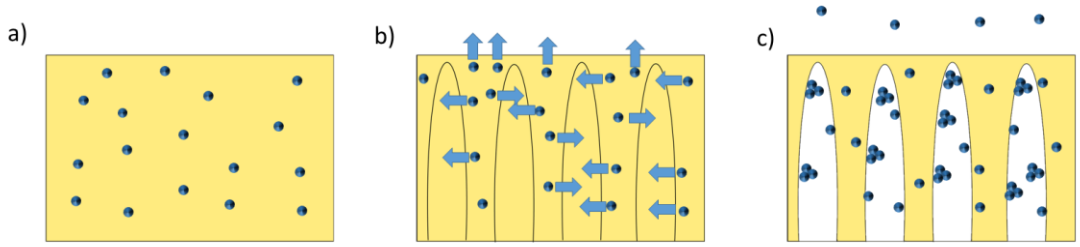

Figure 119 Behavior of not aggregated nanoparticles during the phase separation.

In the figure, the initial situation can be seen under a). It displays the well dispersed nanoparticles in the dope solution. The situation displayed under b) shows that the dope solution has separated into the polymer-rich and polymer-poor phase inside of the coagulation bath. The particles are still in the polymer-rich phase because the phase separation is a relatively fast process. The polymer has not solidified yet. The nanoparticles have the possibility to migrate into the polymer-poor phase. The driving force for this is the hydrophilicity of the particles. The direction of the particle diffusion is indicated by the arrows. Once the particles reach the polymer poor-phase the environment consist of a mixture of NMP and water. Since the particles are not compatible with NMP, they tend to agglomerate. This leads to the situation displayed under c). The polymer has precipitated and some particles are enclosed into the polymer-matrix. Most nanoparticles have formed agglomerates in the void-space of the support structure. The particles which reached the skin layer are not agglomerated since the local NMP concentration is much lower. These particles either migrate into the coagulation bath or they are removed from the skin layer during the rinsing of the membrane. The behavior for the agglomerated particles is presented in Figure 120.

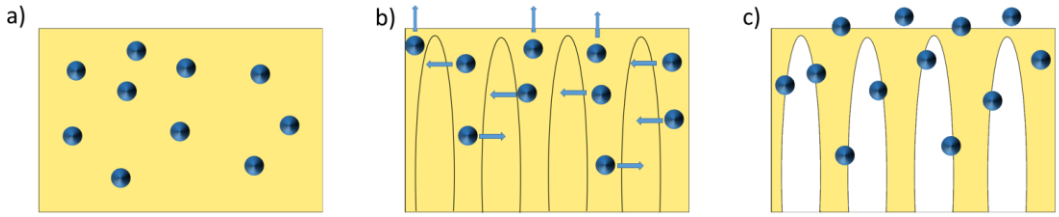

Figure 120 Behavior of aggregated nanoparticles during the phase separation.

As before, the initial dope solution is displayed under a). This time the nanoparticles are agglomerated as indicated by the bigger size of the spheres. The proto-membrane that has separated into polymer-poor and polymer-rich phase is displayed under b). The agglomerated particles exhibit the same diffusion direction but the diffusivity is smaller. This is indicated by the smaller arrows. The time before solidification is virtually identical since this is predominantly a function of the polymer concentration and the solvent non-solvent pair. This

leads to the situation that the agglomerated particles travel a significantly shorter way before the polymer solidifies. Under c) is displayed that the agglomerates are fixed into the interfaces of the membrane during the solidification. This happened because they did not reach the void-space or the bulk of the coagulation bath in the available time frame.

Supporting evidence of this could be seen in the experiment with the acetic acid modified particles in chapter 5.2.7. The viscosity measurements of the dopes solutions with the modified particles indicated that the particles were agglomerated. Consequently, agglomerates were found in the SEM pictures of the membranes which were integrate into the interface of the walls of the macro-voids (cf. Figure 69) and agglomerates on the skin layer (cf. Figure 68). This supports the hypothesis about the influence of the dispersion quality. It was not possible to find a positive influence on the permeability in this experiment. The reason for that is most likely that the used nanoparticle concentrations were high and therefore the effect was overshadowed by pore blocking.

The second phenomenon that was observed in most membranes is the decline of permeability caused by pore blocking. The exceptions to this observation are the membranes with PVP-modified particles and those which were precipitated at slow conditions. This trend correlates with the reduction of agglomerates in the structure. The slower coagulation conditions were achieved by adding solvent into the coagulation bath. In chapter 5.2.5.3 and 5.2.9 this approach lowered the tendency to agglomerate significantly over the precipitation in water. This phenomenon can be explained using the same model that was previously used. The addition of NMP into the coagulation bath lowered the water concentration in the polymer-poor phase during the phase separation. This lead to a reduction of the driving force for the diffusion of the hydrophilic nanoparticles. And consequently, to a longer residence time of the particles in the polymer-rich phase where the agglomeration is hindered by the higher viscosity.

The bonding between the novel base polymer P(VDF-*co*-AA) and the zinc oxide particles enforced this even more as was seen from the better integration. It can also be concluded that high water concentrations interfere with this bonding. Since a similar agglomeration was observed when pure water was used as coagulant. This might also be a contributing factor to the inefficiency of the carboxylic acid based modification of the nanoparticles. From all examined nanoparticle modifications, only the PVP-modification showed an effect on the agglomeration and integration of the particles into the polymer matrix. Both phenomena were

significantly improved over the pristine particles under the same conditions. It can be seen in Figure 108 that the permeability loss caused by pore blocking was reduced significantly. This can be explained by the reduction of agglomerate from the void-space volume, since the particles were integrated into the polymer-matrix. The membrane which were prepared under the slow conditions showed a similar reduction of the agglomerate and no reduction of the permeability could not be observed. This has of course the limitation that the slow precipitation conditions already lowered the performance of the membrane.

7. Conclusion

Regarding the nanoparticle modification, the conclusion is that the use of different carboxylic acids did not provide the expected benefits. While some changes for the stability in relevant solvents were seen, the overall efficiency was limited by the low surface coverage and the instability of the modification. The modification with polyvinylpyrrolidone achieved a high surface coverage with a sufficient stability in comparison. This lead to a significant change in the Hansen solubility parameter of the modified particles.

The preparation of a base membrane with the desired performance was successful in lab scale. The substitution of the solvent required a greater adjustment of the formulation than previously anticipated but the adjusted performance was still within the specifications. The transfer from lab to pilot scale revealed that a dense layer was formed in the support structure. This was unforeseen and most likely caused by the compression of the precipitating membrane by the rollers of the pilot plant. While a similar surface structure was obtained as in lab scale, the performance of the membrane was limited by the dense layer.

The experiments regarding the integration of pristine particles revealed that the sonication conditions were suitable to inhibit the formation of agglomerates in the dope solution. The small particle size enabled the particles to diffuse into the polymer-poor-phase during the phase separation. This led to formation of agglomerated particles in the void-space of the porous structure causing pore blocking. It was possible to suppress this by the employment of slow coagulation conditions and the substitution of PVDF for P(VDF-*co*-AA) which enabled the formation of a bond between the polymer and the particles.

Another successful approach to suppress the agglomeration was the implementation of PVP-modified particles. The change in affinity coupled with the steric stabilization kept the particles in the polymer-rich phase during the phase separation. This led to a good integration into the polymer-matrix and no agglomeration. The other modified particles showed no improvement over the pristine particles which is most likely caused by the aforementioned low surface coverage and instability.

As an overall resume, two significant outcomes have been achieved in the course of this thesis. First, the proposed mechanism (cf. 6.3.6), that explains the influence of the dispersion quality during the phase separation, makes it possible to clarify the differing results between similar system that were found in literature. It should even be possible to transfer this model to other systems and increase the understanding of nanocomposite preparation.

Second, the use of the PVP-based particle modification and P(VDF-*co*-AA) base polymer enable new possibilities for the preparation of nanocomposite membranes. Both methods allow the control of the nanoparticle distribution during the membrane preparation thus allowing the preparation of a nanocomposite membrane with well-integrated and well-distributed particles.

8. Literature

[1] K. Watkins, *Human Development Report 2006 - Beyond Scarcity: Power, Poverty and the Global Water Crisis*, **2006**.

[2] R. W. Baker, *Membrane Technology and Applications*, John Wiley & Sons Ltd, Chichester, **2004**.

[3] T. Melin, R. Rautenbach, *Membranverfahren*, Springer-Verlag, Berlin, **2007**.

[4] M. Ulbricht, *Polymer* **2006**, *47*, 2217–2262.

[5] NANOPUR, *Work Description: Development of Functionalized Nanostructured Polymeric Membranes and Related Manufacturing Processes for Water Purification [NMP.2011.1.2-3]*, **2012**.

[6] C. Velmurugan, N. Radhakrishnan, *Libr. Philos. Pract.* **2016**, 1372.

[7] "Web of Science," can be found under https://apps.webofknowledge.com/, accessed 13.5.2017.

[8] J. Yin, B. Deng, *J. Memb. Sci.* **2015**, *479*, 256–275.

[9] L. Y. Ng, A. W. Mohammad, C. P. Leo, N. Hilal, *Desalination* **2013**, *308*, 15–33.

[10] S. Balta, A. Sotto, P. Luis, L. Benea, B. Van der Bruggen, J. Kim, *J. Memb. Sci.* **2012**, *389*, 155–161.

[11] N. Jones, B. Ray, K. T. Ranjit, A. C. Manna, *FEMS Microbiol. Lett.* **2008**, *279*, 71–76.

[12] S. Liang, K. Xiao, Y. Mo, X. Huang, *J. Memb. Sci.* **2012**, *394–395*, 184–192.

[13] S. H. Wang, J. H. Liu, C. T. Pai, C. W. Chen, P. T. Chung, A. S. T. Chiang, S. J. Chang, *J. Colloid Interface Sci.* **2013**, *407*, 140–147.

[14] K. M. Koczkur, S. Mourdikoudis, L. Polavarapu, S. E. Skrabalak, *Dalt. Trans.* **2015**, *44*, 17883–17905.

[15] M. Mulder, *Basic Principles of Membrane Technology 2nd Edition*, Kluwer Academic Publisher, Dordrecht, **1998**.

[16] M. N. Sarbolouki, *Sep. Sci. Technol.* **1982**, *17*, 381–386.

[17] G. R. Guillen, Y. Pan, M. Li, E. M. V Hoek, *Ind. Eng. Chem. Res.* **2011**, *50*, 3798–3817.

[18] F. Liu, N. A. Hashim, Y. Liu, M. R. M. Abed, K. Li, *J. Memb. Sci.* **2011**, *375*, 1–27.

[19] A. Bottino, G. Camera-Roda, G. Capannelli, S. Munari, *J. Memb. Sci.* **1991**, *57*, 1–20.

[20] G. Kang, Y. Cao, *J. Memb. Sci.* **2014**, *463*, 145–165.

[21] A. Bottino, G. Capannelli, S. Munari, A. Turturro, *J. Polym. Sci. Part B Polym. Phys.* **1988**, *26*, 785–794.

[22] P. Sukitpaneenit, T. S. Chung, *J. Memb. Sci.* **2009**, *340*, 192–205.

[23] ISO, *Nanotechnologies–Terminology and Definitions for Nano-objects–Nanoparticle, Nanofibre and Nanoplate (ISO/TS 27687: 2008)*, **2008**.

[24] H.-D. Dörfler, *Grenzflächen Und Kolloid-Disperse Systeme*, Springer-Verlag, Berlin, **2002**.

[25] S. Abbott, C. M. Hansen, H. Yamamoto, *Hansen Solubility Parameters in Practice*, Hansen-Solubility.com, Leeds, **2013**.

[26] C. M. Hansen, *Hansen Solubility Parameters A User's Handbook*, CRC Press, Boca Raton, **2013**.

[27] E. Wiberg, *Hollemann-Wiberg, Lehrbuch Der Anorganischen Chemie*, Walter De Gruyter, Berlin, **1985**.

[28] C. Jagadish, S. J. Pearton, *Zinc Oxide Bulk, Thin Films and Nanostructures*, Elsevier, Oxford, **2006**.

[29] J. Labille, J. Brant, *Nanomedicine* **2010**, *5*, 985–998.

[30] H. Ma, P. L. Williams, S. A. Diamond, *Environ. Pollut.* **2013**, *172*, 76–85.

[31] P. J. P. Espitia, N. de F. F. Soares, J. S. dos R. Coimbra, N. J. de Andrade, R. S. Cruz, E. A. A. Medeiros, *Food Bioprocess Technol.* **2012**, *5*, 1447–1464.

[32] R. Y. Hong, J. H. Li, L. L. Chen, D. Q. Liu, H. Z. Li, Y. Zheng, J. Ding, *Powder Technol.* **2009**, *189*, 426–432.

[33] Evonik, "AEROSIL - Fumed Silica Technical Overview," can be found under http://www.aerosil.com/sites/lists/IM/Documents/Technical-Overview-AEROSIL-Fumed-Silica-EN.pdf, accessed 1.5.2017.

[34] S. J. Chung, J. P. Leonard, I. Nettleship, J. K. Lee, Y. Soong, D. V. Martello, M. K. Chyu, *Powder Technol.* **2009**, *194*, 75–80.

[35] X. Hou, F. Zhou, B. Yu, W. Liu, *Mater. Sci. Eng. A* **2007**, *452–453*, 732–736.

[36] L. Guo, S. Yang, C. W. Bay, H. Kong, C. Yang, P. Yu, J. Wang, W. Ge, G. K. L. Wong, *Chem. Maters.* **2000**, *12*, 2268–2274.

[37] E. Tang, G. Cheng, X. Ma, X. Pang, Q. Zhao, *Appl. Surf. Sci.* **2006**, *252*, 5227–5232.

[38] S. J. Oh, N. Kim, Y. T. Lee, *J. Memb. Sci.* **2009**, *345*, 13–20.

[39] L. Yan, Y. S. Li, C. B. Xiang, S. Xianda, *J. Memb. Sci.* **2006**, *276*, 162–167.

[40] L.-Y. Yu, H.-M. Shen, Z.-L. Xu, *J. Appl. Polym. Sci.* **2009**, *113*, 1763–1772.

[41] X. Cao, J. Ma, X. Shi, Z. Ren, *Appl. Surf. Sci.* **2006**, *253*, 2003–2010.

[42] E. Yuliwati, A. F. Ismail, T. Matsuura, M. A. Kassim, M. S. Abdullah, *Desalination* **2011**,

283, 206–213.

[43] H. Song, J. Shao, Y. He, B. Liu, X. Zhong, *J. Memb. Sci.* **2012**, *405–406*, 48–56.

[44] C. Dong, G. He, H. Li, R. Zhao, Y. Han, Y. Deng, *J. Memb. Sci.* **2012**, *387–388*, 40–47.

[45] F. Liu, M. R. M. Abed, K. Li, *J. Memb. Sci.* **2011**, *366*, 97–103.

[46] S. W. Bian, I. A. Mudunkotuwa, T. Rupasinghe, V. H. Grassian, *Langmuir* **2011**, *27*, 6059–6068.

[47] E. Yuliwati, A. F. Ismail, *Desalination* **2011**, *273*, 226–234.

[48] Y. Wei, H. Q. Chu, B. Z. Dong, X. Li, S. J. Xia, Z. M. Qiang, *Desalination* **2011**, *272*, 90–97.

[49] R. Marczak, D. Segets, M. Voigt, W. Peukert, *Adv. Powder Technol.* **2010**, *21*, 41–49.

[50] Z. Niu, Y. Li, *Chem. Mater.* **2014**, *26*, 72–83.

[51] Amicon, *Stirred Ultrafiltration Cells: User Guide*, **2004**.

[52] R. M. Boom, T. van den Boomgaard, C. a. Smolders, *J. Memb. Sci.* **1994**, *90*, 231–249.

[53] M. Hesse, H. Meier, B. Zeeh, *Spektroskopische Methoden in Der Organischen Chemie*, Thieme Georg Verlag, Stuttgart, **2005**.

[54] SDBSWeb, “Zinc oxide (SDBS No.: 40168),” can be found under http://sdbs.db.aist.go.jp, accessed 3.3.2017.

[55] SDBSWeb, “Oxalic acid (SDBS No.: 2659),” can be found under http://sdbs.db.aist.go.jp, accessed 3.3.2017.

[56] G. Socrates, *Infrared and Raman Characteristic Group Frequencies : Tables and Charts*, John Wiley & Sons, Chichester, **2008**.

[57] SDBSWeb, “Acetic acid (SDBS No.: 306),” can be found under http://sdbs.db.aist.go.jp, accessed 3.3.2017.

[58] SDBSWeb, “Trifluoroacetic acid (SDBS No.: 746),” can be found under http://sdbs.db.aist.go.jp, accessed 3.3.2017.

[59] SDBSWeb, “Polyvinylpyrrolidone (SDBS No.: 16268),” can be found under http://sdbs.db.aist.go.jp, accessed 3.3.2017.

[60] GESTIS-Stoffdatenbank, “N-Methyl-2-pyrrolidon,” can be found under http://www.dguv.de/ifa/gestis/gestis-stoffdatenbank/index.jsp, accessed 1.9.2016.

[61] T. Mezger, *Das Rheologie Handbuch*, Vincentz Network, Hannover, **2012**.

[62] J. Jordan, K. I. Jacob, R. Tannenbaum, M. A. Sharaf, I. Jasiuk, *Mater. Sci. Eng. A* **2005**, *393*, 1–11.

[63] Malvern instruments Ltd., *Zetasizer Nano Series User Manual*, Malvern Instruments Ltd,

Worcestershire, **2004**.

[64] S. Sakohara, M. Ishida, M. a Anderson, *J. Phys. Chem. B* **1998**, *102*, 10169–10175.

[65] J. M. Berg, A. Romoser, N. Banerjee, R. Zebda, C. M. Sayes, *Nanotoxicology* **2009**, *3*, 276–283.

[66] R. L. Redington, K. C. Lin, *Spectrochim. Acta Part A Mol. Spectrosc.* **1971**, *27*, 2445–2460.

[67] G. D. Clayton, F. E. Clayton, *Patty's Industrial Hygiene and Toxicology: Volume 2A, 2B, 2C: Toxicology.*, John Wiley Sons, New York, **1982**.

[68] S. S. Madaeni, A. H. Taheri, *Chem. Eng. Technol.* **2011**, *34*, 1328–1334.

[69] F. G. Paulsen, S. S. Shojaie, W. B. Krantz, *J. Memb. Sci.* **1994**, *91*, 265–282.

[70] M. Pattanaik, S. K. Bhaumik, *Mater. Lett.* **2000**, *44*, 352–360.

[71] G. Wu, S. Gan, L. Cui, Y. Xu, *Appl. Surf. Sci.* **2008**, *254*, 7080–7086.

[72] M. L. Luo, J. Q. Zhao, W. Tang, C. S. Pu, *Appl. Surf. Sci.* **2005**, *249*, 76–84.

[73] F. Duan, D. Kwek, A. Crivoi, *Nanoscale Res. Lett.* **2011**, *6*, 248–252.

[74] A. Bottino, G. Capannelli, A. Comite, *Desalination* **2002**, *146*, 35–40.

[75] S. H. Zhi, L. S. Wan, Z. K. Xu, *J. Memb. Sci.* **2014**, *454*, 144–154.

9. Appendix

9.1. List of used chemicals

Substance	Quality	Manufacturer
1.4-Dioxane	p.a.	Merck
2-Butanol	ReagentPlus®, ≥ 99 %w	Sigma-Aldrich
Acetic acid	≥ 99.5 %w	Aldrich
Acetone	p.a.	Fluka
Acetonitrile	p.a.	Merck
Benzene	p.a.	Merck
Carbon tetrachloride	99 %	Aldrich
Chloroform	p.a.	Acros
Cyclohexane	AnalaR NORMAPUR	VWR Chemicals
Cyclohexanone	Reagent grade, ≥ 99 %w pure	Sigma-Aldrich
Dichloromethane	p.a.	Aldrich
Dimethyl sulfoxide	p.a.	Merck
Dimethylacetamide	> 98 %	Fluka
Dimethylformamide	Puris	AppliChem
DI-water	deionized	In-house system
Ethanol	p.a.	VWR Chemicals
Ethyl acetate	p.a.	Fluka
Ethylene glycol	Reagent grade, ≥ 99 %w pure	Sigma-Aldrich
n-Hexane	95 %	Sigma-Aldrich
Methanol	p.a.	VWR Chemicals
Methyl ethyl ketone	≥ 99.5 %w pure	Aldrich
N-Methyl-2-pyrrolidone	> 99.5 %w pure	Merck
PEG 35 kDa		Fluka
PEO 100 kDa		Aldrich
PVDF Solef 6010	powder	Solvay Specialty Polymers
PVP Luvitec K-30	≥ 95 %w pure	BASF
p-Xylene	p.a.	Merck
Sodium chloride	ACS, ISO, Reag. Ph. Eur.	Merck
Sodium azide	> 99 %w pure	Sigma-Aldrich
Tetrahydrofuran	p.a.	Merck
Triethylene glycol	ReagentPlus®, ≥ 99 %w pure	Sigma-Aldrich

Trifluoroacetic acid	Reagent grade, ≥ 99 %w pure	Sigma-Aldrich
Water	Ultrapure (18.1 mΩ cm^{-1})	Milli-Q RO System
VP ZnO 20	≥ 99.5 %w pure	Evonik Industries AG

9.2. Additional data

Table 55 Solvent properties for DLS.

No. in HSPiP	Solvent	CAS	n [-]	T1 [°C]	η1 [cPs]	T2 [°C]	η2 [cPs]
7	Acetone	67-64-1	1.359	20	0.331	50	0.256
10	ACN	75-05-8	1.350	15	0.374	25	0.345
52	Benzene	71-43-2	1.501	20	0.649	50	0.436
93	2-Butanol	78-92-2	1.397	25	3.004	40	1.788
156	Chloroform	67-66-3	1.450	20	0.580	25	0.542
181	Cyclohexane	110-82-7	1.430	17	1.020	20	0.696
183	Cyclohexanone	108-94-1	1.430	17	1.020	20	0.696
285	DMAc	127-19-5	1.438	20	1.020	40	0.780
297	DMF	68-12-2	1.430	20	0.920	25	0.802
303	DMSO	67-68-5	1.479	20	2.140	30	1.808
306	1.4-Dioxane	123-91-1	1.422	25	1.197	40	0.942
325	Ethanol	64-17-5	1.360	20	1.200	30	1.003
328	Ethyl Acetate	141-78-6	1.370	20	0.455	25	0.441
368	EG	107-21-1	1.460	20	19.900	30	12.200
417	Hexane	110-54-3	1.380	20	0.326	25	0.294
456	MeOH	67-56-1	1.330	20	0.597	25	0.547
481	MEK	78-93-3	1.379	20	0.420	25	0.410
521	NMP	872-50-4	1.470	20	1.700	25	1.650
524	DCM	75-09-2	1.424	20	0.625	25	0.410
617	THF	109-99-9	1.407	20	0.480	25	0.454
657	TEG	112-27-6	1.456	20	46.400	25	35.530
696	Water	7732-18-5	1.333	20	1.002	30	0.797
697	*p*-Xylene	106-42-3	1.495	20	0.648	40	0.513
862	CCl_4	56-23-5	1.463	21	0.958	35	0.793

Table 56 Hansen parameter of solvents for HSPiP.

No. In HSPiP	Solvent	CAS	δD [MPa$^{1/2}$]	δP [MPa$^{1/2}$]	δH [MPa$^{1/2}$]
7	Acetone	67-64-1	15.5	10.4	7.0
10	ACN	75-05-8	15.3	18.0	6.1
52	Benzene	71-43-2	18.4	0.0	2.0
93	2-Butanol	78-92-2	15.8	5.7	14.5
156	Chloroform	67-66-3	17.8	3.1	5.7
181	Cyclohexane	110-82-7	16.8	0.0	0.2
183	Cyclohexanone	108-94-1	17.8	8.4	5.1
285	DMAc	127-19-5	16.8	11.5	9.4
297	DMF	68-12-2	17.4	13.7	11.3
303	DMSO	67-68-5	18.4	16.4	10.2
306	1.4-Dioxane	123-91-1	17.5	1.8	9.0
325	Ethanol	64-17-5	15.8	8.8	19.4
328	Ethyl Acetate	141-78-6	15.8	5.3	7.2
368	EG	107-21-1	17.0	11	26.0
417	Hexane	110-54-3	14.9	0.0	0.0
456	MeOH	67-56-1	14.7	12.3	22.3
481	MEK	78-93-3	16.0	9.0	5.1
521	NMP	872-50-4	18.0	12.3	7.2
524	DCM	75-09-2	17.0	7.3	7.1
617	THF	109-99-9	16.8	5.7	8.0
657	TEG	112-27-6	16.0	12.5	18.6
696	Water	7732-18-5	15.5	16.0	42.3
697	p-Xylene	106-42-3	17.8	1.0	3.1
862	CCl_4	56-23-5	16.1	8.3	0.0

Table 57 Zinc oxide data for monolayer calculation.

ZnO nanoparticle	
d [nm]	100
density [cm³/g]	5.61
A_{NP} [m²]	3.14E-14
V_{NP} [m³]	5.24E-22
m_{NP} [g]	9.33E-17

Table 58 Monolayer calculation data for low molecular agents.

	TFA	Ox	Ac
density [cm³/g]	1.48	1.9	1.05
M [g/Mol]	114.02	90.04	60.05
specific volume			
V_m [cm³/Mol]	7.7E+01	4.7E+01	5.7E+01
V_m [m³/molecule]	1.3E-28	7.9E-29	9.5E-29
r_m [m] for sphere	3.1E-10	2.7E-10	2.8E-10
area of adsorption			
A_m [m²]	3.4E-19	2.4E-19	2,8E-19
monolayer			
$N_{monolayer}$ [molecules]	93194	128329	113213
$m_{monolayer}$ [g]	1.8E-17	1.9E-17	1.1E-17
$w_{monolayer}$ [%]	15.9	17.1	10.8

Table 59 Monolayer calculation data for polyvinylpyrrolidone.

	polyvinylpyrrolidone	
	repetition unit	**polymer**
density [cm³/g]	1.04	n.d.
M [g/Mol]	114.14	40000
specific volume		
V_m [cm³/Mol]	109.75	n.d.
V_m [m³/molecule]	1.82E-28	n.d.
r_m [m] for sphere	3.51E-10	n.d.
r_H [m]	n.a.	3.34E-09
area of adsorption		
A_m [m²]	4.3E-19	1.9E-17
Monolayer		
molecules	73312	811
mass [g]	1.3895E-17	5.3872E-17
$w_{monolayer}$ [%]	13.0	36.6
mean	24.8	

Table 60 DLS data for influence of sonication time.

sonication time [min]	time [d]	1	2	3	4	5	6	7	8	observation
0	d_H [nm]	142.5	n.d.	n.d.	n.d.	n.d.	n.d.	n.d.	n.d.	unstable
	SD [nm]	141.9	n.d.	n.d.	n.d.	n.d.	n.d.	n.d.	n.d.	
1	d_H [nm]	290.1	113.7	131.6	n.d.	n.d.	n.d.	101.9	104.2	unstable
	SD [nm]	114.8	94	100	n.d.	n.d.	n.d.	65	68.2	
2	d_H [nm]	86.6	n.d.	n.d.	n.d.	n.d.	n.d.	n.d.	n.d.	unstable
	SD [nm]	45.5	n.d.	n.d.	n.d.	n.d.	n.d.	n.d.	n.d.	
3	d_H [nm]	122.1	103.8	101.9	n.d.	104.6	97.1	109.1	n.d.	stable
	SD [nm]	7.7	17.1	15	n.d.	12	1.4	11	n.d.	
4	d_H [nm]	106.9	96.7	95.2	n.d.	80.2	95	94.6	n.d.	stable
	SD [nm]	10.6	11.7	12.5	n.d.	5.5	12.7	12.3	n.d.	
5	d_H [nm]	103.5	99	112.9	n.d.	79.1	86.1	94.5	n.d.	stable
	SD [nm]	12.6	9.5	14.1	n.d.	15.1	13.9	6.9	n.d.	
6	d_H [nm]	102.3	93.1	85.8	n.d.	95.9	85.3	123.8	n.d.	stable
	SD [nm]	8.6	1	16.7	n.d.	32.9	12.2	34.1	n.d.	
7	d_H [nm]	107.7	100	89.8	n.d.	89.7	88.6	83.7	n.d.	stable
	SD [nm]	6.9	6.7	8.8	n.d.	7.5	14.8	6.1	n.d.	
8	d_H [nm]	111.6	90.8	84.5	n.d.	89.8	89	85.1	n.d.	stable
	SD [nm]	3.5	16.9	9.7	n.d.	7.6	7.9	6.9	n.d.	
9	d_H [nm]	116.7	103.8	68.2	n.d.	88.1	92	88.7	n.d.	stable
	SD [nm]	6.6	7.2	12.4	n.d.	12	14.7	6.7	n.d.	
10	d_H [nm]	121.3	101.1	96.1	n.d.	89.7	80.7	88.7	n.d.	stable
	SD [nm]	5.2	6.8	2.6	n.d.	6.7	14.6	14	n.d.	
15	d_H [nm]	105.5	97.8	n.d.	n.d.	n.d.	83.4	105.9	n.d.	stable
	SD [nm]	7.1	8.3	n.d.	n.d.	n.d.	9.9	10.6	n.d.	
20	d_H [nm]	108.6	109.7	117.2	n.d.	n.d.	n.d.	90.4	107.1	stable
	SD [nm]	16.1	6.1	9.5	n.d.	n.d.	n.d.	12.2	7.4	
25	d_H [nm]	108.4	94.5	134.8	n.d.	n.d.	n.d.	96.1	156.9	unstable
	SD [nm]	16.4	13.8	8.5	n.d.	n.d.	n.d.	18.4	20.4	
30	d_H [nm]	107.7	136.2	151.9	106.6	n.d.	n.d.	102.3	106.1	unstable
	SD [nm]	10.9	5.6	10.1	24	n.d.	n.d.	25.4	11.7	
45	d_H [nm]	103.8	112.8	n.d.	n.d.	n.d.	92.2	94.3	n.d.	stable
	SD [nm]	8.4	10.3	n.d.	n.d.	n.d.	9.1	12.7	n.d.	
60	d_H [nm]	275	175.6	239.5	146.8	n.d.	n.d.	197.9	123.8	unstable
	SD [nm]	28.9	17.9	4.7	11.9	n.d.	n.d.	27.6	41	

Table 62 All data NP modification with TFA.

c(TFA)	pH	m (ZnO)	m (TFA)	mass retrieved	mass retrieval
[%w/w(ZnO)]	[-]	[g]	[g]	[g]	[%]
5	2.35	1.00	0.05	0.90	85.7
15	1.9	1.00	0.15	0.87	75.4
20	1.7	1.00	0.20	0.83	69.5
30	1.6	1.00	0.30	0.84	67.3
75	1.2	1.00	0.75	0.68	54.6
100	1.0	1.00	1.00	0.56	45.1
200	0.7	1.00	2.00	0.26	20.8
200	6.3	5.00	10.00	4.88	78.3
200	7.0	2.00	4.00	2.00	80.3
200	10.0	2.00	4.00	2.00	80.3
500	7.0	5.00	25.00	4.99	80.1
1000	7.0	5.00	50.00	5.00	80.3

Table 63 All data NP modification with PVP.

	c(PVP)	m (ZnO)	m (PVP)	mass retrieved	mass retrieval
	[%w/w(ZnO)]	[g]	[g]	[g]	[%]
codispersion	500	5.0	25.0	4.93	80.9
modification	500	5.0	25.0	5.14	84.2

Table 64 All data NP modification with other carboxylic acids.

mod. Agent	c(Mod)	pH	m (mod)	m (TFA)	mass retrieved	mass retrieval
	[%w/w(ZnO)]	[-]	[g]	[g]	[g]	[%]
Ac	200	2.5	5.0	10.0	0.0	0.0
Ac	200	5.0	15.0	30.0	11.95	67.1
Ox	200	2.65	5.0	10.0	11.16	176.0

Table 65 DLS data for HSP rating for pristine ZnO.

No.	solvent	time [days]	1	2	3	4	5	6	7	rating
7	Acetone	d_H [nm]	611.6	1.3	1.8	unstable	n.d.	n.d.	n.d.	6
		SD [nm]	479.7	0.2	1.3	unstable	n.d.	n.d.	n.d.	
10	ACN	d_H [nm]	457.0	450.8	unstable	n.d.	n.d.	n.d.	n.d.	6
		SD [nm]	75.4	181.0	unstable	n.d.	n.d.	n.d.	n.d.	
52	Benzene	d_H [nm]	1061.7	654.2	unstable	n.d.	n.d.	n.d.	n.d.	6
		SD [nm]	192.2	462.2	unstable	n.d.	n.d.	n.d.	n.d.	
93	2-Butanol	d_H [nm]	1160.7	137.2	n.d.	95.1	84.9	n.d.	n.d.	2
		SD [nm]	181.3	23.9	n.d.	25.9	7.1	n.d.	n.d.	
156	Chloroform	d_H [nm]	619.7	337.9	unstable	n.d.	n.d.	n.d.	n.d.	6
		SD [nm]	102.5	75.3	unstable	n.d.	n.d.	n.d.	n.d.	
181	Cyclohexane	d_H [nm]	225.6	unstable	n.d.	n.d.	n.d.	n.d.	n.d.	6
		SD [nm]	3.8	unstable	n.d.	n.d.	n.d.	n.d.	n.d.	
285	DMAc	d_H [nm]	150.4	89.1	144.6	125.3	n.d.	n.d.	n.d.	2
		SD [nm]	2.9	9.0	5.4	21.5	n.d.	n.d.	n.d.	
297	DMF	d_H [nm]	94.5	113.9	n.d.	n.d.	n.d.	83.2	119.4	1
		SD [nm]	17.9	3.4	n.d.	n.d.	n.d.	13.3	13.3	
303	DMSO	d_H [nm]	136.1	unstable	n.d.	n.d.	n.d.	n.d.	n.d.	6
		SD [nm]	32.6	unstable	n.d.	n.d.	n.d.	n.d.	n.d.	
306	1,4-Dioxane	d_H [nm]	439.3	496.9	890.0	n.d.	n.d.	n.d.	n.d.	3
		SD [nm]	83.3	176.6	234.6	n.d.	n.d.	n.d.	n.d.	
325	EtOH	d_H [nm]	124.1	115.1	115.2	116.6	n.d.	n.d.	n.d.	1
		SD [nm]	0.7	14.8	2.9	9.5	n.d.	n.d.	n.d.	
328	EtAc	d_H [nm]	1024.2	217.2	252.3	227.0	264.1	n.d.	n.d.	2
		SD [nm]	1391.5	15.9	22.7	22.3	28.2	n.d.	n.d.	
368	EG	d_H [nm]	85.4	78.1	69.2	n.d.	n.d.	n.d.	n.d.	1
		SD [nm]	27.5	24.5	19.2	n.d.	n.d.	n.d.	n.d.	
417	Hexane	d_H [nm]	567.0	unstable	n.d.	n.d.	n.d.	n.d.	n.d.	6
		SD [nm]	182.2	unstable	n.d.	n.d.	n.d.	n.d.	n.d.	
456	MeOH	d_H [nm]	92.9	129.5	109.0	69.9	n.d.	n.d.	n.d.	1
		SD [nm]	31.8	13.8	22.6	6.2	n.d.	n.d.	n.d.	
481	MEK	d_H [nm]	134.1	170.3	214.2	n.d.	n.d.	n.d.	n.d.	4
		SD [nm]	1.6	9.6	96.8	n.d.	n.d.	n.d.	n.d.	
521	NMP	d_H [nm]	408.4	652.1	unstable	n.d.	n.d.	n.d.	n.d.	6
		SD [nm]	220.1	339.0	unstable	n.d.	n.d.	n.d.	n.d.	
524	DCM	d_H [nm]	182.7	unstable	n.d.	n.d.	n.d.	n.d.	n.d.	6
		SD [nm]	58.3	unstable	n.d.	n.d.	n.d.	n.d.	n.d.	
617	THF	d_H [nm]	152.5	176.2	206.6	n.d.	n.d.	n.d.	n.d.	2
		SD [nm]	32.2	29.0	23.5	n.d.	n.d.	n.d.	n.d.	
696	Water	d_H [nm]	104.4	114.0	8.6	85.7	75.7	n.d.	n.d.	1
		SD [nm]	1.4	9.2	1.3	0.2	7.1	n.d.	n.d.	
697	*p*-Xylene	d_H [nm]	872.0	unstable	n.d.	n.d.	n.d.	n.d.	n.d.	6
		SD [nm]	376.9	unstable	n.d.	n.d.	n.d.	n.d.	n.d.	
862	CCl_4	d_H [nm]	225.8	unstable	n.d.	n.d.	n.d.	n.d.	n.d.	6
		SD [nm]	145.6	unstable	n.d.	n.d.	n.d.	n.d.	n.d.	

Table 66 DLS data for HSP rating for modified ZnO NP with 200% Ox.

No.	solvent	time [days]	1	2	3	4	5	rating
7	Acetone	d_H [nm]	1.0	unstable	n.d.	n.d.	n.d.	6
		SD [nm]	0.1	unstable	n.d.	n.d.	n.d.	
10	ACN	d_H [nm]	145.0	unstable	n.d.	n.d.	n.d.	6
		SD [nm]	14.5	unstable	n.d.	n.d.	n.d.	
93	2-Butanol	d_H [nm]	677.0	unstable	n.d.	n.d.	n.d.	6
		SD [nm]	623.8	unstable	n.d.	n.d.	n.d.	
156	Chloroform	d_H [nm]	949.0	unstable	n.d.	n.d.	n.d.	6
		SD [nm]	67.1	unstable	n.d.	n.d.	n.d.	
183	Cyclohexanone	d_H [nm]	367.9	unstable	n.d.	n.d.	n.d.	6
		SD [nm]	224.5	unstable	n.d.	n.d.	n.d.	
285	DMAc	d_H [nm]	161.0	unstable	n.d.	n.d.	n.d.	6
		SD [nm]	97.8	unstable	n.d.	n.d.	n.d.	
297	DMF	d_H [nm]	169.5	unstable	n.d.	n.d.	n.d.	6
		SD [nm]	60.1	unstable	n.d.	n.d.	n.d.	
303	DMSO	d_H [nm]	289.9	unstable	n.d.	n.d.	n.d.	6
		SD [nm]	113.4	unstable	n.d.	n.d.	n.d.	
306	1,4-Dioxane	d_H [nm]	333.8	unstable	n.d.	n.d.	n.d.	6
		SD [nm]	99.3	unstable	n.d.	n.d.	n.d.	
325	EtOH	d_H [nm]	120.5	unstable	n.d.	n.d.	n.d.	6
		SD [nm]	67.6	unstable	n.d.	n.d.	n.d.	
328	EtAc	d_H [nm]	256.3	unstable	n.d.	n.d.	n.d.	6
		SD [nm]	92.1	unstable	n.d.	n.d.	n.d.	
368	EG	d_H [nm]	402.0	377.7	83.8	70.6	192.1	3
		SD [nm]	22.1	44.3	47.6	4.6	242.3	
417	Hexane	d_H [nm]	871.1	unstable	n.d.	n.d.	n.d.	6
		SD [nm]	670.2	unstable	n.d.	n.d.	n.d.	
456	MeOH	d_H [nm]	334.8	unstable	n.d.	n.d.	n.d.	6
		SD [nm]	131.2	unstable	n.d.	n.d.	n.d.	
481	MEK	d_H [nm]	229.9	unstable	n.d.	n.d.	n.d.	6
		SD [nm]	80.8	unstable	n.d.	n.d.	n.d.	
521	NMP	d_H [nm]	98.9	unstable	n.d.	n.d.	n.d.	6
		SD [nm]	25.5	unstable	n.d.	n.d.	n.d.	
524	DCM	d_H [nm]	4393.3	unstable	n.d.	n.d.	n.d.	6
		SD [nm]	2272.2	unstable	n.d.	n.d.	n.d.	
617	THF	d_H [nm]	321.5	unstable	n.d.	n.d.	n.d.	6
		SD [nm]	103.2	unstable	n.d.	n.d.	n.d.	
696	Water	d_H [nm]	177.0	unstable	n.d.	n.d.	n.d.	6
		SD [nm]	94.3	unstable	n.d.	n.d.	n.d.	

Table 67 DLS data for HSP rating for modified ZnO NP with 200% Ac at pH 5.

No.	solvent	time [days]	1	2	3	4	5	rating
7	Acetone	d_H [nm]	1.0	0.9	0.9	1.0	n.d.	1
		SD [nm]	0.0	0.0	0.0	0.0	n.d.	
10	ACN	d_H [nm]	98.5	87.7	84.5	79.8	n.d.	1
		SD [nm]	9.8	9.4	6.9	7.2	n.d.	
93	2-Butanol	d_H [nm]	380.3	unstable	n.d.	n.d.	n.d.	6
		SD [nm]	157.4	unstable	n.d.	n.d.	n.d.	
156	Chloroform	d_H [nm]	318.7	unstable	n.d.	n.d.	n.d.	6
		SD [nm]	5.3	unstable	n.d.	n.d.	n.d.	
183	Cyclohexanone	d_H [nm]	426.7	302.5	538.0	520.3	536.0	3
		SD [nm]	58.4	39.6	246.0	51.4	94.8	
285	DMAc	d_H [nm]	89.7	87.5	91.5	99.0	99.9	1
		SD [nm]	6.4	9.9	12.4	4.2	15.9	
297	DMF	d_H [nm]	434.6	unstable	n.d.	n.d.	n.d.	6
		SD [nm]	191.1	unstable	n.d.	n.d.	n.d.	
303	DMSO	d_H [nm]	952.0	unstable	n.d.	n.d.	n.d.	6
		SD [nm]	253.6	unstable	n.d.	n.d.	n.d.	
306	1,4-Dioxane	d_H [nm]	765.0	942.7	unstable	n.d.	n.d.	6
		SD [nm]	222.1	567.3	unstable	n.d.	n.d.	
325	EtOH	d_H [nm]	236.8	unstable	n.d.	n.d.	n.d.	6
		SD [nm]	86.7	unstable	n.d.	n.d.	n.d.	
328	EtAc	d_H [nm]	96.8	2081.3	121.6	123.5	125.4	2
		SD [nm]	12.6	2771.0	3.4	2.0	7.7	
368	EG	d_H [nm]	45.5	198.7	60.1	71.7	62.4	1
		SD [nm]	11.9	177.2	15.1	12.5	15.7	
417	Hexane	d_H [nm]	3.5	unstable	n.d.	n.d.	n.d.	6
		SD [nm]	0.5	unstable	n.d.	n.d.	n.d.	
456	MeOH	d_H [nm]	86.4	67.8	122.5	74.6	75.5	1
		SD [nm]	15.7	11.4	19.2	8.3	29.5	
481	MEK	d_H [nm]	157.9	unstable	n.d.	n.d.	n.d.	6
		SD [nm]	20.6	unstable	n.d.	n.d.	n.d.	
521	NMP	d_H [nm]	83.7	87.4	96.6	85.3	94.7	1
		SD [nm]	17.5	9.4	15.6	13.0	24.3	
524	DCM	d_H [nm]	201.5	unstable	n.d.	n.d.	n.d.	6
		SD [nm]	3.8	unstable	n.d.	n.d.	n.d.	
617	THF	d_H [nm]	189.1	237.6	178.3	183.9	436.0	2
		SD [nm]	13.6	64.4	25.8	78.3	0.0	
696	Water	d_H [nm]	85.7	96.3	70.2	71.5	81.3	1
		SD [nm]	6.2	33.4	8.2	5.7	20.6	
697	*p*-Xylene	d_H [nm]	871.7	unstable	n.d.	n.d.	n.d.	6
		SD [nm]	1032.6	unstable	n.d.	n.d.	n.d.	

Table 68 DLS data for HSP rating for ZnO NP modified with 100% TFA at pH 1.

No.	solvent	time [days]	1	2	3	4	5	rating
7	Acetone	d_H [nm]	1199.7	333.6	unstable	n.d.	n.d.	6
		SD [nm]	383.6	49.4	unstable	n.d.	n.d.	
10	ACN	d_H [nm]	93.7	1.0	0.9	unstable	n.d.	6
		SD [nm]	1.1	0.0	0.0	unstable	n.d.	
52	Benzene	d_H [nm]	446.2	unstable	n.d.	n.d.	n.d.	6
		SD [nm]	186.6	unstable	n.d.	n.d.	n.d.	
93	2-Butanol	d_H [nm]	754.0	148.8	86.8	83.6	78.8	1
		SD [nm]	94.2	22.8	16.2	14.0	17.2	
156	Chloroform	d_H [nm]	403.3	unstable	n.d.	n.d.	n.d.	6
		SD [nm]	56.6	unstable	n.d.	n.d.	n.d.	
183	Cyclohexanone	d_H [nm]	782.0	2006.7	1536.3	1292.3	950.3	4
		SD [nm]	69.2	310.9	229.0	564.2	201.5	
285	DMAc	d_H [nm]	94.4	84.3	81.4	92.3	n.d.	1
		SD [nm]	13.8	15.1	6.2	12.6	n.d.	
297	DMF	d_H [nm]	91.2	85.7	108.1	88.7	n.d.	1
		SD [nm]	14.8	7.9	6.5	18.8	n.d.	
303	DMSO	d_H [nm]	661.3	unstable	n.d.	n.d.	n.d.	6
		SD [nm]	269.6	unstable	n.d.	n.d.	n.d.	
306	1,4-Dioxane	d_H [nm]	208.0	284.1	324.3	n.d.	n.d.	4
		SD [nm]	9.7	61.0	54.5	n.d.	n.d.	
325	EtOH	d_H [nm]	129.7	772.0	255.7	n.d.	n.d.	3
		SD [nm]	20.4	24.8	146.3	n.d.	n.d.	
328	EtAc	d_H [nm]	87.2	83.9	77.0	82.4	91.6	1
		SD [nm]	3.2	7.0	1.8	6.2	0.9	
368	EG	d_H [nm]	13.1	54.8	81.7	n.d.	n.d.	1
		SD [nm]	0.1	12.9	27.2	n.d.	n.d.	
417	Hexane	d_H [nm]	1807.0	unstable	n.d.	n.d.	n.d.	6
		SD [nm]	210.7	unstable	n.d.	n.d.	n.d.	
456	MeOH	d_H [nm]	77.4	64.8	73.9	61.1	113.4	1
		SD [nm]	20.8	11.6	7.7	13.2	8.6	
481	MEK	d_H [nm]	1178.0	unstable	n.d.	n.d.	n.d.	6
		SD [nm]	102.6	unstable	n.d.	n.d.	n.d.	
521	NMP	d_H [nm]	540.8	105.2	unstable	n.d.	n.d.	6
		SD [nm]	281.3	23.9	unstable	n.d.	n.d.	
524	DCM	d_H [nm]	200.6	239.4	unstable	n.d.	n.d.	6
		SD [nm]	44.0	108.7	unstable	n.d.	n.d.	
617	THF	d_H [nm]	97.5	91.2	87.0	n.d.	n.d.	1
		SD [nm]	5.1	4.5	13.5	n.d.	n.d.	
696	Water	d_H [nm]	31.9	1.0	96.9	89.4	n/a	1
		SD [nm]	3.0	0.0	5.9	10.0	n/a	
697	*p*-Xylene	d_H [nm]	395.8	unstable	n.d.	n.d.	n.d.	6
		SD [nm]	154.5	unstable	n.d.	n.d.	n.d.	
862	CCl_4	d_H [nm]	4215.3	unstable	n.d.	n.d.	n.d.	6
		SD [nm]	1793.6	unstable	n.d.	n.d.	n.d.	

Table 69 DLS data for HSP rating for modified ZnO NP with 200% TFA at pH 6.

No.	solvent	time [days]	1	2	3	4	rating
7	Acetone	d_H [nm]	0.9	unstable	n.d.	n.d.	6
		SD [nm]	0.0	unstable	n.d.	n.d.	
10	ACN	d_H [nm]	160.5	133.9	174.2	unstable	2
		SD [nm]	29.0	6.7	8.9	unstable	
93	2-Butanol	d_H [nm]	177.9	unstable	n.d.	n.d.	6
		SD [nm]	51.1	unstable	n.d.	n.d.	
156	Chloroform	d_H [nm]	328.8	unstable	n.d.	n.d.	6
		SD [nm]	91.5	unstable	n.d.	n.d.	
183	Cyclohexanone	d_H [nm]	6000.0	558.3	537.7	473.3	2
		SD [nm]	0.0	27.9	124.9	130.7	
285	DMAc	d_H [nm]	161.2	unstable	n.d.	n.d.	6
		SD [nm]	51.3	unstable	n.d.	n.d.	
297	DMF	d_H [nm]	91.3	111.3	120.3	125.2	1
		SD [nm]	12.2	19.6	13.0	26.4	
303	DMSO	d_H [nm]	541.3	unstable	n.d.	n.d.	6
		SD [nm]	68.7	unstable	n.d.	n.d.	
306	1,4-Dioxane	d_H [nm]	350.3	384.3	311.3	458.0	2
		SD [nm]	27.5	7.8	8.3	109.0	
325	EtOH	d_H [nm]	201.8	unstable	n.d.	n.d.	6
		SD [nm]	88.5	unstable	n.d.	n.d.	
328	EtAc	d_H [nm]	87.0	85.5	81.8	79.2	1
		SD [nm]	85.3	13.3	0.2	10.0	
368	EG	d_H [nm]	60.3	37.8	47.2	64.7	1
		SD [nm]	19.1	5.2	23.6	29.8	
417	Hexane	d_H [nm]	1663.6	unstable	n.d.	n.d.	6
		SD [nm]	2323.8	unstable	n.d.	n.d.	
456	MeOH	d_H [nm]	73.6	120.3	86.3	101.0	1
		SD [nm]	3.9	25.8	41.4	39.3	
481	MEK	d_H [nm]	132.4	unstable	n.d.	n.d.	6
		SD [nm]	4.7	unstable	n.d.	n.d.	
521	NMP	d_H [nm]	263.4	unstable	n.d.	n.d.	6
		SD [nm]	38.5	unstable	n.d.	n.d.	
617	THF	d_H [nm]	54.0	79.6	92.8	82.4	1
		SD [nm]	2.7	17.8	10.3	14.9	
696	Water	d_H [nm]	84.3	74.2	77.4	74.7	1
		SD [nm]	9.5	9.4	15.4	5.8	
697	*p*-Xylene	d_H [nm]	323.3	unstable	n.d.	n.d.	6
		SD [nm]	27.3	unstable	n.d.	n.d.	

Table 70 DLS data for HSP rating for modified ZnO NP with 200% TFA at pH 7.

No.	solvent	time [days]	1	2	3	4	rating
7	Acetone	d_H [nm]	1.5	unstable	n.d.	n.d.	6
		SD [nm]	0.9	unstable	n.d.	n.d.	
10	ACN	d_H [nm]	600.0	unstable	n.d.	n.d.	6
		SD [nm]	123.9	unstable	n.d.	n.d.	
52	Benzene	d_H [nm]	508.6	unstable	n.d.	n.d.	6
		SD [nm]	194.1	unstable	n.d.	n.d.	
156	Chloroform	d_H [nm]	557.5	566.3	352.5	n.d.	2
		SD [nm]	84.8	132.5	55.1	n.d.	
183	Cyclohexanone	d_H [nm]	1167.3	unstable	n.d.	n.d.	6
		SD [nm]	51.7	unstable	n.d.	n.d.	
285	DMAc	d_H [nm]	116.6	143.5	117.0	119.1	2
		SD [nm]	9.5	23.1	6.8	10.5	
297	DMF	d_H [nm]	100.5	113.9	157.2	215.4	2
		SD [nm]	7.5	9.8	20.9	54.6	
303	DMSO	d_H [nm]	594.0	unstable	n.d.	n.d.	6
		SD [nm]	203.1	unstable	n.d.	n.d.	
306	1,4-Dioxane	d_H [nm]	539.7	522.0	351.5	369.0	2
		SD [nm]	16.7	85.5	103.4	37.2	
325	EtOH	d_H [nm]	120.7	167.4	123.3	128.2	2
		SD [nm]	18.8	11.7	17.5	18.6	
328	EtAc	d_H [nm]	1587.0	93.9	94.5	92.7	1
		SD [nm]	2779.1	9.0	55.1	2.3	
368	EG	d_H [nm]	2.5	69.2	191.9	103.6	2
		SD [nm]	0.6	22.4	96.6	5.9	
417	Hexane	d_H [nm]	359.5	unstable	n.d.	n.d.	6
		SD [nm]	492.6	unstable	n.d.	n.d.	
456	MeOH	d_H [nm]	104.7	85.6	83.7	78.8	1
		SD [nm]	34.6	10.8	13.2	16.4	
481	MEK	d_H [nm]	102.6	143.0	227.5	n.d.	4
		SD [nm]	7.6	27.9	153.3	n.d.	
521	NMP	d_H [nm]	100.0	190.1	unstable	n.d.	6
		SD [nm]	9.7	76.1	unstable	n.d.	
524	DCM	d_H [nm]	157.5	276.1	305.3	250.2	3
		SD [nm]	63.3	63.1	38.5	24.0	
617	THF	d_H [nm]	111.5	95.1	108.9	110.4	1
		SD [nm]	10.8	20.9	9.2	1.2	
696	Water	d_H [nm]	90.2	92.6	83.4	77.8	1
		SD [nm]	3.4	10.3	12.5	9.7	
697	*p*-Xylene	d_H [nm]	1000.0	unstable	n.d.	n.d.	6
		SD [nm]	131.4	unstable	n.d.	n.d.	

Table 71 DLS data for HSP rating for modified ZnO NP with 200% TFA at pH 10.

No.	solvent	time [days]	1	2	3	4	rating
7	Acetone	d_H [nm]	1.0	unstable	n.d.	n.d.	6
		SD [nm]	0.0	unstable	n.d.	n.d.	
10	ACN	d_H [nm]	322.8	unstable	n.d.	n.d.	6
		SD [nm]	32.9	unstable	n.d.	n.d.	
156	Chloroform	d_H [nm]	377.5	380.7	352.5	333.6	2
		SD [nm]	26.0	91.7	55.1	51.4	
183	Cyclohexanone	d_H [nm]	1354.0	380.7	unstable	n.d.	6
		SD [nm]	501.5	91.7	unstable	n.d.	
285	DMAc	d_H [nm]	118.5	153.7	140.3	129.2	2
		SD [nm]	26.3	25.6	17.1	21.0	
297	DMF	d_H [nm]	94.0	98.1	82.3	105.3	1
		SD [nm]	8.3	3.5	6.9	17.8	
306	1,4-Dioxane	d_H [nm]	443.2	471.0	333.4	357.0	2
		SD [nm]	148.3	31.4	95.1	125.0	
325	EtOH	d_H [nm]	103.2	103.2	115.7	104.4	1
		SD [nm]	12.9	13.6	17.5	29.5	
328	EtAc	d_H [nm]	54.6	97.0	93.5	86.4	1
		SD [nm]	30.7	15.1	3.6	9.2	
417	Hexane	d_H [nm]	371.0	unstable	n.d.	n.d.	6
		SD [nm]	95.5	unstable	n.d.	n.d.	
456	MeOH	d_H [nm]	72.9	80.8	66.3	78.1	1
		SD [nm]	7.1	4.8	14.3	15.9	
481	MEK	d_H [nm]	89.4	127.5	188.3	n.d.	4
		SD [nm]	1.8	16.2	45.8	n.d.	
524	DCM	d_H [nm]	349.6	481.3	unstable	n.d.	6
		SD [nm]	79.1	36.4	unstable	n.d.	
617	THF	d_H [nm]	109.6	83.9	105.1	456.3	1
		SD [nm]	15.8	12.6	0.5	93.4	
696	Water	d_H [nm]	79.0	76.9	105.1	92.9	1
		SD [nm]	6.3	15.1	10.0	16.8	
697	*p*-Xylene	d_H [nm]	826.8	unstable	n.d.	n.d.	6
		SD [nm]	75.6	unstable	n.d.	n.d.	

Table 72 DLS data for HSP rating for modified ZnO NP with 500% TFA at pH 7.

No.	solvent	time [days]	1	2	3	4	5	rating
7	Acetone	d_H [nm]	1.4	unstable	n.d.	n.d.	n.d.	6
		SD [nm]	0.6	unstable	n.d.	n.d.	n.d.	
10	ACN	d_H [nm]	153.1	unstable	n.d.	n.d.	n.d.	6
		SD [nm]	67.9	unstable	n.d.	n.d.	n.d.	
52	Benzene	d_H [nm]	151.2	unstable	n.d.	n.d.	n.d.	6
		SD [nm]	14.2	unstable	n.d.	n.d.	n.d.	
93	2-Butanol	d_H [nm]	708.3	unstable	n.d.	n.d.	n.d.	6
		SD [nm]	422.7	unstable	n.d.	n.d.	n.d.	
156	Chloroform	d_H [nm]	909.4	100.2	536.7	87.4	n.d.	3
		SD [nm]	452.7	4.5	122.6	60.4	n.d.	
183	Cyclohexanone	d_H [nm]	735.3	478.7	1219.7	542.2	n.d.	3
		SD [nm]	157.6	56.9	94.8	386.6	n.d.	
285	DMAc	d_H [nm]	250.9	unstable	n.d.	n.d.	n.d.	6
		SD [nm]	128.0	unstable	n.d.	n.d.	n.d.	
297	DMF	d_H [nm]	101.7	167.5	unstable	n.d.	n.d.	6
		SD [nm]	10.3	108.2	unstable	n.d.	n.d.	
303	DMSO	d_H [nm]	711.0	unstable	n.d.	n.d.	n.d.	6
		SD [nm]	166.4	unstable	n.d.	n.d.	n.d.	
306	1,4-Dioxane	d_H [nm]	320.8	416.3	384.4	296.8	295.8	3
		SD [nm]	29.9	16.3	72.9	51.2	69.9	
325	EtOH	d_H [nm]	284.9	unstable	n.d.	n.d.	n.d.	6
		SD [nm]	331.7	unstable	n.d.	n.d.	n.d.	
417	Hexane	d_H [nm]	359.3	unstable	n.d.	n.d.	n.d.	6
		SD [nm]	40.5	unstable	n.d.	n.d.	n.d.	
456	MeOH	d_H [nm]	68.3	74.0	96.5	87.2	100.3	1
		SD [nm]	15.9	11.9	4.8	32.9	6.6	
481	MEK	d_H [nm]	302.9	unstable	n.d.	n.d.	n.d.	6
		SD [nm]	197.9	unstable	n.d.	n.d.	n.d.	
521	NMP	d_H [nm]	310.2	unstable	n.d.	n.d.	n.d.	6
		SD [nm]	61.3	unstable	n.d.	n.d.	n.d.	
524	DCM	d_H [nm]	304.3	198.6	203.5	3.8	204.2	3
		SD [nm]	14.2	69.7	13.6	0.1	27.7	
617	THF	d_H [nm]	50.7	69.4	83.6	64.9	73.8	1
		SD [nm]	12.0	19.4	8.3	18.8	7.2	
696	Water	d_H [nm]	98.5	80.7	76.6	80.3	87.4	1
		SD [nm]	18.1	11.2	15.8	3.1	4.6	
697	*p*-Xylene	d_H [nm]	6000.0	unstable	n.d.	n.d.	n.d.	6
		SD [nm]	0.0	unstable	n.d.	n.d.	n.d.	
862	CCl_4	d_H [nm]	464.7	unstable	n.d.	n.d.	n.d.	6
		SD [nm]	49.5	unstable	n.d.	n.d.	n.d.	

Table 73 DLS data for HSP rating for modified ZnO NP with 1000% TFA at pH 7.

No.	solvent	time [days]	1	2	3	4	5	rating
7	Acetone	d_H [nm]	0.9	unstable	n.d.	n.d.	n.d.	6
		SD [nm]	0.0	unstable	n.d.	n.d.	n.d.	
10	ACN	d_H [nm]	142.7	unstable	n.d.	n.d.	n.d.	6
		SD [nm]	9.9	unstable	n.d.	n.d.	n.d.	
52	Benzene	d_H [nm]	4044.2	unstable	n.d.	n.d.	n.d.	6
		SD [nm]	2765.9	unstable	n.d.	n.d.	n.d.	
93	2-Butanol	d_H [nm]	176.1	256.9	unstable	n.d.	n.d.	6
		SD [nm]	16.8	167.6	unstable	n.d.	n.d.	
156	Chloroform	d_H [nm]	148.9	unstable	n.d.	n.d.	n.d.	6
		SD [nm]	132.7	unstable	n.d.	n.d.	n.d.	
183	Cyclohexanone	d_H [nm]	267.3	680.7	578.9	208.7	n.d.	3
		SD [nm]	76.6	139.9	213.8	100.7	n.d.	
285	DMAc	d_H [nm]	589.1	unstable	n.d.	n.d.	n.d.	6
		SD [nm]	273.9	unstable	n.d.	n.d.	n.d.	
297	DMF	d_H [nm]	124.2	132.0	114.7	264.2	102.3	2
		SD [nm]	28.3	21.1	39.6	39.5	5.4	
303	DMSO	d_H [nm]	623.3	unstable	n.d.	n.d.	n.d.	6
		SD [nm]	89.9	unstable	n.d.	n.d.	n.d.	
306	1,4-Dioxane	d_H [nm]	211.0	417.3	486.3	387.7	508.3	2
		SD [nm]	22.2	75.1	123.2	33.1	27.2	
325	EtOH	d_H [nm]	407.0	unstable	n.d.	n.d.	n.d.	6
		SD [nm]	207.8	unstable	n.d.	n.d.	n.d.	
417	Hexane	d_H [nm]	203.7	unstable	n.d.	n.d.	n.d.	6
		SD [nm]	5.2	unstable	n.d.	n.d.	n.d.	
456	MeOH	d_H [nm]	71.1	80.7	65.9	87.8	90.2	1
		SD [nm]	22.1	24.2	13.2	21.1	11.6	
481	MEK	d_H [nm]	131.7	unstable	n.d.	n.d.	n.d.	6
		SD [nm]	39.8	unstable	n.d.	n.d.	n.d.	
521	NMP	d_H [nm]	116.5	unstable	n.d.	n.d.	n.d.	6
		SD [nm]	16.5	unstable	n.d.	n.d.	n.d.	
524	DCM	d_H [nm]	4088.4	273.1	101.9	199.0	n.d.	4
		SD [nm]	2703.4	18.7	8.9	35.4	n.d.	
617	THF	d_H [nm]	105.9	74.3	85.8	85.9	74.5	1
		SD [nm]	14.8	10.5	22.2	18.4	25.3	
696	Water	d_H [nm]	95.0	79.3	73.0	88.5	77.1	1
		SD [nm]	3.9	1.9	4.4	14.1	7.4	
697	*p*-Xylene	d_H [nm]	2068.2	unstable	n.d.	n.d.	n.d.	6
		SD [nm]	2780.4	unstable	n.d.	n.d.	n.d.	
862	CCl_4	d_H [nm]	587.3	unstable	n.d.	n.d.	n.d.	6
		SD [nm]	156.7	unstable	n.d.	n.d.	n.d.	

Table 74 DLS data for HSP rating for PVP modified NP by standard procedure.

No.	solvent	time [days]	1	2	3	4	5	rating
7	Acetone	d_H [nm]	0,9	unstable	n.d.	n.d.	n.d.	6
		SD [nm]	0,0	unstable	n.d.	n.d.	n.d.	
10	ACN	d_H [nm]	150,8	147,3	153,0	153,4	175,8	2
		SD [nm]	2,3	8,0	7,7	1,7	6,4	
93	2-Butanol	d_H [nm]	117,8	115,8	112,8	89,9	106,4	1
		SD [nm]	25,8	15,3	11,9	20,3	33,9	
156	Chloroform	d_H [nm]	2,2	277,2	179,8	270,4	311,0	3
		SD [nm]	0,2	124,7	54,9	191,2	5,1	
183	Cyclohexanone	d_H [nm]	1709,0	unstable	n.d.	n.d.	n.d.	6
		SD [nm]	741,2	unstable	n.d.	n.d.	n.d.	
285	DMAc	d_H [nm]	132,7	124,0	142,9	96,3	129,8	2
		SD [nm]	23,5	30,7	15,9	2,0	4,4	
297	DMF	d_H [nm]	126,8	97,4	122,6	116,6	117,6	1
		SD [nm]	14,0	7,3	9,7	4,0	6,9	
303	DMSO	d_H [nm]	151,0	unstable	n.d.	n.d.	n.d.	6
		SD [nm]	49,6	unstable	n.d.	n.d.	n.d.	
306	1,4-Dioxane	d_H [nm]	265,1	247,0	unstable	n.d.	n.d.	6
		SD [nm]	40,7	89,7	unstable	n.d.	n.d.	
325	EtOH	d_H [nm]	136,9	121,4	120,8	129,5	123,8	2
		SD [nm]	28,4	11,5	12,2	7,4	18,0	
328	EtAc	d_H [nm]	2104,6	377,7	unstable	n.d.	n.d.	6
		SD [nm]	2756,2	189,0	unstable	n.d.	n.d.	
368	EG	d_H [nm]	128,0	120,6	62,9	94,1	82,0	1
		SD [nm]	26,4	32,7	21,5	35,2	25,0	
417	Hexane	d_H [nm]	3,6	unstable	n.d.	n.d.	n.d.	6
		SD [nm]	0,5	unstable	n.d.	n.d.	n.d.	
456	MeOH	d_H [nm]	145,9	120,7	129,6	123,3	119,4	2
		SD [nm]	6,2	3,7	13,1	5,1	2,8	
481	MEK	d_H [nm]	140,2	139,9	123,6	110,4	120,3	2
		SD [nm]	4,2	14,7	9,4	11,1	7,4	
521	NMP	d_H [nm]	119,4	105,5	91,8	129,7	106,4	1
		SD [nm]	3,5	13,4	19,2	12,1	12,0	
524	DCM	d_H [nm]	344,0	2,8	343,8	385,7	184,6	3
		SD [nm]	23,6	0,1	61,9	43,6	91,5	
617	THF	d_H [nm]	217,3	267,6	259,9	200,1	n.d.	2
		SD [nm]	6,5	12,4	128,6	126,2	n.d.	
696	Water	d_H [nm]	101,9	82,8	94,5	104,9	106,8	1
		SD [nm]	14,0	12,6	17,0	8,2	11,8	
697	*p*-Xylene	d_H [nm]	1,8	unstable	n.d.	n.d.	n.d.	6
		SD [nm]	0,2	unstable	n.d.	n.d.	n.d.	

Table 75 DLS data for HSP rating for PVP modified NP by codispersion.

No.	solvent	time [days]	1	2	3	4	5	rating
7	Acetone	d_H [nm]	1.0	unstable	n.d.	n.d.	n.d.	6
		SD [nm]	0.1	unstable	n.d.	n.d.	n.d.	
10	ACN	d_H [nm]	142.2	unstable	n.d.	n.d.	n.d.	6
		SD [nm]	38.8	unstable	n.d.	n.d.	n.d.	
93	2-Butanol	d_H [nm]	136.4	131.8	125.5	126.1	113.0	2
		SD [nm]	24.4	5.4	20.0	6.1	22.5	
156	Chloroform	d_H [nm]	459.8	367.9	372.1	329.0	242.5	3
		SD [nm]	172.7	109.5	95.5	33.7	46.2	
183	Cyclohexanone	d_H [nm]	1033.3	1485.3	unstable	n.d.	n.d.	6
		SD [nm]	43.0	633.7	unstable	n.d.	n.d.	
285	DMAc	d_H [nm]	112.9	139.6	140.0	108.5	134.1	2
		SD [nm]	16.3	12.4	5.2	28.3	10.9	
297	DMF	d_H [nm]	128.4	125.0	254.9	253.3	235.6	2
		SD [nm]	6.8	3.8	5.5	15.9	16.2	
303	DMSO	d_H [nm]	163.7	108.9	124.9	159.3	125.2	2
		SD [nm]	62.3	25.8	11.3	72.8	10.2	
306	1,4-Dioxane	d_H [nm]	379.4	unstable	n.d.	n.d.	n.d.	6
		SD [nm]	94.2	unstable	n.d.	n.d.	n.d.	
325	EtOH	d_H [nm]	153.9	322.7	362.3	377.4	677.2	4
		SD [nm]	54.7	14.0	74.1	93.4	377.0	
328	EtAc	d_H [nm]	2386.7	unstable	n.d.	n.d.	n.d.	6
		SD [nm]	266.0	unstable	n.d.	n.d.	n.d.	
368	EG	d_H [nm]	82.6	78.3	102.5	97.0	82.1	1
		SD [nm]	23.8	34.8	26.3	49.7	31.2	
417	Hexane	d_H [nm]	151.0	unstable	n.d.	n.d.	n.d.	6
		SD [nm]	207.9	unstable	n.d.	n.d.	n.d.	
456	MeOH	d_H [nm]	142.0	170.1	162.0	149.7	156.8	2
		SD [nm]	12.5	7.7	14.0	15.7	19.4	
481	MEK	d_H [nm]	141.0	unstable	n.d.	n.d.	n.d.	6
		SD [nm]	25.9	unstable	n.d.	n.d.	n.d.	
521	NMP	d_H [nm]	111.5	118.4	121.2	123.2	124.6	1
		SD [nm]	18.4	20.2	18.5	13.7	16.9	
524	DCM	d_H [nm]	140.5	119.7	304.5	224.8	283.3	3
		SD [nm]	29.8	76.1	87.1	20.7	88.1	
617	THF	d_H [nm]	265.7	511.5	unstable	n.d.	n.d.	6
		SD [nm]	20.9	310.6	unstable	n.d.	n.d.	
696	Water	d_H [nm]	102.9	112.7	116.0	61.2	108.7	1
		SD [nm]	16.5	12.9	18.1	4.6	15.8	
697	*p*-Xylene	d_H [nm]	2001.3	unstable	n.d.	n.d.	n.d.	6
		SD [nm]	2827.5	unstable	n.d.	n.d.	n.d.	

Table 76 Performance of membranes (16% PVDF, 1% PVP K-30) with pristine ZnO nanoparticles.

c(NP)	permeability [L/h m² bar]				rejection [%]				n
[%w/w(PVDF)]	P_0	SD	P_1	SD	PEG 35kDa	SD	PEO 100kDa	SD	
0	1088	101	847	87	3	2	87	0	3
1	968	32	769	7	5	4	n.d.	n.a.	1
3	738	31	572	6	21	22	n.d.	n.a.	1
5	557	131	415	120	14	12	85	3	3
10	570	170	428	147	31	6	89	0	3
15	618	212	509	147	36	7	86	0	2
20	494	133	373	77	28	19	88	2	4
25	482	7	419	4	41	8	n.d.	n.a.	1
40	536	41	411	25	49	4	81	1	2
50	500	232	400	222	57	21	78	11	33

Table 77 Performance of membranes (16% PVDF) with pristine ZnO nanoparticles.

c(NP)	permeability [L/h m² bar]				rejection [%]				n
%w/w(PVDF)	P_0	SD	P_1	SD	PEG 35kDa	SD	PEO 100kDa	SD	
0	48	17	31	4	65	17	78	7	4
5	64	15	43	5	45	19	71	10	3
10	39	2	31	1	83	1	92	2	1
20	55	1	41	1	85	1	87	3	1
25	47	17	40	6	54	23	76	13	3
50	29	2	23	1	76	13	85	3	2

Table 78 Performance of membranes (20% PVDF, 1% PVP) with pristine ZnO nanoparticles coagulated in solvent blend.

c(NP)	permeability [L/h m² bar]				rejection [%]				n
%w/w(PVDF)	P_0	SD	P_1	SD	PEG 35kDa	SD	PEO 100kDa	SD	
0	144	15	88	14	48	22	60	35	2
5	86	3	70	7	15	10	15	1	2
10	100	40	81	41	31	4	56	2	2
20	126	5	99	0	94	2	66	1	2
50	128	23	95	20	13	2	26	2	2

Table 79 Performance of membranes (16% PVDF, 1%PVP) with TFA-modified nanoparticles.

c(NP)	permeability [L/h m² bar]				rejection [%]				n
%w/w(PVDF)	P_0	SD	P_1	SD	PEG 35kDa	SD	PEO 100kDa	SD	
0	1088	101	847	87	3	2	87	0	3
5	741	230	501	139	23	16	88	1	2
10	570	79	405	87	24	21	68	3	2
20	570	28	409	3	22	3	88	1	2

Table 80 Performance of membranes (16% PVDF) with Ac-modified nanoparticles.

c(NP)	permeability [L/h m² bar]				rejection [%]				n
%w/w(PVDF)	P_0	SD	P_1	SD	PEG 35kDa	SD	PEO 100kDa	SD	
0	48	17	31	4	65	17	78	7	4
5	38	12	28	6	62	3	83	5	2
10	21	13	20	7	67	12	76	7	3
20	6	3	9	5	85	6	89	3	2
50	17	1	21	0	64	5	70	2	2

Table 81 Performance of membranes (16% PVDF) with PVP modified nanoparticles.

c(NP)	permeability [L/h m² bar]				rejection [%]				n
%w/w(PVDF)	P_0	SD	P_1	SD	PEG 35kDa	SD	PEO 100kDa	SD	
0	65	7	35	1	51	9	74	5	2
5	83	11	66	8	87	5	89	2	2
10	172	1	115	0	80	1	66	21	2
20	322	15	196	12	70	3	87	2	2
50	957	77	759	81	29	15	80	1	2

Table 82 Performance of membranes (16% copolymer, 1% PVP in dope) from novel copolymer with ZnO nanoparticles

c(NP)	permeability [L/h m² bar]				rejection [%]				n
%w/w(PVDF)	P_0	SD	P_1	SD	PEG 35kDa	SD	PEO 100kDa	SD	
0	2637	87	2018	102	5	0	n.d.	n.d.	2
3	258	n.a.	252	n.a.	49	n.a.	n.d.	n.d.	1
10	245	n.a.	243	n.a.	51	n.a.	74	n.a.	1
15	139	n.a.	144	n.a.	72	n.a.	76	n.a.	1
20	205	n.a.	191	n.a.	51	n.a.	76	n.a.	1
25	144	n.a.	124	n.a.	69	n.a.	81	n.a.	1
50	365	n.a.	343	n.a.	37	n.a.	n.d.	n.d.	1

Table 83 Performance of membranes (20% copolymer, 1% PVP in dope) from novel copolymer with ZnO nanoparticles

c(NP)	permeability [L/h m² bar]				rejection [%]				n
%w/w(PVDF)	P_0	SD	P_1	SD	PEG 35kDa	SD	PEO 100kDa	SD	
0	144	15	86	10	42	4	61	5	2
5	86	3	57	8	64	2	69	6	2
10	100	40	79	2	28	5	47	1	2
20	126	5	128	15	38	5	58	2	2
50	128	23	70	1	24	12	20	3	2

Table 84 TGA result of membranes (16 % PVDF and 1 % PVP) with pristine ZnO nanoparticles.

c(ZnO) in dope solution	residual mass	measured c(ZnO) in membrane
[%w/w(PVDF)]	at T = 502 °C [%]	[%w/w(PVDF)]
0	40.43	0
3	46.83	11
50	61.41	54

9.3. List of figures

9.4. List of tables

9.5. Curriculum Vitae

The C.V. is not included in the online version for privacy reasons.